Formation of Stöber silica supported gold nanoparticles : mechanism and application

Jingjie Luo

UNIVERSITÉ DE STRASBOURG

EDSC Ecole Doctorale des Sciences Chimiques

ÉCOLE DOCTORALE DES SCIENCES CHIMIQUES

Institut de chimie et procédés pour l'énergie, l'environnement et la santé (ICPEES)

THÈSE

présentée par

Jingjie LUO

soutenue le : **19 Septembre 2013**

pour obtenir le grade de

Docteur de l'université de Strasbourg

Discipline / Spécialité : Chimie

Formation of Stöber silica supported gold nanoparticles: mechanism and application

Formation de nanoparticules d'or supportées sur silice Stöber: mécanismes et applications

THÈSE préparée dans l'ICPEES (UMR 7515) et dirigée par :

Mme PETIT Corinne	Professeur, UDS, Strasbourg
Mme PITCHON Véronique	Directeur de recherche, UDS, Strasbourg

RAPPORTEURS :

M. TUEL Alain	Directeur de recherche, CNRS, Lyon
Mme PLUCHERY Olivier	Maître de conférences, Université Paris-6, Paris

MEMBRES DU JURY :

M. BOUR Christophe	Maître de conférences, Université Paris 11, Paris
Mme BEGIN -COLIN Sylvie	Professeur, UDS, Strasbourg

Acknowledgments

I would like to thank a lot of people during my study for the PhD degree of Université de Strasbourg (UDS) in ICPEES (Institut de Chimie et Procédés pour L'Énergie, L'Environnement et la Santé). This study work is under the supervision of Professor Corinne PETIT, and the co-supervisor Véronique PITCHON. The China Scholarship Council (CSC) for the PhD grant during my staying at the ICPEES in UDS is greatly acknowledged.

First of all, I would like to give my most regardful appreciation to Prof. Corinne PETIT, who is directly responsible for the organization and communication of the work during my study. She gives me the opportunity to study abroad, makes me understand the meaning as being a PhD student, and also induces me to realize that being a learner in the Chemistry field is just what I like. She is like a beacon in the sea, shedding light on the way for the passing travelers. Under the discussion with her, I find out that the investigation work is not only a task for getting a degree, but also one part of my splendid life. I am also grateful for the supervision of my co-supervisor Dr. Véronique PITCHON. Her humorous words and passionate smile is her personal mark, giving me the home-like feeling even I am thousands of miles away from home.

I also would like to thank Prof. Wei CHU for the recommendation of me to study abroad in UDS. He introduced me the basic methods for my expedition in research, accelerating my pace stepping into this field. Thanks for him to give me meticulous concern on my study and my daily life.

I am also thankful to Dr. Cuong Pham-huu, the director of the ICPEES, UMR 7515. He gave me abundant support including the experimental equips and useful discussions on a section of the PhD work.

I am grateful to all the members of my jury: Professor Alain TUEL- research director of

CNRS; Dr. Olivier PLUCHERY from UPMC of Paris; Professor Sylvie BEGIN-COLIN from ECPM in Strasbourg; and Dr. Christophe BOUR from the University of Paris 11. Thanks for them to read and appraise the report and providing helpful comments.

Special thanks to the engineers and technicians, Alain- the kind man “forcing” me to learn French, Sécou- enthusiastic with lovely smile, Fabrice- the “if you have any problem, find Fabrice”, Pierre- the handsome gentlemen, Thierry (Dintzer)- busy man running between IPCMS-ICPEES, Thierry (Romero)…; to all my colleges: Anais, Cuong (Duong-Viet), Loubna, Janina…; and the “powerful backing” of my Chinese friends: Yunjie, Xiaojie, Wen, Quan, Yige… for all their helpful discussions on the work and support in my daily life.

I also want to thank my parents. My mother and father are the most normal Chinese. I appreciate their courage to give birth to me and lead me the real way to become a human. When I was very young, I was in poor health and always crying. My parents brought me up with tears and sweats. When I was in primary school, I was as naughty as a boy. But my mother never blamed me, only telling me that a girl as naughty as a boy is usually a clever one. While my father acts as controller with few words unless influential mistakes occurred, showing his wordless but intensive love. I may say I only studied for my parents when I was too young to understand the value of knowledge. My mother taught me to be alive with smile and passion, and my father makes me to treat the problems calmly and patiently. I owe my current results partially to some of the genetic personalities they gave.

Finally, I would like to thank my husband- Yuefeng, who was acting as a counselor during my whole postgraduate career. He provided me the hope and fresh idea for my fighting with the appeared challenges. He is a straightforward man who is ready to show his tenderness and release all my potential pressure. Thanks to my family, I can insist my belief until now with optimistic and relaxed attitude.

Table contents

Résumé

1. Introduction Générale

Les nanoparticules d'or sont utilisées pour des réactions catalytiques depuis environ une vingtaine d'années et montrent d'excellentes activités dans des réactions particulières telles que l'oxydation du monoxyde de carbone et la chloration du méthane. Ces nanoparticules étant très actives, elles favorisent l'économie de matières premières et diminuent le coût en énergie. De nos jours, les nanoparticules colloïdales d'or sont également utilisées dans divers domaines mais seulement de manière préliminaire dans le champ de la catalyse. Etant utilisées comme précurseur d'or, les nanoparticules d'or présentent quelques avantages intéressants comme de pouvoir obtenir un catalyseur particulièrement contrôlé au cours de leurs synthèses et du dépôt sur un large spectre de matériaux ; leur taille, forme, densité étant maîtrisées dans l'étape de la préparation de la solution colloïdale. Pour l'or, ces paramètres peuvent être préalablement estimés à partir de la couleur de l'échantillon sur des matériaux blancs, et l'effet plasmon de surface. Les propriétés ci-dessus illustrent le potentiel intérêt des nanoparticules colloïdales d'or dans le champ de catalyse car elles permettent d'affiner la connaissance de ses différentes étapes.

Un matériau transparent ou blanc, la silice est habituellement utilisée comme support pour des catalyseurs, en particulier pour former une structure cœur-coquille. Cependant, quand la silice est employée en tant que support pour des catalyseurs d'or par des méthodes traditionnelles de préparation et appliquées pour des réactions telles que l'oxydation du monoxyde de carbone, l'activité du catalyseur est généralement faible. Quelques investigations ont été engagées dans la préparation des catalyseurs Au/SiO_2 avec une activité plus élevée par certaines méthodes spéciales telles que la déposition en phase vapeur, à l'aide d'un solvant ainsi que la technique de la dispersion d'agrégats métalliques. Cependant la plupart de ces méthodes sont chères et inapplicables à grande échelle. De plus, la silice étant un support inerte pour les

nanoparticules d'or, il limite également l'interaction Métal - Support, interaction utile pour activer les nanoparticules d'or pendant les réactions d'oxydation.

Les nanoparticules colloïdales d'or étant peu utilisées dans le domaine catalytique, nous avons pour but d'augmenter leur usage en essayant de combiner les avantages définis des nanoparticules colloïdaux d'or avec ceux de la silice. Nous avons choisi de développer nos recherches en synthétisant une silice non poreuse préparée par la célèbre méthode de Stöber et donnant des nanoparticules de silice de taille et de distribution en taille contrôlée. La raison pour laquelle nous avons choisi la silice Stöber est que la variété des sphères de silice est importante en taille et en microporosité. Nous nous sommes intéressées à des sphères de silice non poreuses et de petites tailles (<1 μm). Les nanoparticules d'or peuvent être fortement dispersées à la surface de cette silice. Par l'absence de porosité dans les sphères, les nanoparticules d'or ne seront pas emprisonnées dans des pores et pourront être totalement exposés aux réactifs. De cette façon, le mécanisme de réaction et le rôle des nanoparticules d'or peuvent être étudiés avec précision.

Dans cette thèse, les nanoparticules d'or de très petites tailles et homogènes en taille ont été synthétisées par une méthode colloïdale améliorée au laboratoire à partir de la littérature. La silice préparée par la méthode Stöber, a été utilisée comme support pour disperser les nanoparticules d'or. De très petites quantités d'oxydes métalliques, CuO, Fe_2O_3 ou Co_2O_3 ont été ajoutées aux nanoparticules d'or déposées sur la silice pour améliorer l'activité catalytique. L'oxydation du monoxyde de carbone (CO) a été utilisée comme réaction modèle. Le mécanisme d'oxydation du CO des nanoparticules d'or (métal dopé) déposées sur la silice Stöber a été étudié en détail.

2. Préparations et caractérisations des solutions colloïdales d'or

La préparation étant une partie cruciale de cette thèse, la première partie de ce travail s'est concentrée sur la façon d'obtenir une solution colloïdale stable avec de très petites

nanoparticules d’or (par exemple 3 nm) et avec une distribution en taille étroite. Une série de solutions colloïdales d’or a d’abord été préparée en utilisant $NaBH_4$ comme réducteur et l’alcool polyvinylique (APV, PVA en anglais) comme protecteur. Les tailles et les distributions de tailles des nanoparticules d’or dans les solutions peuvent être variées en changeant les conditions de réaction comme la température de réaction, le solvant et la concentration et le rapport relatif des réactifs. La variation de morphologies et les agglomérats de nanoparticules d’or changent leurs propriétés optiques, ce qui peut être vu directement par la couleur de l’échantillon et détecté par les spectres d’absorption UV–Vis.

Dans cette partie, un des objectifs principaux a été de préparer des solutions colloïdales par une méthode simple avec une distribution étroite de nanoparticules d’or de petites tailles pour de futures applications (c'est-à-dire en les utilisant comme précurseurs de catalyseurs hétérogènes). Un rapport approprié de protecteur : Au : réducteur à savoir APV : Au : $NaBH_4$ de 0.0197: 1: 5 en rapport molaire (le rapport APV: Au exprimé en masse est égal à 5: 1) et une réaction dans l’eau à température ambiante (25^oC) sont les conditions adéquates pour produire les nanoparticules d’or attendues.

Un autre objectif a été d’estimer la taille des nanoparticules d’or et leur distribution obtenues dans les solutions colloïdales en utilisant certaines propriétés particulières de l’or, incluant leurs propriétés optiques. Comme présentées sur la Figure 1, les solutions colloïdales donnent des teintes dérivées de couleur violette qui sont le résultat de la variation en tailles, morphologies agrégations des nanoparticules d’or. Ces observations peuvent être complétées et confirmées par l’étude des spectres d’absorption UV-Vis en liaison directe avec la résonance de plasmon de surface.

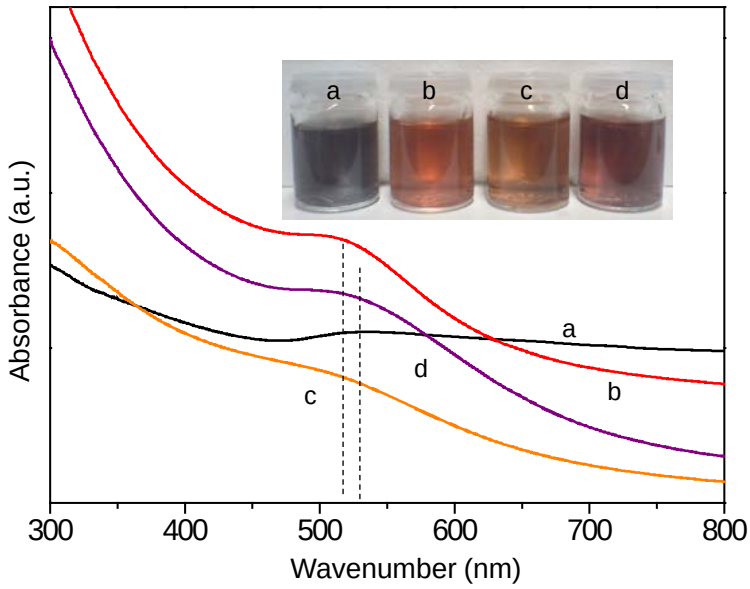

Figure 1. Spectres UV-vis (Absorbance en fonction de la longueur d'onde) et couleur des solutions colloïdales d'or pour différentes concentrations de réactifs. $NaBH_4$: Au = 5: 1 (rapport molaire) et PVA: Au = 5: 1 (rapport en poids). a: $[NaBH_4]$ = 0.1 M, $[HAuCl_4] = 10^{-2}$ M, b: $[NaBH_4]$ = 0.1 M, $[HAuCl_4] = 10^{-3}$ M, c: $[NaBH_4]$ = 0.1 M, $[HAuCl_4] = 10^{-4}$ M, et d: $[NaBH_4]$ = 0.01 M, $[HAuCl_4] = 10^{-4}$ M

La solution colloïdale possédant les particules d'or les plus petites, diluées et homogènes doit présenter un pic de résonance plasmonique à la longueur d'onde la plus petite par rapport aux autres solutions. Pour la solution colloïdale attendue avec une distribution homogène de nanoparticules autour de 3 nm, le spectre UV donne une bande plasmonique symétrique avant 520 nm et de faible intensité (b ou c de la Figure 1).

Dans certains cas, l'étude des observations des couleurs et des spectres UV ne peuvent pas directement indiquer les différences des solutions colloïdales, spécialement quand les spectres sont similaires pour des origines distinctes. Dans ce chapitre, nous discutons d'une méthode originale pour assigner les tailles, la forme et la distribution des cristallites d'or que nous proposons sous le terme «test maison de diffusion liquide» avec une traduction anglaise "Home-made liquid diffusion (HMD) test".

Cette idée s'inspire de la méthode classique développée dans le domaine de la chimie organique par chromatographie couche mince. De la même manière que cette technique permet de séparer et d'identifier différents produits en chimie organique, la méthode peut servir potentiellement à déterminer la nature d'un mélange de nanoparticules et d'en déterminer l'ordre de grandeur de la taille. Le gel de silice déposé sur une feuille d'aluminium est utilisé pour étudier la diffusion des solutions colloïdales d'or. Une goutte de la solution d'or (One drop of gold colloid) est déposée sur la plaque de silice, les processus de diffusion sont étudiés par la prise de 3 photos en fonction du temps (la première à l'ajout, la seconde à la fin de la diffusion et la troisième lorsque la plaque est sèche). La conduite du test est illustrée sur le Schéma 1.

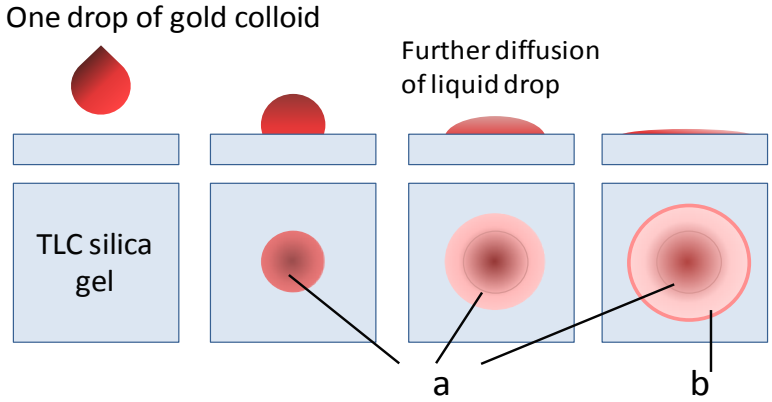

Schéma 1. L'illustration de la procédure de diffusion liquide "maison" et présentation colorée des différents cercles de diffusion. Une goutte de la solution colloïdale d'or (one drop of gold colloïd) est déposée sur la plaque de gel de silice (TLC silica gel). On observe la diffusion de la goutte avec le temps (Further diffusion of liquid drop). 2 cas limites sont obtenus.

a. les particules les plus larges de la solution colloïdale restent sur la surface mouillée par la goutte initiale pour former le disque interne
b. les plus petites particules se déplacent plus facilement jusqu'à la limite de diffusion et forment un bord coloré.

Le premier contact entre la solution colloïdale et le gel forme un disque de liquide concentré illustré par la partie a du schéma. Les particules les plus larges, les agglomérats et les bâtonnets présents dans l'eau sont plus limités dans leur diffusion que les petites particules et restent proche de leur dépôt. Les petites, plus libres de migrer vont diffuser jusqu'à un front

pendant le processus et se situent sur un cercle externe comme le présente la partie b du schéma 1.

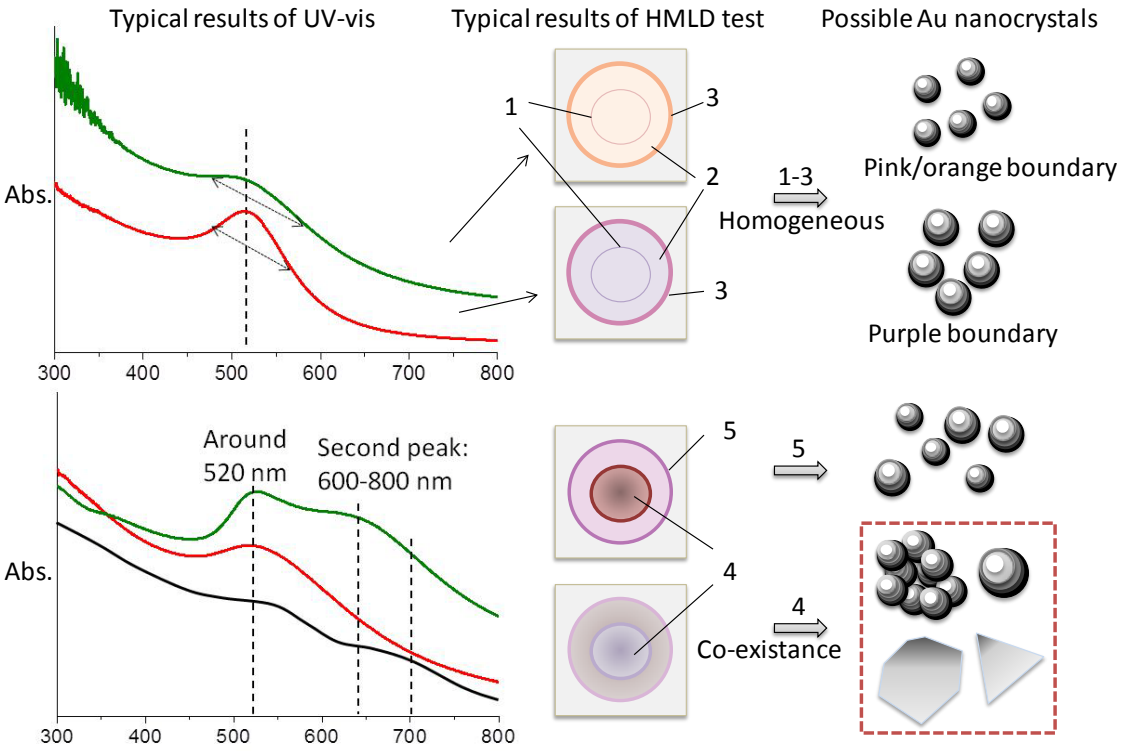

Schéma 2. Illustration de la correspondance entre un spectre d'absorbance, (typical results of UV-vis), son résultat final de diffusion (typical results of HMLD test), avec les couleurs des cercles rose/orange ou violet (pink/orange or purple boundary) et la possible morphologie des nanoparticules d'Au.

[1] zone de contact initial [2] cercle de diffusion avec une couleur unique; [3] front coloré large; [4] zone de couleur claire (pourpre); [5] front coloré fin ou peu visible (pourpre ou violet).

Finalement, la théorie des tests de diffusion (HMLD tests) a été confirmée par une étude en microscopie à balayage directement par l'étude de la plaque. Différentes solutions colloïdales ayant différentes propriétés optiques ont été estimées comme le montre le schéma 2. La méthode de diffusion proposée (the HMLD method) est essentielle pour organiser ce travail, particulièrement lorsque les couleurs et les résultats obtenus par spectrométrie UV-vis se révèlent complexes ou trop peu informatifs. Cette technique est avantageuse pour les groupes engagés dans l'étude des solutions colloïdales d'or, étude qui nécessite un travail important de

préparation. En utilisant en complément cette méthode de diffusion (HMLD), qui est simple et répétable, la formation des nanoparticules d'or peut être rapidement estimée de façon préliminaire et permet de limiter le nombre d'échantillons pour les caractérisations plus complexes et plus chères aux échantillons les plus significatifs.

3. Préparation des silices Stöber et le dépôt de nanoparticules d'or sur ces supports

De façon récente, des matériaux de type silicique préparés par la méthode Stöber sont de plus en plus utilisés dans le domaine de la science des matériaux. Dans le domaine de la catalyse hétérogène, les supports développés habituellement sont des matériaux mésoporeux possédant une grande surface spécifique. Cet oxyde de silicium est différent car il est de grande surface par la petitesse de ses particules et peut-être préparé soit microporeux soit non poreux. Ce type de matériau n'est pas couramment utilisé ou considéré potentiel comme support en catalyse jusqu'à aujourd'hui. Cependant, un fait indéniable est que la silice a un faible coût, facile à produire et possède une faible capacité de transfert électronique ou de conduction. S'il s'avère applicable dans la catalyse à l'or, il sera intéressant dans la compréhension des mécanismes réactionnels et de frittage des nanoparticules d'or.

Dans cette partie, on s'est intéressé à la préparation des sphères de silice Stöber avec les méthodes de dépôt de nanoparticules d'or pour des applications catalytiques. Les sphères de silice avec différents diamètres ont été préparées par le contrôle du dosage des réactifs et nommées SSn (n=1-5, SS1<SS2…<SS5). Dans les méthodes classiques des matériaux Silice Stöber – Au, des ajouts d'organosilanes ou de thiols ont toujours été introduits pour fixer l'or sur la silice, ce qui limite leurs applications en catalyse. Dans notre cas, les nanoparticules d'or (de 2-4 nm) par la voie colloïdale sur des sphères de silice Stöber sont déposées par une voie simple. Deux silices (SS1 et SS5) ont été choisies comme support avec des diamètres respectifs de 49 nm et 490 nm. Un dépôt d'or de 1 wt% d'or est réalisé sur la silice. C'est la première fois que l'ajout de composés organosilanes et thiols n'est pas fait pour ce couple

SiO_2-Au et qu'une méthode dérivée d'une méthode d'imprégnation est développée.

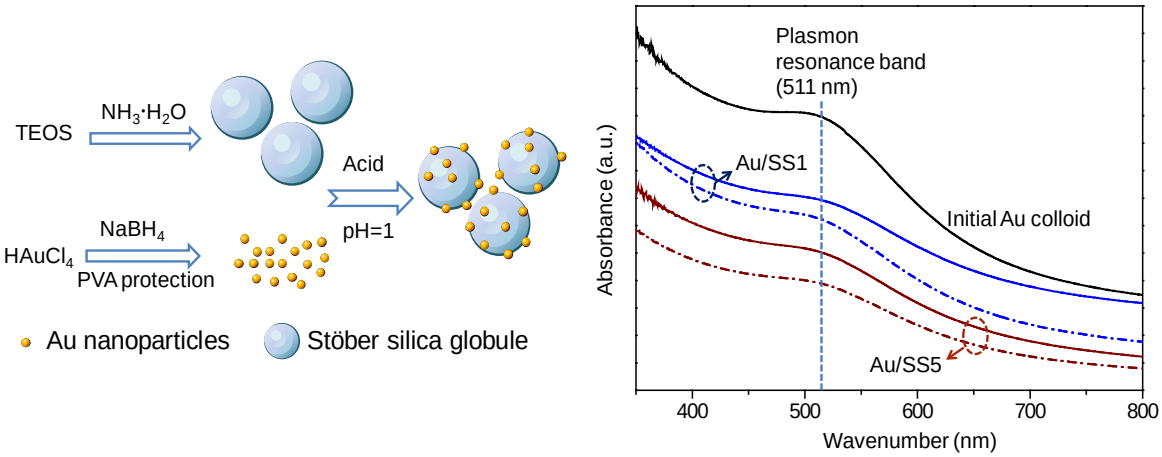

Figure 2. Illustration des étapes de la méthode de préparation (gauche) and spectres UV-vis (droite) de la solution colloïdale pendant la préparation des échantillons Au/SS1 et Au/SS5. Les lignes pleines correspondent à la solution agitée pendant 10 min après l'ajustement du pH à 1, les lignes en pointillés correspondent à la solution mère après centrifugation.

La Figure 2 montre la méthode de préparation et le suivi du dépôt d'or sur les silices SS1 and SS5 à partir de la solution colloïdale. Les silices Stöber sont préalablement obtenues à partir de l'orthosilicate de tétraéthyle (en anglais TEOS) dans l'éthanol absolu par ajout d'ammoniaque dans un mélange éthanol-eau. La poudre de silice séchée est mélangée avec la solution colloïdale d'or et imprégnée à un pH acidifié à 1. Une agitation de 10 min et une centrifugation se sont avérées indispensables pour collecter et déposer les particules d'or sur le support.

Les images des échantillons par les microscopies à balayage (MEB) et à transmission (TEM) avant la calcination montrent une répartition en taille très homogène à la surface des sphères de silice. Les particules sont de petites tailles et centrées sur 3 nm sans agrégation importante de nanoparticules. Après traitement sous air à 300 °C pendant 4 heures, les nanoparticules d'or évoluent. Une partie des nanoparticules des systèmes grossit comme on peut le voir sur la Figure 3. Cependant une grande quantité de petites particules identiques à la taille initiale

existent à la surface des sphères de silice, celles-ci sont capables de satisfaire les conditions pour rendre les matériaux à base d'or intéressants dans le domaine de la catalyse hétérogène.

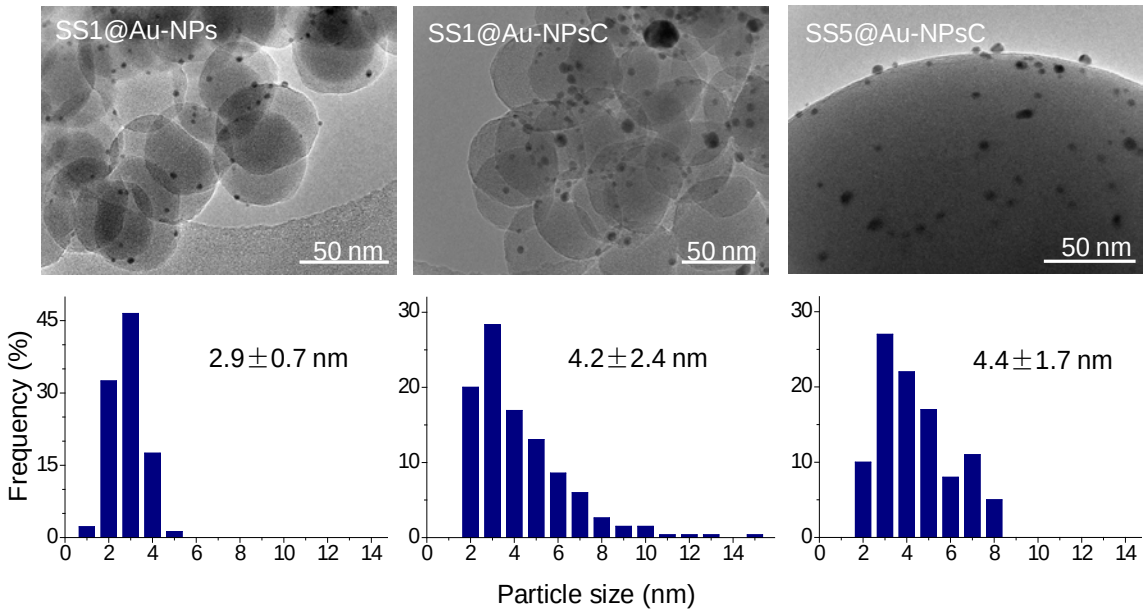

Figure 3. Images MET des échantillons Au/SS1, Au/SS1-C, et Au/SS5-C accompagnées du calcul de leur distribution en taille des nanoparticules d'or; C = après traitement thermique à 300 °C.

Le mode de dépôt des nanoparticules d'or à la surface des sphères de silice a été étudié par la combinaison des techniques de spectroscopies de photoélectron X et infra-rouge (X-ray Photoelectron Spectrum (XPS) et Operando Fourier Transform Infrared Spectroscopy (FTIR)). Pendant le procédé de dépôt, les nanoparticules d'or sont protégées par l'alcool APV (en anglais PVA) qui interagit avec les fonctions hydroxydes de la surface silice, hydroxydes qui existent en grand nombre et de façon très dispersée. Le traitement thermique qui suit le dépôt facilite à la fois la destruction du PVA et la déshydroxylation de la silice. Les nanoparticules d'or sont ensuite déposées à la surface de la silice et sont peut-être faiblement bloquées géométriquement.

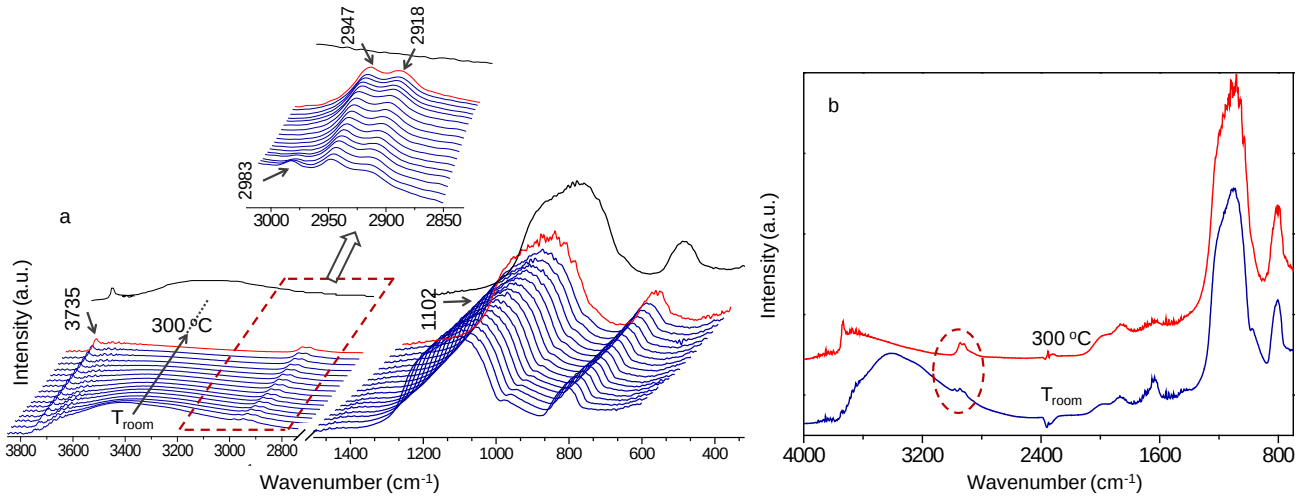

Figure 4. Spectres obtenus par infra-rouge à Transformée de Fourier par la technique Operando (intensité en fonction de la longueur d'onde) pour l'échantillon en montée Au/SS5 de la température ambiante à 300°C

(a) Evolution des spectres de Au/SS5 à la T_{amb} et 300 ^{o}C

(b) Comparaison des spectres initial et final de Au/SS5 à 300 ^{o}C

Ce travail montre la possibilité de préparer par une manière simple et respectueuse de l'environnement des nanoparticules d'or sur des sphères de silice Stöber sans ajout de composés organiques comme c'est souvent le cas ; ces composés sont de plus susceptibles d'être des poisons pour l'or. Cette méthode a conduit à une fine distribution de nanoparticules de petites tailles, correctement distribuées sur la surface de la silice. Ces matériaux sont des matériaux potentiels pour la catalyse hétérogène.

4. Application de matériaux Au/SSn pour des applications catalytiques avec l'ajout d'un second métal.

Dans cette partie du travail, le système Au/SS5 après calcination (Au/SS5-C) a été choisi comme catalyseur type et testé pour la réaction d'oxydation du monoxyde de carbone (CO). Bien que la taille des nanoparticules d'or soit vraiment homogène et autour de 3 nm - en accord de taille avec des applications pour cette réaction - ce système présente une très faible

activité pour la réaction d'oxydation du CO en dessous de 300°C. Ceci est en accord avec la littérature qui indique que ces particules ne peuvent être actives qu'avec une très bonne interaction Métal- Support et ceci n'est pas réalisé avec ce système en raison à la fois de l'utilisation de la silice et de l'utilisation de solutions colloïdales. Pour aller plus loin, le système Au/SS5 avant traitement thermique a été modifié par l'addition d'un second métal réductible. La méthode de synthèse est comme une méthode par dépôt et les échantillons sont nommés: Au/SS5@M-C (M=Co, Fe, et Cu, Au: M= 1: 1 rapport atomique, dépôt d'Au 1 wt% sur la silice), C indique que le traitement thermique est fait (à 300 ^{o}C - 4 h).

4.1 Impact de l'addition d'un second métal sur l'activité du système Au/SS5-C pour l'oxydation du CO

Les échantillons Au/SS5-C and Au/SS5@M-C ont tout d'abord été testés dans la réaction classique d'oxydation du CO. Différents de l'inactif Au/SS5-C, les échantillons chargés d'un second métal augmentent significativement leur activité vis-à-vis du CO.

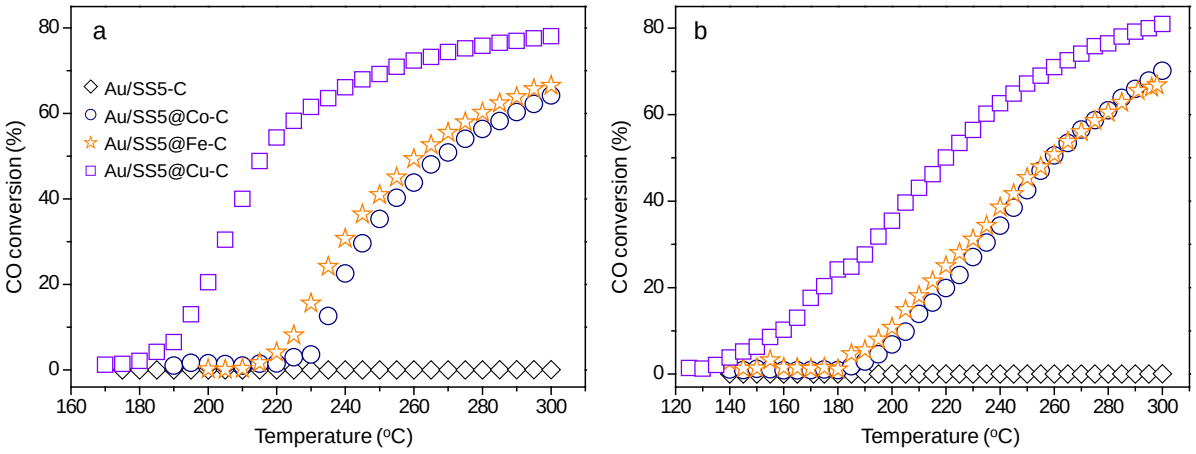

Figure 5. Conversion du CO pendant l'oxydation CO en fonction de la température pour 50 mg de catalyseurs Au/SS5@M-C:

(a) Pour la première montée en température (b) pour la seconde montée

"C" indique que le traitement thermique est effectué (air à 300 ^{o}C sur 4 h).

Pour l'oxydation du monoxyde de carbone, pendant la première montée en température, les échantillons s'activent et lors de la seconde montée présentent une activité supérieure. Comme montré dans la Figure 5, les échantillons Au/SS5@M-C sont actifs, et celui dopé au Cu, présente la meilleure activité dans les conditions testées.

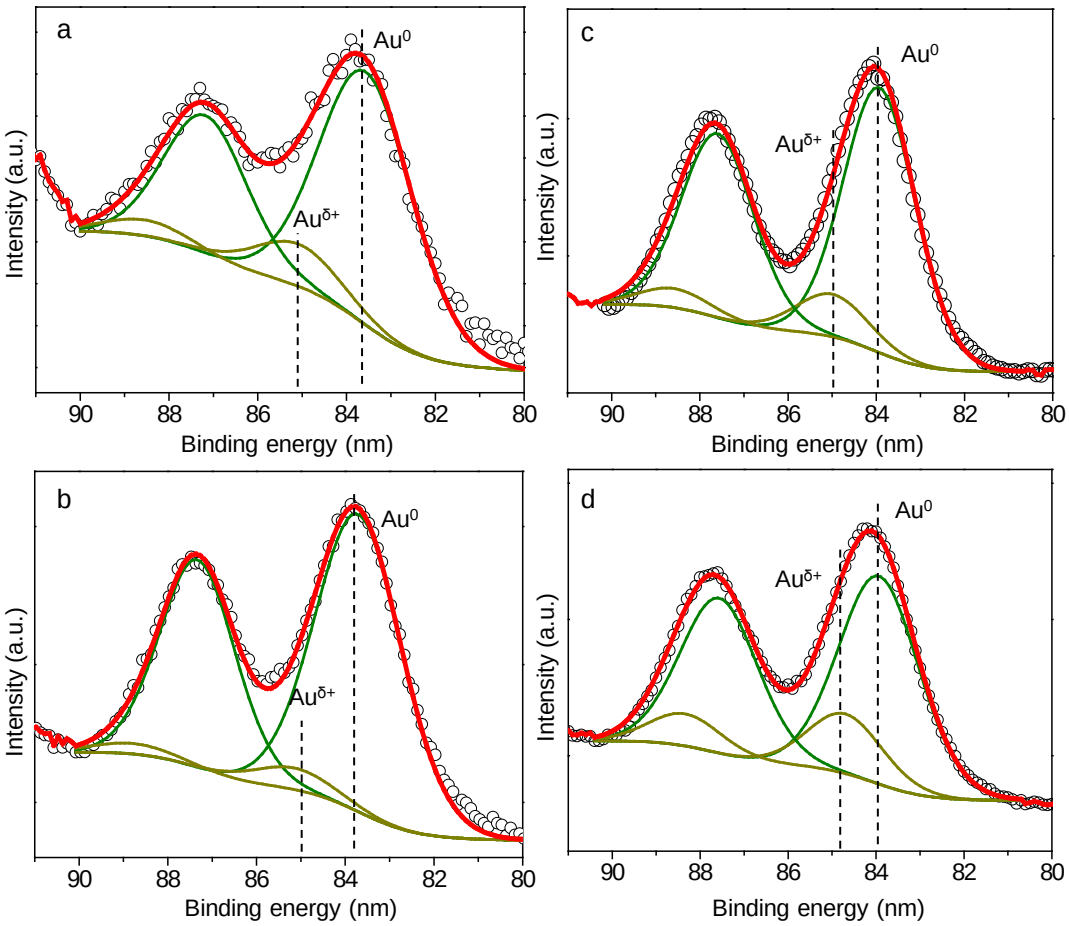

Figure 6. Spectre Au 4f XPS des catalyseurs à l'or avant et après la réaction d'oxydation du CO.

(a-b) échantillon Au/SS5-C frais et vieilli, (c-d) Au/SS5@Cu-C frais et vieilli. Les ronds illustrent le spectre initial et les lignes continues la dé-sommation.

L'étude par XPS des échantillons frais et vieillis donne de précieuses informations. La phase majoritaire pour cette série d'échantillons présente en surface un état métallique (Au^0), une petite portion est oxydée ($Au^{\delta+}$) comme on peut le voir sur la Figure 6. De façon différente à l'échantillon Au/SS5-C, tous les échantillons Au/SS5@M-C avec des ajouts métalliques

contiennent en moyenne 2 fois plus d'espèce $Au^{\delta+}$ après réaction qu'avant. Ceci est interprété par le fait que les nanoparticules d'or sont fixées au support et lié par l'oxygène agissant comme une "glue". L'interaction entre l'or et le support est augmentée. D'un autre côte, l'ajout métallique change également partiellement le degré d'oxydation de l'or.

La microscopie à transmission MET sur l'échantillon Au/SS5@Cu-C frais et vieilli montre que des nanoparticules d'or pur, Cu_2O pure et des agrégats coexistent à la surface des sphères de silice. Cependant les particules sont modifiées pendant la réaction d'oxydation du CO. La taille moyenne des particules diminue de 5.3 nm (frais) à 4.8 nm après la réaction (Figure 7). En combinant les résultats XPS avec ceux du MET, il apparait que les nanoparticules d'or sont entourées de fragment de Cu_2O dans l'échantillon frais. Ces particules ne changent pas de taille significativement après la réaction, modifiant seulement leur environnement moins chargé en Cu_2O.

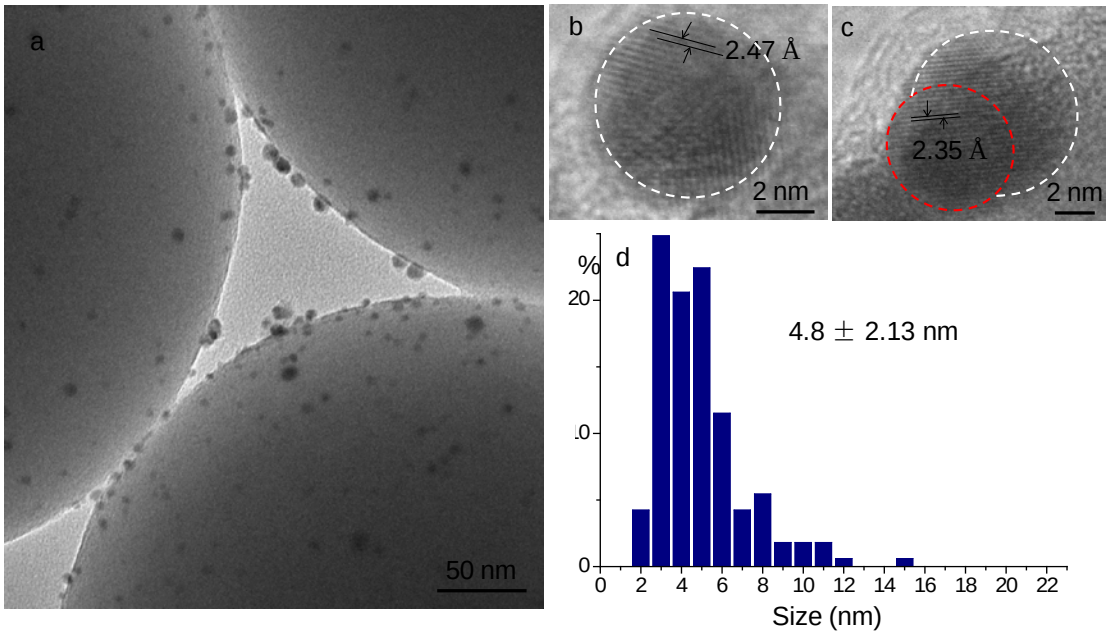

Figure 7. MET de l'échantillon frais Au/SS5@Cu-C (a-c) Images (d) distribution en taille obtenue après l'examen de 200 particules.

Durant le test, l'espèce Cu_2O se détache des particules d'or et une petite part se transforme

en CuO qui est conservée à l'interface Au-Silice. Cette espèce facilite l'encrage et la conservation des nanoparticules d'or à la surface des sphères de silice. Par ce biais, les espèces actives d'oxygène peuvent être remplacées par les lacunes des oxydes métalliques comme le montre les résultats obtenus par XPS. L'adition d'un second métal aide à la fois les nanoparticules d'or à être fixées au support et augmente significativement l'interface entre l'or et la silice. Cette interaction Au-support a été trouvée comme étant un point aussi important de l'activité de ces systèmes à base d'or que les effets de taille. La méthode choisie permet d'identifier de façon claire les paramètres de taille par rapport aux paramètres d'interaction Métal-support car ces paramètres sont contrôlés par la méthode colloïdale. Elle a donc permis de séparer les effets de taille de ceux d'interface de façon explicite. De plus, la structure particulière des sphères de silice Stöber non poreuses contribue également à la dispersion des nanoparticules métallique. Elle se distingue des supports classiques mésoporeux et peut être considérée comme un support nouveau et approprié dans le cadre des catalyseurs à base d'or.

4.2 Nouvelle application pour les catalyseurs à base d'or? - Au/SS5-C et Au/SS5@Cu-C pour l'oxydation sélective de H_2S

En prenant en compte les régulations très strictes des émissions de SO_x, le sulfure d'hydrogène (H_2S) contenu dans les gaz acides doit être spécifiquement piégé/détruit pour ne pas être libéré dans l'atmosphère. La technologie la plus usitée pour retirer l' H_2S est le procédé industriel bien connu: le procédé Claus. Cependant, en raison des limitations thermodynamiques, 3 à 5% du H_2S ne sont pas convertis en soufre. Dans des conditions catalytiques, l'oxydation sélective de H_2S peut être conduite dans la gamme de température de 210- 240 ^oC en une seule étape. C'est un fait admis que les catalyseurs à l'or présentent une activité fortement réduite si une petite quantité de H_2S ou de produits soufrés est présente dans le mélange gazeux en raison de leur forte affinité. L'effet d'empoissonnement des nanoparticules d'or est du à l'adsorption forte de certains produits sur les sites actifs et par là-même l'inhibition de l'adsorption des réactants que l'on désire transformer. On peut également

observer que les poisons peuvent changer la structure de l'échantillon, par exemple en favorisant l'agrégation des particules. Le travail présenté dans cette partie cherche à évaluer l'affinité des particules d'or pour des composés soufrés (H_2S et SO_2) malgré ces réserves. On peut également envisage l'affinité élevée de l'or avec les produits soufrés comme un avantage. Il y a des chances qu'il puisse exister un état d'activation compatible avec les autres étapes de la réaction : adsorption et dissociation, transformation sélective en soufre et régénération des sites actifs. Alors dans ce cas, il pourrait s'avérer que les catalyseurs à base d'or soient actifs pour cette réaction comme le sont un certain nombre de sulfures.

Les échantillons Au/SS5-C et Au/SS5@Cu-C ont été testés pour l'oxydation sélective de H_2S et leurs résultats sont présentés sur la Figure 8.

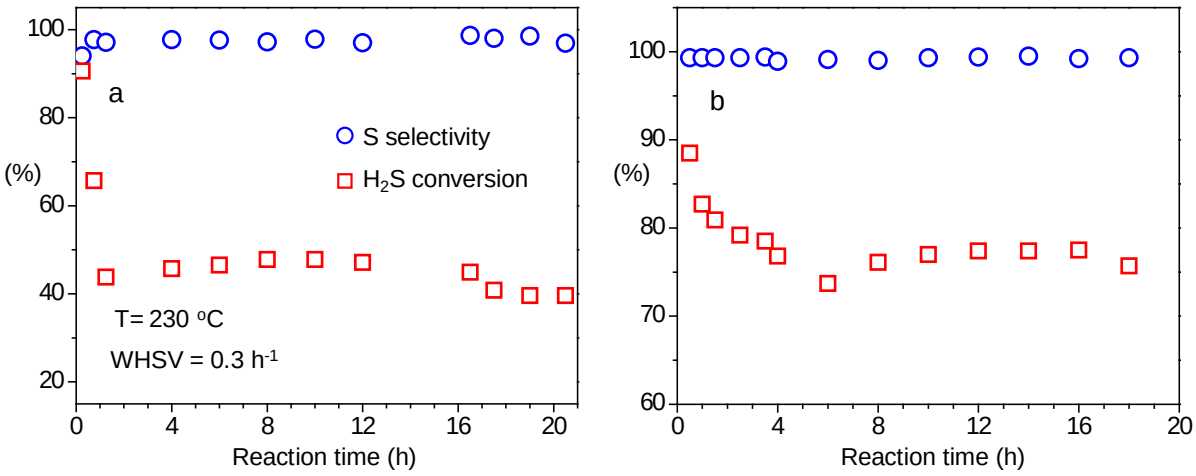

Figure 8. Performances (conversion et sélectivité) de 100 mg Au/SS5-C (a) et Au/SS5@Cu-C (b) dilués dans 200 mg de SiC en fonction du temps pour l'oxydation sélective de H_2S en Soufre à la température de 230 °C (conditions expérimentales)

Les deux échantillons Au/SS5-C et Au/SS5@Cu-C présentent une excellente sélectivité pour la formation de S à partir de H_2S. Si la silice seule possède une très faible activité/sélectivité pour cette réaction de Claus comme rapporté dans la littérature, la sélectivité très élevée (95%-98%) observée dans ce cas doit être attribuer aux nanoparticules d'or. La conversion de H_2S sur Au/SS5-C n'est pas aussi élevée que celle obtenue avec

Au/SS5@Cu-C. En revenant à un débit horaire de 0.15 h^{-1} à 0.6 h^{-1}, la conversion H_2S obtenue plus basse indique que l'échantillon Au/SS5-C a évolué et que cet échantillon n'est pas stable dans les conditions de réaction. Au contraire, le comportement de l'échantillon Au/SS5@Cu-C montre une conversion de H_2S et une sélectivité en soufre très stable dans le temps. Les images obtenues par MET et présentées dans la Figure 9 confirment que les nanoparticules d'or de l'échantillon Au/SS5-C s'agrègent durant le test; la taille moyenne des particules passant de 5.5 nm à 9.2 nm.

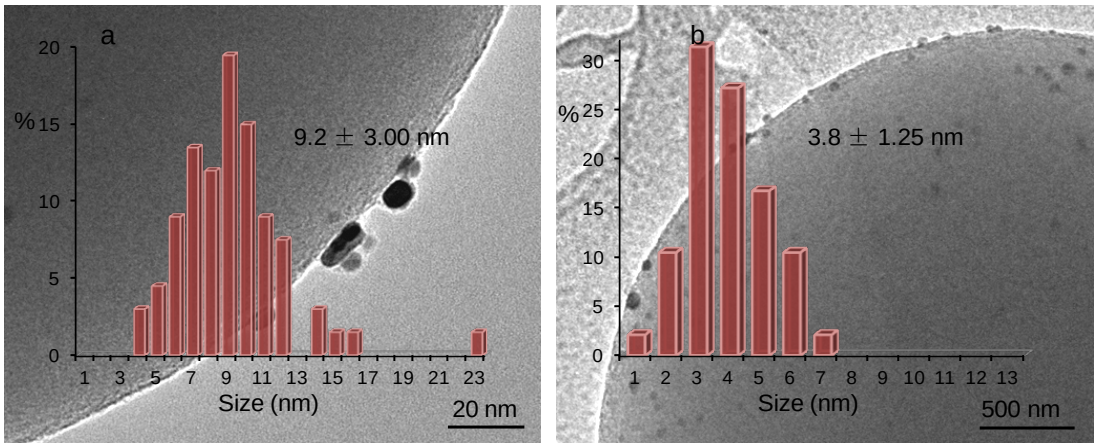

Figure 9. images MET et distribution des particules d'or des systèmes Au/SS5-C et Au/SS5@Cu-C après le test d'oxydation sélective de H_2S.

Dans le cas de l'échantillon Au/SS5@Cu-C, il est surprenant de constater que la taille moyenne des particules décroît à 3.8 nm, valeur bien plus petite que pour l'échantillon frais. Les images MET obtenues en haute résolution sur l'échantillon testé Au/SS5@Cu-C illustrent également la formation d'un nouveau composant, à savoir l'alliage AuCu qui a du se produire sous le mélange réactionnel H_2S et O_2. Cet alliage peut jouer un rôle redox dans la catalyse et faciliter la réorganisation de la structure des particules Au et Cu_2O que l'on trouvait au contact l'une de l'autre avant test.

Les résultats Au 4f obtenus par XPS sur les catalyseurs usés prouvent l'existence d'or Au^{3+} qui peut être reliée aux espèce sulfures et/ou sulfates dans le cas de l'échantillon Au/SS5-C

(Figure 10). Les pics O 1s XPS suggèrent également la formation d'espèces sulfates pour Au/SS5-C qui laisse présager d'une adsorption irréversible de H_2S et permet d'expliquer la diminution observée de l'activité avec le temps. Au contraire, l'échantillon Au/SS5@Cu-C s'avère beaucoup plus stable et présente aucun changement pendant le test et aucune évolution des spectres XPS.

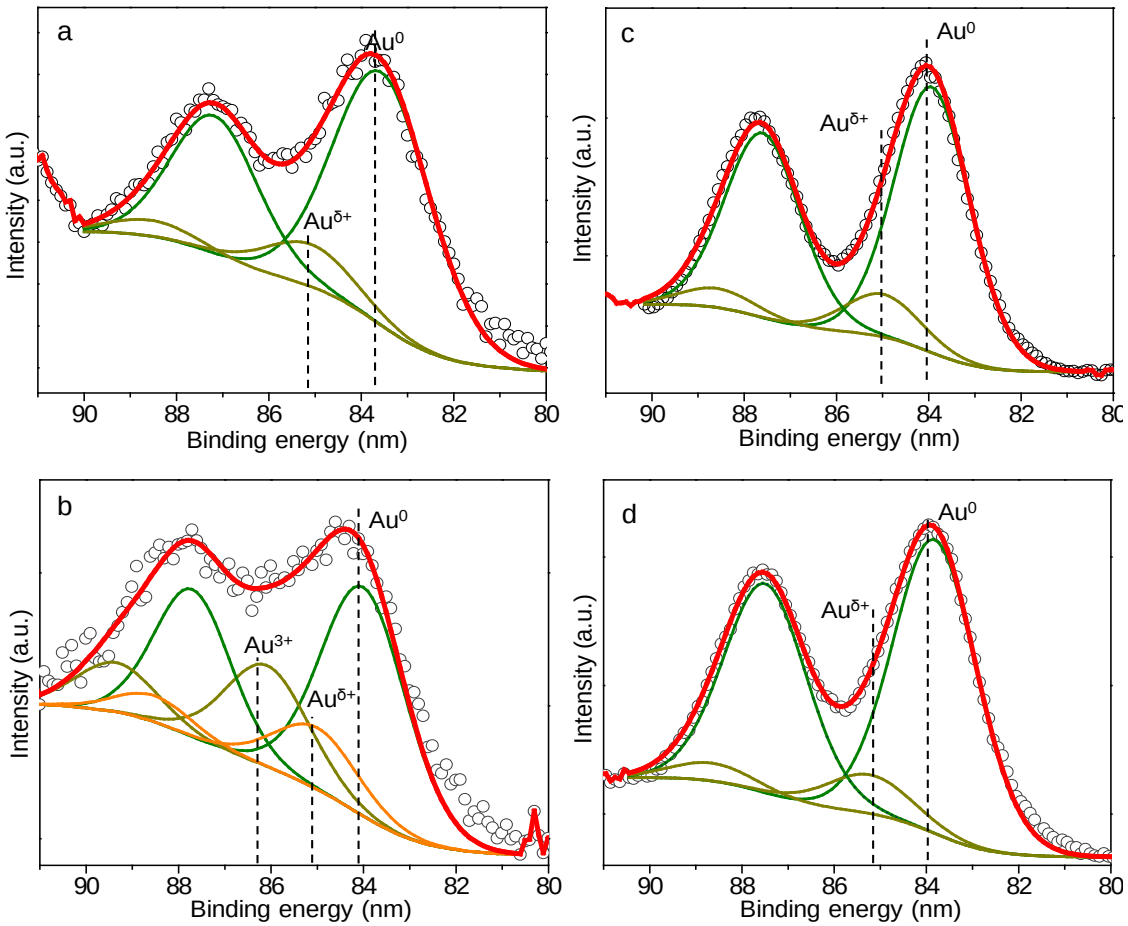

Figure 10. Spectres Au 4f XPS de Au/SS5-C et Au/SS5@Cu-C: (a-b) échantillon frais et usé Au/SS5-C, (c-d) échantillon frais et usé Au/SS5@Cu-C avant et après le test d'oxydation de H_2S. Les ronds sont les données initiales, et les lignes les courbes de dé-sommation et la courbe somme.

Dans ce travail, l'oxydation sélective de H_2S en S a été testée sur les particules d'or déposées sur des sphères de silice Stöber, avec ou sans addition de cuivre. L'addition de Cu élimine l'empoissonnement partiel de l'or par les sulfates et rend le catalyseur stable sur un

temps raisonnablement long dans cette réaction. La silice Stöber s'avère être un support adéquat pour les nanoparticules d'or préparées par voie colloïdale. La supériorité de ce support réside dans le fait que les sphères étant non poreuses, elles permettent à la fois de disperser les nanoparticules et d'optimiser le contact du gaz avec les sites actifs. Ceci limite la pression de surface et le transfert thermique et facilite le départ du soufre à l'état vapeur , ce qui explique à nouveau son intérêt pour cette réaction particulière. Ce travail semble également indiquer que les nanoparticules d'or supportées peuvent être intéressantes pour des réactions catalysées ou non, contenant du soufre ou des produit soufrés en raison de leur résistance potentielle au soufre qui n'agit pas sur elles comme poison.

5. Perspectives

Le travail présenté dans cette thèse est principalement axé sur un nouveau matériau constitué de nanoparticules d'or sur des sphères de silice Stöber, nanoparticules préparées par voie colloïdale. Nous avons essayé de montrer leur potentialité pour des applications catalytiques avec et sans modification. Par l'étude de ces matériaux, la croissance et l'évolution des nanoparticules, leur rôle pendant une réaction catalytique et l'évaluation dans de nouvelles applications sont aisés à comprendre et à évaluer. En se basant sur le travail fait, on peut citer différentes perspectives qui peuvent se résumer comme suit.

En étudiant la couleur de l'échantillon pour des supports blancs, les pics de résonance plasmonique par UV-vis et les résultats de diffusion des particules par dépôt sur un gel de silice «décrit et nommé en anglais: the home-made liquid diffusion test», la morphologie of nanoparticules d'or de la solution colloïdale peut être utilement estimé et confirmé par une étude par MEB ou MET éventuellement. Ce couplage de méthodes simples devrait favoriser la baisse des coûts des études et être un guide pour débuter les études des colloïdes d'or mais aussi d'argent et de cuivre en raison des propriétés plasmoniques communes.

Le procédé de dépôt développé de la solution colloïdale contenant des nanoparticules d'or

calibrées sur des sphères de silice Stöber, sans usage d'agent de couplage, limite le risque d'un empoisonnement des nanoparticules d'or. Cet aspect ouvre des perspectives pour les systèmes Au/Stöber-silice à partir de solutions colloïdales pour des applications en catalyse hétérogène.

La structure de la silice Stöber non poreuse est une structure avantageuse pour disperser des nanoparticules et augmenter l'activité d'or mais également pour d'autres métaux nobles. Les silices mésoporeuses ne sont plus les seules silices potentielles pour la dispersion et le confinement des nanoparticules d'or.

Au vu de la capacité du système Au-silice Stöber (avec l'addition d'un co-métal comme le cuivre) à être insensible au soufre, les applications des catalyseurs d'or peuvent s'élargir, y compris pour les systèmes préparés par l'ajout de stabilisants tels que les thiols. On peut espérer que les nanoparticules d'or ont des potentialités pour des besoins très importants et traités par la catalyse hétérogène.

Chapter I General Introduction

1.1 The initial and current background of gold research

During the past thousands of years, gold was always viewed as one of the most stable metals. The bulk metallic gold is inert and possesses the golden luster. This specific property of gold together with high malleability made gold as the specialized material for coin, jewelry, and artifact. Besides, gold material can also be applied in medical science such as cancer treatment and dental operation. However, the gold material utilized in catalysis field was neglected for such long time. In fact, gold compounds in chemistry used field were concerned since last century and became more and more vivid.[1] Haruta et al. suggested that when the gold was supported onto metal/nonmetal carriers as nanoparticles, the chemical properties of gold became definitely distinctive to the bulk metallic gold. Applying the supported gold nanoparticles for CO oxidation, excellent reaction activity was found by reducing the reaction temperature to room temperature or even lower. The period for nano-scale gold used as indispensible catalyst material was thus came into the world.[2, 3] Gold species as the active species for catalysts is now widely applied to various catalytic reactions, which include oxidation of alcohol and aldehyde, propylene epoxidation, acetylene hydrochlorination, and formation of carbon-carbon bonds.[4, 5] It is no doubt that the investigations over supported nano-scale gold catalyst are receiving more and more attention. For one appropriate target reaction, using nano-scale gold material as catalyst, it may help enhance the selectivity and yield of target production under the same operation conditions, or largely reduce the reaction temperature and catalyst amount at the same yield. No matter how, it lowers the cost, saves energy and lays great importance for the industrial procedure. Investigation over gold catalysts can be shown by the exponential growth of publications during recent years (1994-2012) by searching the subject ‘gold catalysis’ as shown in Figure 1.1.

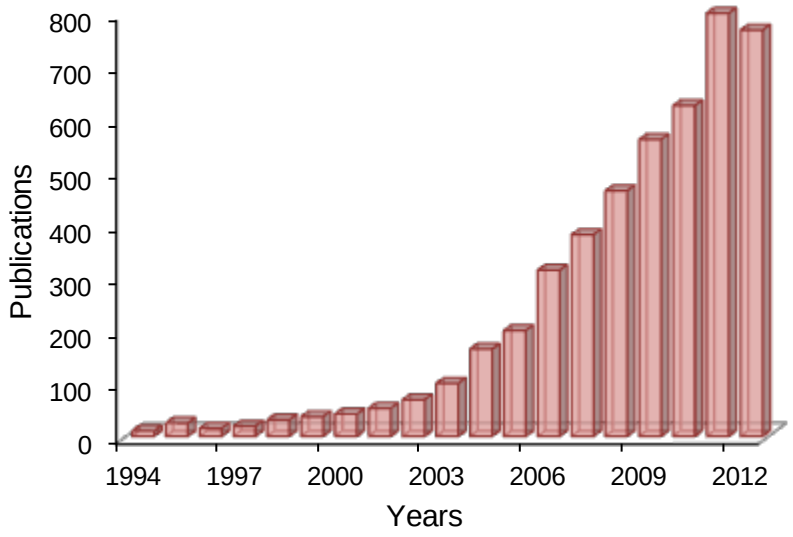

Figure 1.1 Publications from 1994 to 2012 with the subject ‘gold catalysis’.

1.2 Catalysts based on gold nanoparticles

1.2.1 Preparation of gold nanoparticles

√ Impregnation method (IM)

The gold precursor solution- $HAuCl_4$ solution is added into the carrier powder. After stirring, the solution is aged for the absorption of the active species onto the surface and into the pores of support. The catalyst can then be obtained by washing, filtration, drying and calcination. The impregnation method includes incipient wetness impregnation and isometric impregnation. The previous method is also called excessive solution impregnation, by which excessive amount of gold precursor solution is used to prepare the catalyst. Whilst during the isometric impregnation method, the solution of nitrate salt used for impregnation is required to be totally entered into inner pores of support to make the support precisely saturated with the solution. Sometimes, the isometric impregnation method cannot be operated very precisely. The BET tests can help the operator preliminarily understand the porosity parameters of the supports, and the synthesis process can be carried out more accurately. The impregnation method is one of the

earliest preparation methods for synthesizing gold catalyst.[6] This method is still used for the current production of gold catalysts due to its facile process and low price. However, the residual Cl^- that is somewhat difficult to be totally washed results in the formation of larger gold aggregations; besides, for the gold catalysts prepared by incipient wetness impregnation method, since the excessive amount of solution is applied, the gold species cannot totally absorbed into the pores of carrier leading to the less loading amount of gold than the theoretical amount. Herein there are plenty of investigation focusing on how to improve the operation conditions of the impregnation method, including using the $Au(PPh_3)(NO_3)$ as the gold precursor and remove the Cl^- under protection of gaseous ammonia.[7, 8]

√ Deposition-precipitation method (DP)

In the DP method, the gold precursor is mixed with the carrier. The precipitator is added into the mixture under stirring until the pH is appropriate for the formation of required gold nanoparticles (e.g. pH = 9~11, depending on the properties of supports). Thus after filtration, wash, drying and calcination procedures the catalysts can be synthesized. The reported precipitators generally used include ammonia, Na_2CO_3, and $NaHCO_3$ solutions, etc. Xu et al.[9] prepared MgO-doped nanoscale gold catalysts by using the DP method and studied the influences of precipitator on the particles size distribution and the activity for CO oxidation. The results turned out that Na_2CO_3 solution was helpful for the formation of gold catalyst possessing smaller nanoparticles performing much better activity for CO oxidation. However, the catalytic activity of gold catalysts from DP method largely depends on the isoelectric point (IEP). The DP method is very efficient for obtaining and dispersive gold nanoparticles (Au-NPs) on the surface of supports such as TiO_2 (IEP = 6), CeO_2 (IEP = 6.75) and FeO_x (IEP = 6.5-6.9).[10, 11] Well this method does not favorable the very acidic supports such as SiO_2 and heteropolyacid (IEP = 1-2); and also the very basic MgO (IEP = 12) that makes the $AuCl_4^-$ rapidly change into $Au(OH)_3$ deposited in the aqueous solution and losses most of the gold source.

√ Direct anionic exchange (DAE)

The direct anionic exchange (DAE) method was for the first time put forward by our lab.[11-14] The aqueous solution of $HAuCl_4$ is added into the baker with support. The above solution is heated to 70 ^oC for 1 h. The sample powder can be obtained by washed with ammonia (ammonia is advocated for the high dispersion of gold nanoparticles), filtered, dried at 120 ^oC overnight, and calcined in air at 300 ^oC for 4 h. The direct anionic exchange, namely, is to exchange the gold species with the hydroxide species in the support. Ivanova et al.[11] investigated the impacts of the concentration of the $HAuCl_4$ solution. They found out that the gold species $Au(OH_n)Cl_{4-n}^-$ changed along with the concentration of gold source. The best condition of solution for the exchange to get a bidendate ligand is with pH around 4-5. The Au/Al_2O_3 prepared by the DAE method possessed better activity for CO oxidation than the traditional DP method prepared Au/Al_2O_3 sample. This method can also be widely applied for various of supports with IEP ≥ 2 (to make the exchange of Cl^- to OH^- available) at pH ≤ 8-9 (to eliminate the formation of $Au(OH)_3$ deposition).

Table 1.1 Reported preparation methods for gold catalysts.

Preparation	Typical catalyst	Referen	Comments
Impregnation (IM)	TiO_2, C, etc	[15, 16]	Low dispersion & loading of
Deposition-Precipitation (DP)	TiO_2, CeO_2, ZrO_2, etc.	[17, 18]	Fit for carriers with IEP of 5-8
Co-precipitation (CP)	CeO_2-M_2O_3, etc.	[19]	
Chemical Vapor Deposition (CVD)	Al_2O_3, etc.	[20]	Volatile organic Au precursor
Direct anionic exchange (DAE)	Al_2O_3, Nb_2O_5, TiO_2, ZrO_2,	[11, 13, 21]	Support IEP≥ 2, at pH ≤ 8-9
Liquid Grafting	Au/Fe_2O_3, etc.	[22]	Not fit for high Au loading.
Cation Exchange	Au/Y-type zeolite, etc.	[23]	Irreversible deactivation
Photochemical Deposition	TiO_2, etc.	[24]	Activity is modest
Sol-gel	γ-Al_2O_3/MgO-Al_2O_3, etc.	[25]	Organic metal precursor
Magnetron sputtering	WO_3, C, etc.	[26]	Special apparatus is in need

The above three methods are the earliest methods for synthesizing supported Au-NPs,

which are now still widely utilized (sometimes with modifications) in the catalysis field. Of cause there are many other methods for obtaining much finer supported Au-NPs with better size distribution. The most popular methods are listed in Table 1.1.

In general, researchers suggested series methods for synthesizing supported Au-NPs to cater to both the commercial and industrial demands. However, obtaining Au-NPs with satisfied size distribution for target reactions is still a main research objective. Herein, we would like to introduce a preparation method for synthesizing Au-NPs that is fashionable in the material science recently.

√ Preparation methods for colloidal gold nanoparticles

The synthesis of colloidal Au-NPs becomes a fashion in the field of material due to its special chemical, optical, and photoelectric properties. The investigators in the field of catalysis are also trying to focus on the colloidal Au-NPs as precursor for gold catalysts in the consideration of their reasonable advantages. By using the gold colloid as precursor, the Au-NPs can be obtained before supported onto carriers. This is a very importance parameter of gold catalyst for some structure sensitive reactions such as CO oxidation. The interaction between gold and support can also be understood more detailed. Besides, it is also a worthy note that the optical of gold colloids- especially the color change, is really interesting and can be utilized during the synthesis of colloidal Au-NPs for understanding the process. The detail is elaborated in the later 1.3.2 part. Here we would like to introduce the synthesis methods of gold colloid that are most commonly used in the publications. The colloidal Au-NPs can be made by reduction of gold source (e.g. $HAuCl_4$) with a strong reduce agent under protection of organic compound. The organic compound as protect agent is added before the addition of reduce agent to obtain the demanded size of gold nanoparticles. The most two famous and widely used agents for reducing the gold source are the sodium citrate and the sodium borohydride ($NaBH_4$).

☺ Reduction of $HAuCl_4$ with sodium citrate

For the using of sodium citrate, a certain amount of gold precursor (e.g. $HAuCl_4$ aqueous solution) is added to the beaker and heated to reflux with vigorous stirring. The sodium citrate is rapidly added into the above solution. The solution is then boiled for a while to get a stable gold colloid solution. By this method, gold colloid about 10-20 nm[27, 28] or even larger particles (80-160 nm)[29] can be prepared according to the variation of the pH value, the concentration of sodium salt and chloroauric acid, the addition of other protect agents such as gelatin, bis (psulfonatophenyl) phenylphosphine dihydrate dipotassium (BSPP), 4-carboxythiophenol (4-CTP), etc[30-32].

☺ Reduction of $HAuCl_4$ with sodium borohydride

The method using $NaBH_4$ as reduce agent is generally operated under room temperature. The gold precursor and the protect agent are mixed under stirring for several minutes. The certain amount of $NaBH_4$ solution is then quickly added into the solution. The color variation of the solution indicates the successful formation of gold colloid. The $NaBH_4$ solution possesses strong reducibility, and however not very stable, which should be freshly prepared for using. Zhang et al.[33] applied the apoferritin compound as protect agent and synthesized the Au-NPs under reduction of $NaBH_4$. The gold colloid with average particle size of 3.6 nm was obtained. The Cetylpyridinium chloride(CPC) was applied as the protect agent by Ghosh et al.[34] to get the gold colloid with 3-10 nm Au-NPs. The poly (amidoamine) dendrimer (PAMAM) was proved to be very effective to synthesize gold colloid with very small and homogeneous Au-NPs when it was used as protect agent. However, this compound was really expensive and made the cost of preparation quite huge.[35] Some other compounds such as C_{16}/C_8 Xanthate[36], 4-carboxythiophenol (4-CTP),[37] and cetylpyridinium chloride (CPC)[34] can also be applied as the protect agent for stabilizing colloidal Au-NPs. By using the $NaBH_4$ as reduce agent comparing to the sodium citrate, the gold colloid with smaller nanoparticles can be made by choosing the appropriate protect agent in general.

☺ Other agents for the reduction and protection of gold colloid

There are also some agents can be applied both as the protect agents and reduce agents. The quaternary ammonium-based room-temperature ionic liquids (QAILs) is one of the agents for successfully prepared 20-40 nm colloidal Au-NPs with good stability and reproducibility.[38] Sun et al.[39] prepared the 10-20 m nm colloidal Au-NPs using branched polyethylenimine (BPEI). The N-(2-Aminoethyl-3-aminopropyl) trimethoxy silane (DIAMO) was also applied as both the protect agent and reduce agent for preparing 13-20 nm colloidal Au-NPs.[40] There are some special techniques facilitating the preparation of gold colloids.[41, 42]

However, to prepare gold colloid with small and homogeneous Au-NPs with simple and low cost agents under reduction of $NaBH_4$ is still a current challenge until now.

1.2.2 Supports for gold nanoparticles

The large amounts of publications demonstrated that the activities of supported gold catalysts are much higher than the unsupported gold catalysts.[43] It is found out that the Au $4f_{7/2}$ binding energy from XPS spectra of unsupported and supported Au-NPs are different even when the average particle size is similar. Some investigators ascribed this phenomenon to the gold-support interaction. In fact, the supporting process may change the chemical state of gold nanoparticles. In this case, the appearance of the XPS peak of $Au^{\delta+}$ ($0<\delta<3$) and/or Au^{3+} could make the overlapped peaks of Au^0 and oxidative Au species to shift to higher binding energy comparing to the unsupported neutral Au-NPs. The synergistic effect between gold and support will largely enhance the Au-support interaction, the redox properties, and the catalytic reactivity of gold catalysts. The application of support is also a key role for dispersing Au-NPs, making the Au-NPs more stable. Generally speaking, the physical and chemical properties of supports are one of the factors essentially impacting the catalytic activity of the Au-NPs. The supports used for Au-NPs in research can be divided into two groups according to whether it is reducible or not, in most cases. The first group is the supports

that largely enhance the catalytic activity of gold catalysts. These supports include the Fe_2O_3, CeO_2, TiO_2 (TiO_2 is a special case with poor reducibility but it is excellent support for Au-NPs for many reactions), etc, most of which are reducible and may perform catalytic activities on their own. Another group is called the inert support for gold catalysts including SiO_2, MgO, Al_2O_3, ZrO_2, etc, which is impossible to transfer the oxygen species from the supports to gold impossible. It is generally considered that the Au-NPs loading on reducible supports are generally more efficient than those supported on the inert ones.[44] But there also exist exceptions. In the investigation of Rossignol et al,[45] it was found out that the inert supports (Al_2O_3 and ZrO_2) possessed the activity as good as Au/TiO_2 for CO conversion in the preferential oxidation (PROX) of CO under H_2. A further study of this group suggested that the presence of H_2 changed the mechanism of CO oxidation.[46] The reaction mechanism evolved the H*, OH* and OOH* intermediates.[47] The CO oxidation rate was largely promoted before the hydrogen oxidation.

1.3 Surface Plasmon Resonance effect of gold nanoparticles

Gold colloids have received considerable attention recently in research because of their renowned optical properties.[48] It shows different Surface Plasmon Resonance (SPR) absorption by different dispersion states, which is reflected by the color change of the colloid solution.[49]

1.3.1 Surface Plasmon Resonance

Surface plasmon (SP) is a kind of electromagnetic wave that transmitted parallel along with the contact surface of metal/dielectric.[50] Since the wave occurred on the boundary of the metal and medium solvent, great changes can be provided by even slightly modify on the surface. Surface plasmon resonance (SPR) is the frequency upon which the conductive electrons in the solid resonantly and collectively oscillated after excited by the incident light. The resonance will occur only if the frequency of the incident light photons is consistent with that of the

oscillation of electrons against the restoring force of positive nucleus. For the nano-scale particles dispersed in medium solution, the condition is different.

In the gold colloid, unlike the surface between planar metal and medium solvent, the radius of Au-NPs is much smaller than the wavelength of incident light.[51] In this case, the oscillation is locally around the nanoparticles, which is called localized surface plasmon resonance (LSPR)[52, 53]. The incoming radiation induces formation of a dipole in the nanoparticle of the colloid (the mechanism as shown in the mechanism of Figure 1.2). For a complementary, the restoring force is formed in the positive nucleus part. The electrons resonant oscillating under incident light will display enhanced near-field aptitude at the resonant wavelength, whilst largely reduced at the surface of nanoparticles/dielectric and medium solution.[54] LSPRs are basic fundamental for many application and optical phenomenon of colloidal nanoparticles.[55] Materials as gold, copper, silver, and alkai metals having free electrons possess such properties, depending only on the shape, size, and medium solution.[56] From this point of aspect, gold colloids with different size and shapes of particles should display regulation about the color and surface plasmon bond observed by UV-vis that can be followed. For the non-spherical gold, gold nanoparticles on carriers, gold concerned core-shell structure, the situation is different and more complex.

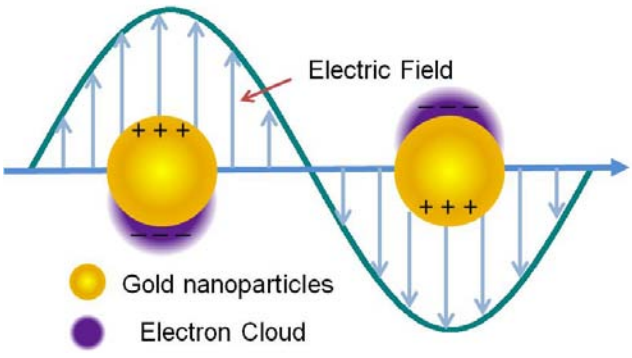

Figure 1.2 Scheme of localized surface plasmon resonance (LSPR) of gold nanoparticles in gold colloid (according to ref.[57]).

1.3.2 SPR effect revealed by UV-vis

1.3.2.1 SPR effect of spherical and anisotropic gold nanocrystals

√ Plasmon resonance peaks of spherical gold nanoparticles

UV-visible (UV-vis) is an efficient technique to capture the SPRs of colloidal Au-NPs. Spherical colloidal Au-NPs display one surface plasmon resonance bond at around 520 nm in general.[58] Of cause, this bond changes in detail along with the shape, the size and the medium solvent of the colloid.

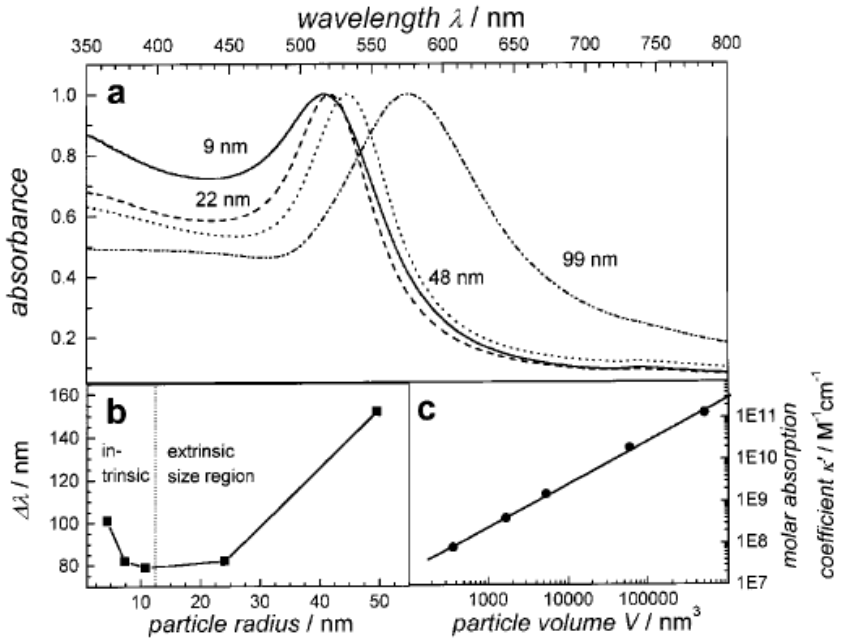

Figure 1.3 Size effects on the surface plasmon absorption of spherical gold nanoparticles. The UV-vis absorption spectra of colloidal solutions of gold nanoparticles with diameters varying between 9 and 99 nm show that the absorption maximum red-shifts with increasing particle size in part a, while the plasmon bondwidth follows the behavior illustrated in part b. The bondwidth increases with decreasing nanoparticle radius in the intrinsic size region and also with increasing radius in the extrinsic size region as predicted by theory. In part c the extinction coefficients of these gold nanoparticles at their respective plasmon absorption maxima are

plotted against their volume on a double logarithmic scale.[59]

The variation of surface plasmon effect also possesses the size effect, e.g., the growing up of the gold aggregations made the distances between each particle differs, thus the surface plasmon effect will be changed, which is reflected by the red/blue-shift of the surface plasmon absorbance location revealed from the UV-vis spectra. A systemic investigation has been taken out by Link and El-Sayed.[59] In fact, they didn't find a continuous red-shift or blue-shift of the absorbance peak along with the increasing of the gold nanoparticles. As shown in Figure 1.3, it can be seen that for smaller size in the region of quasi-static limit, the peak blue-shifted and becomes wider with the decreasing particle size of Au colloid due to the intrinsic size effect. While for the larger particles (> 25 nm), the plasmon bondwidth increases with the particle size further growing.

√ Plasmon resonance peaks of anisotropic gold nanocrystals

Not only the nanoparticle sizes, but also the shapes of the gold particles greatly impact the surface plasmon resonance effect.

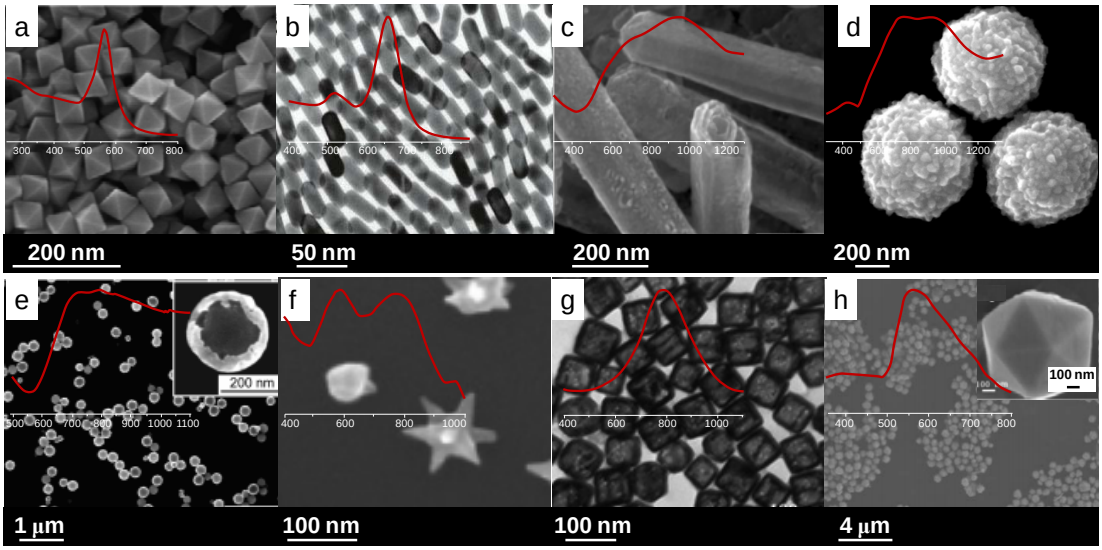

Figure 1.4 Other kinds of gold nanocrystals with different shapes and optical properties: (a) gold nanooctahedras, (b) gold nanorods, (c) gold multiple-walled nanotubes, (d) gold

nanomeatballs, (e) gold nanobowls, (f) gold nanostars, (g) gold nanocages, and (h) gold nanoicosahedras. The inset red lines display the UV-vis spectra of the corresponding gold nanocrystals, in which the x-axes and y-axes are wavelength (in nm) and adsorption (a.u.), respectively. The TEM and SEM images are adapted from ref.[60-67]

General for the spherical gold nanoparticles, there is a surface plasmon resonance bond around 520 nm that typically characterizing the existence of Au-NPs. While if the Au-NPs size is too smaller, for example, only several nanometer, such bond might shift to a much lower wavelength with weak intensity.[68] In the current investigation, novel Au-NPs with non-spherical shapes have been prepared, including gold nanorods, nanooctahedras, nanotubes, nanomeatballs, nanobowls, nanostars, and nanocages.[69, 70] All of them display particular resonance peaks according to the surface plasmon resonance effect as shown in Figure 1.4. Taking the gold nanorods for instance, two resonance peals can be observed- one at about 520 nm due to the transversal modes of gold nanorods, the other at about 600-700 nm or even higher wavelength attributed to the longitudinal modes of gold nanorods.

1.3.2.2 Effect of the presence of support and solvent

When the Au-NPs are evolved in the core-shell structure, the surface plasmon resonance effect will be largely modified as well as the UV-vis spectra. Hirsch et al.[71] made the investigation on metal nanoshells with silica as the core. When the Au-NPs with different sizes (5, 7, 10, and 20 nm) were coated on the 60 nm silica core to form the SiO_2@Au core-shell structure, the UV-vis spectra of particles red shifted with decreasing thickness of the gold shell. Ravindranath et al.[72] synthesized the Ag@Au core-shell structure and tested the material by UV-vis spectra. It was turned out (Figure 1.5) that the Ag@Au material displayed one broad UV adsorption peak at around 600 nm, which differed from either the pure Ag-NPs or the Au-NPs. Comparing to the Au-NPs, the peak of Ag@Au largely red shifted. The surface plasmon resonance effect of Au-NPs can be easily changed by the variation of surrounding environment.

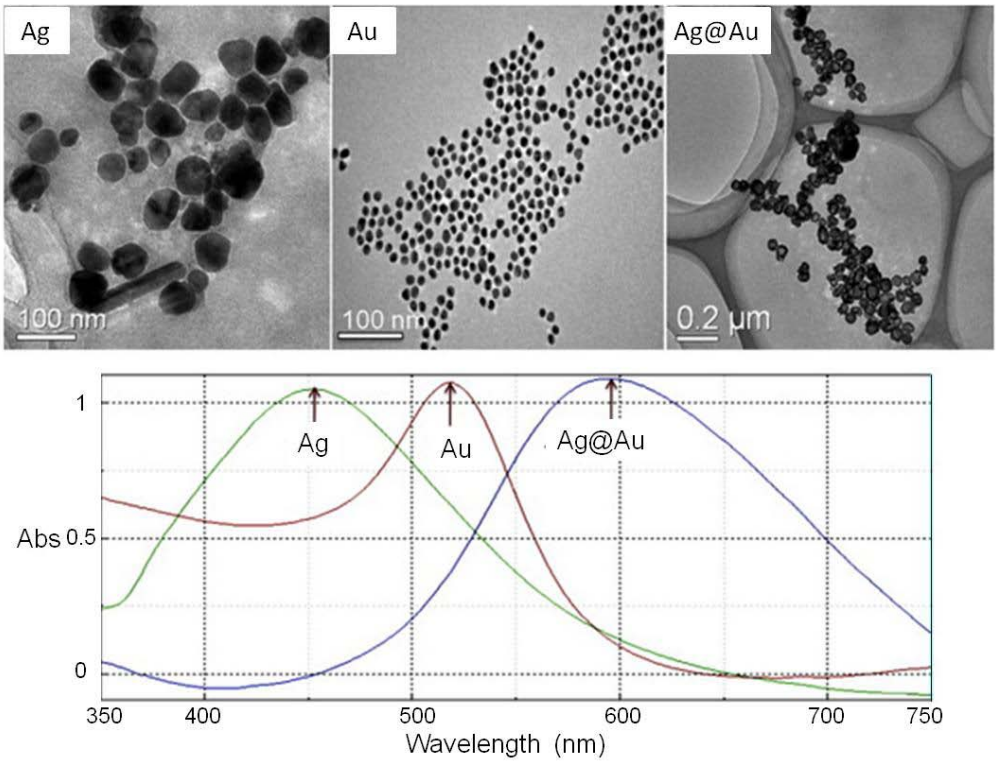

Figure 1.5 Characterization of nanoparticles: TEM images of synthesized silver (a), gold (b) and Ag-Au core-shell nanoparticles (c) UV-visible absorbance spectrographs displaying their characteristic plasmon peaks.[72]

Besides, the Au-NPs supporting onto carriers also changes the location of the UV-vis spectra. Fang et al.[73] studied the optical properties of Au/TiO_2 samples with different loading of gold by the UV-vis spectra. It was found that the location of adsorption peak for supported gold nanoparticles blue-shifts along with the rising of gold loading, although the particles sizes in all the samples were around 3-4 nm. In addition, the adsorption peak of supported gold nanoparticles located around 590 nm, which differed much from the bare small gold nanoparticles (around 520 nm for small particles around 2-50 nm) reported everywhere.[74, 75]

Silica is an excellent transparent, dielectric material, which never absorbs light or conducts electrons.[76] The silica materials are very similar as glasses in the Lycurgus Cup, which are only host for nanoparticles and the mixture of gold-silica can display the parallel optical properties of Au-NPs. Kobayashi and co-workers[77] synthesized the silica-coated Au-NPs by

a sol-gel method. It was found out that the Au@SiO_2 generally remained the initial optical properties of gold sol, disregarding the loading contents of gold. In fact the thickness of SiO_2 matters sometimes and controlled the optical properties of the Au-NPs when the SiO_2 shell coated the same gold sol. Liz-Marzán et al.[78] found out that the thin silica shell around gold nanoparticles displayed the red color of gold nanoparticles. The intensity of the plasmon resonance peaks increased with the rise of silica thickness, due to the local reflective around particles. However when the silica shell was thick enough, the adsorption at lower wavelength became stronger due to the scattering covering the plasmon resonance of Au-NPs. In this situation, the thick silica (about 80 nm) masked the initial color of initial gold colloid and only displayed very light pink color.

Besides, it was turned out that the solvent also lay importance on the optical properties of silica coated Au-NPs.[78] For the Au@SiO_2 with silica shell of 83 nm, the solvents' reflective index displayed a volcano-type curve impacting the maximum location of plasmon resonance peaks, that is, the plasmon peaks first red-shifted with the increase of the solvent's reflective index (1.36-1.45), and then blue-shifted with the further rise of the solvent's reflective index (1.45-1.49). For a tested sample with 15 nm gold core and 60 nm silica shell, the color of Au@SiO_2 in solvents with reflective index from 1.45 to 1.36 displayed the color from turbid to transparent.

1.3.2.3 Application of SPR effect of gold nanocrystals during Cancer treatment

It has to be mentioned that the Au-NPs and gold nanorods (Au-NRs) can be efficiently used during the cell imaging and cancer and treatment. The epithelial growth factor receptor (EGFR) is a kind of protein that is very important for the control of growth, multiplication and differentiation of cells. The gold nanoparticles can be conjugated with the anti-EGFR antibody, which is able to bond the cell surface and possesses the molecular specificity labeling capacity under laser excitation.[79]

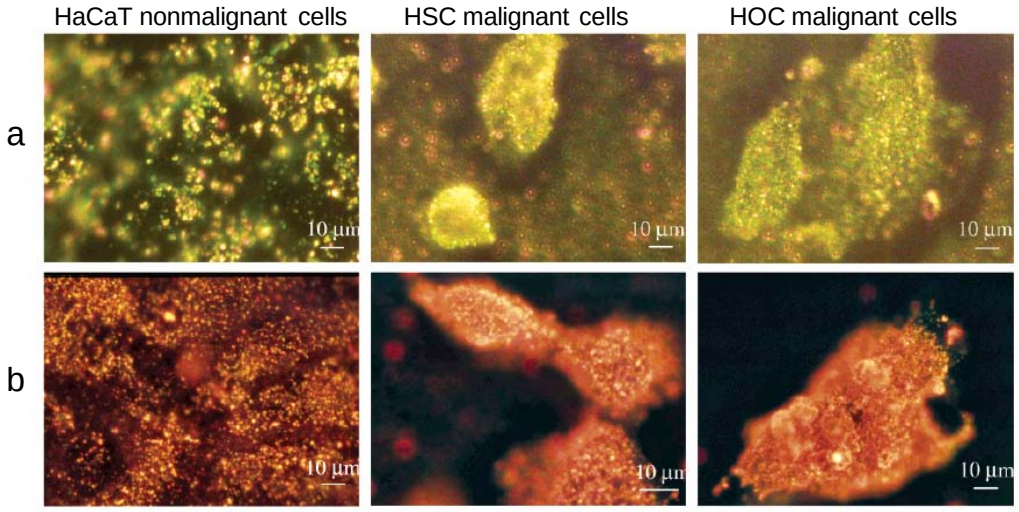

Figure 1.6 Light scattering images of anti-EGFR/Au nanospheres after incubation with cells for 30 min at room temperature (a), and light scattering images of anti-EGFR/Au nanorods after incubation with cells for 30 min at room temperature (b). From gold nanospheres, the green to yellow color is most dominant, corresponding to the surface plasmonic enhancement of scattering light in the visible region, and from gold nanorods, the orange to red color is most dominant, corresponding to the surface plasmonic enhancement of the longitudinal oscillation in the near-infrared region.[80]

Besides, the Au-NPs possess high ability to absorb the visible light and transfer the optical energy into heat. Since the heat for killing cancer cells is only half comparing to the normal cells, the cancer cells can be killed by this method without damage of the healthy cells.[81] The spherical Au-NPs were proved to be excellent for cancer cells of subcutaneous tissue. However, the spherical Au-NPs are powerless for biological tissues too difficult to be penetrated by visible light. Under such circumstance, the Au-NRs with certain aspect ratio are more preferential due to the fact that they perform great absorption and scattering ability in the near-infrared range (800-1200 nm). By applying the appropriate light source (near infrared laser) according to the LSPR of Au-NRs, it can heat the Au-NRs to treat the cancer cells. Huang et al.[80] applied the oligopeptides-gold nanorods to mark the nucleus. Under the Dark field optical microscope, the cancer cells and normal cells can be clearly separated as shown

in Figure 1.6. By using the laser of 800 nm, the cancer can be selectively killed.

1.3.3 Color of gold colloid and application

The beautiful and vivid colors of gold colloids are also results of the changes of SPR effect variation.

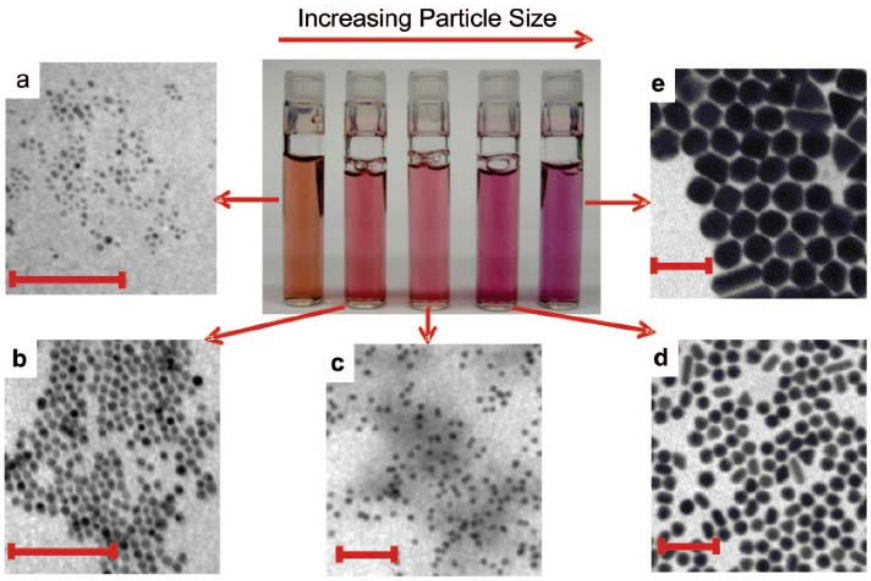

Figure 1.7 Photographs of aqueous solutions of gold nanospheres as a function of the particles sizes. The scale bar of each image is 100 nm.[82]

When the gold colloids are exposed under the incident light, the photons of the incident light at the same frequency of the colloid SPRs will be absorbed, the left photons consisting the reflect light displays the color visualized by eyes.[83] Polymers with different ligands are utilized as the agents for varying the aggregation degree of the gold nanoparticles as well as the color of the gold colloid. In the research of synthesize of gold colloids, the color change is a very important signal to disclose the size and distribution, even the shapes of the Au-NPs. The colloid with spherical Au-NPs generally shows red color as shown in Figure 1.7.[82, 84, 85] The colloid with Au-NPs about 3-5 nm particles, the color might be wine-red, or reddish orange depending on the used reduce and protect agents.[37, 86, 87] For gold colloids with very larger

Au-NPs (> 100 nm) or gold aggregations, the colloid displays purple or even grayish blue color.[88, 89]

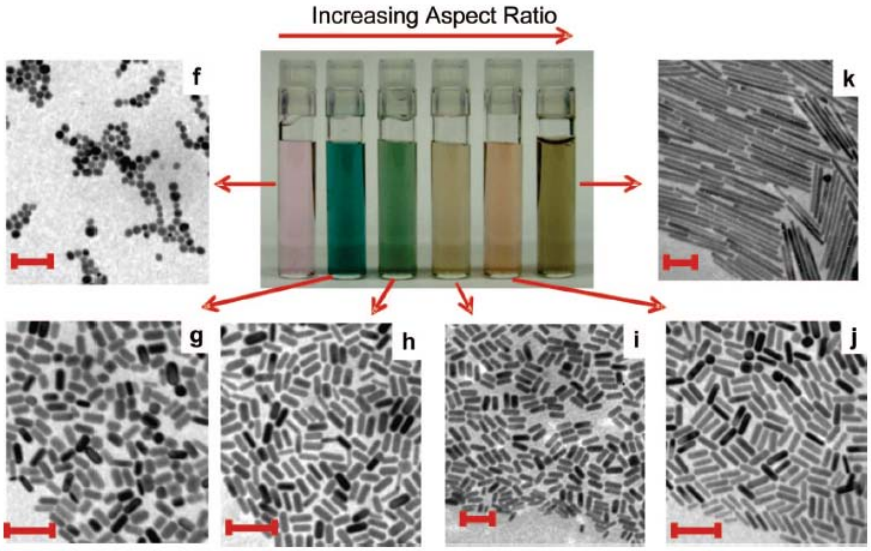

Figure 1.8 Photographs of aqueous solutions of gold nanorods as a function of increasing dimensions. The scale bar of each image is 100 nm.[82]

The color of the colloids with non-spherical Au-NPs is more vivid.[90, 91] Taking the gold nanorods for instance as shown in Figure 1.8, the color can be green, blue, purple, red, and brownish yellow according to the aspect ratio (the ratio between the transverse and longitudinal diameters).[92, 93] Such color variation is very sensitive to the changes of gold sizes and shapes, which provides a facile and macroscopical measurement during the synthesis of Au-NPs. However, it ought to be very careful if the shapes of Au-NPs are not the same. For example, if the colloids, one with Au-NPs and another with Au-NRs, the different of the gold particles sizes is uneasy to tell.

In the work of this thesis, the homogeneous spherical Au-NPs with narrow size distribution are required by using the colloidal method with simple and low cost reactants, which is until now still a challenge in the heterogeneous catalysis field. Based on the SPR effect, it will be very interesting to consider the reflection between sizes of Au-NPs and the color of gold colloid in a reversible way. It also means that the size distribution can be estimated partially

from the color of the gold colloid. By combining with the UV-vis spectra and home-made simple methods, it is hopeful that the morphology of as-synthesized colloidal Au-NPs can be firstly inferred by simple measurements. This, is just what it has to be done in the first section of the whole thesis. The understanding of relationship between the plasmon resonance and the change of color of colloid with spherical Au-NPs may shed light on the study for the further beginners.

1.4 Supported gold nanoparticles for CO oxidation

1.4.1 Main parameters impacting the catalytic activity

The discovery of supported Au-NPs used for low-temperature CO oxidation arouses enthusiastic wave over researchers. However, the catalytic performance over Au-NPs for CO oxidation differs very much according to the properties of gold catalysts. The main factors impacting the catalytic activity of Au-NPs are suggested as below according to the existed literatures.

√ The size of nanoparticles

It is understood that the physical property of gold will transfer from metal to non-metal when the particle sizes decrease to certain value. The threshold level for metallic gold change into non-metallic is 100 to 800 atoms for one particle, which is about 2 to 3 nm for a particle.[44] By the way, the conduction property of gold will also urgently decrease with the reducing of the particle size. This is in accordance with plenty of work declaring that the favorable size of Au-NPs is around 3 nm for CO oxidation, during which the non-metallic property of gold acts as a raw driving force for catalyzing the reaction.[94]

As it is well know that some of the reactions are rather sensitive to the sizes of Au-NPs. As it is mentioned above, the size of Au-NPs is viewed as a most important parameter for reactions

such as CO oxidation especially when inert supports are utilized.[95] The supported small gold particles (< 5 nm) are more capable for activating the reactions.[44, 96, 97] In this case, plenty of investigations have been focused on how to prepare excellent Au-NPs with homogeneous small particles for the promotion of various reactions. It was previously reported that the CO reaction rate over 2 to 4 nm gold nanoparticles will be 2 orders of magnitude larger than that over 20 to 30 nm gold nanoparticles.

√ The interaction between gold particles and supports

As it was introduced above, there are mainly two groups of materials used as supports: the active support (TiO_2, ZnO_2, FeO_x, etc) and inert support (SiO_2, ZrO_2, Al_2O_3, etc). It is general considered that when supported on the active supports, the Au-NPs display much higher activity than supported on the inner supports. Of cause, there are still some arguments for the absoluteness of this conclusion. Take Al_2O_3 for instance, the catalytic activity of Au/Al_2O_3 prepared by deposition of gold colloid was reported to be futile for the CO oxidation.[98] However, some other researchers also reported that the Au/Al_2O_3 from indirect colloid deposition method possessed excellent catalytic activity for CO oxidation even comparable to the Au/TiO_2.[99] Besides, as it is mentioned above in the 1.2.2 section, the presence of hydrogen in the PROX CO oxidation may also promoted the catalytic activity of gold catalysts supported on inert carrier as Al_2O_3 and ZrO_2.[45] The gold particles can interact with the surface of support for the sake of a higher activity. When the gold particles move together, or get into the inner bulk face of the support, or blocking the pores of the supports such as the MCM-41 and SBA-15, the predominant catalytic reactivity of Au-NPs will be destroyed. Even when the sizes of Au-NPs are similar for the gold catalysts supported on different materials, the catalytic activity will be distinctive according to different chemical and physical states of metal oxides.[100] On the other hand, it was demonstrated that for the Au-NPs supported on the active supports, the active oxygen can be provided from the support and the reaction will be carried out on the perimeter between the gold particles and support[101]. While for Au-NPs supported on the inert materials, the support do not take part in the reaction[102].

√ The gold loading

The amounts of gold loading on the surface of the support are also one of the factors influencing the catalytic activity. An appropriate amount of gold loading will accelerated the reaction rate, due to the highly dispersed Au-NPs offering large amounts of active sites for the reaction to be taken place. There is a volcanic-like relationship between the amounts of gold loading and the catalytic activity. When the gold content is very low, the gold active sites are not enough for the reaction and thus results to unsatisfied reactant conversion and productivity. When the gold content is too high, the excessive Au-NPs will encounter aggregation during the high temperature treatment and the catalytic activity largely decreases.

√ The calcination temperature

For gold catalysts, small Au-NPs around 3 nm are most active for reactions such as CO oxidation. However, the smaller Au-NPs possess much lower melting point than the larger Au-NPs. Under a higher calcination temperature, the smaller Au-NPs will be melted, move and aggregated into one larger particle which is not good for the catalytic activity. The temperature of calcination is generally located at 300 °C for several hours in most of the work. Higher temperature is very dangerous for the smaller Au-NPs. Li and colleagues[103] even found out that the calcination process displayed no good for the gold catalyst even at 300 °C. The T_{50} (the temperature at 50% CO conversion) of uncalcined Au/TiO_2 was about 50 °C lower than the calcined one. There also exist some exceptions. In a previous work of our group, the stoichiometric mixtures of TiO_2 and ZrO_2 ($TiZrO_4$) were applied as the support for gold catalysts.[104] By using the direct anionic exchange method, the as-synthesized gold catalysts maintained most of the satisfied small particles and excellent activity for CO oxidation even when the calcinations temperature was 750^{o}C.

√ The pH value

Deposition-precipitation method is widely used for preparation of gold catalyst. During this

process, the pH value of the solution should be adjusted by basic solution such as NaOH and ammonia water. It was found out that the pH value greatly impacted the size of gold nanoparticles, the real gold loading amount, and the catalytic activity for CO oxidation. Independent of the supports, the T_{50} over gold catalyst for CO oxidation decreased about 150°C when the pH value changed from 5 to 9.[100] On the other hand, the previous investigation of our group applied the direct anionic exchange method to obtained supported Au-NPs. And it was found out that the pH value of the gold precursor laid great importance on the formation of gold catalysts.[11] The graphical mechanism is shown in Figure 1.9. The $[AuCl_x(OH)_{4-x}]^-$ species changed a lot along with the pH value of the solution. When the pH value of the solution was lower than 2 or higher than 7, there would exist only the $[AuCl_4]^-$ or $[Au(OH)_4]^-$, respectively. Based on this mechanism, it was available to control the gold species in the solution by carefully changing the pH value, which was very important for the interaction between the gold and support.

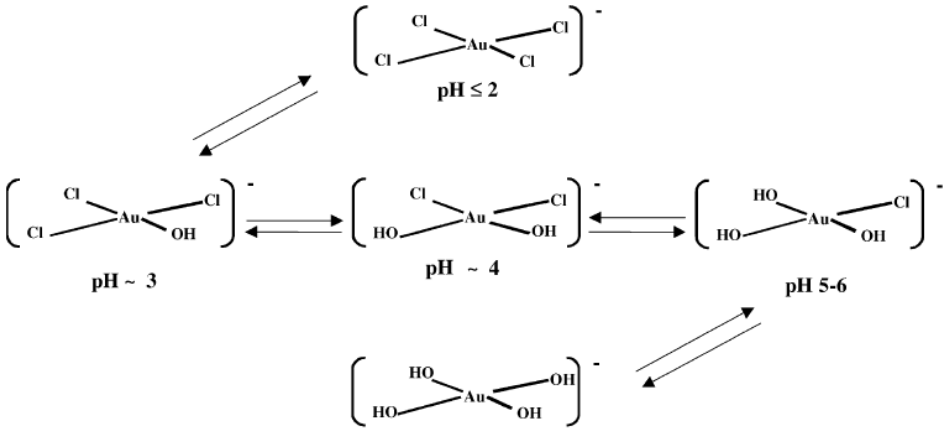

Figure 1.9 Equilibrium between gold species according to pH.[11]

1.4.2 Chemisorption of gas molecules over gold

There are two major measurements most commonly applied for testing the chemisorptions over Au-NPs, which include the dynamic (volumetric method)/static (pulse method) measurement,[105, 106] and the Fourier Transformed Infrared Spectroscopy (FTIR).[107-109] The

additional measurements are the ^{129}Xe NMR[110], Diffuse Reflectance Infra-red Fourier Transform (DRIFTS),[111, 112] and temperature programmed desorption, etc.[113, 114]

√ Chemisorption of CO

The CO adsorption onto the Au/TiO_2 catalyst was studied by the volumetric method,[105, 106] and the results turned out that large amount of the CO molecules were reversibly adsorbed on the surface of TiO_2. Only very small amount of CO molecules could be irreversibly adsorbed on the Au-NPs, which was responsible for the production of CO_2. For the catalyst after O_2 pretreatment, irreversible adsorption of CO could be taken under 0^oC.[105] Besides, the adsorption amount of CO species decreases with the raising of temperature.

The Fourier Transformed Infrared Spectroscopy (FTIR) is very helpful for identifying the different adsorption species of CO molecules. The reported CO species adsorbed on different supports and supported Au-NPs are listed in Table 1.2. For the Au-NPs supported on TiO_2, CeO_2 and ZnO, the overlapped adsorption peaks in 1100-1800 cm^{-1} can be ascribed to the CO_3^{2-} or carboxylate species.[115-118] The CO molecules adsorbed on TiO_2 display peaks around 2180 cm^{-1}.[119] The CO species adsorbed on metallic gold (Au^0) locate ranging from 2100 to 2110 cm^{-1} depending on the carriers.[120, 121] In the Au/ZnO system, the peaks appeared at about 2115 cm^{-1} are resulted from the CO species adsorbed on the gold species with positive charge ($Au^{\delta+}$);[122] whilst the peaks of such CO adsorption species ($Au^{\delta+}$-CO) corresponding to Al_2O_3, MgO and SiO_2 supported gold blue-shift to about 2130 cm^{-1}.[123, 124] In addition, the adsorption peaks of CO species can shift a little due to the variation the synthesize methods. Taking the results from Table 1.2 for example, the authors synthesized the Au/ZnO catalysts by DP method and sol-gel method, in which the adsorption peak of $Au^{\delta-}$-CO of the former catalyst red-shifted about 30 cm^{-1}.[117, 122] It is a worth note that the CO adsorption species also change with some other operation conditions. For example, the frequency of Au^0-CO species decrease with the rise of operation pressure,[125] while increases with the reduction of surface coverage ratio.[126]

Table 1.2 The corresponding CO adsorption species and their frequency in FTIR form literatures.

Support	Preparation	Peak frequency (cm^{-1})	Assignment	Ref.
TiO_2	DP	2186	TiO_2-CO	[120]
		2110	Au^0-CO	
ZnO	Colloidal deposition	2180	ZnO-CO	[117]
		2077	$Au^{\delta-}$-CO	
ZnO	DP	2113	$Au^{\delta+}$-CO	[122]
		2101	Au^0-CO	
		2048	$Au^{\delta-}$-CO	
Al_2O_3, MgO	DP	2131	$Au^{\delta+}$-CO	[123]
		2114	Au^0-(O)-CO	
SiO_2	DP	2130	$Au^{\delta+}$-CO	[124]
		2106	Au^0-CO	
CeO_2	DP	2159, 2155	Ce^{4+}-CO	[121]
		2142, 2137	Ce^{3+}-CO	
		2100	Au^0-CO	

It is suggested that there exists the interaction between gold atoms at the edge of Au-NPs and the neighbor support particles, especially when gold interacted with the Ti^{4+}. The CO species adsorbed on such kind of gold atoms display (Au^0-CO) obvious different peak locations,[127, 128] the frequency of which is slightly lower at about 2100-2110 cm^{-1}. Raskó et al.[128] attributed the peaks locating at 2051 and 2026 cm^{-1} to the CO adsorbed on the edged and kinked gold atoms. Boccuzzi et al.[129] also identified the CO species adsorbed on gold atoms. They suggested that the peaks of linearly and bridged adsorbed CO species with gold clusters located at 2055 and 1990 cm^{-1} as shown in Figure 1.10, respectively.

During the measurements by FTIR, the isotopes of CO species (^{12}CO and ^{13}CO) and O species ($^{18}O_2$ and $^{16}O_2$) can be introduced for identification the source of the adsorption species,[107, 108, 130, 131] whether from the support or the gaseous CO. Boccuzzi et al.[108] made the investigation of competitive adsorption of CO and O_2 on gold active sites by using isotopic FTIR technique. It was found out that the pretreatment under CO gas was helpful for the activation of oxygen species and facilitated the reaction, while the pretreatment under oxygen went against the process of reaction.

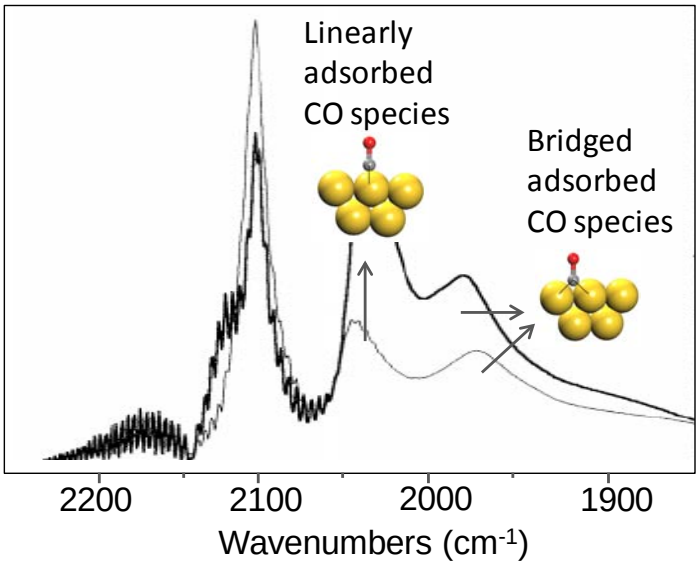

Figure 1.10 FTIR spectra in the carbonyl region of the Au/TiO_2 reduced sample contacted with 60 mbar CO (bold curve) and of the sample previously contacted with 1 mbar O_2 for 2 h at RT and then exposed to 60 mbar CO (thin curve).

Chiorino and co-worker[107] also studied the mechanism of CO oxidation over Au/TiO_2, Au/CeO_2, and Au/ZrO_2 by detection of CO adsorption using isotopic FTIR technique. The results turned out that the gold active sites could activate the CO and $^{18}O_2$ from the gas mixture, and only $C^{16}O^{18}O$ was produced in the outcome. Besides, the negatively charged gold clusters on the surface of support in the Au/CeO_2 catalyst effectively activated the oxygen species in the gas and produced large amount of $C^{16}O^{18}O$.

√ Chemisorption of O_2

The conclusions of O_2 adsorption on the supported Au-NPs in the literature still lack of unanimousness until now. Haruta et al[132] tested the Au/TiO_2 catalyst by the temperature programmed desorption (TPD) process and found out evident amount of adsorbed oxygen species. The hydroxide titration method can also be applied for semi-quantitatively estimating the dispersion and sizes of Au-NPs.[133, 134]

Some investigations suggested the influences of pretreatment under oxygen and the calcination, announcing the great importance of oxygen-active sites that lay on the catalytic activity of catalysts.[135, 136]

√ Chemisorption of H_2

The adsorption of H_2 on gold surface is trace amount and very hard to be detected.[137] The small positively charged Au-NPs with less than 15 atoms can reacted with deuterium or hydrogen, while there is no reaction over the negatively charged Au-NPs. There are very few reports concerning the chemisorption of H_2 on Au-NPs, except the preferential oxidation of CO (PROX) in the presence of H_2. The recent research of Caps and her colleagues[47] found out that the Au-OOH, Au-OH and Au-H intermediates involved in the present of H_2. Besides, the present of H_2 also changed the reaction path of CO oxidation and largely promoted the reactivity over Au/Al_2O_3.

√ Chemisorption of gases such as NO_x, SO_2 and H_2S

Now that it comes down to the gas molecules adsorption over gold, the other gas molecules such as NO_x, SO_2 and H_2S is concisely mentioned by the way. The NO and N_2O won't adsorb onto the surface of bulk gold. For the adsorption of NO gas on the surface of Au/CeO_2 catalyst, Ilieva et al.[138] considered that there existed only a reversible non-dissociated adsorption. They also proved that the NO adsorbed on the surface of gold was essentially distinct from adsorbed on the surface of Pt. Hussain[139] applied the Density Functional Theory (DFT) to imitate the NO adsorption on the (111), (100) and (111) crystal faces of Au-NPs. The molecular adsorption energy increased with the rise of unsaturation degree of the coordination of gold atoms. Besides, the adsorption of NO_x was also related to the sizes of Au-NPs, the pressure of NO_x and the adsorption temperature. Bukhtiyarov et al.[140] investigated the adsorption of NO_x onto the surface of 2-7 nm Au-NPs. They found out that only automatically adsorbed N_2 molecules existed on the surface of Au-NPs under high

vacuum state ($P_{NO} > 10^{-5}$ Pa).

His et al.[141] investigated the sulphonate adsorption on the surface of Au-NPs. They first applied the H_2S gas to pretreatment the gold surface, and found out that the adsorption amount of sulphonate was largely decreased. The authors ascribed such phenomenon to that the H_2S was first adsorbed on the surface of gold and blocked the adsorption active sites for sulphonate, thus decreased the adsorption of sulphonate. The report of Geng et al.[142] revealed that Au-NPs were easily to be attracted and formed large gold clusters when the colloidal Au-NPs were exposed in the H_2S atmosphere. Feria and co-workers[143] also confirmed the effective dissociation of SO_2 on the Au(001) crystal face of Au/TiC using both the experiments and theoretical calculation.

1.4.3 Mechanism of CO oxidation over gold catalysts

The chosen of different carriers induces different reaction mechanism. Take the CO oxidation as the example model, the mechanism of oxygen species adsorption and activation is still complex with contradictions. For gold supported on inert carriers such as SiO_2, the absorption of oxygen species is not occurred on the support but on the surface of gold particles with defect sites.[144, 145] During the reaction, the CO and O_2 gas molecules competitively absorb on the Au-NPs (path a in Figure 1.11). The oxygen molecule dissociated on the surface of gold, reacts with the CO adsorption species and thus release the CO_2 molecules. In this case the desired gold particles with higher activity should be very dispersive with small sizes to facilitate the exposure of the steps, edges, and kinks defect site on the gold particles for the oxygen species adsorption.

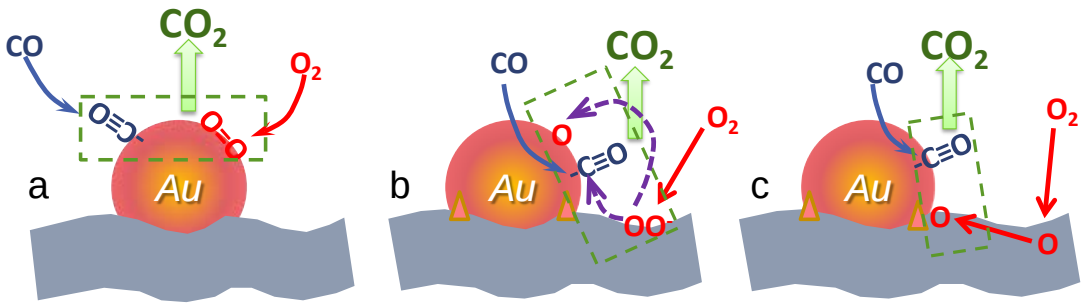

Figure 1.11 Three possible reaction paths of CO oxidation over supported Au-NPs depending on properties of carriers.

For Au-NPs supported on reducible supports, the supports themselves can be effective for the reaction individually. Sometimes, the oxygen species adsorption and the reaction can be occurred at the gold-metal oxide interface and the supports surface (paths b and c in Figure 1.7). For path b, the oxygen gaseous molecule is absorbed as superoxide species (O_2^- species),[146] and the CO_2 production then fulfilled by reaction between adsorbed CO species with either the O_2^- species or adsorbed oxygen species from O_2^- dissociation. The previous species is like carbonate-like transition state and more likely to be happened.[132] Besides, the lattice oxygen species in support can also participate into the reaction as shown in path c of Figure 1.7. During the reaction, the lattice oxygen species can be replenished by the dissociation of gaseous oxygen molecules and then reacts at the gold-support interface.[147] Thus the dissociation of oxygen no longer acts as the rate-determining step, and the sizes of Au-NPs are not the only determined role for the catalytic activity.

1.5 The goal of the research

Supported Au-NPs have been applied for catalytic reaction during the past several decades. The researches among this field so far are still developed rapidly to purchase novel nanoscale gold materials with better activity for the catalysis field. Researchers are looking for new preparation methods and special approaches to improve the catalytic activity of supported Au-NPs. Currently, one special topic becoming the hot spot concerning the colloidal Au-NPs

is also utilized into various aspects, and the catalysis field is also involved.[147, 148] Applying the colloidal Au-NPs as precursor, the sizes and distribution of Au-NPs can be controlled before supported onto carriers. What's more, the Au-NPs in gold colloid can be preliminarily estimated directly from the color, the UV-vis resonance peaks, and other special measurements such as liquid diffusion test due to the famous surface plasmon resonance effect of Au-NPs. The above properties illustrate the decent prospective of colloidal Au-NPs introduced into the catalysis field, which means that the sizes and distribution of supported Au-NPs from colloid method can be availably controlled, give unlimited superiorities for understanding the famous size effect of gold catalysts.

Besides, it is well-known that the silica is excellent for gold materials such as core-shell structures and coating techniques. However, when silica is used as support for gold catalysts by traditional preparation methods and applied for reactions such as CO oxidation, the activity of the catalysts is generally unsatisfied.[100, 149] Some investigations were engaged into the preparation of Au/SiO_2 catalysts with higher activity by some special methods such as chemical vapor deposition (CVD) and solvated metal atom dispersion (SMAD) technique.[150, 151] However most of them were expensive and unavailable to be generally applied. No matter how, the reactions over various silica supported Au-NPs wipe off the impact from gold-support interaction, which is helpful for easily understanding the action roles of the Au-NPs. According to these above advantages, researchers applied the Au/SiO_2 as model catalysts both for studying the reaction mechanism and searching modification for high efficient novel materials. By using the colloidal Au-NPs concerned materials, non-supported Au-NPs within special structures with excellent catalytic activity can also be synthesized by using gold colloid. Arnal and his co-workers[152] synthesized a special core-shell structured gold catalyst, in which the Au-NPs were encapsulated into the porous ZrO_2. The Au-NPs were on the one hand separated by the ZrO_2 and on the other hand possessed super high cluster-resistant ability, which thus performed attractive stability and activity for CO oxidation.

However in fact, the colloidal Au-NPs are still not universally applied in the catalysis field. Under this circumstance, we are trying to combine the colloidal Au-NPs with the silica material, in which the non-porous silica was chosen to be prepared by the famous Stöber method. The reason why we chosen the non-porous Stöber silica is that the Au-NPs can be highly dispersed on the surface of silica. All the Au-NPs won't be trapped into the pores and can be totally exposed to the reactants. Thus the reaction mechanism and the role of Au-NPs can be precisely studied.

In the thesis, the CO oxidation is applied as the model reaction because of its simple operation and wide applications such as CO_2 laser, gas sensor, and environmental protection. Besides, although the researches among the mechanism of CO oxidation over supported Au-NPs never stop, the mechanism of reaction is still complex. We are engaged to put forward a facile but efficient method for synthesizing Stöber silica supported Au-NPs with very small and homogeneous particle sizes (e.g. 2-3 nm). The supported Au-NPs prepared by the colloid method can be easily controlled and applied for CO oxidation (before and after modification). The growth of Au-NPs and their reaction mechanism for CO oxidation can thus be understood.

1.6 Short introduction of the author and the goal for this work

1.6.1 The working background

The author was enrolled by the Sichuan University of China since the year 2008 and engaged into the study of material and catalysis field. During 2008-2010, the job is focusing on efficient gold and copper catalysts for CO oxidation. At the second year as a Master student, she published the first paper[153] and made herself a chance to pursue doctoral degree in advance.

At the end of 2010, her subject was changed into the methane adsorption/desorption in coal

bed gas due to the foundation of the *Key National Basic Research and Development Program* (the 973 program). This is absolutely a new aspect in the whole laboratory (However it does not connected much with the current investigation field). She engaged into constructing the experimental instruments and published the first paper on this aspect in the lab.

From September of 2011 until now, she was send to ***The University of Strasbourg*** working on the synthesis of gold nanoparticles and their growing mechanism to prepare her thesis.

The above arrangements partly explain the shifting of her job during the last four years. No matter how, she is no longer a beginner of the current research project. On the one hand, she is partially familiar with the research project since her master stage; on the other hand, she knows how to use the current equipments and resources to process the study as soon as possible. The favorite investigation parts of the author are the researches on synthesizing novel materials both with amazing morphologies and satisfied application in some fields such as catalysis, and understanding the processes and mechanism.

1.6.2 Why the current subject was chosen

The author took part in the researches of supported Au-NPs for CO oxidation in the master stage, which was very similar with the current research project. The author understands the reported mechanism of CO oxidation over gold catalysts very well. The current work applies the colloidal Au-NPs and the Stöber silica for purchasing novel gold materials. The author wants to explore an environmental and simple method to synthesize supported Au-NPs for catalytic reactions, which would be a very good starting point for the application of gold colloid in the catalysis field but also a challenge. Besides, the controllable preparation of Au-NPs and the available exposed gold on the surface of non-porous Stöber silica will be helpful for understanding what happened and the evolution of the gold materials during the catalytic reactions.

1.6.3 The ICPEES group in the University of Strasbourg

The Institute of Chemistry and Processes for Energy, Environment and Health (ICPEES) is a joint research unit under the joint supervision of the CNRS and the University of Strasbourg.

The transversal skills present in ICPEES can solve global problems ranging from the synthesis of molecules to the development of the final object based on targeted applications. The ICPEES institute possesses the new technologies for the development of innovative materials.

The MARI team "Matériaux Avancés pour la Réactivité des Interfaces" of the ICPEES (the author worked in) is mainly engaged in preparing and modifying potential solid catalysts (in powder form). During the past several years, gold catalysts by novel preparation method and applied for reactions such as CO oxidation and aldehydes hydrogenation formed the main part of researches in the team. These detailed studies help explain the mechanisms of adsorption and reaction as well as the evolution of the material under catalysis conditions.

Bibliography

[1] C.H. Fisher, The reactive methyl group in toluene derivatives. I. Oxidation with selenium dioxide and cleavage of benzylpyridinium halides, Journal of the American Chemical Society, 56 (1934) 2056-2057.

[2] M. Haruta, T. Kobayashi, H. Sano, N. Yamada, Novel gold catalysts for the oxidation of carbon-monoxide at a temperature far below 0 ^{o}C, Chemistry Letters, (1987) 405-408.

[3] M. Haruta, H. Kageyama, N. Kamijo, T. Kobayashi, F. Delannay, Fine structure of novel gold catalysts prepared by coprecipitation, in: T. Inui (Ed.) Studies in Surface Science and Catalysis, Elsevier1989, pp. 33-42.

[4] A.S.K. Hashmi, Gold-catalyzed organic reactions, Chemical Reviews, 107 (2007) 3180-3211.

[5] A. Corma, A. Leyva-Pérez, M.J. Sabater, Gold-catalyzed carbon–heteroatom bond -forming

reactions, Chemical Reviews, 111 (2011) 1657-1712.

[6] G.R. Bamwenda, S. Tsubota, T. Nakamura, M. Haruta, The influence of the preparation methods on the catalytic activity of platinum and gold supported on TiO2 for CO oxidation, Catalysis Letters, 44 (1997) 83-87.

[7] J.-D. Grunwaldt, C. Kiener, C. Wögerbauer, A. Baiker, Preparation of Supported Gold Catalysts for Low-Temperature CO Oxidation via “Size-Controlled” Gold Colloids, Journal of Catalysis, 181 (1999) 223-232.

[8] W.-C. Li, M. Comotti, F. Schüth, Highly reproducible syntheses of active Au/TiO2 catalysts for CO oxidation by deposition–precipitation or impregnation, Journal of Catalysis, 237 (2006) 190-196.

[9] H.Y. Xu, W. Chu, J.J. Luo, T. Zhang, Impacts of MgO promoter and preparation procedure on meso-silica supported nano gold catalysts for carbon monoxide total oxidation at low temperature, Chemical Engineering Journal, 170 (2011) 419-423.

[10] N. Hammer, I. Kvande, X. Xu, V. Gunnarsson, B. Tøtdal, D. Chen, M. Rønning, Au–TiO2 catalysts on carbon nanofibres prepared by deposition-precipitation and from colloid solutions, Catalysis Today, 123 (2007) 245-256.

[11] S. Ivanova, C. Petit, V. Pitchon, A new preparation method for the formation of gold nanoparticles on an oxide support, Applied Catalysis a-General, 267 (2004) 191-201.

[12] S. Ivanova, W. Pitchon, Y. Zimmermann, C. Petit, Preparation of alumina supported gold catalysts: Influence of washing procedures, mechanism of particles size growth, Applied Catalysis a-General, 298 (2006) 57-64.

[13] Y. Azizi, C. Petit, V. Pitchon, Role of support in the oxidation of acetylene over gold catalysts, Journal of Catalysis, 269 (2010) 26-32.

[14] Y. Azizi, C. Petit, V. Pitchon, Formation of polymer-grade ethylene by selective hydrogenation of acetylene over Au/CeO_2 catalyst, Journal of Catalysis, 256 (2008) 338-344.

[15] M. Bowker, A. Nuhu, J. Soares, High activity supported gold catalysts by incipient wetness impregnation, Catalysis Today, 122 (2007) 245-247.

[16] H.Y. Tsai, Y.D. Lin, W.T. Fu, S.D. Lin, The activation of supported Au catalysts prepared by impregnation, Gold Bulletin, 40 (2007) 184-191.

[17] A. Hugon, L. Delannoy, C. Louis, Supported gold catalysts for selective hydrogenation of 1,3-butadiene in the presence of an excess of alkenes, Gold Bulletin, 41 (2008) 127-138.

[18] L. Delannoy, R.L. Chantry, S. Casale, Z.Y. Li, Y. Borensztein, C. Louis, HRTEM and STEM-HAADF characterisation of Au-TiO_2 and Au-Al_2O_3 catalysts for a better understanding of the parameters influencing their properties in CO oxidation, Physical Chemistry Chemical Physics, 15 (2013) 3473-3479.

[19] D. Andreeva, I. Ivanov, L. Ilieva, M.V. Abrashev, R. Zanella, J.W. Sobczak, W. Lisowski, M. Kantcheva, G. Avdeev, K. Petrov, Gold catalysts supported on ceria doped by rare earth metals for water gas shift reaction: Influence of the preparation method, Applied Catalysis a-General, 357 (2009) 159-169.

[20] B.L. Moroz, P.A. Pyrjaev, V.I. Zaikovskii, V.I. Bukhtiyarov, Nanodispersed Au/Al_2O_3 catalysts for low-temperature CO oxidation: Results of research activity at the Boreskov Institute of Catalysis, Catalysis Today, 144 (2009) 292-305.

[21] B.C. Campo, S. Ivanova, C. Gigola, C. Petit, M.A. Volpe, Crotonaldehyde hydrogenation on supported gold catalysts, Catalysis Today, 133 (2008) 661-666.

[22] G. Neri, A. Bonavita, S. Galvagno, P. Siciliano, S. Capone, CO and NO_2 sensing properties of doped-Fe_2O_3 thin films prepared by LPD, Sensors and Actuators B-Chemical, 82 (2002) 40-47.

[23] Y.-M. Kang, B.-Z. Wan, Gold and iron supported on Y-type zeolite for carbon monoxide oxidation, Catalysis Today, 35 (1997) 379-392.

[24] G.R. Bamwenda, S. Tsubota, T. Nakamura, M. Haruta, Photoassisted hydrogen-production from a water-ethanol solution - a comparison of activities of Au-TiO_2 and Pt-TiO_2, Journal of Photochemistry and Photobiology a-Chemistry, 89 (1995) 177-189.

[25] M.A. Al-Daous, A.A. Manda, H. Hattori, Acid-base properties of gamma-Al_2O_3 and MgO-Al_2O_3 supported gold nanoparticles, Journal of Molecular Catalysis a-Chemical, 363 (2012) 512-520.

[26] G.M. Veith, A.R. Lupini, S.J. Pennycook, A. Villa, L. Prati, N.J. Dudney, Magnetron sputtering of gold nanoparticles onto WO_3 and activated carbon, Catalysis Today, 122 (2007) 248-253.

[27] A. Currao, V.R. Reddy, G. Calzaferri, Gold-golloid-modified AgCl photocatalyst for water oxidation to O_2, ChemPhysChem, 5 (2004) 720-724.

[28] K.C. Grabar, P.C. Smith, M.D. Musick, J.A. Davis, D.G. Walter, M.A. Jackson, A.P. Guthrie, M.J. Natan, Kinetic control of interparticle spacing in Au colloid-based surfaces: Rational nanometer-scale architecture, Journal of the American Chemical Society, 118 (1996) 1148-1153.

[29] F. Xie, M.S. Baker, E.M. Goldys, Enhanced fluorescence detection on homogeneous gold colloid self-assembled monolayer substrates, Chemistry of Materials, 20 (2008) 1788-1797.

[30] K.S. Mayya, V. Patil, M. Sastry, Lamellar multilayer gold cluster films deposited by the Langmuir-Blodgett technique, Langmuir, 13 (1997) 2575-2577.

[31] J. Ye, B.V. de Broek, R. De Palma, W. Libaers, K. Clays, W. Van Roy, G. Borghs, G. Maes, Surface morphology changes on silica-coated gold colloids, Colloids and Surfaces a-Physicochemical and Engineering Aspects, 322 (2008) 225-233.

[32] M.P. Neupane, S.J. Lee, I.S. Park, M.H. Lee, T.S. Bae, Y. Kuboki, M. Uo, F. Watari, Synthesis of gelatin-capped gold nanoparticles with variable gelatin concentration, Journal of Nanoparticle Research, 13 (2011) 491-498.

[33] L. Zhang, J. Swift, C.A. Butts, V. Yerubandi, I.J. Dmochowski, Structure and activity of apoferritin-stabilized gold nanoparticles, Journal of Inorganic Biochemistry, 101 (2007) 1719-1729.

[34] S.K. Ghosh, S. Nath, S. Kundu, K. Esumi, T. Pal, Solvent and ligand effects on the localized surface plasmon resonance (LSPR) of gold colloids, Journal of Physical Chemistry B, 108 (2004) 13963-13971.

[35] M.E. Garcia, L.A. Baker, R.M. Crooks, Preparation and characterization of dendrimer-gold colloid nanocomposites, Analytical Chemistry, 71 (1999) 256-258.

[36] O. Tzhayik, P. Sawant, S. Efrima, E. Kovalev, J.T. Klug, Xanthate capping of silver, copper, and gold colloids, Langmuir, 18 (2002) 3364-3369.

[37] V. Patil, R.B. Malvankar, M. Sastry, Role of particle size in individual and competitive diffusion of carboxylic acid derivatized colloidal gold particles in thermally evaporated fatty amine films, Langmuir, 15 (1999) 8197-8206.

[38] W. Huang, S.M. Chen, Y.S. Liu, H.Y. Fu, G.Z. Wu, The controlled synthesis of stable gold nanoparticles in quaternary ammonium ionic liquids by simple heating, Nanotechnology, 22 (2011).

[39] X.P. Sun, S.J. Dong, E.K. Wang, One-step preparation of highly concentrated well-stable gold colloids by direct mix of polyelectrolyte and $HAuCl_4$ aqueous solutions at room temperature, Journal of Colloid and Interface Science, 288 (2005) 301-303.

[40] G. Suyal, M. Mennig, H. Schmidt, Effect of glass substrates on the formation of gold-silver colloids in nanocomposite thin films, Journal of Sol-Gel Science and Technology, 29 (2004) 11-18.

[41] K. Zhu, L.Q. Huang, J. Zhu, Z.Y. Zhuang, Influence of TX-100 on the size controlled synthesis of gold colloid, Spectrochimica Acta Part a-Molecular and Biomolecular Spectroscopy, 69 (2008) 566-571.

[42] S.I. Stoeva, A.B. Smetana, C.M. Sorensen, K.J. Klabunde, Gram-scale synthesis of aqueous gold

colloids stabilized by various ligands, Journal of Colloid and Interface Science, 309 (2007) 94-98.

[43] M. Haruta, N. Yamada, T. Kobayashi, S. Iijima, Gold catalysts prepared by coprecipitation for low-temperature oxidation of hydrogen and of carbon monoxide, Journal of Catalysis, 115 (1989) 301-309.

[44] G.C. Bond, The effect of the metal to non-metal transition on the activity of gold catalysts, Faraday Discussions, 152 (2011) 277-291.

[45] C. Rossignol, S. Arrii, F. Morfin, L. Piccolo, V. Caps, J.L. Rousset, Selective oxidation of CO over model gold-based catalysts in the presence of H_2, Journal of Catalysis, 230 (2005) 476-483.

[46] E. Quinet, F. Morfin, F. Diehl, P. Avenier, V. Caps, J.L. Rousset, Hydrogen effect on the preferential oxidation of carbon monoxide over alumina-supported gold nanoparticles, Applied Catalysis B-Environmental, 80 (2008) 195-201.

[47] E. Quinet, L. Piccolo, F. Morfin, P. Avenier, F. Diehl, V. Caps, J.L. Rousset, On the mechanism of hydrogen-promoted gold-catalyzed CO oxidation, Journal of Catalysis, 268 (2009) 384-389.

[48] M.C. Daniel, D. Astruc, Gold nanoparticles: Assembly, supramolecular chemistry, quantum-size-related properties, and applications toward biology, catalysis, and nanotechnology, Chemical Reviews, 104 (2004) 293-346.

[49] S.K. Ghosh, T. Pal, Interparticle coupling effect on the surface plasmon resonance of gold nanoparticles: From theory to applications, Chemical Reviews, 107 (2007) 4797-4862.

[50] H. Raether, Excitation of plasmons and interband transitions by electrons, Springer-Verlag, Berlin ; New York, 1980.

[51] K.A. Willets, R.P. Van Duyne, Localized surface plasmon resonance spectroscopy and sensing, Annual Review of Physical Chemistry, 58 (2007) 267-297.

[52] C.R. Yonzon, D.A. Stuart, X.Y. Zhang, A.D. McFarland, C.L. Haynes, R.P. Van Duyne, Towards advanced chemical and biological nanosensors - An overview, Talanta, 67 (2005) 438-448.

[53] A.J. Haes, L. Chang, W.L. Klein, R.P. Van Duyne, Detection of a biomarker for Alzheimer's disease from synthetic and clinical samples using a nanoscale optical biosensor, Journal of the American Chemical Society, 127 (2005) 2264-2271.

[54] J.B. Gonzalez-Diaz, A. Garcia-Martin, J.M. Garcia-Martin, A. Cebollada, G. Armelles, B. Sepulveda, Y. Alaverdyan, M. Kall, Plasmonic Au/Co/Au nanosandwiches with enhanced magneto-optical activity, Small, 4 (2008) 202-205.

[55] U. Kreibig, M. Vollmer, Optical properties of metal clusters, Springer, Berlin ; New York, 1995.

[56] L. Wang, C. Clavero, Z. Huba, K.J. Carroll, E.E. Carpenter, D.F. Gu, R.A. Lukaszew, Plasmonics and enhanced magneto-optics in core-shell Co-Ag nanoparticles, Nano Letters, 11 (2011) 1237-1240.

[57] S. Tokonami, Y. Yamamoto, H. Shiigi, T. Nagaoka, Synthesis and bioanalytical applications of specific-shaped metallic nanostructures: A review, Analytica Chimica Acta, 716 (2012) 76-91.

[58] F. Xia, X.L. Zuo, R.Q. Yang, Y. Xiao, D. Kang, A. Vallee-Belisle, X. Gong, J.D. Yuen, B.B.Y. Hsu, A.J. Heeger, K.W. Plaxco, Colorimetric detection of DNA, small molecules, proteins, and ions using unmodified gold nanoparticles and conjugated polyelectrolytes, Proceedings of the National Academy of Sciences of the United States of America, 107 (2010) 10837-10841.

[59] S. Link, M.A. El-Sayed, Spectral properties and relaxation dynamics of surface plasmon electronic oscillations in gold and silver nanodots and nanorods, Journal of Physical Chemistry B, 103 (1999) 8410-8426.

[60] C.C. Li, K.L. Shuford, M.H. Chen, E.J. Lee, S.O. Cho, A facile polyol route to uniform gold octahedra with tailorable size and their optical properties, Acs Nano, 2 (2008) 1760-1769.

[61] X.C. Ye, L.H. Jin, H. Caglayan, J. Chen, G.Z. Xing, C. Zheng, D.N. Vicky, Y.J. Kang, N. Engheta, C.R. Kagan, C.B. Murray, Improved size-tunable synthesis of monodisperse gold nanorods through the use of aromatic additives, Acs Nano, 6 (2012) 2804-2817.

[62] Y.G. Sun, Y.N. Xia, Multiple-walled nanotubes made of metals, Advanced Materials, 16 (2004) 264-+.

[63] H. Wang, N.J. Halas, Mesoscopic Au "Meatball" particles, Advanced Materials, 20 (2008) 820-+.

[64] J. Ye, P. Van Dorpe, W. Van Roy, G. Borghs, G. Maes, Fabrication, characterization, and optical properties of gold nanobowl submonolayer structures, Langmuir, 25 (2009) 1822-1827.

[65] C.L. Nehl, H.W. Liao, J.H. Hafner, Optical properties of star-shaped gold nanoparticles, Nano Letters, 6 (2006) 683-688.

[66] Y.P. Chen, Y.Y. Zhang, W.X. Liang, X.D. Li, Gold nanocages as contrast agents for two-photon luminescence endomicroscopy imaging, Nanomedicine-Nanotechnology Biology and Medicine, 8 (2012) 1267-1270.

[67] C.X. Zhang, J.L. Zhang, B.X. Han, Y.J. Zhao, W. Li, Synthesis of icosahedral gold particles by a simple and mild route, Green Chemistry, 10 (2008) 1094-1098.

[68] L.H. Lu, I. Randjelovic, R. Capek, N. Gaponik, J.H. Yang, H.J. Zhang, A. Eychmuller, Controlled fabrication of gold-coated 3D ordered colloidal crystal films and their application in surface-enhanced Raman spectroscopy, Chemistry of Materials, 17 (2005) 5731-5736.

[69] Q. Xie, J. Zhou, L. Kang, Q. Zhao, B. Li, Y.H. Wang, R.L. Zong, X.G. Huang, Preparation of optically anisotropic nanocomposites with oriented gold nanorods embedded in polyvinyl alcohol, Journal of Nanoscience and Nanotechnology, 10 (2010) 1829-1833.

[70] H.J. Chen, L. Shao, K.C. Woo, T. Ming, H.Q. Lin, J.F. Wang, Shape-dependent refractive index sensitivities of gold nanocrystals with the same plasmon resonance wavelength, Journal of Physical Chemistry C, 113 (2009) 17691-17697.

[71] L.R. Hirsch, A.M. Gobin, A.R. Lowery, F. Tam, R.A. Drezek, N.J. Halas, J.L. West, Metal nanoshells, Annals of Biomedical Engineering, 34 (2006) 15-22.

[72] S.P. Ravindranath, Y.L. Wang, J. Irudayaraj, SERS driven cross-platform based multiplex pathogen detection, Sensors and Actuators B-Chemical, 152 (2011) 183-190.

[73] J. Fang, S.W. Cao, Z. Wang, M.M. Shahjamali, S.C.J. Loo, J. Barber, C. Xue, Mesoporous plasmonic Au-TiO_2 nanocomposites for efficient visible-light-driven photocatalytic water reduction, International Journal of Hydrogen Energy, 37 (2012) 17853-17861.

[74] Y.R. Zhang, Y.Z. Xu, Y. Xia, W. Huang, F.A. Liu, Y.C. Yang, Z.L. Li, A novel strategy to assemble colloidal gold nanoparticles at the water-air interface by the vapor of formic acid, Journal of Colloid and Interface Science, 359 (2011) 536-541.

[75] A.K. Suresh, D.A. Pelletier, W. Wang, M.L. Broich, J.W. Moon, B.H. Gu, D.P. Allison, D.C. Joy, T.J. Phelps, M.J. Doktycz, Biofabrication of discrete spherical gold nanoparticles using the metal-reducing bacterium Shewanella oneidensis, Acta Biomaterialia, 7 (2011) 2148-2152.

[76] N.J. Halas, Nanoscience under glass: The versatile chemistry of silica nanostructures, Acs Nano, 2 (2008) 179-183.

[77] Y. Kobayashi, M.A. Correa-Duarte, L.M. Liz-Marzan, Sol-gel processing of silica-coated gold nanoparticles, Langmuir, 17 (2001) 6375-6379.

[78] L.M. Liz-Marzan, M. Giersig, P. Mulvaney, Synthesis of nanosized gold-silica core-shell particles, Langmuir, 12 (1996) 4329-4335.

[79] K. Sokolov, M. Follen, J. Aaron, I. Pavlova, A. Malpica, R. Lotan, R. Richards-Kortum, Real-time vital optical imaging of precancer using anti-epidermal growth factor receptor antibodies conjugated to gold nanoparticles, Cancer Research, 63 (2003) 1999-2004.

[80] X.H. Huang, I.H. El-Sayed, W. Qian, M.A. El-Sayed, Cancer cell imaging and photothermal therapy in the near-infrared region by using gold nanorods, Journal of the American Chemical Society, 128 (2006) 2115-2120.

[81] I.H. El-Sayed, X. Huang, M.A. El-Sayed, Selective laser photo-thermal therapy of epithelial carcinoma using anti-EGFR antibody conjugated gold nanoparticles, Cancer Letters, 239 (2006) 129-135.

[82] C.J. Murphy, A.M. Gole, J.W. Stone, P.N. Sisco, A.M. Alkilany, E.C. Goldsmith, S.C. Baxter, Gold nanoparticles in biology: Beyond toxicity to cellular imaging, Accounts of Chemical Research, 41 (2008) 1721-1730.

[83] Y. Wang, Voltage-induced color-Selective absorption with surface-plasmons, Applied Physics Letters, 67 (1995) 2759-2761.

[84] T. Makiabadi, A. Bouvree, V. Le Nader, H. Terrisse, G. Louarn, Preparation, optimization, and characterization of SERS sensor substrates based on two-dimensional structures of gold colloid, Plasmonics, 5 (2010) 21-29.

[85] C.D. Geddes, H.S. Cao, J.R. Lakowicz, Enhanced photostability of ICG in close proximity to gold colloids, Spectrochimica Acta Part a-Molecular and Biomolecular Spectroscopy, 59 (2003) 2611-2617.

[86] A. Currao, V.R. Reddy, G. Calzaferri, Gold-colloid-modified AgCl photocatalyst for water oxidation to O_2, ChemPhysChem, 5 (2004) 720-724.

[87] J. Qian, C. Wang, X. Pan, S. Liu, A high-throughput homogeneous immunoassay based on Förster resonance energy transfer between quantum dots and gold nanoparticles, Analytica Chimica Acta, 763 (2013) 43-49.

[88] M. Kahraman, M.M. Yazici, F. Sahin, M. Culha, Experimental parameters influencing surface-enhanced Raman scattering of bacteria, Journal of Biomedical Optics, 12 (2007).

[89] Z.G. Liu, Y.G. Zu, Y.J. Fu, R.H. Meng, S.L. Guo, Z.M. Xing, S.N. Tan, Hydrothermal synthesis of histidine-functionalized single-crystalline gold nanoparticles and their pH-dependent UV absorption characteristic, Colloids and Surfaces B-Biointerfaces, 76 (2010) 311-316.

[90] V. Sebastian, S.K. Lee, C. Zhou, M.F. Kraus, J.G. Fujimoto, K.F. Jensen, One-step continuous synthesis of biocompatible gold nanorods for optical coherence tomography, Chemical Communications, 48 (2012) 6654-6656.

[91] M. Hu, J.Y. Chen, Z.Y. Li, L. Au, G.V. Hartland, X.D. Li, M. Marquez, Y.N. Xia, Gold nanostructures: engineering their plasmonic properties for biomedical applications, Chemical Society

Reviews, 35 (2006) 1084-1094.

[92] J. Perez-Juste, I. Pastoriza-Santos, L.M. Liz-Marzan, P. Mulvaney, Gold nanorods: Synthesis, characterization and applications, Coordination Chemistry Reviews, 249 (2005) 1870-1901.

[93] K.C. Ng, W.L. Cheng, Fine-tuning longitudinal plasmon resonances of nanorods by thermal reshaping in aqueous media, Nanotechnology, 23 (2012).

[94] M.S. Chen, D.W. Goodman, Catalytically active gold: From nanoparticles to ultrathin films, Accounts of Chemical Research, 39 (2006) 739-746.

[95] N. Lopez, T.V.W. Janssens, B.S. Clausen, Y. Xu, M. Mavrikakis, T. Bligaard, J.K. Norskov, On the origin of the catalytic activity of gold nanoparticles for low-temperature CO oxidation, Journal of Catalysis, 223 (2004) 232-235.

[96] F. Moreau, G.C. Bond, Preparation and reactivation of Au/TiO_2 catalysts, Catalysis Today, 122 (2007) 260-265.

[97] Y.S. Chi, H.P. Lin, C.Y. Mou, CO oxidation over gold nanocatalyst confined in mesoporous silica, Applied Catalysis a-General, 284 (2005) 199-206.

[98] D. Widmann, Y. Liu, F. Schuth, R.J. Behm, Support effects in the Au-catalyzed CO oxidation - Correlation between activity, oxygen storage capacity, and support reducibility, Journal of Catalysis, 276 (2010) 292-305.

[99] L. Wen, J.K. Fu, P.Y. Gu, B.X. Yao, Z.H. Lin, J.Z. Zhou, Monodispersed gold nanoparticles supported on gamma-Al_2O_3 for enhancement of low-temperature catalytic oxidation of CO, Applied Catalysis B-Environmental, 79 (2008) 402-409.

[100] A. Wolf, F. Schuth, A systematic study of the synthesis conditions for the preparation of highly active gold catalysts, Applied Catalysis a-General, 226 (2002) 1-13.

[101] X.Y. Liu, A.Q. Wang, L. Li, T. Zhang, C.Y. Mou, J.F. Lee, Structural changes of Au-Cu bimetallic catalysts in CO oxidation: In situ XRD, EPR, XANES, and FT-IR characterizations, Journal of Catalysis, 278 (2011) 288-296.

[102] K. Qian, Z.Q. Jiang, W.X. Huang, Effect of oxygen treatment on the catalytic activity of Au/SiO_2 catalysts, Journal of Molecular Catalysis a-Chemical, 264 (2007) 26-32.

[103] W.C. Li, M. Comotti, F. Schuth, Highly reproducible syntheses of active Au/TiO_2 catalysts for CO oxidation by deposition-precipitation or impregnation, Journal of Catalysis, 237 (2006) 190-196.

[104] Y. Azizi, V. Pitchon, C. Petit, Effect of support parameters on activity of gold catalysts: Studies of ZrO_2, TiO_2 and mixture, Applied Catalysis a-General, 385 (2010) 170-177.

[105] Y. Iizuka, H. Fujiki, N. Yamauchi, T. Chijiiwa, S. Arai, S. Tsubota, M. Haruta, Adsorption of CO on gold supported on TiO_2, Catalysis Today, 36 (1997) 115-123.

[106] N.W. Cant, N.J. Ossipoff, Cobalt promotion of Au/TiO_2 catalysts for the reaction of carbon monoxide with oxygen and nitrogen oxides, Catalysis Today, 36 (1997) 125-133.

[107] A. Chiorino, M. Manzoli, F. Menegazzo, M. Signoretto, F. Vindigni, F. Pinna, F. Boccuzzi, New insight on the nature of catalytically active gold sites: Quantitative CO chemisorption data and analysis of FTIR spectra of adsorbed CO and of isotopic mixtures, Journal of Catalysis, 262 (2009) 169-176.

[108] F. Boccuzzi, A. Chiorino, M. Manzoli, P. Lu, T. Akita, S. Ichikawa, M. Haruta, Au/TiO_2 nanosized samples: A catalytic, TEM, and FTIR study of the effect of calcination temperature on the CO oxidation, Journal of Catalysis, 202 (2001) 256-267.

[109] G. Avgouropoulos, M. Manzoli, F. Boccuzzi, T. Tabakova, J. Papavasiliou, T. Ioannides, V. Idakiev, Catalytic performance and characterization of Au/doped-ceria catalysts for the preferential CO oxidation reaction, Journal of Catalysis, 256 (2008) 237-247.

[110] D. Guillemot, V.Y. Borovkov, V.B. Kazansky, M. PolissetThfoin, J. Fraissard, Surface characterization of Au/HY by ^{129}Xe NMR and diffuse reflectance IR spectroscopy of adsorbed CO. Formation of electron-deficient gold particles inside HY cavities, Journal of the Chemical Society-Faraday Transactions, 93 (1997) 3587-3591.

[111] H.Y. Fan, C.A. Shi, X.S. Li, S. Zhang, J.L. Liu, A.M. Zhu, In-situ plasma regeneration of deactivated Au/TiO_2 nanocatalysts during CO oxidation and effect of N_2 content, Applied Catalysis B-Environmental, 119 (2012) 49-55.

[112] H. Wang, H.Q. Zhu, Z.F. Qin, F.X. Liang, G.F. Wang, J.G. Wang, Deactivation of a Au/CeO_2-Co_3O_4 catalyst during CO preferential oxidation in H_2-rich stream, Journal of Catalysis, 264 (2009) 154-162.

[113] T.A. Ntho, J.A. Anderson, M.S. Scurrell, CO oxidation over titanate nanotube supported Au: Deactivation due to bicarbonate, Journal of Catalysis, 261 (2009) 94-100.

[114] T.A. Zepeda, A. Martinez-Hernandez, R. Guil-Lopez, B. Pawelec, Preferential CO oxidation in excess of hydrogen over Au/HMS catalysts modified by Ce, Fe and Ti oxides, Applied Catalysis B-Environmental, 100 (2010) 450-462.

[115] B.K. Chang, B.W. Jang, S. Dai, S.H. Overbury, Transient studies of the mechanisms of CO

oxidation over Au/TiO_2 using time-resolved FTIR spectroscopy and product analysis, Journal of Catalysis, 236 (2005) 392-400.

[116] J.D. Henao, T. Caputo, J.H. Yang, M.C. Kung, H.H. Kung, In situ transient FTIR and XANES studies of the evolution of surface species in CO oxidation on Au/TiO_2, Journal of Physical Chemistry B, 110 (2006) 8689-8700.

[117] K. Kahler, M.C. Holz, M. Rohe, J. Strunk, M. Muhler, Probing the reactivity of ZnO and Au/ZnO nanoparticles by methanol adsorption: A TPD and DRIFTS study, ChemPhysChem, 11 (2010) 2521-2529.

[118] M. Kantcheva, O. Samarskaya, L. Ilieva, G. Pantaleo, A.M. Venezia, D. Andreeva, In situ FT-IR investigation of the reduction of NO with CO over Au/CeO_2-Al_2O_3 catalyst in the presence and absence of H_2, Applied Catalysis B-Environmental, 88 (2009) 113-126.

[119] J. Kiss, nos, R. meth, bert, Ko, s, kos, Rask, J., Characterization of Au-Rh/TiO_2 bimetallic nanocatalysts by CO and CH_3CN adsorption: XPS, TEM and FTIR measurements, Journal of Nanoscience and Nanotechnology, 9 (2009) 3828-3836.

[120] G. Wu, T. Chen, W. Su, G. Zhou, X. Zong, Z. Lei, C. Li, H_2 production with ultra-low CO selectivity via photocatalytic reforming of methanol on Au/TiO_2 catalyst, International Journal of Hydrogen Energy, 33 (2008) 1243-1251.

[121] T. Tabakova, M. Manzoli, F. Vindigni, V. Idakiev, F. Boccuzzi, CO-free hydrogen production for fuel cell applications over Au/CeO_2 catalysts: FTIR insight into the role of dopant, Journal of Physical Chemistry A, 114 (2010) 3909-3915.

[122] X. Liu, M.-H. Liu, Y.-C. Luo, C.-Y. Mou, S.D. Lin, H. Cheng, J.-M. Chen, J.-F. Lee, T.-S. Lin, Strong metal-support interactions between gold nanoparticles and ZnO nanorods in CO oxidation, Journal of the American Chemical Society, 134 (2012) 10251-10258.

[123] E.G. Szabó, M. Hegedűs, F. Lónyi, Á. Szegedi, A.K. Datye, J.L. Margitfalvi, Preparation, characterization and activity of Au/Al_2O_3 catalysts modified by MgO, Catalysis Communications, 10 (2009) 889-893.

[124] F. Somodi, I. Borbáth, M. Hegedűs, A. Tompos, I.E. Sajó, Á. Szegedi, S. Rojas, J.L.G. Fierro, J.L. Margitfalvi, Modified preparation method for highly active Au/SiO_2 catalysts used in CO oxidation, Applied Catalysis a-General, 347 (2008) 216-222.

[125] F. Boccuzzi, A. Chiorino, S. Tsubota, M. Haruta, FTIR study of carbon monoxide oxidation and scrambling at room temperature over gold supported on ZnO and TiO_2 .2., Journal of Physical Chemistry, 100 (1996) 3625-3631.

[126] J.Y. Lee, J. Schwank, Infrared spectroscopic study of NO reduction by H_2 on supported gold catalysts, Journal of Catalysis, 102 (1986) 207-215.

[127] I.X. Green, W.J. Tang, M. Neurock, J.T. Yates, Spectroscopic observation of dual catalytic sites during oxidation of CO on a Au/TiO_2 catalyst, Science, 333 (2011) 736-739.

[128] J. Rasko, J. Kiss, CO oxidation in the presence of hydrogen on Au/TiO_2 catalyst: an FTIR-MS study, Catalysis Letters, 111 (2006) 87-95.

[129] F. Boccuzzi, A. Chiorino, M. Manzoli, D. Andreeva, T. Tabakova, FTIR study of the low-temperature water-gas shift reaction on Au/Fe_2O_3 and Au/TiO_2 catalysts, Journal of Catalysis, 188 (1999) 176-185.

[130] J.T. Calla, M.T. Bore, A.K. Datye, R.J. Davis, Effect of alumina and titania on the oxidation of CO over Au nanoparticles evaluated by ^{13}C isotopic transient analysis, Journal of Catalysis, 238 (2006) 458-467.

[131] M. Ojeda, B.Z. Zhan, E. Iglesia, Mechanistic interpretation of CO oxidation turnover rates on supported Au clusters, Journal of Catalysis, 285 (2012) 92-102.

[132] M. Haruta, S. Tsubota, T. Kobayashi, H. Kageyama, M.J. Genet, B. Delmon, Low-temperature oxidation of CO over gold supported on TiO_2, alpha-Fe_2O_3, and Co_3O_4, Journal of Catalysis, 144 (1993) 175-192.

[133] H. Berndt, I. Pitsch, S. Evert, K. Struve, M.M. Pohl, J. Radnik, A. Martin, Oxygen adsorption on Au/Al_2O_3 catalysts and relation to the catalytic oxidation of ethylene glycol to glycolic acid, Applied Catalysis a-General, 244 (2003) 169-179.

[134] D.G. Barton, S.G. Podkolzin, Kinetic study of a direct water synthesis over silica-supported gold nanoparticles, Journal of Physical Chemistry B, 109 (2005) 2262-2274.

[135] L. Ilieva-Gencheva, G. Pantaleo, N. Mintcheva, I. Ivanov, A.M. Venezia, D. Andreeva, Nano-Structured Gold Catalysts Supported on CeO_2 and CeO_2-Al_2O_3 for NO_x Reduction by CO: Effect of Catalyst Pretreatment and Feed Composition, Journal of Nanoscience and Nanotechnology, 8 (2008) 867-873.

[136] Y.N. Shen, X.Z. Yang, Y.Z. Wang, Y.B. Zhang, H.Y. Zhu, L. Gao, M.L. Jia, The states of gold species in CeO_2 supported gold catalyst for formaldehyde oxidation, Applied Catalysis B-Environmental, 79 (2008) 142-148.

[137] S. Lin, M.A. Vannice, Gold dispersed on TiO_2 and SiO_2 - Adsorption properties and catalytic behavior in hydrogenation reactions, Catalysis Letters, 10 (1991) 47-62.

[138] L. Ilieva, G. Pantaleo, G. Munteanu, A.M. Venezia, D. Andreeva, Temperature programmed desorption of CO and NO over gold/ceria catalysts for NO_x reduction, Revue Roumaine De Chimie, 52 (2007) 975-+.

[139] A. Hussain, D. Curulla Ferré, J. Gracia, B.E. Nieuwenhuys, J.W. Niemantsverdriet, DFT study of CO and NO adsorption on low index and stepped surfaces of gold, Surface Science, 603 (2009) 2734-2741.

[140] A.V. Bukhtiyarov, R.I. Kvon, A.V. Nartova, V.I. Bukhtiyarov, An XPS and STM study of the size effect in NO adsorption on gold nanoparticles, Russian Chemical Bulletin, 60 (2012) 1977-1984.

[141] A. Ihs, K. Uvdal, B. Liedberg, Infrared and photoelectron spectroscopic studies of ethyl and octyl xanthate ions adsorbed on metallic and sulfidized gold surfaces, Langmuir, 9 (1993) 733-739.

[142] J.F. Geng, B.F.G. Johnson, M.D.R. Thomas, D.S. Shephard, L. Jiang, Behaviour of two-dimensional arrays of gold nanoparticles under H_2S: agglomeration and regeneration, Inorganica Chimica Acta, 330 (2002) 33-37.

[143] L. Feria, J.A. Rodriguez, T. Jirsak, F. Illas, Interaction of SO_2 with Cu/TiC(001) and Au/TiC(001): Toward a new family of $DeSO_x$ catalysts, Journal of Catalysis, 279 (2011) 352-360.

[144] M.M. Schubert, S. Hackenberg, A.C. van Veen, M. Muhler, V. Plzak, R.J. Behm, CO oxidation over supported gold catalysts-“Inert” and “active” support materials and their role for the oxygen supply during reaction, Journal of Catalysis, 197 (2001) 113-122.

[145] R. Zanella, A. Sandoval, P. Santiago, V.A. Basiuk, J.M. Saniger, New preparation method of gold nanoparticles on SiO_2, Journal of Physical Chemistry B, 110 (2006) 8559-8565.

[146] Z.P. Hao, L.B. Fen, G.Q. Lu, J.J. Liu, L.D. An, H.L. Wang, In situ electron paramagnetic resonance (EPR) study of surface oxygen species on Au/ZnO catalyst for low-temperature carbon monoxide oxidation, Applied Catalysis a-General, 213 (2001) 173-177.

[147] J.D. Grunwaldt, A. Baiker, Gold/titania interfaces and their role in carbon monoxide oxidation, Journal of Physical Chemistry B, 103 (1999) 1002-1012.

[148] J.-D. Grunwaldt, M. Maciejewski, O.S. Becker, P. Fabrizioli, A. Baiker, Comparative study of Au/TiO_2 and Au/ZrO_2 catalysts for low-temperature CO oxidation, Journal of Catalysis, 186 (1999) 458-469.

[149] K. Qian, W.X. Huang, Z.Q. Jiang, H.X. Sun, Anchoring highly active gold nanoparticles on SiO_2 by CoO_x additive, Journal of Catalysis, 248 (2007) 137-141.

[150] M.P. Casaletto, A. Longo, A.M. Venezia, A. Martorana, A. Prestianni, Metal-support and preparation influence on the structural and electronic properties of gold catalysts, Applied Catalysis a-General, 302 (2006) 309-316.

[151] H.T. Beyene, F.D. Tichelaar, M.A. Verheijen, M.C.M. van de Sanden, M. Creatore, Plasma-Assisted Deposition of Au/SiO_2 Multi-layers as Surface Plasmon Resonance-Based Red-Colored Coatings, Plasmonics, 6 (2011) 255-260.

[152] P.M. Arnal, M. Comotti, F. Schuth, High-temperature-stable catalysts by hollow sphere encapsulation, Angewandte Chemie-International Edition, 45 (2006) 8224-8227.

[153] J.J. Luo, W. Chu, H.Y. Xu, C.F. Jiang, T. Zhang, Low-temperature CO oxidation over $CuO-CeO_2/SiO_2$ catalysts: Effect of CeO_2 content and carrier porosity, Journal of Natural Gas Chemistry, 19 (2010) 355-361.

Chapter II Materials and methods

2.1 Synthesis of materials

2.1.1 Materials

Sodium borohydride ($NaBH_4$) (Across Organics, >98%), poly(vinyl alcohol) (PVA) (Aldrich, Average M_W = 50,000 g/mol, >90%, hydrolyzed), chloroauric acid ($HAuCl_4$) (Aldrich, 99.99% purity), H_2SO_4 (Aldrich, >98%) were utilized in this work. Tetraethyl orthosilicate (100%) was purchased from VWR BDH Prolabo. The ammonia solution (28-30% in water) and ethanol (EtOH) were purchased from Carlo Erba Reagents.

2.1.2 Preparation of gold colloid

The gold colloid solution was prepared from $HAuCl_4$ solution reduced by $NaBH_4$ in the presence of PVA. Certain amounts of $HAuCl_4$ solution and PVA (1 wt%) was added together into a 250 ml beaker. After stirring at 750 r/min for 20 min, the $NaBH_4$ solution was then injected into the mixed liquid rapidly. The color of the solution changed from light yellow to vivid color depending on the preparation conditions. The detail of the preparation conditions are listed in Table 2.1 and Table 2.2.

Table 2.1 The list of Au colloid under different preparation conditions of system I.

Sample	Concentration (M)[a]		Agent	T[b]	Sample	Concentration (M)		Agent	T
	$HAuCl_4$	$NaBH_4$				$HAuCl_4$	$NaBH_4$		
I.1-ref[c]	10^{-4}	0.1	H_2O	25°C	I.5-GH[d]	10^{-2}	0.1	H_2O	25°C
I.2-Et	10^{-4}	0.1	Ethanol	25°C	I.6-GM[c]	10^{-3}	0. 1	H_2O	25°C
I.3-35	10^{-4}	0.1	H_2O	35°C	I.7-SL[c]	10^{-3}	0.01	H_2O	25°C
I.4-50	10^{-4}	0.1	H_2O	50°C					

[a] The molar ratio between $NaBH_4$ and Au is 5:1, and the weight ratio between PVA and gold is 5: 1. The 1 wt% PVA is dissolved in water. [b] Temperature for preparation of Au colloid. [c] Before testing the UV-vis spectra of all the colloids, the volumes are transferred to be the same by diluting the solution. [d] For better memory and

identification of the samples, every sample in this system is labeled as I.n-special condition. Here the I.5-GH, I.6-GM, and I.7-SL are referred to gold colloids prepared by using gold precursor with higher concentration (GH, 10^{-2} M), gold precursor with middle concentration (GM, 10^{-3} M), and sodium borohydride with lower concentration (SL) comparing with the reference sample I.1-ref, respectively.

The as-prepared gold colloids were tested by UV-vis Spectrophotometer 10 min, 24 h, and 15 days after the $NaBH_4$ solution was added. During the measurement of the UV-vis spectra, every time the tested colloids are diluted into the same concentration and 50 drops were used for test.

Table 2.2 The preparation condition of Au colloid with various amounts of $NaBH_4$ or PVA of system II.

Sample	Ratio			Sample	Ratio		
	gold	PVA[a]	$NaBH_4$[b]		gold	PVA[a]	$NaBH_4$[b]
II.1-S0.5[c]	1	5	0.5	III.1-P0	1	0	5
II.2-S1	1	5	1	III.2-P0.5	1	0.5	5
II.3-S2	1	5	2	III.3-P0.85	1	0.85	5
II.4-S3	1	5	3	III.4-P3	1	3	5
II.5-S5[d]	1	5	5	III.5-P5[d]	1	5	5
II.6-S10	1	5	10	III.6-P10	1	10	5

[a] The weight ratio between PVA and Au. The 1 wt% PVA is dissolved in water. [b] The molar ratio between $NaBH_4$ and Au. The concentration of $NaBH_4$ solution is 0.1 M. [c] For better memory and identification of the samples, every sample in Table 2.2 is labeled as II.n-Sx (x is molar ratio of sodium borohydride: Au) and III.n-Py (y is weight ratio of PVA: Au). [d] The preparation of II.5-S5 and III.5-P5 is totally the same of the I.6-GM Table 2.1, unless that the I.6-GM is diluted to be the same volume of I.1-ref in Table 2.1.

2.1.3 Synthesis of Stöber silica

The Stöber silica was prepared according to the previous work by Stöber et al [1]. Certain amounts of TEOS and 50 ml EtOH were added into a 250 ml baker. The scheduled amounts of H_2O and $NH_3 \cdot H_2O$ in 50 ml EtOH were injected at one time into the baker without contacting

the baker wall (this procedure is very important for getting homogeneous silica globules). The stirring speed was controlled at 1100 r/min for 5 min to get a homogeneous blend of reactant and then was slowed down to 500 r/min for uniform generation of spherical silica. The above solution changed from colorless to transparent opalescent after 1 h and was stirred over night at 25 ^{o}C. After in situ dried in the baker at 60 ^{o}C, the powder was washed and filtered with water and ethanol. During the whole process, the silica went through no further centrifugation. The powder was at last dried, collected, and marked as SSn (n=1-5). The corresponding information for preparing the Stöber silica is listed in Table 2.3. Five types of silica with different spherical diameters were successfully prepared and the average size of the spherical Stöber silica was easily controlled by varying the reactant amounts, e.g. the amounts of H_2O, the dosages ratio between TEOS and ammonia.

Table 2.3 The detailed information of the as-prepared Stöber silica-the from different dosages of reactants.

Stöber	Dosages of reactants (ml)				Stöber	Dosages of reactants (ml)			
silica	TEOS	$NH_3 \cdot H_2O$	H_2O	EtOH	silica	TEOS	$NH_3 \cdot H_2O$	H_2O	EtOH
SS1	5	5	1	110	SS4	5	10	10	110
SS2	5	3	1	110	SS5	5	15	10	110
SS3	5	5	10	110					

2.1.4 Synthesis of gold nanoparticles supported by Stöber silica

The Stöber silica supported gold nanoparticles were prepared by the modified incipient wetness impregnation. The theoretical gold loading was aimed to be 1 wt%. After 1 g Stöber silica was introduced into the as-prepared colloidal gold nanoparticles, the pH of the gold was adjusted to about 1 with 0.1 M H_2SO_4 solution. After stirred for 10 min, the mixture solution was then centrifuged at 3000 r/min for 10 min. After washing and filtered, the gold nanoparticles supported on the Stöber silica was at last obtained, and marked as Au/SSn (n=1 or 5). For comparison, the gold nanoparticles supported on the commercial silica were also applied as the support material. The only difference of the preparation is than there is no pH adjusting procedure for the commercial silica supported gold nanoparticles. The comparison

sample was labeled as Au/CS below. The three silica supported gold samples were further calcined in pipe furnace under air at 300 ^{o}C for 4 h. The catalysts were labeled as Au/SS1-C, Au/SS5-C, and Au/CS-C, corresponding gold nanoparticles supported on SS1, SS5, and commercial silica after calcination.

2.1.5 Synthesis of metal (oxide) doped M-Au/SS5 samples

The metal (oxide) doped M-Au/SS5 samples (M=Co, Fe, Cu) were prepared. The above as-prepared Au/SS5 (1 g, without calcination) sample was put into a 50 ml baker. The certain amounts of initial metal nitrate ($Co(NO_3)_3 \cdot 6H_2O$), $Fe(NO_3)_3 \cdot 9H_2O$, or $Cu(NO_3)_2 \cdot 3H_2O$) were dissolved into 10 ml water and mixed with the Au/SS5 sample. After 20 min stirring for the uniform blend of the solution, the 0.1 M $NaBH_4$ solution ($NaBH_4$: M=5: 1, molar ratio) was added into the mixture to reduce the metallic ions into metal. The transformation of color was observed gradually along with the injection of $NaBH_4$. After stirring for 0.5 h, the mixed solution was washed and filtered by water for several times to remove the excessive Na^+ and other pollutants. The powder was dried in water bath at 60 ^{o}C over night. The obtained dry powders are noted as Au/SS5@M (Au/SS5@Cu, Au/SS5@Fe and Au/SS5@Co, respectively). Before the reaction tests, each sample was calcined under air at 300 ^{o}C for 4 h to eliminate the organic compounds during preparation. The corresponding samples are named as Au/SS5@Cu-C, Au/SS5@Fe-C and Au/SS5@Co-C, respectively.

2.2 Characterization and instruments

2.2.1 Ultraviolet-visible (UV-vis) spectroscopy

The Ultraviolet-visible spectroscopy is the adsorption spectroscopy or reflectance spectroscopy of samples operated in the range of visible or near-infrared.

√ Basic theory of ultraviolet-visible absorption

In the tested scope of electromagnetic spectrum, electronic transitions take place. The energy from incident light can be absorbed by the molecules possessing π- and nonbonding electrons which are stimulated into antibonding orbital. The molecules that are facile to be stimulated generally absorb incident light at longer wavelength.

Beer-Lambert law

This principle is useful for estimating the concentration of adsorption species in the tested sample.

$$A = \log_{10}(I_0/I) = \varepsilon \cdot c \cdot L \quad (2.1)$$

In equation (2.1), A is the absorbance that can be known from the UV-vis spectra. I_0 is the transmitted intensity of the incident light at certain wavelength. L corresponds to the path from the incident light to the sample. c is the tested concentration of the adsorption species. And ε is a parameter named extinction coefficient, which is consistent for a solution at the same temperature and pressure.

The Beer-Lambert Law is very beneficial for many compounds. However, it is sometimes inapplicable for some complex molecules such as organic compounds.

The UV-vis spectrophotometer records the intensity of the light passing through the sample which is marked as I. The initial intensity of the incident light is labeled as I_0. The ratio between the intensity of incident light and reflected light (I/I_0) is named the transmittance (marked as T). The absorbance (A) can be expressed as equation (2.2):

$$A = -\log (T\%/100\%) \quad (2.2)$$

√ Double beam UV-vis spectrophotometer

The UV-vis spectrophotometer used in this work is UV-1800 double beam with absorbance

range of -4~4 Abs and transmittance of 0-400%. The light source is consisted by 20 W halogen lamp and deuterium lamp. The measurements can be taken in the range of 290-1100 nm. The scheme of the double beam instrument is illustrated in Figure 2.1. The incident light can be divided into two beams by a beam splitting before it gets through the sample, one passing through the reference cell and the other going through the sample cell. The light through the reference cell is viewed as zero absorbance/100% transmission, and the result from the detector comes from the sample cell.

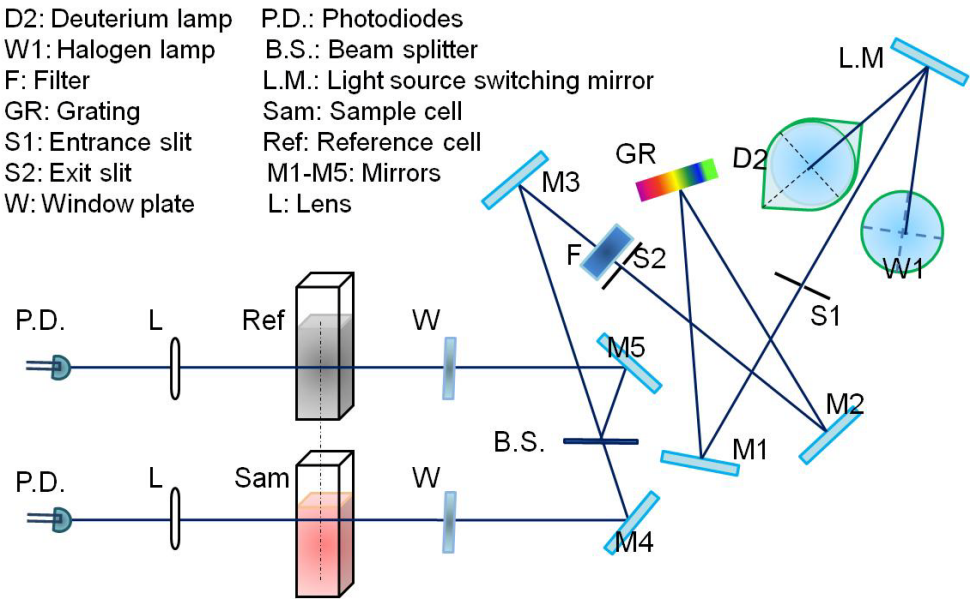

Figure 2.1 Schematic of double beam UV-1800 optical system.

√ Sample preparation for the UV-vis measurement

Before measured by the UV-vis, the as-prepared gold colloids in the same system were diluted into the same concentration for a better comparison. 50 drops of tested colloid was added into the 1.0 cm quartz cells and put into the chamber. The data were collected in the range of 290-1100 nm.

2.2.2 N_2 adsorption/desorption measurement

√ Theory of gas molecules adsorption over materials

The porous structure parameters including surface area, pore size distribution and average pore volume are important for estimating the textures of materials. The specific surface area is consisted by the internal irregular opening and small holes, and cannot be calculated directly from the size of bulk particles.

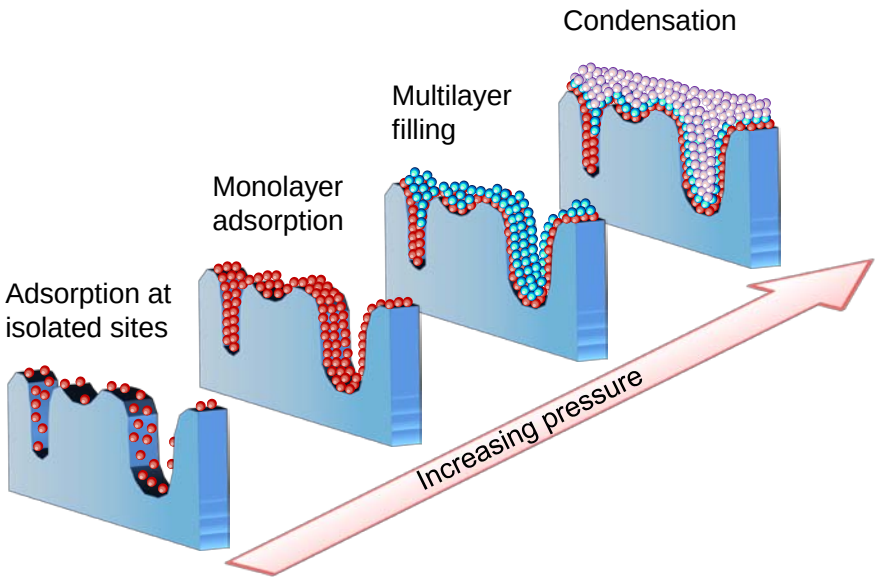

Figure 2.2 Adsorption of gas molecules over porous materials.

The specific surface area is an important parameter for estimating the thermal properties, chemical stability, and adsorption capacity. The adsorption of inert gases over the atoms in the tested materials can help understanding the surface area. The adsorbed amount is defined as X, which is not only a function of exposed surface but also related to the temperature, gas pressure and the interaction intensity between gas and solid. Since the interaction between most of the gas and solid is very weak, the low temperature is necessary for the sufficient adsorption to occur and cover the entire surface. The surface adsorption amount is generally increases with the raise of pressure as a linear relationship. However, when the adsorbed gas cover the entire

surface with the thickness of one atom (the amount of monolayer adsorption is named as X_m), the gas adsorption do not finished but then adsorbed as multilayer adsorption with pressure as shown in Figure 2.2.

√ The measurement method

The surface area, average pore volume and the average pore size were measured by a Tristar Micromeritics sorptometer as shown in Figure 2.3, which allows the simultaneous degas of six samples and analysis of three samples. The liquid nitrogen was used as adsorbate at liquid nitrogen temperature (-196 ^{o}C). Before measurement, each sample was outguessed at 250 °C for 10 h in order to desorb impurities and moisture on its surface and in the inner pores.

Figure 2.3 The Tristar Micromeritics sorptometer at ICPEES in University of Strasbourg. The machine on the left side is for the degass of samples which is possible for six samples simultaneously degass. The machine on the right side is for the analysis of the porosity, which can detect three samples ensemble.

2.2.3 Superficial detection by XPS

√ Constitution of XPS instrument and the main theory

The X-ray photoelectron spectroscopy (XPS) is a quantitative technique for measuring the

composition of surface elements, the ratio and homogeneity between elements, and their corresponding valence states. This technique should be carried out under ultrahigh vacuum condition and can generally detect the 1-10 nm subsurface.

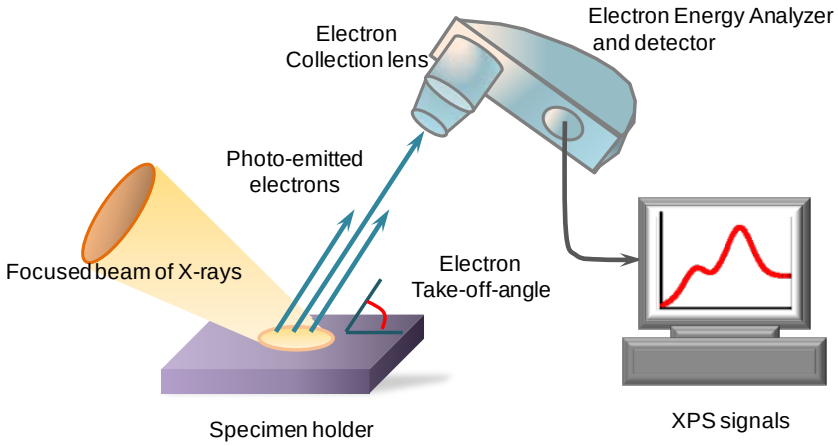

Figure 2.4 The major constitution of monoenergetic XPS instrument.

The basic theory of the XPS is that the inner electrons or valence electrons in the atoms or molecules are excited as photo-emitted electrons as shown in Figure 2.4. The focused beam of light of X-ray is usually the monochrome Al Kα (1486.6 eV, the X-ray for this work) with 20-200 μm beam of light or Mg Kα (1253.6 eV) with 10-30 μm beam of light. The electrons are then detected by the apparatus. The energy at certain wavelength is known and the binding energy of the emergent electrons can be calculated by the equation below:

$$E_{BD} = E_{photon} - E_{kinetic} + \Phi \quad (2.3)$$

The E_{BD} is binding energy of electrons, the E_{photon} is the energy of photons from X-ray, the $E_{kinetic}$ is the kinetic energy of measured electrons, and Φ is parameter of the Energy Disperse Spectroscopy. The photoelectron spectroscopy can thus be obtained by making the binding energy as the x-axis and relative intensity as the y-axis.

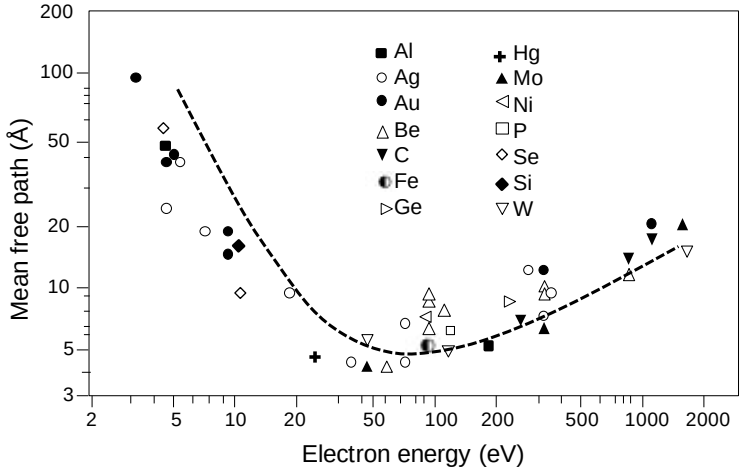

Figure 2.5 The mean free path of electrons of different metal.[2]

Generally speaking, the surface sensitivity of analysis depends on the detected radiation. The characteristic electrons are emitted from the electron beam or the X-ray irradiation, and then arrive the electron energy analyzer and detector. Although the X-ray photons or the high-energy electrons bombarding the surface can permeate as deep as ~ 1 μm, only small amount of electrons overflow the surface maintaining the initial energy. The detectable emergent electrons without energy lose can be only from about 1-8 nm on the surface. In fact, the electrons in the deep of the solid also have chances to be overflowed, however the energy of which will be lost because of the collision with other electrons during the overflow path. The experimental results suggested that the inelastic scattering cross section of electrons in the solid is huge, and the inelastic mean free path (IMFP, the average distance of the paths between two times of valid inelastic collision of electrons possessing certain energy) is short as shown in Figure 2.5 for only lower than 10 nm. In this case, only small amount of electrons at the superficial surface can escape to the surface with unchanged characteristic energy. The XPS is really sensitive to the surface contamination, and this is also why the ultra high vacuum is in use- to remove the contamination from the surface.

√ The current condition of XPS instrument in this work

The X-ray photoelectron spectra (XPS) were recorded on a XSAM800 spectrometer with an Al Kα (1486.6 eV, 15mA) X-ray source. Charging effects were corrected by adjusting the binding energy of Si 2p peak to 103.4 eV. In this work the standardization did not apply the carbon contamination of 284.6 eV because of the present of satellites peaks ranging from 293-285 eV, making the definition of carbon peaks to be complex. In order to get a more precise identification of the peaks, the separation of overlapped peaks for the same element was based on the following principles: (1) the width of the peak is consistent, (2) the binding energy of the corresponding species is generally consident with an allowable fluctuation of 0.3 eV, (3) the energy difference from spin-orbit splitting of metal species, e.g. 3.65 eV between Au $4f_{7/2}$ and $4f_{5/2}$, should be identical during different data anlysis.

√ Quantitative analysis

During the XPS measurement of samples, not only the qualitative detection of the elements and their states are required, the ratio between each element and the contents are also demanded for understanding the composition of material. The quantitative analysis by XPS is transformation of the intensity/area of signal peaks into the ratio of corresponding elements. The practical methods for quantitative analysis of XPS mainly include the standard method, the first principle model and the sensitivity method. In this work we use the sensitivity method for estimating the contents of each element.

The sensitivity method is applying the intensity of certain elements as reference, measure the relative intensity of other elements, and thus get the relative contents of the other elements, which is herein a semi-quantitative analysis method.

For the single-phase homogeneous surface with unlimited thickness, the surface area of number j peak corresponding to i element (I_{ij}) can be described as following:

$$I_{ij} = K \cdot T(E) \cdot L_{ij}(\gamma) \cdot \sigma_{ij} \cdot n_i \cdot \lambda(E)\cos\theta \quad (2.4)$$

$$\text{Thus } n_i = I_{ij}/K \cdot T(E) \cdot L_{ij}(\gamma) \cdot \sigma_{ij} \cdot \lambda(E)\cos\theta = I_{ij}/S_{ij} \quad (2.5)$$

$$S_{ij} = K \cdot T(E) \cdot L_{ij}(\gamma) \cdot \sigma_{ij} \cdot \lambda(E)\cos\theta \approx T(E) \cdot L_{ij}(\gamma) \cdot \sigma_{ij} \cdot \lambda(E) \quad (2.6)$$

$L_{ij}(\gamma)$, the asymmetry factor of j orbit of the i element, σ_{ij}, the cross section of photo ionization of the j orbit in the i element, n_i, the atom concentration of the i element, $\lambda(E)$, the inelastic mean free path of the photoelectron, θ, the angle between the surface and the emitted photoelectrons as shown in Figure 2.7. T(E), the transfer function of the analyzer, and K and a are the parameters of the apparatus.

The S_{ij} is the sensitivity factor of element. The 1s orbit of F element can be made as references as $S_{F1s} = 1$. In this case, for a sample with two kinds of elements a and b, the sensitivity of which is known as S_a and S_b, together with the peak areas of I_a and I_b, the atoms ratio can be calculated as:

$$n_a/n_b = \frac{I_a/I_b}{S_a/S_b} \quad (2.7)$$

The general atom concentration of an element is:

$$C_a = \frac{I_a/S_a}{\sum_i I_i/S_i} \quad (2.8)$$

2.2.4 SEM and TEM

The Scanning electron microscopy (SEM) is a technique scanning the surface of samples by the electron beam. The 3D high resolution images of material surface can be obtained by this technique. The SEM images in this work were carried out on a JEOL 6700F microscope working at 10 kV accelerated voltage. The solid was fixed on the sample holder by a graphite paste for examination.

In the Transmission electron microscope (TEM), electron beam after speed-up is cast onto a very thin layer of sample. The schema of the apparatus is shown in Figure 2.6. The electrons collide with the atoms in the sample and then change the moving orientation and perform the solid angle scattering. The scattering angle depends on the density and thickness of the sample, which forms the images with different intensity. The images can be modified and focused on the image device. The distinguish ability of the TEM is much higher than the optical microscope due to the very short De Broglie wavelength of electrons, which can be modified to about 0.1-0.2 nm. Therefore, the fine structure or even a series of atoms in the target sample can be observed by this technique. The TEM is an important technique in many disciplines corresponding to physics, chemistry, and biology. It is also an indispensible technique for the investigation of nano-scale materials especially in our current work concerning the growth and function of gold nanoparticles. It is a most directive path for surveying the morphology of the gold nanoparticles.

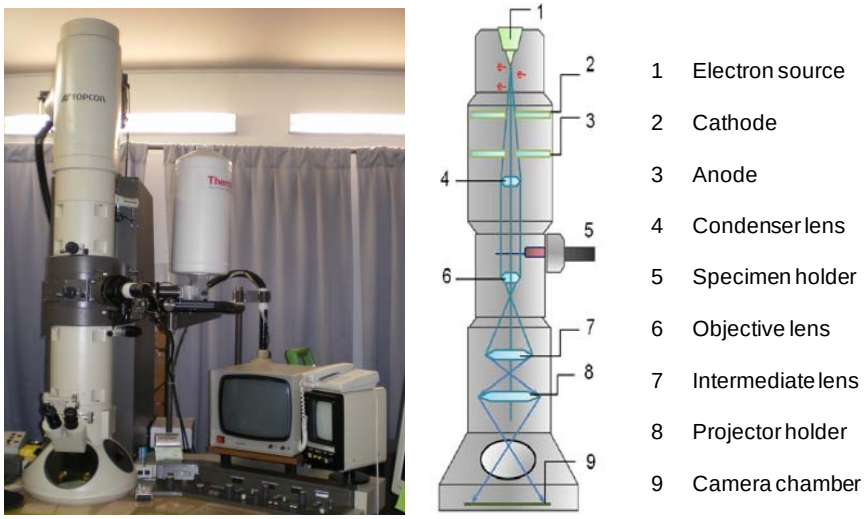

Figure 2.6 The Transmission electron microscopy and the schema of the apparatus.

The TEM images in this work are operated on a Topcon EM002B microscope (accelerating voltage of 200 kV) as shown in Figure 2.6, using a 2048 × 2048 pixels Ultrascan cooled CCD array detector, and a high tilt sample holder. The sample preparation for tomography TEM was done according to the following process: the solid was crushed in a mortar into a very

fine powder. The powder was then dispersed in water with gentle shake. A drop of the solution was deposited on a holey copper grid and the solvent was evaporated at room temperature before introducing of the sample holder into the microscope chamber.

2.2.5 X-ray diffraction

The atomic planes of a crystal cause an incident beam of X-rays to interfere with one another as they leave the crystal. The phenomenon is called X-ray diffraction. The X-ray diffraction is a useful technique for measuring the average distance between layers or atoms, determine the orientation of single crystal, detect the structure of novel material, and find out the sizes and shapes of grains. The XRD analysis in this work is carried out on a Bruker D-8 Advance Diffractometer with a Cu Kα radiation in the range of 2θ = 20-80^o.The sample is crushed into powder and deposited on a glass plate for analysis. The average size of gold crystalline grains is calculated from Au(111) crystal face by Scherrer Equation:

$$d = \frac{0.89\lambda}{B\cos\theta} \times \frac{180^o}{\pi} \quad (2.9)$$

In which d is the average size of crystalline grains, λ is the wavelength of incident X-ray, and B is the full width at half maximum of the diffraction peak.

2.2.6 Operando Inferred Spectroscopy

The operating principal of Inferred Spectroscopy (IR) is according to the different frequency of chemical bonds due to the different vibration energy level. The resonance frequency or the vibrational frequency depends on the shapes of equipotential plane of molecules, the atomic mass, and the coupling. The Operando Inferred Spectroscopy (Operando IR) is recorded using a Bruker Vertex 70 infrared spectrophotometer with 2 cm^{-1} resolution under desired atmosphere of gases. Small amount of sample is mixed with KBr, and grinded into fine powder. The data is recorded from 4000 - 600 cm^{-1}.

2.3 Measurement of catalytic performances

2.3.1 CO oxidation

The CO oxidation was carried out under atmospheric pressure in a fixed bed reaction. 50 mg or 100 mg catalyst is added into the U-shaped quartz micro-reactor. The reaction flow is consisted by 1.5 vol.% CO and 5 vol.% O_2 balanced with He at the speed of 50 ml/min controlled by Tylan flow controllers. The temperature ranges from room temperature to 300^{o}C monitored and controlled by a Eurotherm system. The amounts of CO and CO_2 are detected by a TDX-01 chromatographic column. The conversion of CO is calculated by the following equation:

$$C_{CO} = \frac{CO^{in} - CO^{out}}{CO^{in}} \times 100\% \quad (2.10)$$

CO^{in} and CO^{out} are the initial inlet amount and the outlet amount of the CO gas, respectively.

2.3.2 H_2S selective oxidation

The selective oxidation of H_2S is performed under atmospheric pressure under different temperature, the apparatus of which is displayed as Figure. 2.7. 100 mg catalyst SiC is fixed with silica wool in the middle of Pyrex (18 mm inner diameter and 600 mm height) mixing with 200 mg for the seek of lower pressure drop and better contact surface.[3] The mixture of gases goes through the vertical bed thoroughly. The temperature of the furnace is detected by a K-type thermocouple and a Minicor regulator. The flow rate of gas mixture is composed of H_2S (1 vol.%), O_2 (2.5 vol.%), water vapor (30 vol.%) and balanced by He, which are monitored by Brooks 5850TR flowmeters linked to a control unit. The gas hourly space velocity (GHSV) varies from 3000 to 4000 h^{-1}.

$$H_2S + \frac{1}{2}O_2 \rightarrow H_2O + \frac{1}{n}S_n \quad \Delta H = -222\ kJ/mol \quad (2.11)$$

The water vapor (30 vol.%) is introduced by He bubbling method in order to catch up with the industrial conditions of Claus reaction, in which the water is produced and remains in the gas phase during the reaction. The produced sulfur can be melted down by using a heating tape and collective for continuable reaction. The conversion of H_2S and the selectivity for S can be obtained from the following equations:

$$C_{H_2S} = \frac{H_2S^{in} - H_2S^{out}}{H_2S^{in}} \times 100\% \quad (2.12)$$

$$S_S = \left(1 - \frac{SO_2^{out}}{H_2S^{in}}\right) \times 100\% \quad (2.13)$$

$$Y_s = C_{H_2S} \cdot S_S \quad (2.14)$$

The C_{H2S}, S_S, and Y_S are corresponding to the conversion of H_2S, the selectivity of S, and the yield of S, respectively; the H_2S^{in}, H_2S^{out}, and SO_2^{out} means the injected amount of H_2S, the detected amount of H_2S after reaction, and the detected SO_2 after reaction.

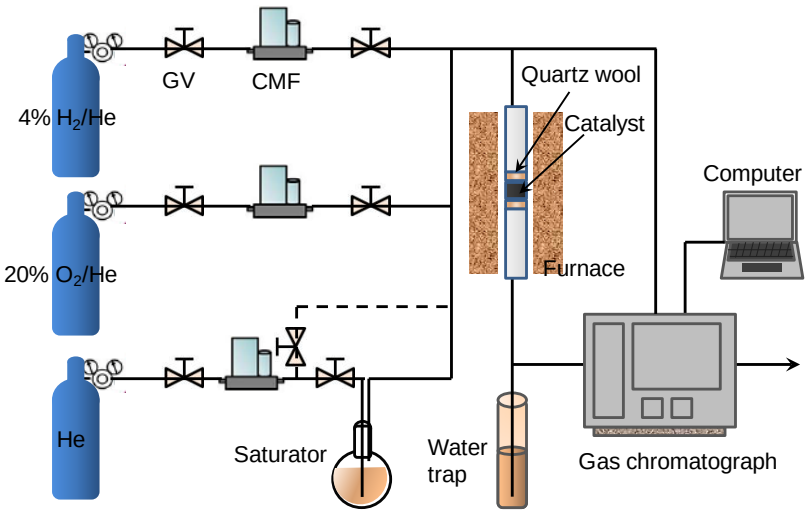

Figure 2.7 Schematic diagram of the apparatus for selective H_2S oxidation.

Analysis of the inlet and outlet gases was performed on-line using a Varian CP-3800 gas chromatograph equipped with a Chrompack CP-SilicaPLOT capillary column allowing the detection of O_2, H_2S, H_2O and SO_2, a catharometer detector (TCD) and a calibrated six-port

loop (250 ml). Before the reaction, the reactor was purged with helium at room temperature until no trace of oxygen could be detected by gas chromatography at the exit of the reactor, then the dry helium flow was replaced by the one containing steam. The catalyst was heated from room temperature to the reaction temperature and the wet helium flow was replaced by the reactant flow.

$$S_{H_2S} = \frac{H_2S^{in} - H_2S^{out}}{H_2S^{in}} \times 100\% \quad (2.15)$$

Bibliography

[1] W. Stöber, A. Fink, E. Bohn, Controlled growth of monodisperse silica spheres in the micron size range, Journal of Colloid and Interface Science, 26 (1968) 62-69.

[2] D. Briggs, M.P. Seah, Practical surface analysis, 2nd ed. ed., Wiley, Chichester, 1990.

[3] Y.F. Liu, L.D. Nguyen, T.H. Tri, Y. Liu, T. Romero, I. Janowska, D. Begin, P.H. Cuong, Macroscopic shaping of carbon nanotubes with high specific surface area and full accessibility, Materials Letters, 79 (2012) 128-131.

Chapter III Preparation and practical characterization of gold colloids

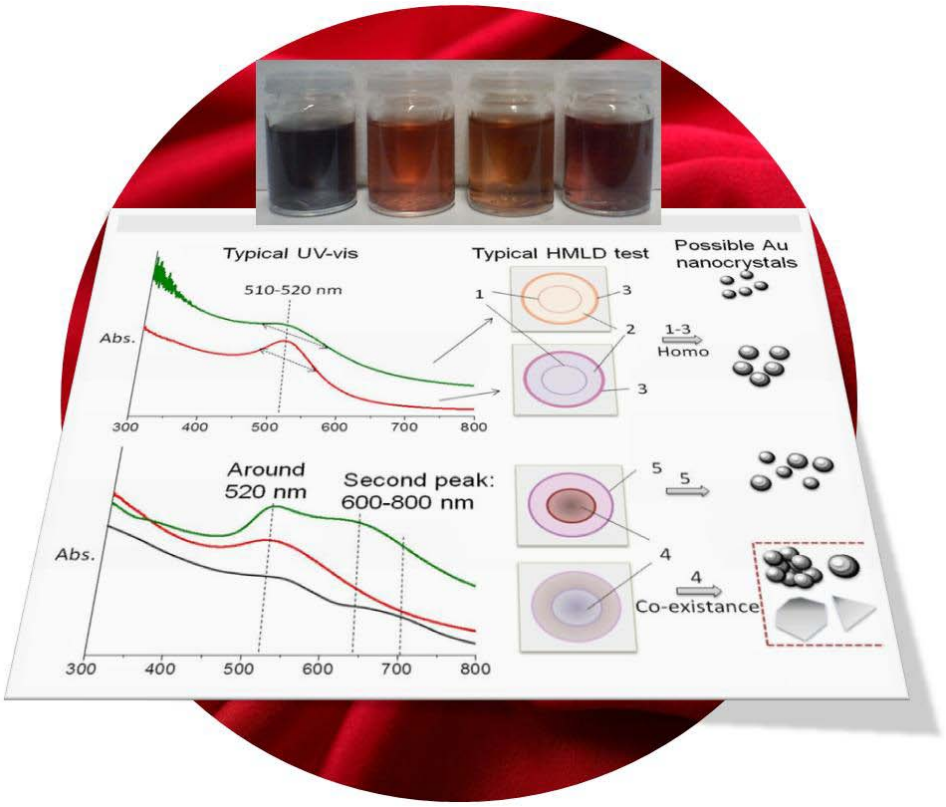

- Gold colloids were made by using $NaBH_4$ as reducer and PVA as protector.
- Small and homogeneous gold nanoparticles (Au-NPs) were finally synthesized.
- Forms and sizes of Au-NPs were roughly estimated from color and UV spectra.
- Home-made liquid diffusion (HMLD) is helpful for comparing and choosing small Au-NPs before expensive TEM.

As a fundamental work of the thesis, this chapter was focused on how to prepare the satisfactory gold colloid with very small gold nanoparticles (e.g. about 2.5 nm) and narrow size distribution. The gold colloid was synthesized by reduction of chloroauric acid with sodium borohydride ($NaBH_4$) under polyvinyl alcohol (PVA) protection. The growth and stability of gold colloids were controlled by modifying the reaction agent, the reaction temperature, the reactant concentration, and the addition amounts of $NaBH_4$ and PVA. The different operation conditions influencing the formation of gold nanoparticles were discussed in detail. Appropriate ratio of PVA: Au: $NaBH_4$ of 0.0197: 1: 5 of molar ratio (PVA: Au weight ratio is equal to 5: 1) reacting in water at room temperature (25^oC) was helpful to produce small colloidal gold nanoparticles. For a simple and effective estimation, the techniques including color observation, UV-visible spectrometry, and home-made liquid distribution (HMLD) test were applied to comparing and understand the formation of different gold colloid. The results turn out that the applying of HMLD test was proved very helpful for choosing gold colloid with fine and homogeneous particles.

3.1 Introduction

Gold colloid is a kind of suspension that consisted of gold particles (Au-NPs) less than 100 nm in fluid such as water. In fact, gold colloid has been applied since very ancient periods, e.g. as colorant for staining glass. However it was really understood from aspect of material science until the amazing discovery of Faraday that the color resulted from the sub-micrometer-size of gold particles.[1] Zsigmondy was then prepared the gold colloid in a dilute solution, and gained the Nobel Prize in Chemistry 1925 due to him outstanding work in this filed.[2] The theories established by Mie and many other researchers, such as the famous Mie scattering theory for scattering and absorption by spherical particles, further helped understanding the mechanism of gold colloid preparation and application.[3, 4] Gold colloid can be synthesized by reduction of gold precursor (chloroauric acid in general) under reducer agent with or without protect agent. The simple method was provided by Turkevich[5] with sodium citrate as both reducer and protector, obtaining Au-NPs ranging from 10-20 nm or even larger. Since the citrate reduction possesses lots of advantages such as low price of the reagents, non-toxic water solvent, and low-pollution in the reaction,[6] it remains as a most available method for preparing gold colloid in the current work. But how to reduce the size of nanoparticles is a challenge of this method. Sodium borohydride ($NaBH_4$) is also applied as a very strong reducer for acquiring colloidal metal nanoparticles.[7-10] During the preparation of gold colloid by using $NaBH_4$ as reducer, the organic compounds such PVA, PVP, dendrimer are always applied as the protectors to stable the Au-NPs.[11-15] Unusual methods by using complex organic compounds and expensive instrument are also provided recently for preparing homogeneous smaller gold nanoparticle.[16-19]

The absolute superiority of colloidal Au-NPs in catalysis filed is that, the size distribution and shapes of Au nanoparticles can be previously understood and controlled before loading onto the supports. It is well-known that size dependent effect acting as one important part varying the optical properties, is a most essential problem that must be considered for supported

Au-NPs,[20, 21] e.g. an excellent gold catalyst for CO oxidation possesses very narrow unimodal size distribution of Au-NPs around 2.5 nm.[22-24] Theoretically, the supported Au-NPs from colloid method with desired size distribution and shape can be obtained by varying the preparation conditions such as reaction temperature, pH value, protector and reducer, thus applying rather facile process for studies, e.g. the size effect and gold-metal interaction of catalysts.

Besides, gold colloids possess their unique optical and electronic properties.[25-27] Gold colloids display vivid colors due to the effect of localized surface plasmon resonance, largely depending on their sizes, shapes, and medium solutions. Gold colloid with small spherical nanoparticles generally shows color more red, whilst colloid with elongated Au-NPs may display other color such as beautiful green or blue.[28]

Surface plasmon resonance (SPR) is the frequency upon which the conductive electrons in the solid resonantly and collectively oscillated after excited by incident light. The resonance will only occur if the frequency of the incident light photons is consistent with that of the oscillated electrons. For the nanoscale particles dispersed in medium solution, the condition is different. Unlike the surface between planar metal and medium solvent, the radius of Au-NPs is much smaller than the wavelength of incident light.[29] In this case, the oscillation is locally around the nanoparticles under the frequency named localized surface plasmon resonance (LSPR).[30-32] Materials as gold, copper, and alkali metals having free electrons possess such properties, depending only on the shape, size, and medium solution.[33] From this point of view, gold colloids with different sizes and shapes of particles should display regulation about the color and surface plasmon resonance bond observed by UV-vis spectra.

UV-visible (UV-vis) absorbance spectroscopy is an efficient technique to reflect the SPRs of colloidal Au-NPs. Spherical colloidal Au-NPs display one resonance bond at around 520 nm in general.[34] Of cause, this bond changes in detail along with the shapes, the sizes and the medium solvents of the colloid. Besides, the beautiful and vivid colors of gold colloids are also

results of the changes of surface plasmon resonance. When the gold colloids are exposed under the incident light, the photons of the incident light at the same frequency of the SPRs of colloid will be absorbed, the left photons consisting the reflect light displays the color visualized by eyes.[35]

In this work, we applied the $NaBH_4$ and PVA (polyvinyl alcohol, 1 wt%) as the reducer and protector to prepare various gold colloid. The impacts of the $NaBH_4$ and PVA amounts, the concentration of reaction agents, the reaction solvent, and the reaction temperature were investigated in detail. We correlated the results from UV-vis spectra, the color of colloid, and the home-made liquid diffusion test (one drop of colloid onto TLC silica gel) together for understanding and estimating the gold colloids. The result showed that the home made liquid diffusion test can easily help to compare and chose one suitable gold colloid with small particles and narrow size distribution based on the preliminary results selected by UV-vis spectra and colloid color.

3.2 UV-vis spectra of a typical gold colloid

Gold colloids prepared by using $NaBH_4$ as reduce agent and PVA as protect agent have been widely investigated in recent years. However, the colloid Au-NPs obtained by this method ranges from 1-100 nm largely depend on the preparation conditions and the ratio between reducer/protector and gold. Work obtaining Au-NPs around 3-5 nm generally applied the $NaBH_4$: Au molar ratio around 3-5,[10, 36-38] while the PVA: Au weight ratio varied among very wide range (e.g. the weight ratio from 0.3,[39] 1.5,[36] even to 10[40], however using PVA from different companies with different masses. The molar ratio between PVA and Au is sometimes not mentioned in the literatures).

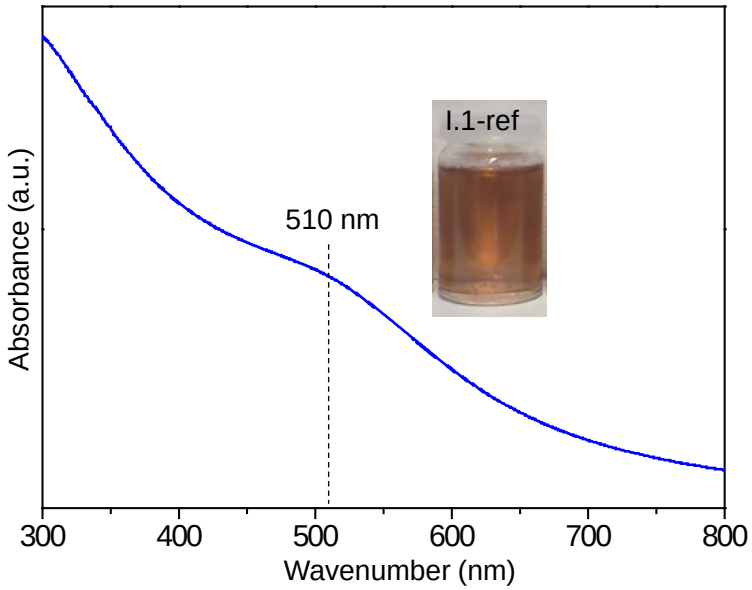

Figure 3.1 UV-vis spectrum and the photograph of colloid I.1-ref. $NaBH_4$: Au = 5: 1 (molar ratio, [$NaBH_4$] = 0.1 M, [Au] = 10^{-4} M) & PVA: Au = 5: 1 (weight ratio), M_W = 50,000 g/mol.

In order to understanding the influences of reaction conditions such as reaction agent, temperature and reactant concentration on the Au-NPs growth, both the $NaBH_4$: Au molar ratio and PVA: Au weight ratio are first fixed at 5: 1 (mass ratio of PVA- M_W = 50 000, the PVA: Au: $NaBH_4$ molar ratio is 0.0197: 1: 5).

Table 3.1 The list of Au colloid under different preparation conditions of system I.

Sample	Concentration (M)[a]		Agent	T[b]	Sample	Concentration (M)		Agent	T
	$HAuCl_4$	$NaBH_4$				$HAuCl_4$	$NaBH_4$		
I.1-ref[c]	10^{-4}	0.1	H_2O	25 °C	I.5-GH[d]	10^{-2}	0.1	H_2O	25 °C
I.2-Et	10^{-4}	0.1	Ethanol	25 °C	I.6-GM[c]	10^{-3}	0. 1	H_2O	25 °C
I.3-35	10^{-4}	0.1	H_2O	35 °C	I.7-SL[c]	10^{-3}	0.01	H_2O	25 °C
I.4-50	10^{-4}	0.1	H_2O	50 °C					

[a] The molar ratio between $NaBH_4$ and Au is 5: 1, and the weight ratio between PVA and gold is 5: 1 (the PVA: Au: $NaBH_4$ molar ratio is 0.0197: 1: 5). The 1 wt% PVA is dissolved in water. [b] Temperature for preparation of Au colloid. [c] Before the UV-vis spectra of all the colloids, the volumes are transferred to be the same by diluting the solution. [d] For better memory and

identification of the samples, every sample in this system I is labeled as I.n-special condition. Here the I.5-GH, I.6-GM, and I.7-SL are referred to gold colloids prepared by using **g**old precursor with **h**igher concentration (GH, 10^{-2} M), **g**old precursor with **m**iddle concentration (GM, 10^{-3} M), and **s**odium borohydride with **l**ower concentration (SL, 0.01 M) comparing with the reference sample I.1-ref, respectively.

Colloid I.1-ref is used as the reference comparing to other colloids in system I. Details of each colloid are listed in Table 3.1. The UV-vis spectrum and photograph of colloid I.1-ref are shown in Figure 3.1 and the inset picture. The as-prepared colloid I.1-ref displays semi-transparent orange-brown color that was reported previously corresponding to 1-2 nm Au-NPs.[41] A very weak and broad resonance bond is observed in the UV-vis spectrum, demonstrating that the colloidal Au-NPs have been successfully prepared. The adsorption peak maximum located around 510 nm also reveals the existence of highly dispersed Au-NPs with very small sizes.

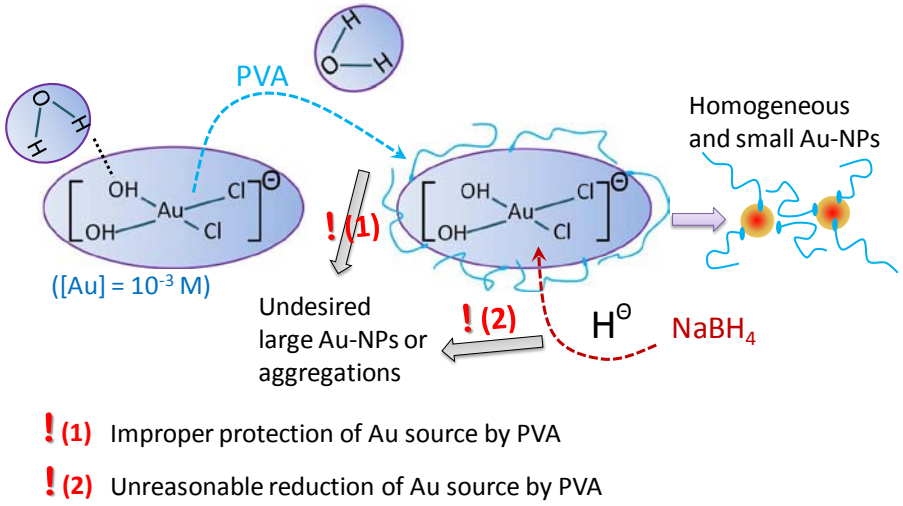

Schema 3.1 The possible paths for Au-NPs formation during synthesize of gold colloid in water at room temperature.

The schema and possible paths for formation of Au-NPs is illustrated in Schema 3.1. The concentration of gold is defined as 10^{-3} M, in which the domain species of gold should be $[Au(OH)_2Cl_2]^-$ according to the previous work of our group.[42] During the synthesis of gold

colloid, the gold precursor ($HAuCl_4$ solution) is first mixed with PVA solution as presented in 2.1.2 part of Chapter II. By stirring the mixture for 20 min, the PVA with abundant hydroxyl species acts as the protect agent and interacts with the gold precursor. The further addition of the fresh $NaBH_4$ solution possessing the negatively charged H^- easily reduces the gold precursor into metallic Au-NPs under the protection of huge PVA molecules. Under certain operation conditions (including the same temperature, solvent, stirring rate, etc.), the condition of PVA and $NaBH_4$ solution lay great importance to the Au-NPs formation. The undesirable reaction conditions will directly result in the formation of large gold nanocrystals or aggregations that are not wanted. In this case, the operation conditions for preparing Au-NPs are detected in detail.

3.3 Influence of reaction conditions

3.3.1 The influence of reaction solvent

The protector- PVA (Mr = 50,000) is very hard to be dissolve in simple organic compound (e.g. ethanol & acetone), and can be totally dissolved in water only at temperature higher than 70 ^oC (70-90 ^oC, the physical property of PVA changes at T higher than 90 ^oC).

In this work, ethanol is also tested to be the reaction medium (colloid I.2-Et) to see the influence of reaction medium on Au-NPs growth. The UV-vis absorbance spectra of colloid I.2-Et 10 min and 2 weeks after preparation are shown in Figure 3.2. Differing from the colloid I.1-ref prepared with distill water, colloid I.2-Et prepared with ethanol displays very broad absorption peaks ranging from 490 nm to 750 nm, which is seemed to be consistent by two overlapped peaks locating at 530 nm and 700 nm, respectively. By the way, deposition of tiny blue powders is observed immediately after addition of $NaBH_4$. The color of the suspension is black-blue as shown in the inset picture of Figure 3.2. Such color with two plasmon bonds in UV-vis spectra is always reported to be related to randomly arranged aggregations, pearl-like connected Au nanoparticles or Au nanorods (gold nanocrystals with both longitude and latitude

diameters).[43-46]

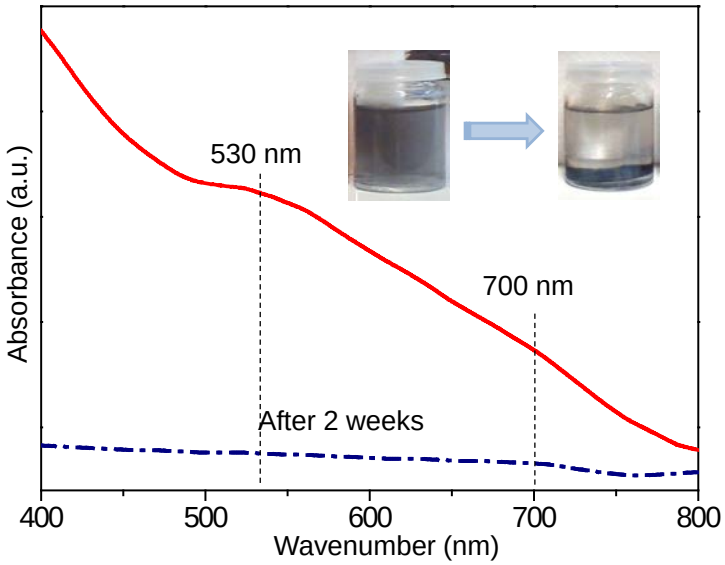

Figure 3.2 UV-vis spectra of Au colloid I.2-Et prepared using ethanol as solvent 10 min (red line) and 2 weeks (blue dotted line) after preparation. [$NaBH_4$] = 0.1 M, [Au] = 10^{-4} M, $NaBH_4$: Au = 5: 1 (molar ratio), PVA: Au = 5: 1 (weight ratio), M_W = 50,000 g/mol.

It is a worthy note that the PVA solution used here is dissolved in water (the PVA used in this work cannot directly dissolved in ethanol without water), whilst the addition of $HAuCl_4$ solution is dissolved in EtOH. In this case, the gold precursor will not be ideally protected by PVA molecules as shown in step (1) of Schema 3.1. Besides, it is well-known that the reducibility of $NaBH_4$ in ethanol will be weakened than in the water. In this case, after addition of $NaBH_4$, the germs are disorderedly formed and more likely to be aggregated without suitable PVA protection. After 2 weeks, the SPR bonds nearly disappear due to the separation of Au-NPs from liquid phase. The nanoparticles in colloid I.2-Et by using EtOH as solvent are very unstable and totally separated from the liquid phase during less than two weeks, which is unavailable for preparing stable Au-NPs with homogeneous small particles.

3.3.2 The influence of reaction temperature

The impact of reaction temperature as a factor turning the sizes and shapes of Au-NPs is also

wondered. As can be seen from Figure 3.3, the widths of SPR bonds the colloids prepared at higher temperature (35 ^{o}C and 50 ^{o}C) are broader and the intensities are much weaker comparing with colloid I.1-ref prepared at 25 ^{o}C.

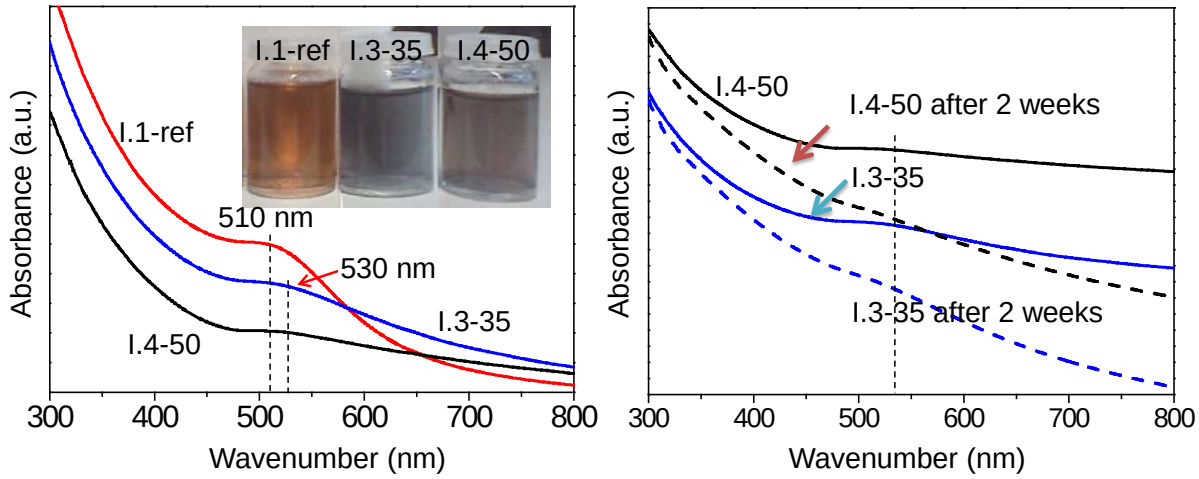

Figure 3.3 UV-vis spectra of Au colloids prepared at different temperature. [$NaBH_4$] = 0.1 M, [Au] = 10^{-4} M, $NaBH_4$: Au = 5: 1 (molar ratio), PVA: Au= 5: 1 (weight ratio), reaction temperature for I.1-ref, I.3-35, and I.4-50 is 25^{o}C, 35^{o}C, and 50^{o}C, respectively.

The SPR bond maximum over colloid I.3-35 is red-shifted to about 530 nm indicating the formation of larger gold nanoparticles. Whilst, the UV-vis spectrum of colloid I.4-50 is a little weird comparing to the other spectra, which displays very weak SPR bond with a large trail until 750 nm. The much more weakened color and intensity of SPR bonds over colloids I.3-35 and I.4-50 suggest that only small amounts of Au-NPs exist in colloids I.3-35 and I.4-50 due to the formation of huge gold aggregates as deposition and cannot be reflected by the UV-vis spectrometer.

The color of colloids also changes from orange into blue and dark brown, respectively. After two weeks aging, the color of colloids is barely changed. However, the colloid VII and VIII seem unstable during the two weeks with largely reduced plasmon bond intensities. All the spectra are tested under room temperature (25^{o}C), thus there is no effect from the temperature on the spectra.[47] The temperature of preparation does impact the formation of Au-NPs. It is a

common knowledge that the gold nuclei are surrounded by PVA and thus separated from each other. Thus the gently raise of temperature (from 20°C to 35°C and 50°C) will not cause the further the further growth or aggregation of formed Au-NPs if the other operation conditions maintain the same. It was previously suggested that the reaction rate could be intensely enhanced under higher temperature and thus form heterogeneous particles.[48] Another problem that cannot be neglected is that, the viscosity of solution largely decreases along with the temperature (e.g. the viscosity of water decreases from 1.004 mPa·s at 25°C to 0.554 mPa·s at 50°C[49]). In the solution possessing lower viscosity under higher reaction temperature, the nuclei are facile to move and form large particles during preparation, making the gold particles unstable and easily deposited.

3.3.3 The influence of reactant concentration

For understanding the impacts of reactant concentration on the formation of Au-NPs, the gold colloids are synthesized using different concentration conditions of both gold source and $NaBH_4$ reduce agent. The corresponding UV-vis absorbance spectra are shown in Figure 3.4. The corresponding colors of gold colloids are displayed in the inset picture.

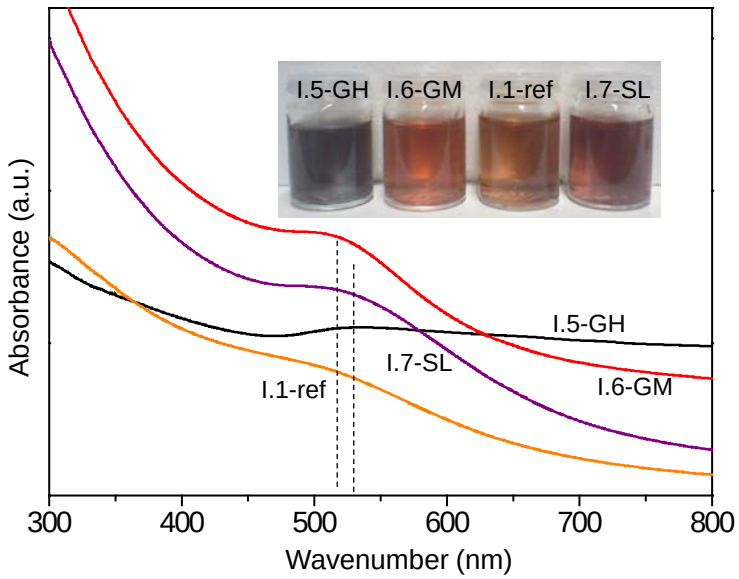

Figure 3.4 UV-vis spectra of Au colloids from different reactant concentration. NaBH4: Au= 5: 1 (molar ratio), PVA: Au= 5: 1 (weight ratio). The [Au] for I.5-GH, 1.6-GM, and I.1-ref is 10^{-2}

M, 10^{-3} M, and 10^{-4} M, respectively, and the [$NaBH_4$] = 0.1 M. The I.7-SL is of the same condition of I.1-ref, except that the [$NaBH_4$] = 0.01 M.

The higher concentration (10^{-2} M) of $HAuCl_4$ solution of colloid I.5-GH results in a black-blue color. A very broad plasmon resonance bond ranging from 470 nm to about 800 nm with low intensity is observed, indicating that the distribution of Au-NPs in colloid I.5-GH is very heterogeneous from very small nanoparticles to large aggregations. The lower concentration of gold precursor receives colloid I.6-GM and I.1-ref with plasmon bonds locating around 510 nm. Although lower $HAuCl_4$ concentration may be good to obtain smaller sizes of Au-NPs, it is not unlimited to reduce the concentration during the industrial production. A highly diluted gold precursor will not only take excessive volume but also difficult for uniformly mixing of reactants during reaction. We suggest that the concentration of gold precursor between 10^{-3} and 10^{-4} M is more suitable for application.

One colloid I.7-SL prepared using a lower $NaBH_4$ concentration (0.01 M) was also tested by the UV-vis measurement. The peak maximum is red-shifted to about 520 nm comparing to the colloid I.1-ref. The color also changes into rose-violet. Combining with the color and SPR bond, the Au-NPs in colloid I.7-SL are believed to be larger than colloid I.1-ref.

The concentration of reactant also largely affects the formation of Au-NPs. Lower concentration of gold precursor or higher concentration of reducer are more appropriate for preparing small nanoparticles with narrow size distribution. When the gold precursor is condensed, the reaction with $NaBH_4$ is rather forceful that the nucleation is too fast and the formed gold nuclei might collide together to form larger gold crystals. When the $NaBH_4$ solution is too diluted, the addition of $NaBH_4$ cannot uniformly react with the gold precursor since the larger volume of reducer solution needs more time to be added and blended equally. Larger nuclei will be formed during the addition of $NaBH_4$. Upon the above two conditions, the formation of Au-NPs is uneven under the same reaction conditions (e.g. stirring speed and temperature). Large sizes or broad size distribution will be formed, which is not the requirement

of general preparation of gold colloid for catalysis application.

3.4 Influence of addition amount of reducer- $NaBH_4$

3.4.1 Characterization of gold colloid by UV-vis

For the sake of the effects of reducer amounts on the Au nanoparticles sizes during Au colloid preparation, six samples are prepared by different $NaBH_4$ amounts as listed in Table 3.2.

Table 3.2 The preparation condition of Au colloids with various amounts of $NaBH_4$ or PVA in system II.

Sample	Ratio			Sample	Ratio		
	gold	PVA[a]	$NaBH_4$[b]		gold	PVA[a]	$NaBH_4$[b]
II.1-S0.5[c]	1	5	0.5	III.1-P0	1	0	5
II.2-S1	1	5	1	III.2-P0.5	1	0.5	5
II.3-S2	1	5	2	III.3-P0.85	1	0.85	5
II.4-S3	1	5	3	III.4-P3	1	3	5
II.5-S5[d]	1	5	5	III.5-P5[d]	1	5	5
II.6-S10	1	5	10	III.6-P10	1	10	5

[a] The weight ratio between PVA and Au. The 1 wt% PVA is dissolved in water. [b] The molar ratio between $NaBH_4$ and Au. The concentration of $NaBH_4$ solution is 0.1 M. [c] For better memory and identification of the samples, every sample in Table 3.2 is labeled as II.n-Sx (x is molar ratio of sodium borohydride: Au) and III.n-Py (y is weight ratio of PVA: Au). [d] The preparation of II.5-S5 and III.5-P5 is totally the same of the I.6-GM Table 3.1, unless that the I.6-GM is diluted to be the same volume of I.1-ref in Table 3.1.

The as-prepared gold colloids are illustrated in the inset picture of top left image of Figure 3.5. The vivid colors demonstrate that the colloidal Au-NPs have been successfully prepared. With the incremental amount of reducer, the color of the Au colloid changes from purple to red and at last dark brown. It is generally reported that the gold colloid with particles around 3-5 nm

possesses red or wine-red color,[50, 51] which is similar with our colloid II.3-S2, II.4-S3, and II.5-S5. When the molar ratio between $NaBH_4$ and Au is lower than 2, the color of Au colloid tends to be purple. When the $NaBH_4$: Au molar ratio is higher than 5, the color of the gold colloid changes into deep brown or even black. These variations are very interesting and are expect to be related with the size of the Au-NPs.

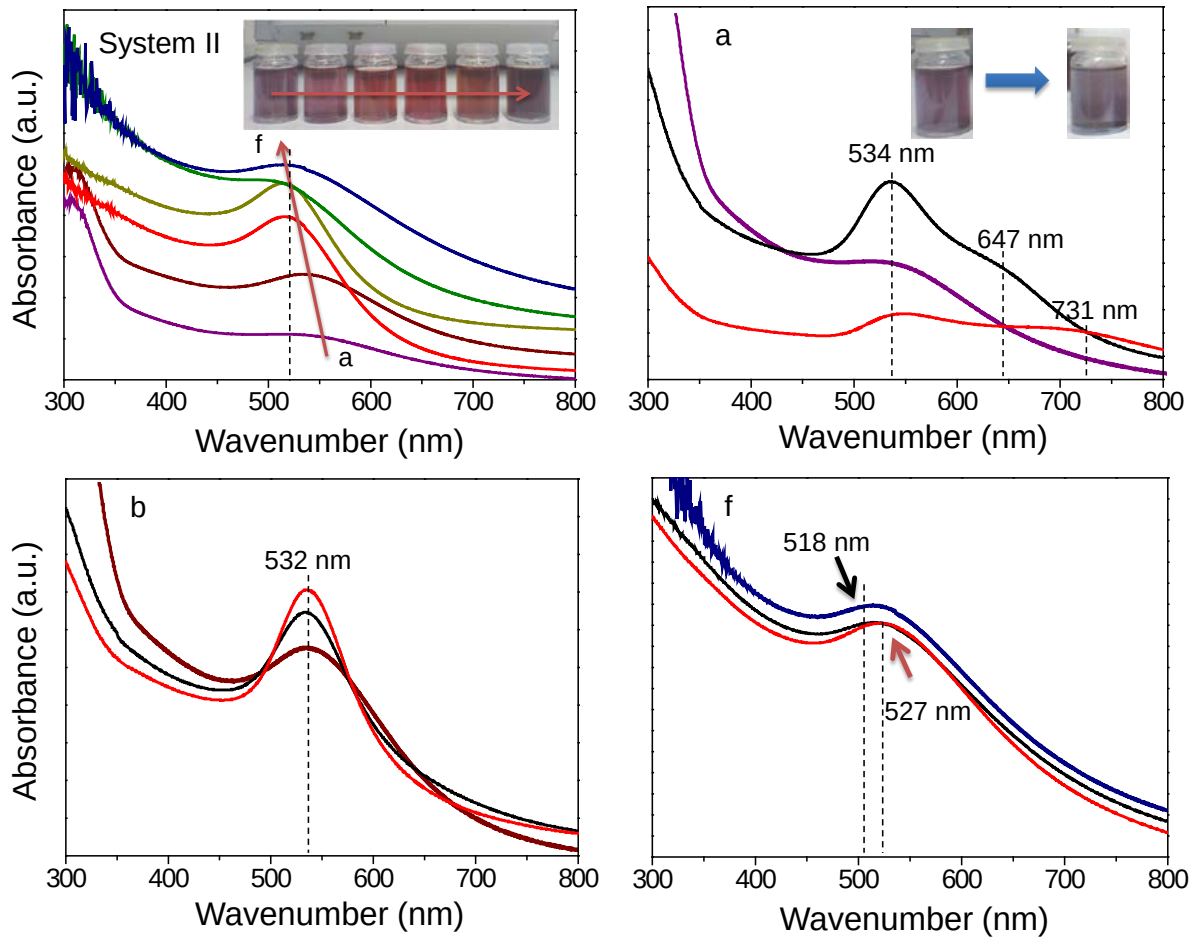

Figure 3.5 UV-vis spectra of Au colloids 10 min after NaBH4 addition (upper left), and the comparison of three gold colloids after prepared for 1 day (black line) and 2 weeks (red line). a. II.1-S.0.5, b. II.2-S1, c. II.3-S2, d. II.4-S3, e. II.5-S5, and f. II.6-S10 respectively, according to different $NaBH_4$: Au molar ratio. [$NaBH_4$] = 0.1 M, [Au] = 10^{-3} M, PVA: Au = 5: 1 (weight ratio).

As previously stated, the visualized color of gold colloid is a reasonable phenomenon that can

be explained by the SPR effect. The incident light at the same frequency of SPR is absorbed by colloid, and the rest of the incident light is reflected as the color. The color of colloid is strictly depending on the sizes and shapes of Au-NPs in this work, which are expected to be applied for the identification of colloids. The UV-vis spectra over six Au colloids are taken 10 min after addition of $NaBH_4$ as shown in top left image of Figure 3.5. All the fresh Au colloids possess single absorption bond in the range of 490- 550 nm, which is a characteristic of Au colloids reported everywhere.[25, 26, 52] The absorption at certain wavelength is a visible phenomenon from the surface plasmon resonance, which causes strong electromagnetic radiation by the excitation of molecules.[17, 53] The differences in sizes and shapes of particles result in distinctive position and shape of the absorption peak, as well as the color. With the $NaBH_4$: Au ratio raises from 0.5 to 5, the position of plasmon resonance bond blue-shifts from 534 nm to 510 nm, revealing the different structures/sizes of nanoparticles.[54] It was suggested that a blue shift of plasmon bond reflected the reduction of particle sizes.[54] It is in this case inferred that the Au-NPs sizes degrade with the addition of reducer. However, there seems to be valve value of the reducer amount for the growth of Au-NPs, since the plasmon bond slightly red-shifts to 518 nm over II.6-S10 with an excessive $NaBH_4$ amount, and the peak becomes broader with trail until 700 nm. In addition, the intensity of plasmon bonds over colloid II.1-S0.5 and II.2-S1 are relatively weak, which means that the amounts of absorption species in colloids are quite low. An obvious peak locates at about 313 nm is observed in both the two colloids, which can be attributed to a ligand-to-metal charge transfer transition in the tetrachloroaurate ion derived from $[AuCl_4]^-$.[55] It is meaning that the small amount of reducer is not sufficient for reducing all the ionic gold species into Au^0. There exist large amounts of unreduced gold species even after the formation of Au-NPs. The intensity of the plasmon bonds raise along with the increase amount of $NaBH_4$ until the ratio between reducer and Au becoming 2: 1. Further increase of the $NaBH_4$ amount does not induce obvious increase of the peak intensity. It is considered that the 2: 1 ratio is generally enough for the reduction from Au^{3+} to Au^0. When the $NaBH_4$: Au ratio is higher than 3, the plasmon bond become much broader. It was reported that for the gold particles possessing plasmon bond at the same location, a broader peak width was related to

smaller Au-NPs.[54]

After one day, the UV-vis spectra of the above six colloids generally remain the similar SPR bonds (including the half-peak width and peak position) as 1 day before, expect the colloid II.1-S0.5 and II.2-S1 (Figure 3.5). A new plasmon bond locating at 647 nm is formed over colloid II.1-S0.5 one day later. Both the absorption peaks of colloid II.1-S0.5 and II.2-S1 become sharper, and the absorption peak at 313 nm depresses gradually. After 2 weeks, deposition is formed in colloid II.1-S0.5 covering the bottom of bottle. The second absorption peak red-shifts to 731 nm and the total intensities are much weakened, proving the growing process during two weeks. The single plasmon bond of colloid II.2-S1 also becomes sharper after 2 weeks, resulting from the development of gold particles from residual precursor. When the amount of $NaBH_4$ is lower (e.g. colloid II.1-S0.5 and II.2-S1), the Au ions cannot be totally reduced into Au^0, and there remain Au^{3+} and even Au^+ species in the solution. In this case, the solution possesses acid property that makes the Au-NPs unstable by the incomplete charging and lack of repulsive electrostatic interaction.[56] The as-formed gold nuclei tend to form larger nanoparticles. No differences are observed from the UV-vis spectra or the colors of colloid II.3-S2, II.4-S3, and II.5-S5. A slight shrinking of the bond together with slight red-shift is observed in colloid II.6-S10 as shown in the lower right image of Figure 3.5, suggesting the further growth of particles within 2 weeks.

Correlating with the color changes over different colloids (the picture was taken 1 day after preparation), the insufficient reduction of Au precursor induces a purple color. The Au colloids from appropriate amount of $NaBH_4$ display color in red. However, when the amount of reducer is too high, the gold colloid turns out to be brown and even black (for the colloid II.6-S10, we have tested several times, the result turns out to be equal). In fact, during the preparation of colloid II.6-S10, the color of solution changes from yellow to red and then brown-black very rapidly. It is inferred that when the $NaBH_4$ amount is high, large amounts of very small germs are formed immediately. However, the intense reduction and huge number of germs provide the opportunity of small germs to be collided during string. The aggregations are more likely

to be formed.

From the above analysis combining the color and SPR peaks of UV-vis spectra, it is still difficult to select one best colloid with small and homogeneous Au-NPs (2-4 nm). In fact, as the paper chromatography made in the organic chemistry for separating and identifying different compounds, the similar consideration also can be probational for comparing and choosing colloids with desired particle sizes and distribution. TLC silica gel is applied in the following work to understand the size distribution of Au-NPs by colloids diffusion. One drop of gold colloid is dropped onto the silica gel, the diffusion process can be complete in about 10 second and the silica gel can be totally dried after about 10 min. In order to keep an equal volume of the tested liquid, the same dropping pipette will be used for transferring different colloids, and one droplet of colloid will be utilized during the test. Before testing, the concentration of gold in each colloid is diluted to be identical. Each diffusion process is recorded by three photos along with time.

3.4.2 Home-made liquid diffusion test of gold colloid

The function of the home-made liquid diffusion (HMLD) test can be illustrated as displayed in Schema 3.2. Immediately after one droplet of gold colloid onto the silica gel, the very initial liquid-solid gel contact layer is formed as shown in phenomenon “a” in Schema 3.2. However, the appearance of the initial contact layer is too fast only in the first 0-1 second. It is still very hard to capture this step by camera. The diffusion of the liquid goes on roundly. During the diffusion of gold colloid, larger gold crystals are easily limited to move with water. Thus the larger gold nanocrystals can be limited in the initial diffusion layer “a”, whereas smaller particles are tend to diffuse further with water until the diffusion procedure ended with boundary, as shown in the “b” of Schema 3.2.

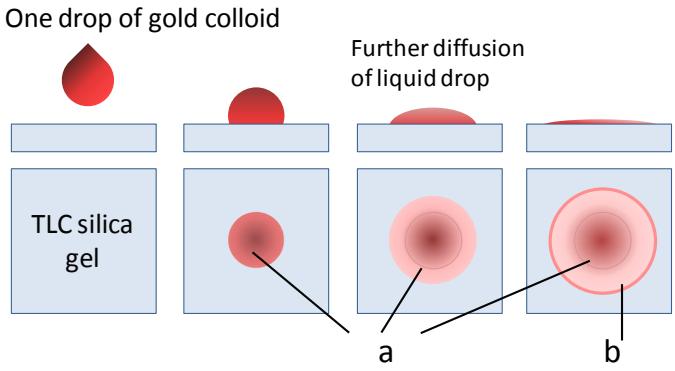

Schema 3.2 The illustration of home-made liquid diffusion procedure and color display of the diffusion circles. a. Initial contacted layer limited the move of larger particles to form the inner diffusion layer, b. Small particles run faster until the end of diffusion and form the colored boundary.

Under this circumstance, for the test of Au colloid with small particles and narrow size distribution, the liquid should diffuse fast to form a thick boundary with color. Whilst the surface of diffusion circle should be homogeneous and surrounded by light color (since most of the small particles diffuse to the boundary). For the colloid with aggregation or heterogeneous gold nanocrystals, the gold nanocrystals will be separated easily depending on their morphologies and sizes. According to the above theory, it should be interesting to apply this simple HMLD test for comparing and understanding the growth and distribution of Au-NPs in different colloids.

3.4.2.1 10^{-3} M $HAuCl_4$ aqueous solution

The diffusion circle of one droplet of water onto the silica gel displays no color influence. Only light yellow boundary can be seen, which should be induced by the restructure of silica gel by water diffusion. Figure 3.6 shows the illustration of one droplet of 10^{-3} M $HAuCl_4$ diffusing on silica gel with time.

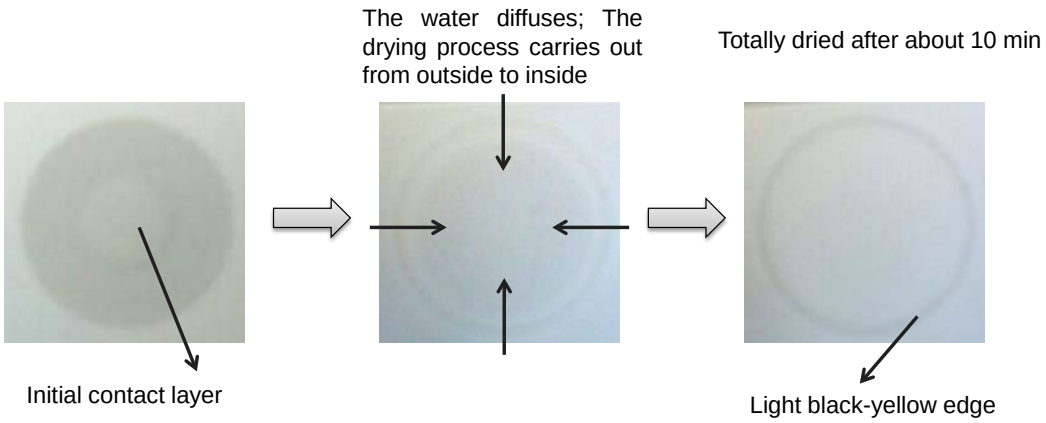

Figure 3.6 The illustration of one droplet of 10^{-3} M $HAuCl_4$ aqueous solution onto TLC silica gel diffusing along with time.

The inner diffusion circle due to the initial contact layer is formed immediately after the liquid is dropped. Along with time, the inner circle become flat after the water diffuses. The color of the main circle tends to be more uniform, and the dry process taken place from the outside to inside as shown in the middle image of Figure 3.6. The large circle with diameter about 1.5 cm and light black-yellow boundary can be observed finally due to the recrystallization of $HAuCl_4$. The totally dry process takes about 10 min. The inside color of the circle is homogeneous and generally the same as the initial silica gel.

3.4.2.2 Mixture of PVA (1 wt%) and $NaBH_4$ solution

The mixture of PVA and $NaBH_4$ solution is also diffusion background as shown in Figure 3.7. The difference from the $HAuCl_4$ diffusion is that, huge water bubble is formed immediately after dropping. This is because of the higher viscosity of PVA from large molecules.

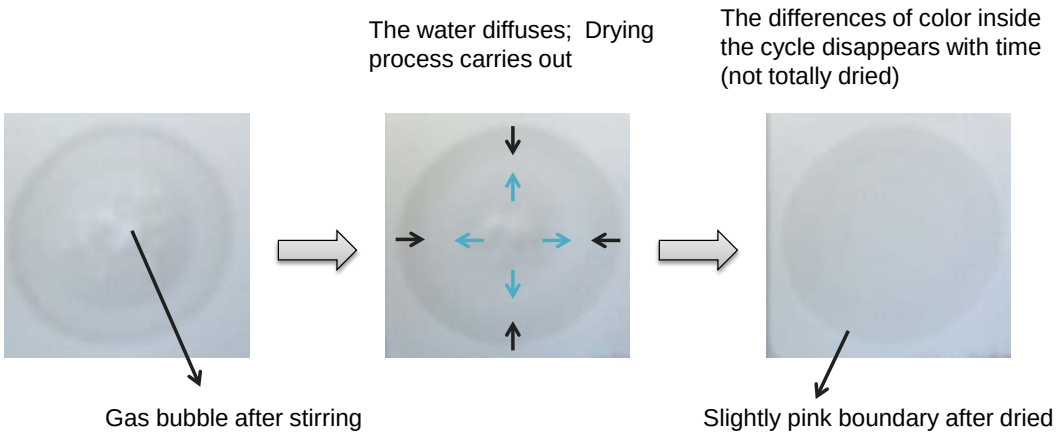

Figure 3.7 The illustration of one droplet of PVA (1 wt%) and $NaBH_4$ solution mixture onto TLC silica gel diffusing along with time.

The inside spots of inner circle is gas bubbles generated during mixture of solutions. Along with time, the water bubble diffuses and at last disappear, and dry process carried out from outside to insides simultaneously. After totally dried, the very light pink boundary is left on the silica gel (the picture is not shown). From the diffusion of background reactant, the basic diffusion role is visualized and the very light color of initial reactants (including $NaBH_4$, $HAuCl_4$, and PVA) very slightly influences the observation of Au-NPs.

3.4.2.3 HMLD test of Colloid II.2-S1 (UV-532 nm)

For colloid II.2-S1, immediately after the liquid is dropped, the initial liquid-silica contact layer is formed and the liquid continue diffuses as shown in the first image of Figure 3.8. The outside diffusion layer is limited by thick pink-purple edge, and the pink color of the outside layer is deeper than the initial contact layer. As the time goes on, the color of outer circle becomes much lighter due to the further diffusion of Au-NPs. The rest particles in the initial contact layer move on (middle image of Figure. 3.8) and slowly step out of the inner boundary.

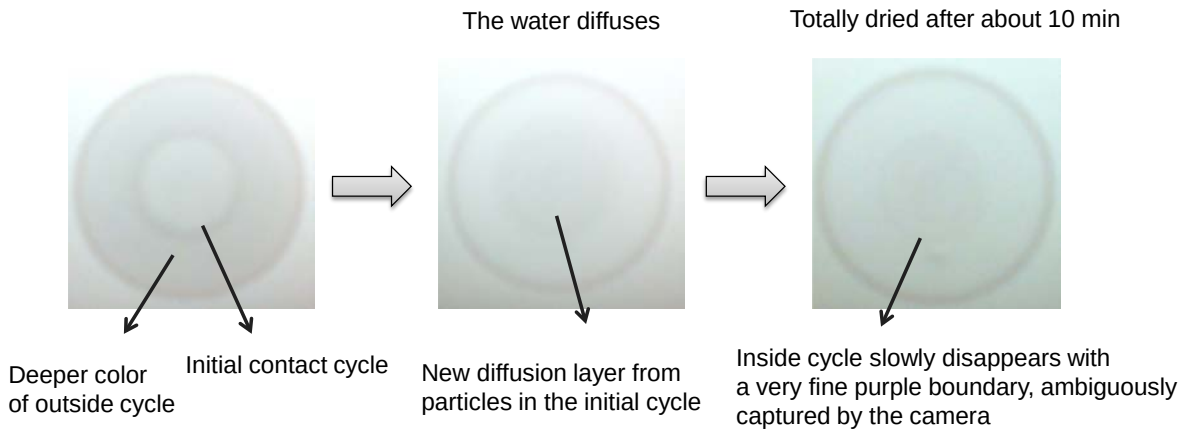

Figure 3.8 Photos with time after one droplet of fresh colloid II.2-S1 onto TLC silica gel.

The diffusion layers become overlapped at last. After the silica gel is totally dried, the main visible layer with thick pink-purple edge is observed. The inner layer with pink color surrounded by fine purple boundary is also observed. The inner fine boundary limits the movement of larger gold crystals. The color centered is deeper pink than the marginal color at last. The multiple colors on the silica gel can be attributed to the heterogeneous distribution of Au nanocrystals.

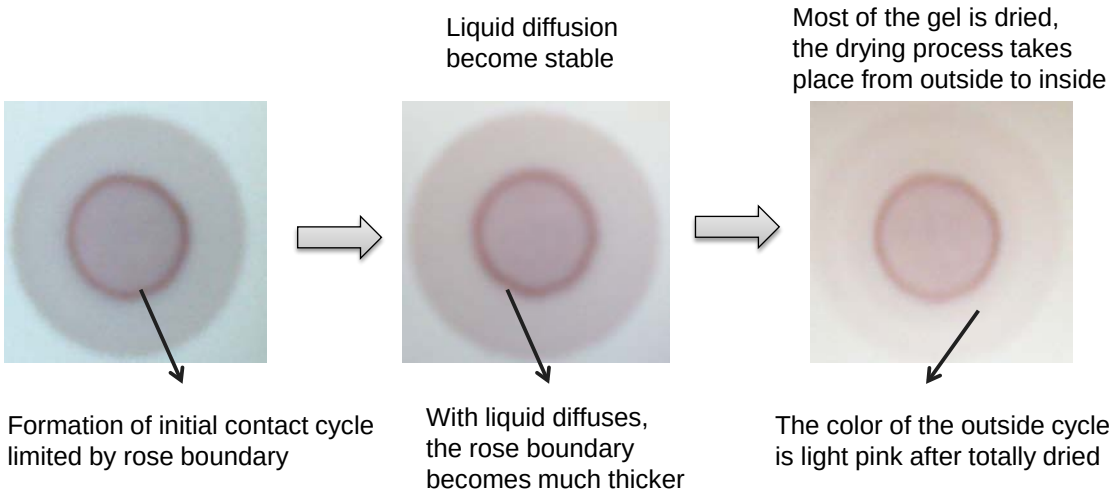

Figure 3.9 Photos with time after one droplet of aged colloid II.2-S1 (after 6 weeks) onto TLC silica gel.

After 6 weeks, the colloid II.2-S1 is retested by dropping one droplet of aged colloid onto silica gel as shown in Figure 3.9. The diffusion process is similar whilst the color diffusion is

quite distinctive. Immediately after the liquid is dropped, the initial contact layer is formed, however with thick rose boundary. The color of the inner circle is deeper than the outside circle. After totally dried, two concentric circles are clearly observed: one large outside circle with light pink color and pink boundary; and one small circle with fresh pink color and deep rose boundary. During the diffusion process, part of the liquid along with very small particles diffuses quickly and radically to the outside boundary, whilst the larger particles move slowly and are limited by the boundary of the initial contact interface. Along with time, parts of particles move on and step over the boundary of initial contact layer to the outside circle. Only very large particles are restrained in the inner circle.

It has to be mentioned that the silica gel is partially separated from the aluminum substrate due to the water infusion in the initial contact layer. After the liquid diffuses into the outside circle, the silica gel becomes stick back to the aluminum substrate again. However, there will be an isolation belt between the inner and outside diffusion circles, because of the second-time water diffusion and the asynchronous drying process of outside and inner circles. For the colloid consisted by small particles, most of the particles move to the outside boundary, the color of isolation belt maintains mainly the same of pure silica gel (white-gray color) and the rest of the circle will be with very light color comparing to the outside boundary. While for the colloid with both small and very large particles, the isolation belt becomes the inner boundary with deep color. And the color of the inner and outside circle should be different. From this point of view, it should be realized that the particles of colloid II.2-S1 is really heterogeneous after 6 weeks aging. Very large particles are formed and centered in the inner circle. The much deeper color of inner circle and boundary also illustrate that the most of the small particles grow into large particles after aging.

Combining the results from Figure 3.5 and Figure 3.9, it can be realized that the insufficient amount of reducer is unsatisfied for obtaining Au colloid with homogeneous small Au nanoparticles and especially high stability. The lack of base condition, on the one hand failed to reduce all gold precursor into metallic Au; on the other hand unable to supply a stable

atmosphere for the as-formed small particles. Heterogeneous Au particles with large aggregations are thus produced. The UV-vis spectra of fresh colloid II.2-S1 and the colloid after 1 day and 6 weeks display the plasmon bonds locating at the similar wavelength with different peak width. It is revealed that only the UV-vis absorbance spectra are not sensitive enough to identify the Au-NPs in the colloid. The application of HMLD test is helpful for pointing out the development of gold colloid and necessary for comparing gold colloids with different Au-NPs distribution conditions.

3.4.2.4 HMLD Theory evidenced by SEM

To control and demonstrate these proposals, the aged II.2-S1 colloid deposition on silica gel is examined by the SEM (Scanning Electron Microscope) technique. The SEM images of TLC silica gel after HMLD test of colloid II.2-S1 are divisionally operated as shown in the inset illustration of Figure 3.10(a-1). It is easy to identify the gold from the support by using the special parameter. Gold nanocrystals on the surface of silica gel display distinct luminance contrast to silica. By observing the inner circle caused by the initial contact layer of water and silica (part “a” of Figure 3.10), both huge nanocrystals larger than 1 μm and aggregations are present. The main morphology of large aggregations is marked by the red lines. The Energy-dispersive X-ray spectroscopy (EDX) demonstrates the existence of gold component. By the global observation, the crystals at the boundary of initial contact layer “b” seem smaller than those in the section “a”. Whereas large gold aggregations still present on the inner boundary b as displayed in Figure 3.10(b).

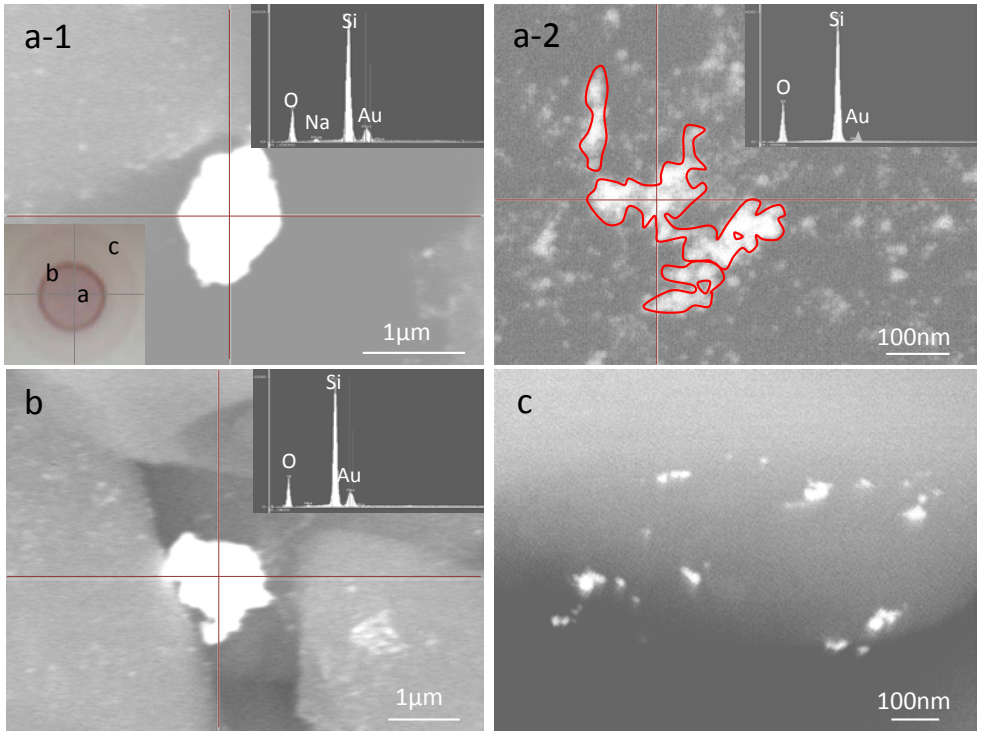

Figure 3.10 SEM images of aged colloid II.2-S1 deposited on TLC silica gel in function of areas. The three insets of a-1, a-2, and b is the EDX results corresponding to the area crossed. The inset photo of silica gel in Fig. 5a illustrates the different diffusion area operated by SEM technique corresponding to: a The inner surface of initial liquid-silica contact layer; b The boundary of initial contact layer; c The boundary of outside diffusion layer.

It is consistent with our theory that the larger and heterogeneous gold nanocrystals are too huge to move with liquid and will be limited in the inside diffusion layer. By changing the detect region to the outside boundary c, there is no observation of large gold aggregations. In fact, there are also some shining compounds on the boundary c (not shown). However by confirming each of them with the SEM/EDX technique, such kind of shining bulks are only resulted from the residual impurity of the substrates. The dispersive shining spots shown in Figure 3.10(c) are inferred to be small Au-NPs, which should be around 5-20 nm. Unfortunately, these particles are too small to be evidenced as gold from the SEM/EDX. Only Si and O elements are revealed from the EDX results by detecting these particles. In fact, fine particles with very small sizes (e.g. < 5 nm) are under the limitation of SEM technique and uneasy to be detected. Nomatterhow, the analysis results of SEM in a word demonstrate the previous consideration for the HMLD test.

3.4.2.5 Colloid II.4-S3 (UV-510 nm) and colloid II.6-S10 (UV-518 nm)

The images of HMLD test over colloid II.4-S3 is shown in Figure 2.11, which possesses the plasmon bond locating around 510 nm. Comparing with colloid II.2-S1, the colloid II.4-S3 displays a more beautiful red color and appropriate position of plasmon bond, which is considered to be with better particle size distribution and smaller sizes. After dropped onto the silica gel, homogeneous pink color covers the surface of silica gel. Different from colloid II.2-S1, there is no inner boundary displayed in the center of the silica gel after totally dried. Uniform pink color covers the circle with only one ambiguous outside boundary.

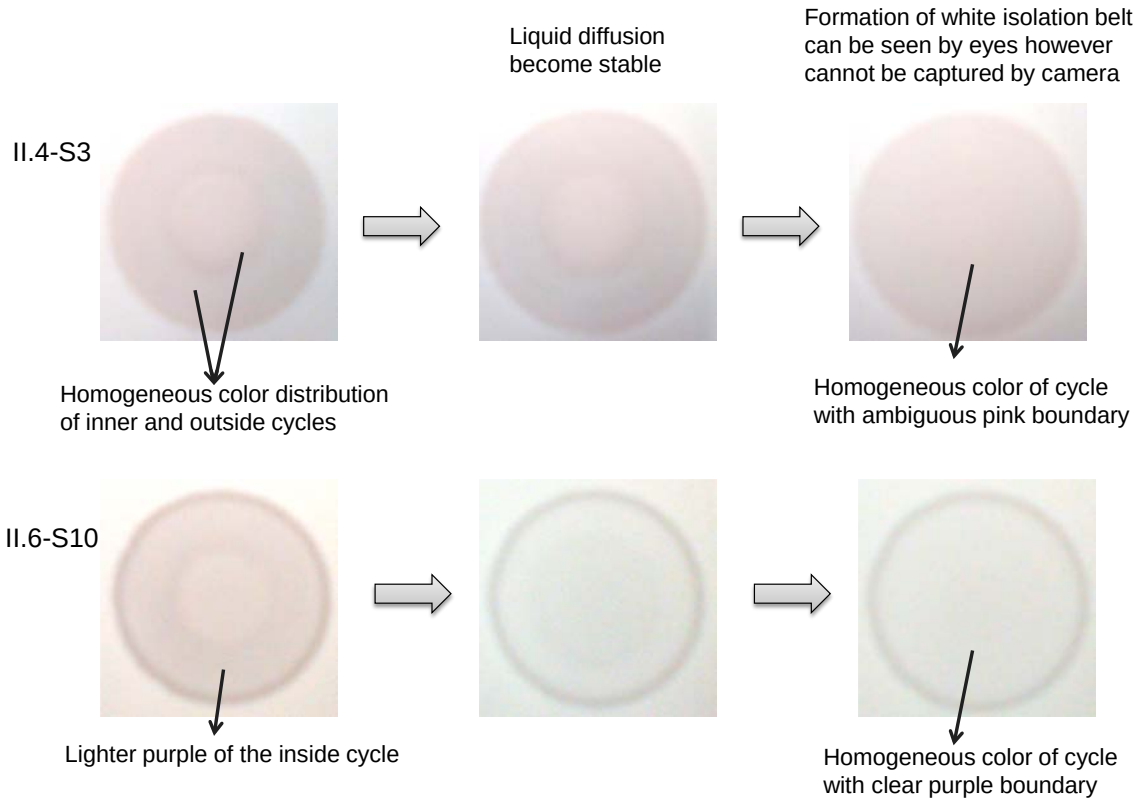

Figure 3.11 Photos after with time after one droplet of colloid II.4-S3 and colloid II.6-S10 onto the TLC silica gel.

The colloid II.6-S10 with the plasmon bond around 518 nm is also studied by the HMLD test as shown in Figure 3.11. The diffusion process is similar as colloid II.4-S3. The only difference is that the main color of silica surface is light purple with a clear and thick purple boundary. The

diffusion performance of colloid II.6-S10 suggests that the Au-NPs are homogeneous enough and more easily diffused to the outside boundary than those in colloid II.2-S1. However, combining the position of plasmon bond and colloid color, it is hard to give a conclusion that the Au-NPs in colloid II.6-S10 are as small as required.

Small/insufficient amount of $NaBH_4$ result in uncompleted reduction of Au-NPs, prejudice the well dispersion of Au-NPs, and even lead to the aggregation of small Au-NPs. While sufficient amount of $NaBH_4$ does help dispersing the Au-NPs, forming Au-NPs with very small sizes, and stabilize particles from aggregation. However, excessive amount of $NaBH_4$ is not that beneficial for the nanoparticles growth as previously reported. During the preparation of gold colloids, we utilize the same stirring speed, transfer pipette, beaker, and even the rotor just to gain the reasonable comparison of each colloid. For colloid II.6-S10 with a deep brown color, we also tested for several times, and the results are proved to be highly repetitive every time. The results turn out that excessive amount of reducer ($NaBH_4$: Au=10) is not suitable. We have also made an additional experiment with $NaBH_4$: Au of 50: 1. Black solution and deposition is formed immediately after the addition of $NaBH_4$. It is conjectured that, the large amount of reducer in colloid II.6-S10 will produce huge amount of fine nuclei. At the same stirring speed, the nuclei are more likely to have collision and form larger aggregations. The ratio of $NaBH_4$: Au as 5: 1 is proved to be a better formula in this work (reaction T: 25^{o}C, stirring speed: 750 r/min), which lasts for nearly 6 months without any deposition, changes in color and plasmon bond position.

3.5 Influence of addition amount of protector- PVA

3.5.1 Characterization of gold colloid by UV-vis

The details of Au colloid prepared from different PVA: Au weight ratios are listed in Table 3.2. The molar ratio between reducer and Au is fixed as 5: 1. It can be seen from the inset picture of Figure 3.12 that the color of colloids from various PVA amount is generally a brown

system. Colloid III.1-P0 displaying purple-brown is a comparison without any addition of PVA. A smaller amount of PVA (PVA: Au ≤ 0.5 weight ratio) makes the gold colloid with dark brown. The higher amount of PVA induces gold colloid with semitransparent light brown.

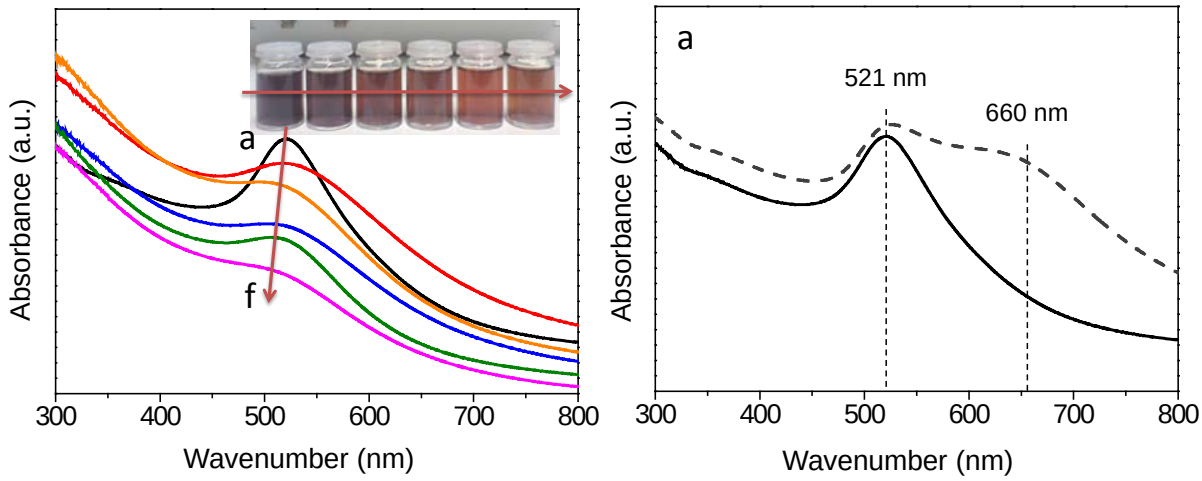

Figure 3.12 Uv-vis spectra of Au colloid prepared from different PVA amounts (left profile, 10 min after $NaBH_4$ is added), and the comparison of fresh colloid III.1-P0 and the colloid after 1 week (right profile). a. III.1-P0, b. III.2-P0.5, c. III.3-P0.85, d, III.4-P3, e, III.5-P5, f. III.6-P10 respectively, corresponding to different PVA: Au weight ratio. [$NaBH_4$] = 0.1 M, [Au] = 10^{-3} M, $NaBH_4$: Au = 5: 1 (molar ratio).

The brown color system also depends on the selected ratio between the reducer and Au ($NaBH_4$: Au=5: 1), which means that the color system might be red if the ratio is based on 3: 1 (as the II.4-S3 in system II). The UV-vis spectra of gold colloids by variation of PVA amount is displayed in Figure 3.12. Colloid III.1-P0 with no PVA give an intensive SPR bond at 521 nm- a characteristic peak of gold colloid as reported. The $NaBH_4$ alone without addition of protect agent can also reduce the gold precursor into metallic gold. Without the addition of PVA, the absorption peak is much sharper than the other tested colloids. After 1 week, an additional peak around 660 nm appears in the aged colloid III.1-P0, whilst the peak around 521 nm does not shift. It is demonstrated that the sizes of the Au-NPs do not change during the aging time. However, some large aggregations are formed due to the lack protection of Au-NPs. With the raise of PVA amount, the plasmon bond blue-shifts from 521 nm (colloid III.1-P0), 517 nm

(colloid III.2-P0.5) to 510 nm (colloid III.3-P0.85) and then become mainly permanent. The intensity of the bonds is also reduced along with the raising of PVA amounts.. The display of plasmon bonds by UV-vis spectra reflects the basic estimation of the Au-NPs, and further information should be obtained by using the HMLD tests.

3.5.2 Home-made liquid diffusion tests of gold colloids

3.5.2.1 Colloid III.1-P0 (UV-521 nm)

The colloid III.1-P0 prepared after one day is dropped on the TLC silica gel as shown in Figure 3.13. Violet boundary formed immediately on the boundary of the initial contact layer. The final shape of the circle is very interesting, there seems two purple diffusion layers separated by an “isolation belt” colored light purple. The drop test of colloid III.1-P0 displays unique purple color much deeper than the other colloids.

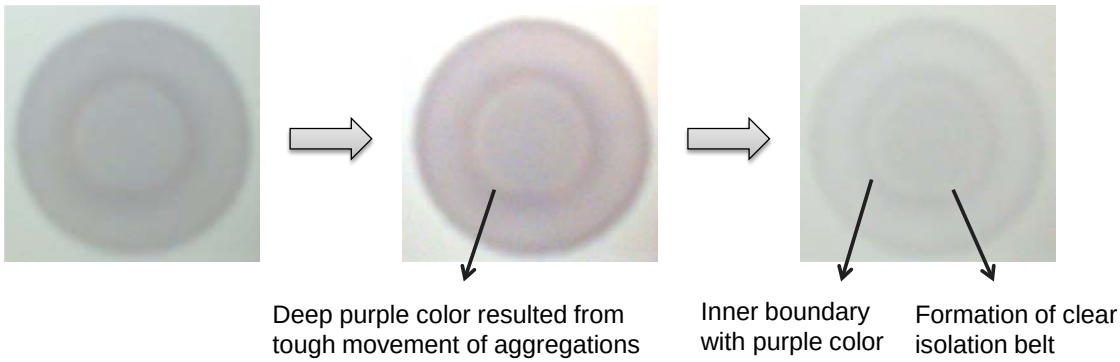

Figure 3.13 Photos of one droplet of colloid III.1-P0 onto the TLC silica gel.

The HMLD test of colloid III.1-P0 evidences the consistent result of UV spectra that this colloid varying with time possesses heterogeneous size distribution and even large aggregations.

3.5.2.2 Colloid III.2-P0.5 (UV-535 nm)

The results of HMLD test over colloid III.2-P0.5 is very similar with that of colloid III.1-P0,

expect that the essential color is light pink and the inner boundary and layer is not that obvious (Figure 3.14). A very thick pink-purple edge is observed during the drying process. If carefully watched under light, the inner diffusion layer can be observed. From the result of HMLD test, it can be seen that only very few amount of PVA (e.g. PVA: Au = 0.5 weight ratio, equal to 0.002: 1 molar ratio) is quite helpful for the protection of Au-NPs from growing.

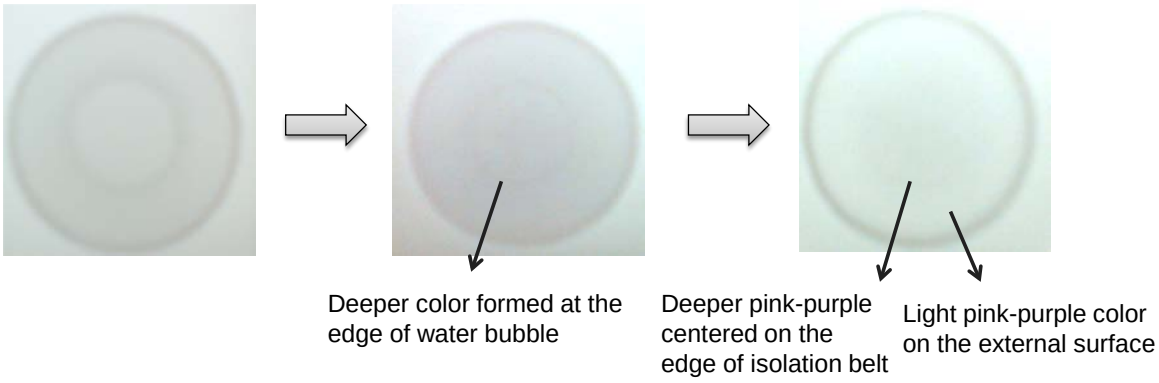

Figure 3.14 Photos with time after one drop of colloid III.2-P0.5 onto the TLC silica gel. The third image is treated by changing the luminance and contrast to be -13% and 41% respectively for a better view of the inner layer.

3.5.2.3 Colloid III.5-P5 (UV-510 nm)

Figure 3.15 displays the photos with time after one droplet of colloid III.5-P5 onto the TLC silica gel. The satisfactory diffusion procedure is performed over this colloid as displayed below. The color of the outside circle becomes deeper pink than the inner circle at the beginning due to the fast diffusion of colloid, indicating that small particles exist in this colloid and are freely move with the liquid. No boundary is formed after the water in the initial contact layer diffuses out, suggesting that the particle sizes of Au-NPs is generally homogeneous. Besides, very thick pink boundary is displayed at the end and the silica surface is covered by uniform light pink, further evidencing that the Au-NPs in this colloid should be small with narrow size distribution.

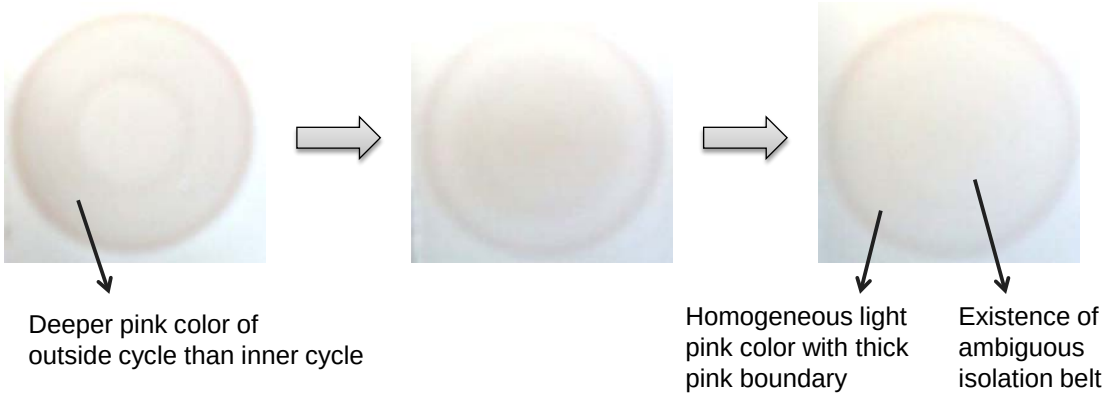

Figure 3.15 Photos with time after one droplet of colloid III.5-P5 onto the TLC silica gel.

Among all the colloids prepared from the applied method, the colloid III.5-P5 (the same of II.5-S5) is applied to be the most favorable sample with both small sizes and narrow size distribution from the combination results of the colloid color, the UV-vis spectra, and the HMLD test.

3.6 Proposal of Au-NPs migration in function of sizes and forms

Based on the above results from the color, the UV-vis spectra, the HMLD test, and the SEM images, the relationship between plasmon bonds, the possible sizes and morphologies, and the migrations of Au-NPs can be revealed as illustrated in Schema 3.3. For the gold colloid with symmetric plasmon bond around 510-520 nm (upper panel of Schema 3.3), the results of HMLD test generally display homogeneous distribution of light pink or purple color (depending on the real color of the colloid) with thick pink/orange or purple color boundary. One very light and thin limitation or isolation belt will show in the inner circle because of the initial contact of liquid and silica. The Au-NPs are homogeneous distributed on the diffusion layer. The color of the inner surface and boundary of the diffusion layer is corresponding to the particles sizes and can be revealed also from the half width of plasmon bonds. The broader plasmon bond related to pink boundary resulted from smaller Au-NPs, whereas the colloid with sharp plasmon bond and larger homogeneous Au-NPs displays purple boundary.

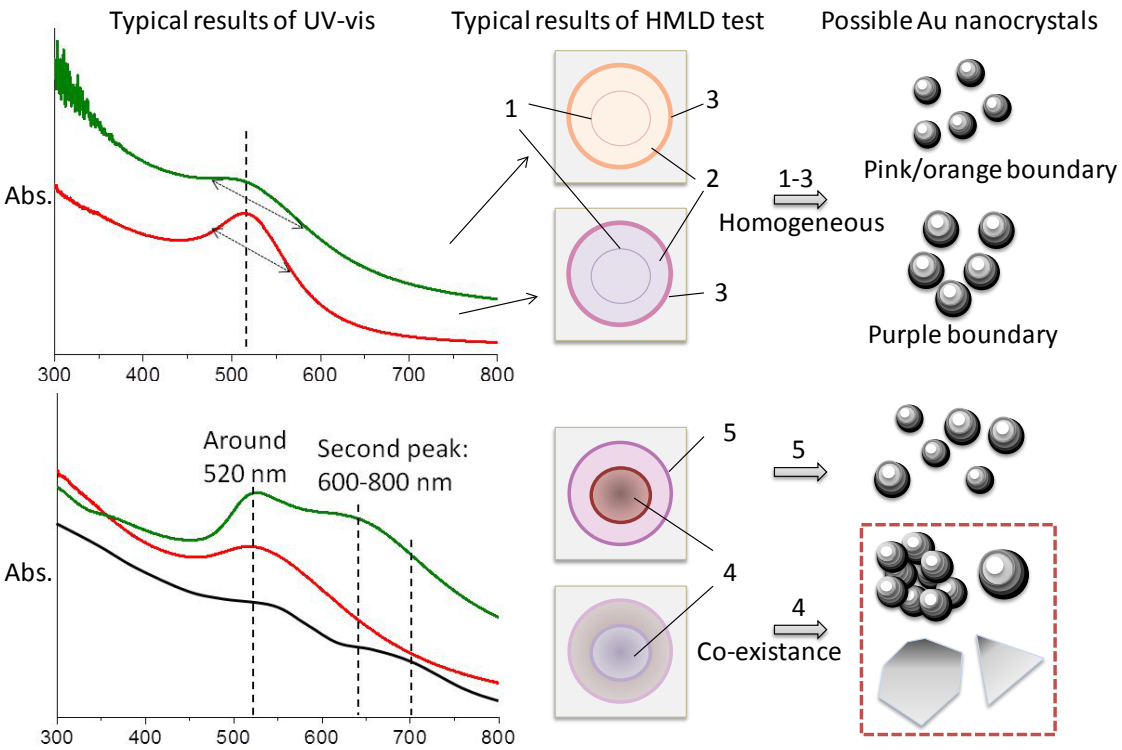

Schema 3.3 Illustration of the relevance between the UV-vis absorbance spectra, the home-made liquid diffusion (HMLD) tests, and the possible morphologies of gold nanocrystals.

1 Initial contact layer; 2 Diffusion circle with homogeneous color: light pink or purple; 3 Thick boundary with pink or purple color; 4 Clear inner diffusion layer with deeper color; 5 The boundary of outside diffusion layer is thin or even unambiguous with purple or violet color.

For the gold colloid with heterogeneous particles, the situation is more complicated. The relative UV-vis absorbance spectra display one asymmetric and broad peak until 700-800 nm, or two or multiple overlapped peaks locating around 520 nm and 600-800 nm, respectively. The typical results of HMLD test can be seen in the lower penal of Schema 3.3. Under these circumstances, the diffusion of liquid during the HMLD test is going to perform two different diffusion circles: the inner diffusion circle caused by the liquid-silica initial contact that forces the restriction of larger particles and aggregations; and the outside diffusion layer contributed by smaller nanoparticles more facile to move. As shown in Schema 3.3 (4-5), the smaller Au-NPs in colloid are ready to move on the outside circle and limited by the boundary. Since

the Au-NPs in these colloids are heterogeneous, the smaller Au-NPs at the boundary 5 are more likely to be consisted by Au-NPs with broad size distribution. The inner circle restrains the mobility of large crystals, which might have the co-existence of larger particles, aggregations, and also huge crystals with various morphologies.

For inorganic heterogeneous catalytic application, the size of Au-NPs must be lower than 5 nm and due to the property of small nanoparticles, it is really important to have a homogeneous distribution of sizes [57]. The best color of colloid solution is red, the profile of UV-vis is broad and centered around 510-520 nm. The result of HMLD test ought to be a uniform light color inside the circle and a thick boundary (e.g. with pink color). This is the case of the sample III.5-P5 = II.5-S5; the most favorable sample with both small sizes and narrow size distribution from the combination results of the color, the UV-vis spectra, and the HMLD test. The TEM profile of this colloid, just supported onto another kind of silica support (Stöber silica), was presented in a previous paper of the Strasbourg's lab [58]. The images show the sizes of gold particles. The average size of colloid III.5-P5 supported on silica spheres is 2.9 nm with a deviation of 0.7 nm.

3.7 Conclusion

Serious of gold colloids were prepared by colloid methods. The best conditions for preparing homogeneous and small colloidal Au-NPs were by using 5: 1 molar ratio of $NaBH_4$: Au, 5: 1 weight ratio of PVA: Au under room temperature. The plasmon resonance bonds revealed from UV-vis spectra and the colors of colloids were applied as basic observation for estimating the morphologies of colloidal Au-NPs. Under the help of a special test named home-made liquid diffusion (HMLD), additional information was obtained and efficient for comparing and choosing gold colloid with different Au-NPs size distributions. The theory was also evidenced by the SEM technique. Although the Transmission Electron Microscopy (TEM) technique could provide the information of Au-NPs more precisely, the technique is expensive and cost of time. For people engaging in the work concerning gold colloid, which might be based on

fussy and mass of fundamental preparation work, the HMLD method in this work is essential for providing further information of colloidal Au-NPs, especially when the color and UV-vis spectra results reveal only complex or insufficient information. The HMLD method is helpful for choosing gold colloid consisting by small and homogeneous Au-NPs before complicated and expensive characterizations.

Bibliography

[1] M. Faraday, The bakerian lecture: Experimental relations of gold (and other metals) to light, Philosophical Transactions of the Royal Society of London, 147 (1857) 145-181.

[2] R. Zsigmondy, E.B. Spear, J.F. Norton, The chemistry of colloids, 1st ed., John Wiley & sons, inc.; etc., New York,, 1917.

[3] E. Prodan, P. Nordlander, N.J. Halas, Electronic structure and optical properties of gold nanoshells, Nano Letters, 3 (2003) 1411-1415.

[4] C.F. Bohren, D.R. Huffman, Absorption and scattering of light by small particles, Wiley, New York, 1983.

[5] J. Kimling, M. Maier, B. Okenve, V. Kotaidis, H. Ballot, A. Plech, Turkevich method for gold nanoparticle synthesis revisited, Journal of Physical Chemistry B, 110 (2006) 15700-15707.

[6] X.H. Ji, X.N. Song, J. Li, Y.B. Bai, W.S. Yang, X.G. Peng, Size control of gold nanocrystals in citrate reduction: The third role of citrate, Journal of the American Chemical Society, 129 (2007) 13939-13948.

[7] M. Luty-Blocho, K. Fitzner, V. Hessel, P. Lob, M. Maskos, D. Metzke, K. Paclawski, M. Wojnicki, Synthesis of gold nanoparticles in an interdigital micromixer using ascorbic acid and sodium borohydride as reducers, Chemical Engineering Journal, 171 (2011) 279-290.

[8] H.S. Fan, X.L. Yu, Y.H. Long, X.Y. Zhang, H.F. Xiang, C.T. Duan, N. Zhao, X.L. Zhang, J. Xu, Preparation of kapok-polyacrylonitrile core-shell composite microtube and its application as gold nanoparticles carrier, Applied Surface Science, 258 (2012) 2876-2882.

[9] S. Patra, J. Das, H. Yang, Selective deposition of Pt on Au nanoparticles using hydrogen presorbed into Au nanoparticles during $NaBH_4$ treatment, Electrochimica Acta, 54 (2009) 3441-3445.

[10] A. Beck, A. Horvath, G. Stefler, R. Katona, O. Geszti, G. Tolnai, L.F. Liotta, L. Guczi, Formation

and structure of Au/TiO_2 and Au/CeO_2 nanostructures in mesoporous SBA-15, Catalysis Today, 139 (2008) 180-187.

[11] S.K. Ghosh, S. Nath, S. Kundu, K. Esumi, T. Pal, Solvent and ligand effects on the localized surface plasmon resonance (LSPR) of gold colloids, Journal of Physical Chemistry B, 108 (2004) 13963-13971.

[12] Y.V. Bokshits, N.P. Osipovich, E.A. Strel'tsov, G.P. Shevchenko, Underpotential deposition of lead on silver and gold colloids, Colloids and Surfaces a-Physicochemical and Engineering Aspects, 242 (2004) 79-83.

[13] O. Tzhayik, P. Sawant, S. Efrima, E. Kovalev, J.T. Klug, Xanthate capping of silver, copper, and gold colloids, Langmuir, 18 (2002) 3364-3369.

[14] B. Pergolese, A. Bigotto, M. Muniz-Miranda, G. Sbrana, Gold/palladium and silver/palladium colloids as novel metallic substrates for surface-enhanced Raman scattering, Applied Spectroscopy, 59 (2005) 194-199.

[15] M.E. Garcia, L.A. Baker, R.M. Crooks, Preparation and characterization of dendrimer-gold colloid nanocomposites., Abstracts of Papers of the American Chemical Society, 215 (1998) U460-U461.

[16] M.A. Sobhan, M.J. Withford, E.M. Goldys, Enhanced stability of gold colloids produced by femtosecond laser synthesis in aqueous solution of CTAB, Langmuir, 26 (2010) 3156-3159.

[17] W. Huang, S.M. Chen, Y.S. Liu, H.Y. Fu, G.Z. Wu, The controlled synthesis of stable gold nanoparticles in quaternary ammonium ionic liquids by simple heating, Nanotechnology, 22 (2011).

[18] K. Zhu, L.Q. Huang, J. Zhu, Z.Y. Zhuang, Influence of TX-100 on the size controlled synthesis of gold colloid, Spectrochimica Acta Part a-Molecular and Biomolecular Spectroscopy, 69 (2008) 566-571.

[19] S.I. Stoeva, A.B. Smetana, C.M. Sorensen, K.J. Klabunde, Gram-scale synthesis of aqueous gold colloids stabilized by various ligands, Journal of Colloid and Interface Science, 309 (2007) 94-98.

[20] R. Kaur, B. Pal, Size and shape dependent attachments of Au nanostructures to TiO_2 for optimum reactivity of Au-TiO_2 photocatalysis, Journal of Molecular Catalysis a-Chemical, 355 (2012) 39-43.

[21] J.A. Lopez-Sanchez, N. Dimitratos, P. Miedziak, E. Ntainjua, J.K. Edwards, D. Morgan, A.F. Carley, R. Tiruvalam, C.J. Kiely, G.J. Hutchings, Au-Pd supported nanocrystals prepared by a sol immobilisation technique as catalysts for selective chemical synthesis, Physical Chemistry Chemical Physics, 10 (2008) 1921-1930.

[22] Y.S. Chi, H.P. Lin, C.Y. Mou, CO oxidation over gold nanocatalyst confined in mesoporous silica,

Applied Catalysis a-General, 284 (2005) 199-206.

[23] G.C. Bond, The effect of the metal to non-metal transition on the activity of gold catalysts, Faraday Discussions, 152 (2011) 277-291.

[24] M. Alhumaimess, Z.J. Lin, W.H. Weng, N. Dimitratos, N.F. Dummer, S.H. Taylor, J.K. Bartley, C.J. Kiely, G.J. Hutchings, Oxidation of benzyl alcohol by using gold nanoparticles supported on ceria foam, Chemsuschem, 5 (2012) 125-131.

[25] C.M. Xue, O. Birel, M. Gao, S. Zhang, L.M. Dai, A. Urbas, Q. Li, Perylene monolayer protected gold nanorods: Unique optical, electronic properties and self-assemblies, Journal of Physical Chemistry C, 116 (2012) 10396-10404.

[26] N. Gandra, A. Abbas, L.M. Tian, S. Singamaneni, Plasmonic planet-satellite analogues: Hierarchical self-assembly of gold nanostructures, Nano Letters, 12 (2012) 2645-2651.

[27] H. Jans, Q. Huo, Gold nanoparticle-enabled biological and chemical detection and analysis, Chemical Society Reviews, 41 (2012) 2849-2866.

[28] J. Perez-Juste, I. Pastoriza-Santos, L.M. Liz-Marzan, P. Mulvaney, Gold nanorods: Synthesis, characterization and applications, Coordination Chemistry Reviews, 249 (2005) 1870-1901.

[29] K.A. Willets, R.P. Van Duyne, Localized surface plasmon resonance spectroscopy and sensing, Annual Review of Physical Chemistry, 58 (2007) 267-297.

[30] C.R. Yonzon, D.A. Stuart, X.Y. Zhang, A.D. McFarland, C.L. Haynes, R.P. Van Duyne, Towards advanced chemical and biological nanosensors - An overview, Talanta, 67 (2005) 438-448.

[31] C.R. Yonzon, E. Jeoungf, S.L. Zou, G.C. Schatz, M. Mrksich, R.P. Van Duyne, A comparative analysis of localized and propagating surface plasmon resonance sensors: The binding of concanavalin a to a monosaccharide functionalized self-assembled monolayer, Journal of the American Chemical Society, 126 (2004) 12669-12676.

[32] A.J. Haes, L. Chang, W.L. Klein, R.P. Van Duyne, Detection of a biomarker for Alzheimer's disease from synthetic and clinical samples using a nanoscale optical biosensor, Journal of the American Chemical Society, 127 (2005) 2264-2271.

[33] L. Wang, C. Clavero, Z. Huba, K.J. Carroll, E.E. Carpenter, D.F. Gu, R.A. Lukaszew, Plasmonics and enhanced magneto-optics in core-shell Co-Ag nanoparticles, Nano Letters, 11 (2011) 1237-1240.

[34] F. Xia, X.L. Zuo, R.Q. Yang, Y. Xiao, D. Kang, A. Vallee-Belisle, X. Gong, J.D. Yuen, B.B.Y. Hsu, A.J. Heeger, K.W. Plaxco, Colorimetric detection of DNA, small molecules, proteins, and ions using

unmodified gold nanoparticles and conjugated polyelectrolytes, Proceedings of the National Academy of Sciences of the United States of America, 107 (2010) 10837-10841.

[35] Y. Wang, Voltage-induced color-Selective absorption with surface-plasmons, Applied Physics Letters, 67 (1995) 2759-2761.

[36] G.M. Veith, A.R. Lupini, S.J. Pennycook, A. Villa, L. Prati, N.J. Dudney, Magnetron sputtering of gold nanoparticles onto WO_3 and activated carbon, Catalysis Today, 122 (2007) 248-253.

[37] M. Comotti, W.C. Li, B. Spliethoff, F. Schuth, Support effect in high activity gold catalysts for CO oxidation, Journal of the American Chemical Society, 128 (2006) 917-924.

[38] N. Dimitratos, A. Villa, C.L. Bianchi, L. Prati, M. Makkee, Gold on titania: Effect of preparation method in the liquid phase oxidation, Applied Catalysis a-General, 311 (2006) 185-192.

[39] F. Porta, L. Prati, M. Rossi, G. Scari, New Au(0) sols as precursors for heterogeneous liquid-phase oxidation catalysts, Journal of Catalysis, 211 (2002) 464-469.

[40] T.M. Wang, W.M. Liu, J. Tian, Preparation and characterization of gold/poly(vinyl alcohol)/MoS_2 intercalation nanocomposite, Journal of Materials Science-Materials in Electronics, 15 (2004) 435-438.

[41] D.G. Duff, A. Baiker, P.P. Edwards, A new hydrosol of gold clusters .1. Formation and particle-size variation, Langmuir, 9 (1993) 2301-2309.

[42] S. Ivanova, C. Petit, V. Pitchon, A new preparation method for the formation of gold nanoparticles on an oxide support, Applied Catalysis a-General, 267 (2004) 191-201.

[43] K.L. Ai, Y.L. Liu, L.H. Lu, Hydrogen-bonding recognition-induced color change of gold nanoparticles for visual detection of melamine in raw milk and infant formula, Journal of the American Chemical Society, 131 (2009) 9496-+.

[44] C.G. Wang, Z.F. Ma, Z.M. Su, Synthesis and self-assembly of silica-coated anisotropic gold nanoparticle films, Nanotechnology, 17 (2006) 1819-1824.

[45] Q. Xie, J. Zhou, L. Kang, Q. Zhao, B. Li, Y.H. Wang, R.L. Zong, X.G. Huang, Preparation of optically anisotropic nanocomposites with oriented gold nanorods embedded in polyvinyl alcohol, Journal of Nanoscience and Nanotechnology, 10 (2010) 1829-1833.

[46] P. Yang, M. Ando, N. Murase, Various Au nanoparticle organizations fabricated through SiO_2 monomer induced self-assembly, Langmuir, 27 (2011) 895-901.

[47] S. Link, M.A. El-Sayed, Size and temperature dependence of the plasmon absorption of colloidal

gold nanoparticles, Journal of Physical Chemistry B, 103 (1999) 4212-4217.

[48] C.F. Li, D.X. Li, G.Q. Wan, J. Xu, W.G. Hou, Facile synthesis of concentrated gold nanoparticles with low size-distribution in water: temperature and pH controls, Nanoscale Research Letters, 6 (2011).

[49] Y.H. Gong, C. Shen, Y.Z. Lu, H. Meng, C.X. Li, Viscosity and density measurements for six binary mixtures of water (methanol or ethanol) with an Ionic liquid ([BMIM][DMP] or [EMIM][DMP]) at atmospheric pressure in the temperature range of (293.15 to 333.15) K, Journal of Chemical and Engineering Data, 57 (2012) 33-39.

[50] A. Currao, V.R. Reddy, G. Calzaferri, Gold-golloid-modified AgCl photocatalyst for water oxidation to O_2, ChemPhysChem, 5 (2004) 720-724.

[51] T. Makiabadi, A. Bouvree, V. Le Nader, H. Terrisse, G. Louarn, Preparation, optimization, and characterization of SERS sensor substrates based on two-dimensional structures of gold colloid, Plasmonics, 5 (2010) 21-29.

[52] L.F. Gou, C.J. Murphy, Fine-tuning the shape of gold nanorods, Chemistry of Materials, 17 (2005) 3668-3672.

[53] P.K. Jain, I.H. El-Sayed, M.A. El-Sayed, Au nanoparticles target cancer, Nano Today, 2 (2007) 18-29.

[54] S. Link, M.A. El-Sayed, Spectral properties and relaxation dynamics of surface plasmon electronic oscillations in gold and silver nanodots and nanorods, Journal of Physical Chemistry B, 103 (1999) 8410-8426.

[55] C. Baatz, N. Decker, U. Prusse, New innovative gold catalysts prepared by an improved incipient wetness method, Journal of Catalysis, 258 (2008) 165-169.

[56] K.S. Mayya, V. Patil, M. Sastry, On the stability of carboxylic acid derivatized gold colloidal particles: The role of colloidal solution pH studied by optical absorption spectroscopy, Langmuir, 13 (1997) 3944-3947.

[57] N. Weiher, E. Bus, L. Delannoy, C. Louis, D.E. Ramaker, J.T. Miller, J.A. van Bokhoven, Structure and oxidation state of gold on different supports under various CO oxidation conditions, Journal of Catalysis, 240 (2006) 100-107.

[58] J. Luo, W. Chu, S. Sall, C. Petit, Facile synthesis of monodispersed Au nanoparticles-coated on Stöber silica, Colloids and Surfaces a-Physicochemical and Engineering Aspects, 425 (2013) 83-91.

Chapter IV Preparation of Stöber silica and its supported gold nanoparticles

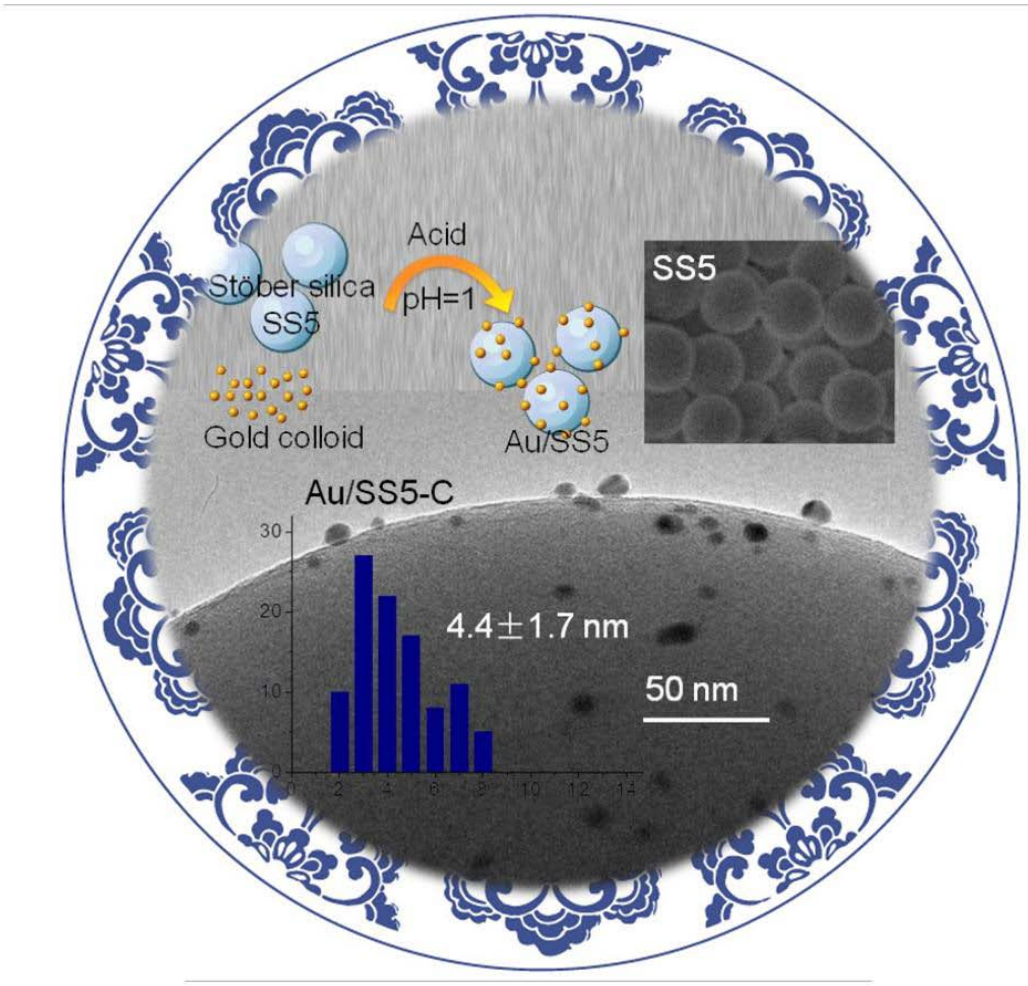

- The 2-4 nm colloidal gold nanoparticles are highly dispersed onto Stöber silica.
- Neither surfactant nor catalytic-poisonous compound is applied during coating.
- Small gold nanoparticles still exist after calcined at 300 ^{o}C for 4 h.
- Calcined gold particles are further fixed on silica by removing hydroxyl species.
- This method provided possibility for SiO_2@Au-like materials used for catalysis.

The homogeneous and tiny colloidal gold nanoparticles (2-4 nm) were utilized as the precursor and coated onto the non-porous Stöber silica by a facile method. For the first time, the coating process is fulfilled without either organosilanes or thiols compounds, which was invariably applied for Stöber silica to fix the gold particles in the previous work and thus limited the application of the gold material in inorganic heterogeneous catalysis field. For better understanding, the mechanism of the synthesis process was further analyzed. During the coating process, the gold nanoparticles protected by polyvinyl alcohol (PVA) surrounded with hydroxyl species were highly dispersed on the surface of Stöber silica. The following calcination facilitated the combining removal of hydroxyl species in both PVA and silica structure, and the gold nanoparticles anchored by residual hydroxyl species on the surface of Stöber silica. Major of the small particles about 3 nm remained their sizes even after calcination, which was just the satisfied size for some reactions such as CO oxidation. This simple and environmental synthesis method provided an available strategy for synthesizing gold catalysts with very small and ordered sizes that can be used for further investigation in the inorganic heterogeneous catalysis field.

4.1 Introduction

Gold nanoparticles (Au-NPs) have released huge attraction because of its unique optical and electric properties when dispersed as nanoscale in the fields such as optics, catalysis, biology, and medical science.[1-5] Recently, the colloidal Au-NPs are synthesized by reducing Au^{3+} solution and widely utilized for preparing novel and interesting materials.[6-8] Even in the catalysis field, the colloidal Au-NPs are also applied as a burgeoning material by several peers to overcome the problems such as high cost, complicated processes, and difficult control of particles size that always occur during general preparation of supported gold nanoparticles.[9, 10] Applying colloidal Au-NPs into the synthesis of gold materials possesses great advantages. People can on the one hand primarily assess metal particle sizes according to the surface plasmon resonance (SPR) effect and on the other hand the particles sizes can be controllable synthesized for supporting.[11] These two superiorities make the colloidal Au-NPs un-blamable to be welcome as the precursor of gold materials or even catalysts in the future. However, the nanoparticles from gold colloid captured by carrier such as silica are not that commonly applied until now.

The Au-NPs contained core-shell structure is one kind of material that is demanded according to its optical and catalytic activity, in which the Au-NPs can be controllably synthesized with demanded properties.[12] Silica is usually used as carrier for some metals such as gold and platinum.[13-16] In this work, we look especially into the silica material cooperated with gold. During the last five decades, a silica material provided by Stöber[17] was afterwards utilized in both fields of catalysis and novel material. The combination of synthesis of Stöber silica and colloidal metal nanoparticles provides broad approaches for plenty of material preparation including the currently hot core-shell structures and even core-shell-shell structures.[18-20] The only problem is that the as-synthesized Stöber silica is generally non-porous. In this circumstance anchoring the metal nanoparticles onto Stöber silica is a current entry point that the nanoparticles (of cause with required size distribution) can be

dispersed totally on the surface of support. Osterloh and co-workers[21] successfully obtained the citrate protected Au-NPs supported on the 3-ammoniumpropylsilyl (APS) modified silica, and observed the structure rearrangement induced by alkanethiol. Kim et al.[22] loaded the tetrakis (hydroxymethyl) phosphonium chloride (THPC) protected gold seeds onto the amine-functionalized silica nanoparticles. Some other researches also combine the colloidal Au-NPs with silica modified with amine or amino- agents.[21, 23] It is almost a common sense that the thiol and amine-contained agents are indispensible during the synthesizing of colloidal silica-gold related materials for the silica fixing the gold. However, such agents might become poison for the Stöber silica doped/coated/supported Au-NPs especially when they are applied in the catalysis field that is another renowned field of gold. Take the thiol- contained agent for instance, the S component as the impurity of the agents can be strongly adsorbed onto Au-NPs,[24] thus hinders the adsorption of reactants and even changes the sample structure.[25] Besides, the removal of these agents requires higher temperature[26] that is undesired for the Au-NPs in the inorganic heterogeneous catalysis field.

Here in this work, we explored a facile and inexpensive method for coating the tiny Au-NPs (2-4 nm) onto the mono-dispersed Stöber silica spheres with controllable sizes. During the whole synthesis procedure, here we used neither thiol nor amine. Two sizes of silica globules diameters were tested for observing the Au-NPs growth during calcination. The colloidal Au-NPs coating on the silica kept the initial small sizes and most of the particles remained small even after calcined at 300^{o}C for 4 h under air. The synthesis mechanism of the Au nanoparticles coated silica was further understood combining the XPS and in situ FTIR that the Au-NPs were anchored on the surface of silica by a seemingly dehydration process.

4.2 Characterization of as-prepared Stöber silica

4.2.1 The morphology of Stöber silica

Several Stöber silica materials with different globule diameters are prepared by varying the

amounts of reactants, named as SS1, SS2…SS5 along with the increase of diameters. The preparation method is shown in part 2.1.3 of Chapter II. Figure 4.1 displays the scanning electron microscope (SEM) images of several types of Stöber silica. The four Stöber silica materials display general spherical morphologies with average diameter about 48 nm, 42 nm, 153 nm and 490 nm, respectively. The SS1 is consisted by homogeneous globular balls around 48 nm. By contrast, the average size of SS2 prepared by less amount of ammonia is a little bit smaller than that of SS1. The silica structures of both SS1 and SS2 are condensed. The SS1 is constituted by generally regular globules, whereas the morphology in SS2 is hardly spherical. The irregular silica particles in SS2 are even connected to each other with ambiguous boundary. Silica globules with very small diameters are reported very hard to be controlled as homogeneous spheres.

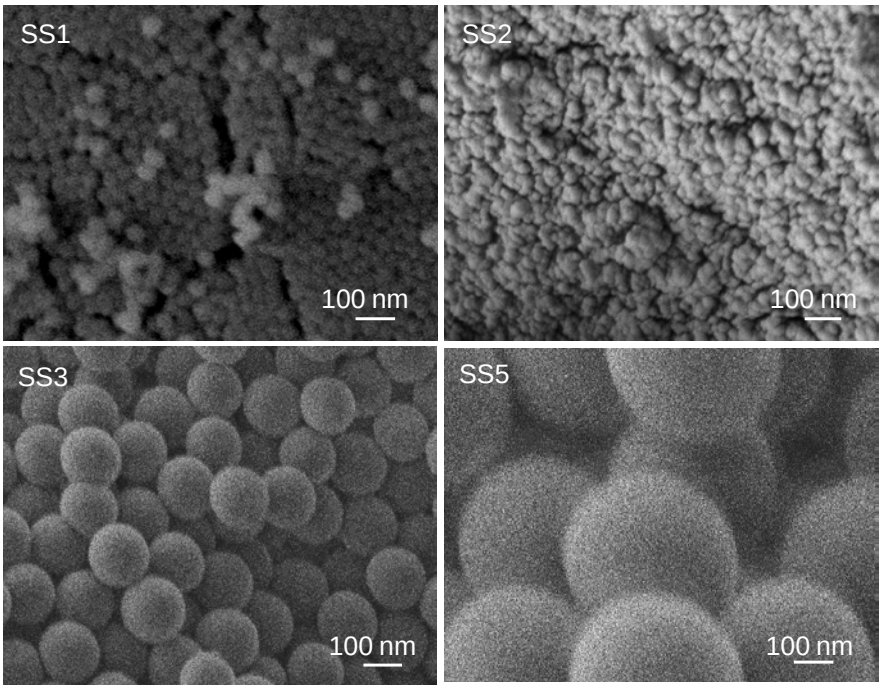

Figure 4.1 SEM images of typical silica prepared by Stöber Method.

The SS3 and SS5 samples prepared with large amount of water and ammonia are compromised of obviously larger globules around 153 nm and 490 nm-both with typical spheres at uniform diameter without any additional small spheres. The purpose of applying the

Stöber silica as support for Au-NPs in this work is to obtain mono-dispersed Au-NPs locating on the surface of silica spheres. In the previous researches, the centrifugation process had to be introduced to remove the unqualified silica spheres to make homogeneous sizes.[22, 27-29] Interestingly, in this work we have controlled the parameters during the synthesis and obtained the very homogeneous mono-dispersed silica spheres using the in situ drying method without further centrifugation, indicating that the nucleation of Stöber silica are considerably uniform under operating conditions. The result is proved to be repetitive.

4.2.2 Chemical and physical properties of as-prepared silica

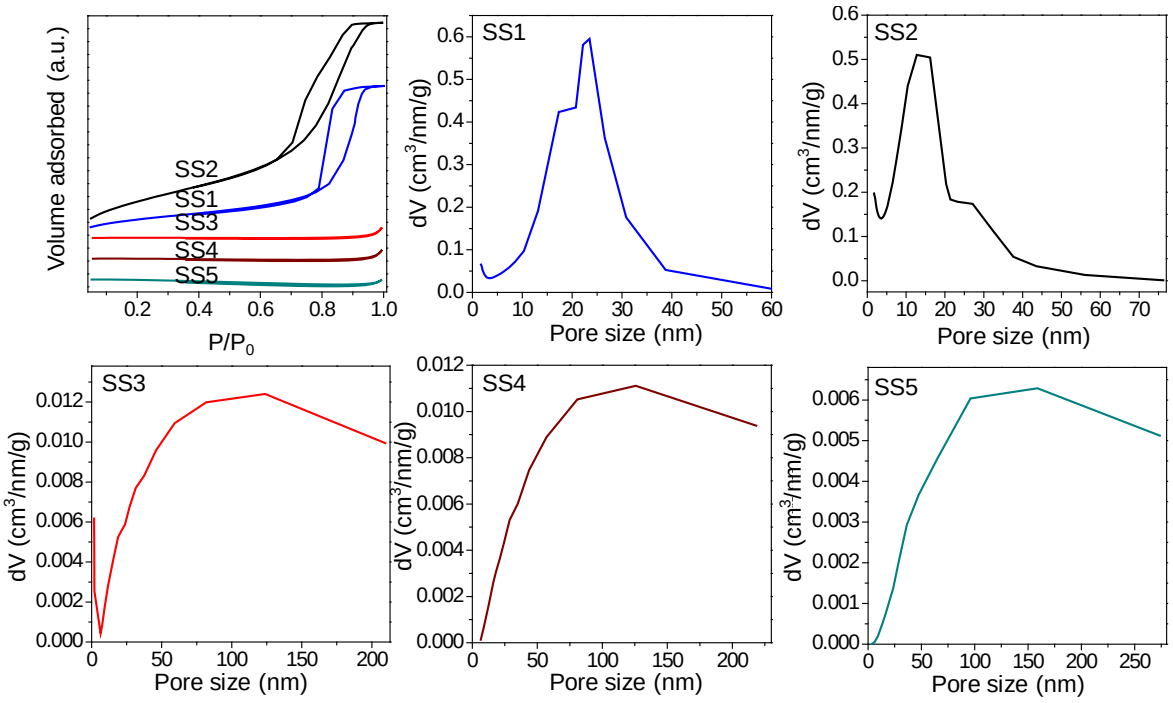

Figure 4.2 N_2 adsorption/desorption of five Stöber silica synthesized by different ratio of reactants and the corresponding size distribution.

The texture properties of Stöber silica are characterized by the N_2 adsorption/desorption measurements are shown in Figure 4.2 and Table 4.1. According to the previous papers [30], the surface area of the Stöber silica was general smaller than the other kind of silica due to their nonporous surface and was only several m^2/g. The synthesized SS1 and SS2 by less amount of

water possess larger surface area (Table 4.1), respectively. And the nominal average pore size is 10.5 nm and 6.5 nm-both the calculated average pore sizes range in the mesoporous domain. The N_2 adsorption/desorption isotherm curves of these two samples are classified to be type IV according to the classification of IUPAC [31]. The other three samples display very small surface area of less than 10 m^2/g, which is in the range of reported literatures. The isotherm curves from SS3 to SS5 display type II classification which are related to non-porous or macroporous structures [32]. H2 type of hysteresis loop reveals wedge-shaped pore structure or intervals between spherical structures which is consistent with the global morphologies of Stöber silica. The size distributions from SS3 to SS5 also indicate that the material possess 'macropores'. Besides, it can be realized from the very small surface area that the surface of the Stöber silica should be non-porous. In order to confirm this information, the microporosity of silica is also tested. From the comparison of the micropore volume (V_{micro}) and whole pore volume (V_{pore}) as listed in Table 4.1, it can be realized that there exist very few amount of micropores contributing to the very small total volume, which are nearly negligible and the materials can be viewed as non-porous. According to the variation of the real diameter observed by SEM (D_{SEM}), it can be seen that the rising dosages of both water and ammonia could help increase the silica globules diameters. When the diameter of silica globule is small (lower than 50 nm), the silica globules are very hard to be prepared as traditional spherical but heterogeneous both on the size and morphology. It has to be mentioned that the tested texture properties such as pore sizes are not real "pores" of Stöber silica taking the very small S_{BET} and the V_{pore} into consideration, but the distances between each large silica globules. However, such measurement is not futile but could give some information of the real morphologies of the silica globules. The very large surface area of SS1 and SS2 samples can be ascribed to the mesopores generated from the intervals between small globules. For the samples composed of larger silica globules, the average pore volumes and surface areas slowly diminished and the tested average pore sizes become huge. It can be observed from Figure 4.1 and 4.2 that the variation tendency of the visible diameters of Stöber silica from SEM (D_{SEM}) and average pore sizes (D_{pore}) seems to be the same orientation.

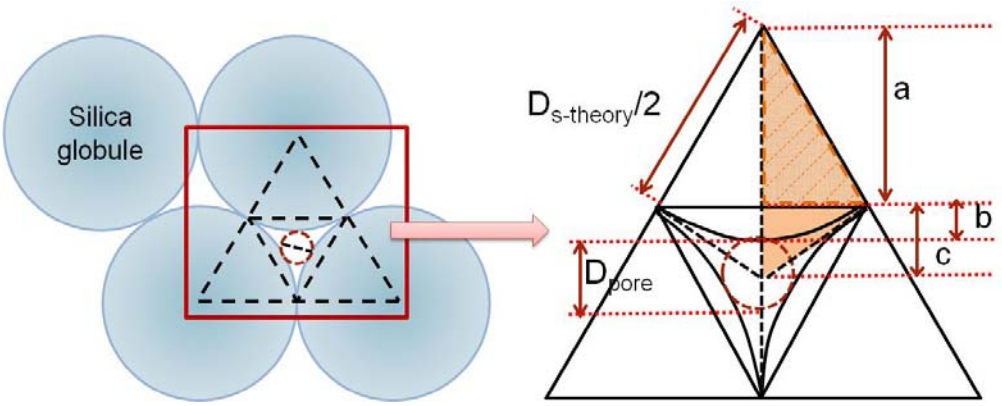

Scheme 4.1 The calculation method of the theoretical average pore diameter of Stöber silica globules.

In order to preliminarily estimate the diameter of the silica globules in each sample, we are trying to find out an available equation of the diameter as a function of D_{pore}, in which each globules in silica is assumed to be regular spherical and orderly arranged one by one as shown in Scheme 4.1. Herein, the pore volume and average pore diameter ought to be calculated from the seemed triangular slit as shown in Scheme 1. We defined the diameter of the centered red circle to be the pore size of the related Stöber silica. The calculation method is accomplished by simplifying the silica structure to be geometric as illustrated in the right image of Scheme 1. Then, the theoretical results that can be calculated by the following equations are listed in Table 4.1 as $D_{s\text{-}theory}$.

$$D_{pore}/2 = c - b \tag{4.1}$$

$$D_{s\text{-}theory} = \sqrt{3}\,(a + c) \tag{4.2}$$

$$b = D_{s\text{-}theory}/2 \tag{4.3}$$

$$a = \sqrt{3}\,/(4\,D_{s\text{-}theory}) \tag{4.4}$$

$$\rightarrow \quad D_{s\text{-}theory} = 6.464 D_{pore} \tag{4.5}$$

From Table 4.1 it can be seen that the theoretical values calculated from the BET results differ not much from D_{SEM} but generally larger than the D_{SEM}. Further investigation is under consideration to explain this interesting phenomenon. No matter how, the theoretical value $D_{s\text{-}theory}$ can be preliminarily help estimating the probable diameter of the as-synthesized Stöber silica before TEM analysis and partly lowered the expenditure. The SS1 and SS5 consisted by spheres around 50 nm and 500 nm are chosen to be the cores for colloidal Au-NPs coating.

Table 4.1 The texture properties and the average diameter of silica globules from theoretical calculation and SEM technique.

Texture properties from N_2 adsorption results						
	S_{BET} (m^2/g)	V_{pore} (cc/g)	V_{micro} (cc/g)	D_{pore} (nm)	$D_{s\text{-}theoryl}$ (nm)	D_{SEM} (nm)
SS1	88.3	0.21	0.021	11	68	48
SS2	324.9	0.34	n.d.[a]	7	42	42
SS3	7.1	0.01	0.008	30	196	153
SS4	5.9	0.01	0.001	53	340	n.a.
SS5	3.7	< 0.01	0.004	90	580	490

[a] n.d.: There is no available data detected.

4.3 Colloidal gold nanoparticles coated Stöber silica

4.3.1 Synthesis of Au/SS5-C

The synthesis method of Au/SS5-C is simple as shown in part 2.1.4 of Chapter II. The as-synthesized silica supported Au-NPs are named as Au/SS1 and Au/SS5. After calcination, the two samples are marked as Au/SS1-C and Au/SS5-C, respectively. In the traditional synthesize methods for preparing supported Au-NPs such as impregnation and deposition-precipitation method, the real variation and development of Au-NPs during deposition and calcination is generally not mentioned.[33, 34] Different from the traditional methods, in this work both the Au-NPs and silica globules were already preformed before the coating process. Thus what happens during the coating process can be clearly understood. Besides, the Stöber silica is non-porous globules unlike normal mesoporous supports. Thus

under this circumstance, the Au-NPs can be totally dispersed on the surface of silica. During the calcination, there is no chance for the Au-NPs to be trapped into the pores of support, which makes the analysis of the growth mechanism much more facile.

The UV-vis measurement is a useful technique for preliminary understanding the sizes and shapes of Au-NPs before microscopy analysis. The illustration in Figure 4.3 displays the desired synthesis path in this work. Correspondingly, the UV-vis spectra of Au/SS1 and Au/SS5 during preparation are also shown.

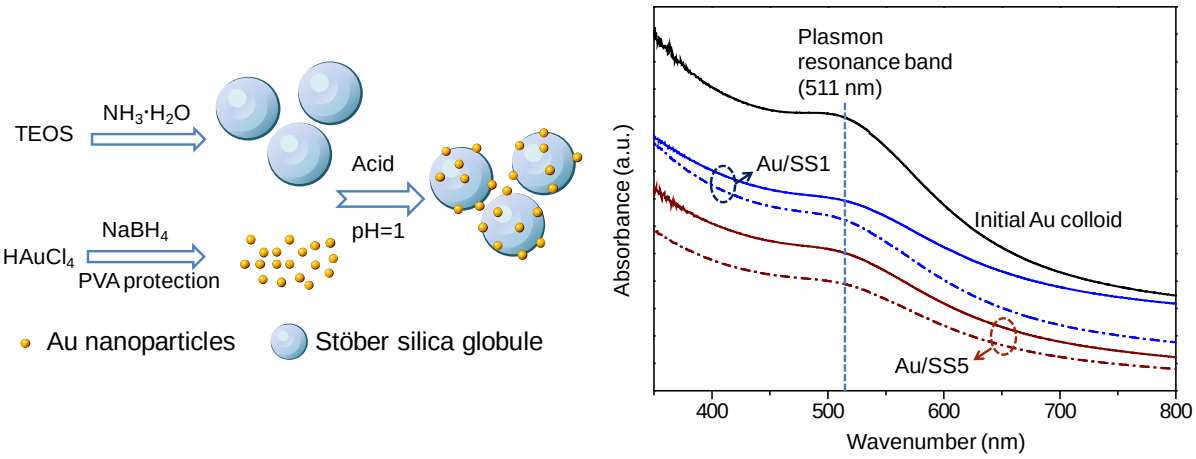

Figure 4.3 Illustration of the expected synthesis progress (left) and UV-vis spectra (right) of liquid during the preparation of Au/SS1 and Au/SS5. The solid lines are taken from the solution stirred for 10 min after the pH value adjusted to 1; the hollow lines are taken from the supernatant solution after centrifugation.

The initial gold colloid displays one peak at about 511 nm that is not very intensive. It was previous reported that the colloid Au-NPs generally possessed the plasmon resonance absorbance at about 520 nm due to the collective oscillation of electrons [35]. The position of this peak will changed along with the shape and size of Au-NPs. The weak peak at 511 nm indicates the existence of very small spherical Au-NPs (only several nm). We have tested the impact of the pH modification. Without the adjustment of pH value, the color of the mother solution is barely changed after the coating procedure and even the centrifugation, the location and the

intensity of the absorption peak perform no differences. Adjusting of pH value to 1 after the silica is added into gold colloid, the color of the supernatant liquid become nearly transparent and the support changes from white to reddish brown. The first UV-vis scanning from the supernatant of mixture solution (solid line in Figure 4.3) is taken 10 min after the pH is settled to 1. As we mentioned before, the as-prepared Stöber silica is non-porous spheres, the initial ten minutes is thus decisive for the adsorption of Au-NPs onto silica surface. The largely reduced intensity of the plasmon resonance absorbance bond of supernatant liquid also reveals that Au-NPs have been partially captured by the surface of silica. After centrifugation, the intensity of the peak further decreased. It is indicated that the Au-NPs coated onto non-porous Stöber silica should be fulfilled under low pH value. Besides, the coating process cannot be fulfilled only by stirring, in which the centrifugation process is indispensible for capturing the Au-NPs. The coating process is more like a precipitation process with force. However the reason why these zero state Au nanoparticles loading onto silica favor the acid condition is still under discussion. It is also remarkable that the position of the absorption peaks over the initial colloid, the colloid after coating and centrifugation is barely shifted, demonstrating that the sizes of Au-NPs won't change during the coating process.

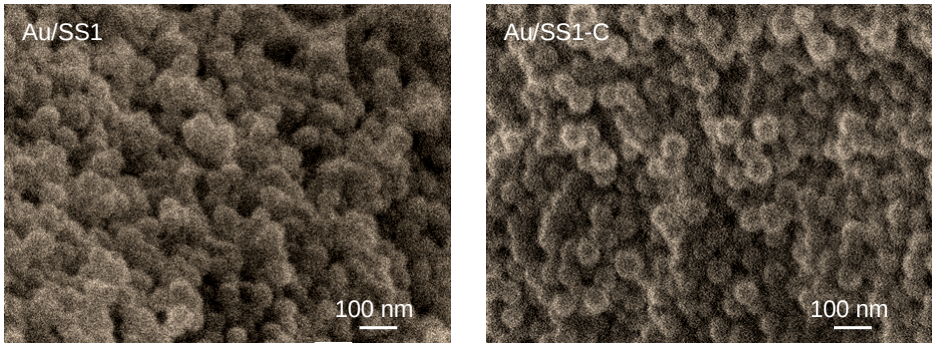

Figure 4.4 SEM images of Au/SS1 before (a) and after (b) calcination in air at 300 ^{o}C for 4 h.

For the view of the morphologies of Au-NPs coated silica samples, the SEM technology of Au/SS1 before and after calcination (300 ^{o}C for 4 h in air) is operated (Figure 4.4). No Au-NPs can be seen in the Au/SS1 sample before and after calcination. As shown in Figure 4.1, the bulk silica is compromised by compact silica globules layer by layer, and intervals exist between

spheres. After the Au-NPs coating on SS1, the globular morphology still maintains unless that the surface of the SS1 seems to be a little modified. There are still intervals between globules, but parts of the globules are connected by the glue-like stuff. After calcination, the Au/SS1-C is visualized to be more dispersed and with more regular globules comparing to the Au/SS1. The glue-like matters are disappeared. However, the images are lack of definition caused by the charge of silica. One cannot confirm that the glue-like matters are from PVA by the SEM images.

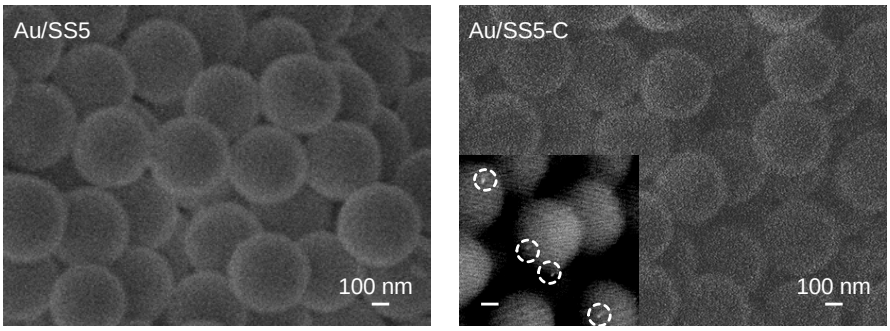

Figure 4.5 SEM images of Au/SS5 sample before (a) and after (b) calcination in air at 300 ^{o}C for 4 h. The bar in the inset picture of left image is 100 nm.

The SEM images of Au/SS5 before and after calcination are also carried out as shown in Figure 4.5. Different from the Au/SS1, the surface of each Au/SS5 globule is smooth without prominence. Glittery ring can be observed on the boundary of each silica sphere, which should be ascribed to the special light parameter when taking photos but not the gold. There is no clear observation of single Au-NPs before calcination. Since the theoretical loading of gold is rather low as 1 wt%, there is no chance for the gold to encapsulate the large SS5 spheres even as thin a layer. It is thus considered that the gold is dispersed on the surface. The inset picture in the right image of Figure 4.5 is a dark field microscopy of Au/SS5-C sample. Sporadic bright spots with size about 5-10 nm can be seen in the calcined Au/SS5-C, which is never found in the same sample before calcination, suggesting that some clustering of smaller Au-NPs occur during calcination. For better evidence, the TEM images are required.

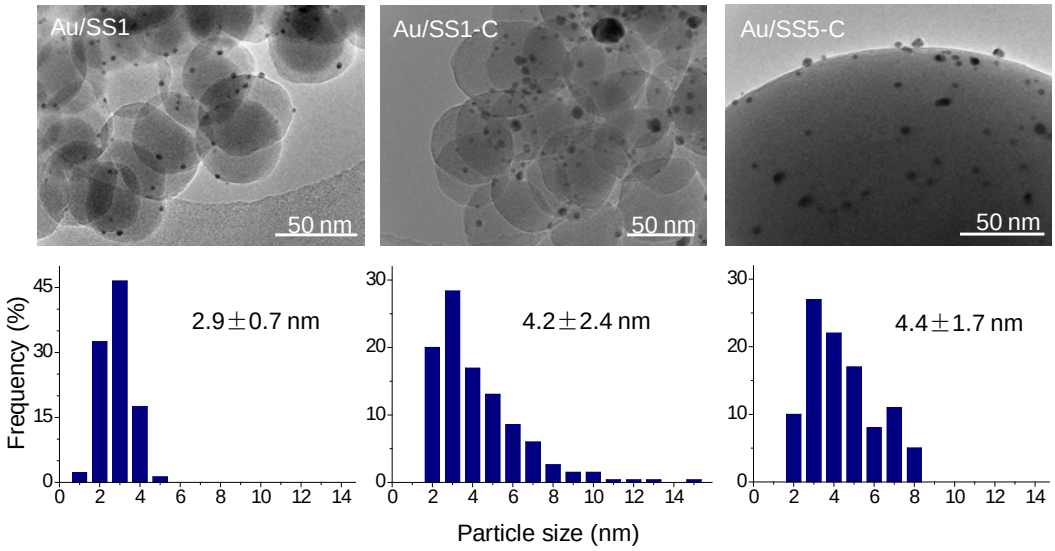

Figure 4.6 TEM images of Au/SS1, Au/SS1-C, and Au/SS5-C samples and the corresponding diameter distribution of three samples.

The TEM images of three samples based on SS1 and SS5 are shown in Figure 4.6. The revealed SS1 globules are mainly spheres with irregular boundaries. This is in accordance with the previous suggestion that the Stöber silica with smaller spherical diameter was more difficult to achieve, especially for those with diameters lower than 100 nm, the circular degree would also be decreased [36, 37]. The diameters of SS1 globules are mainly ranging from 40 nm to 60 nm, which is in accordance with the SEM. The Au-NPs with average size of 2.9 nm are highly dispersed on the surface of Stöber silica. During all the TEM images of Au/SS1, there is no observation of Au-NPs larger than 5 nm, most of which are around 3 nm. There are even black spots much smaller than 2 nm on the surface of the silica spheres. But since they are beyond the limitation of the microscope, it is difficult to declare that it is Au-NPs or not. They are not considered into the calculation of size distribution of Au-NPs. The image suggested that we have the first time successfully anchored the Au-NPs about 3 nm onto the surface of non-porous Stöber silica globules with a modified impregnation method. However, no legible observation of the PVA as layer encapsulating the surface is displayed. While the interesting part is that, during the characterization several Au-NPs was trying to leave the surface of silica spheres, nevertheless they were captured and pulled back by the glue-like substances on the surface

(Figure 4.7), which ought to be from the polymer-PVA. After calcination at 300^{o}C for 4 h under air, the size distribution of Au-NPs becomes much broader with the average diameter of 4.2 nm. Au-NPs larger than 5 nm and even of 15 nm are appeared. Some nanoparticles about 2 to 3 nm still maintain on the SS1 surface. It is indicated that there do exist some extremely small particles with melting-point lower than 300^{o}C (< 2 nm [38]), which are melted under calcination temperature and assembled into larger gold particles. In addition, small parts of the Au-NPs of 3 nm are also diminished. This is because of that during the calcination, the partial of the PVA are removed from the sample. The smaller Au-NPs without the protection of PVA begin to move for the sake of lower energy and formed clusters at higher temperature. No matter how, there are still considerable amounts of Au-NPs about 3 nm remaining on the surface of SS1, which is really interesting for some of the catalysis reaction [39].

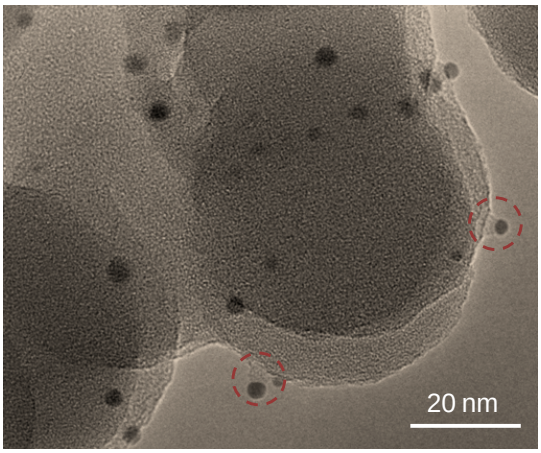

Figure 4.7 TEM image of Au/SS1. In this sample, Au-NPs about 3 nm was successfully loaded on the surface of SS1 support without addition of any organic couplant. The nanoparticles in the red circle on the surface of support are captured by the glue-like stuff, which is inferred to be the PVA.

The colloidal Au-NPs used for coating SS5 are the same of SS1. The TEM image of Au/SS5-C is displayed in Figure 4.6. After calcination, the Au-NPs in Au/SS5-C are also grown larger. Different from the Au/SS1-C sample, there is no gold particles larger than 8 nm were observed in all the images of Au/SS5-C and large amounts of nanoparticles are around 3 nm

which is in the ideal confine for some reactions as reported in previous work [40-42]. Since the single silica globule of SS5 possess much larger area than that of the SS1, the Au-NPs on the SS5 will be much separated from each other than on the SS1. During the calcinations process, the PVA was removed step by step, the smaller gold particles begin to move and have more chance to be clustered. It is inferred that the long distance between particles on SS5 makes the particles more difficult to move toward each other and partially protected the Au-NPs. Thus the Au-NPs in Au/SS5-C won't grow into very large particles as in Au/SS1-C.

4.3.2 Mechanism of gold nanoparticles anchored onto silica

In order to take a view of what happened during the calcination process, the in situ FTIR spectra are carried out during a simulation calcination procedure. The temperature increases from room temperature to 300°C at 1°C/min under air and the chosen spectra are shown in Figure 4.8.

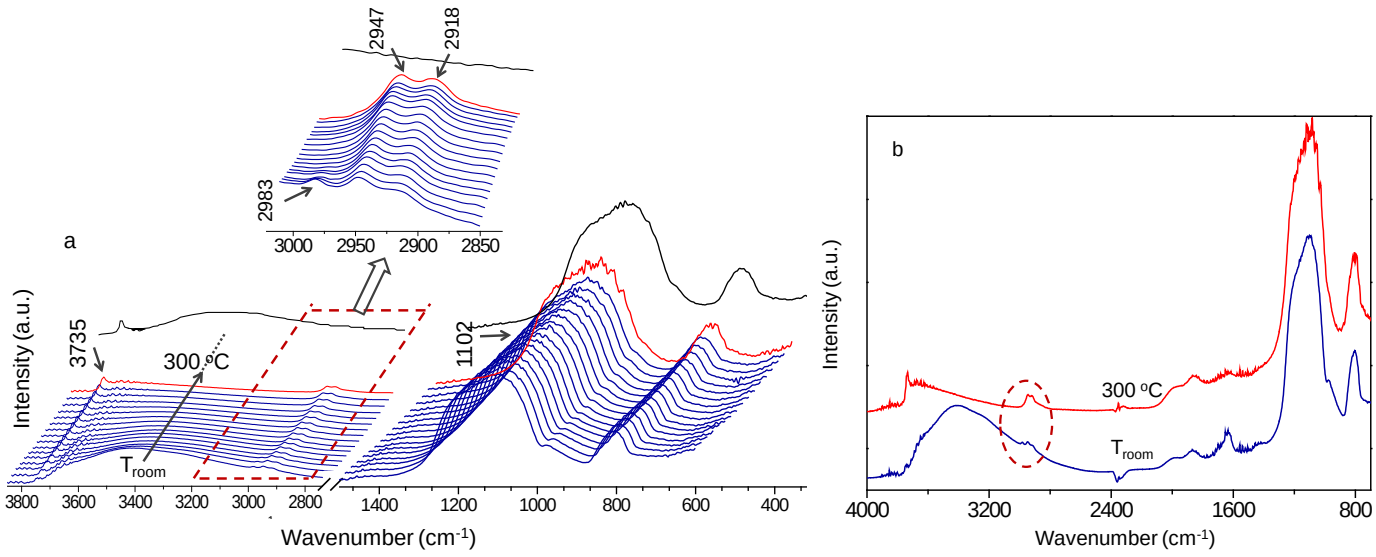

Figure 4.8 Operando FTIR spectra over Au/SS5 sample along with temperature rising from room temperature to 300°C by 1°C/min under air (a) and the comparison of Au/SS5 sample at room temperature and 300°C (b). The last black line in picture (a) is the spectrum of fresh Au/SS5-C after 4 h calcination at 300°C in air.

The multiple peaks ranging from 600-1400 cm^{-1} are belonged to the characteristic of silica structure and do not change much at the very beginning of temperature rising. Three peaks located at 2918, 2947 and 2983 cm^{-1} are observed and due to the C-H sp^3 stretch [43-45] that generated from the residual TEOS or PVA compounds. The large peaks locating at 3000-3700 cm^{-1} and 1400-2100 cm^{-1} are resulted from the Si-OH stretching [44] and water species in the sample, respectively. Along with the raising of temperature, the intensity of Si-OH bond and water species largely reduce at first and then gently decrease with time. The organic compounds are steadily removed from room temperature to 300^{o}C as shown in Figure 4.8(b). Two small peaks around 2950 cm^{-1} still exist until 300^{o}C. For the Au/SS5-C sample after calcined at 300^{o}C for 4 h, the IR spectra (the last black spectrum in Figure 4.8) displays no peak of C-H stretching evidences the totally remove of reactants utilized during the preparation of Au-NPs and silica. A new peak at 3735 cm^{-1} that is attributed to isolated Si-OH vibration [46] is present as well as the hydrate species decreases, indicating the lost of hydrate species from the silica structure. The decrease amount of hydrate species in silica structure together with the slightly increase of Si-O and Si-O-Si species (900-1200 cm^{-1}) demonstrating the variation of silica structure during calcination.

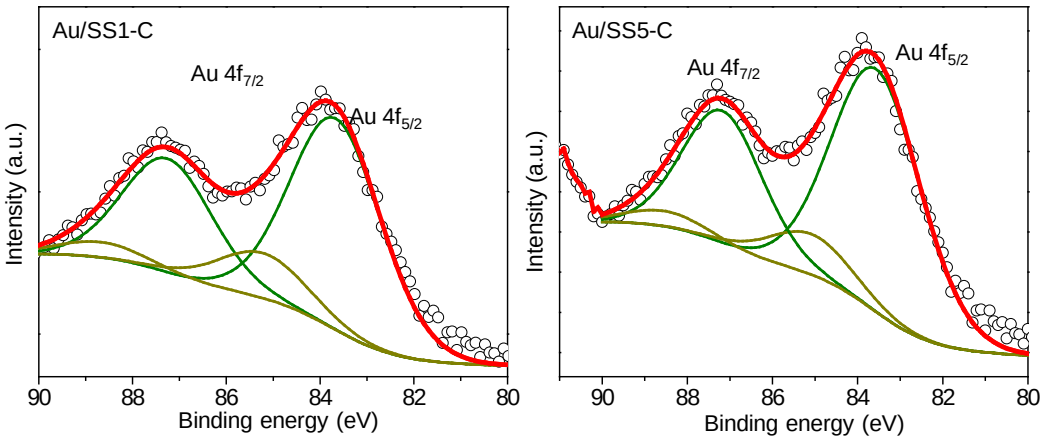

Figure 4.9 Au 4f XPS spectra of Au/SS1-C and Au/SS5-C.

The valence states and components surface ratio over Au/SS1-C and Au/SS5-C are characterized by X-ray photoelectron spectroscopy (XPS) technique. Figure 4.9 shows the Au 4f spectra of the two samples. Both the samples possess two overlapped peaks that can be fitted

by four peaks of o two states-one at about 84 eV- binding energy of Au $4f_{7/2}$ that corresponds to Au^0 species, the other with higher binding energy presenting the existence of $Au^{\delta+}$ species. The binding energy of Au $4f_{5/2}$ is about 3.65 eV higher than that of Au $4f_{7/2}$. Both the two calcined samples possess large amount of metallic Au species and minority of $Au^{\delta+}$ species. The surface ratios between tested elements are listed in Table 4.2 as below. It is surprisingly that the Au/Si ratio in Au/SS1-C is much lower than in Au/SS5-C. Since that the SS5 is non-porous and constructed by spheres much larger than the Au-NPs, it is believed that the Au-NPs are only highly dispersed on the surface of SS5. In this case, the atom ratio between different gold species revealed from XPS ought to be the same value of the real ratio of entire sample. Meanwhile, there is chance that the real atom ratio between Au and Si is larger than measured since the large inner part of the compact Stöber silica may not be directly detected by the machine. For SS1, the much smaller silica globules are more facile for the XPS scan over the Si component. From this point of view, the measured Au/Si ratio over Au/SS1-C should be somewhat lower than over Au/SS5-C. No matter how, the SS5 is considered better for Au-NPs coating for both Au-NPs dispersing and protecting.

Table 4.2 XPS data of Au/SS1-C and Au/SS5-C samples

Sample	Au $4f_{7/2}$ (eV)	Surface gold species	Atom ratio	
			Au/Si	Si/O
Au/SS1-C	83.7 84.5	Au^0 (80.1%) $Au^{\delta+}$ (19.9%)	0.5%	59.7%
Au/SS5-C	83.7 85.2	Au^0 (87.2%) $Au^{\delta+}$ (12.8%)	0.9%	62.5%

Based on the results from in situ FTIR and XPS, a model is put forward for understanding the preparation mechanism of supported Au-NPs on Stöber silica. After coating process, the Au-NPs are deposited on the surface of silica. The Au-NPs are dispersed and protected by PVA, a part of which is linked to the surface of silica globules by hydroxyl species (the first step of Scheme 4.2).

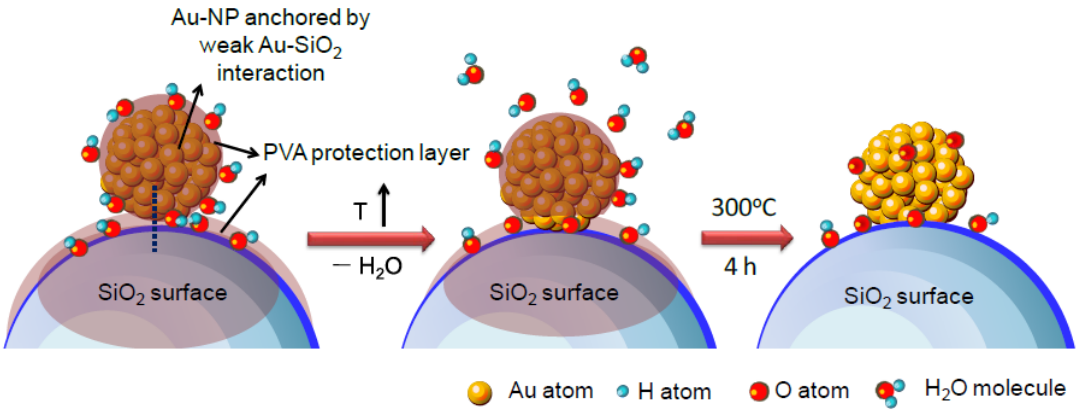

Scheme 4.2 Mechanism of Au-NPs anchored onto silica during calcination.

At the beginning of the calcinations, only absorbed water in the sample is quickly removed. After the temperature becomes higher, hydrate species either in silica structure or PVA layer protecting the Au-NPs are also started to be removed as water. Along with the temperature further raises, the PVA layer begins to be removed steadily by a combustion process. The emerged Au-NPs without covering of PVA are thus anchored on silica surface by the residual hydroxyl species as shown in the second step of Scheme 4.2. During the total calcination that includes temperature increase and maintenance, the PVA is finally burned out and the Au-NPs with edges and corner are exposed and fixed on the surface of Stöber silica. Minority of the gold species after calcination changes into partial oxidative stated $Au^{\delta+}$ species. The morphology of Stöber silica is mainly maintained as spheres as initial.

In fact, the Au-NPs coating globular silica can be both viewed as a basic model for the core-shell structures and the supported nano-gold material. The core-shell structure with this simple synthesis method can also be achieved by increasing the gold loading amounts as previous report [22]. Besides, this small Au-NPs coating silica provides a path for synthesizing gold catalysts that can be used in the inorganic heterogeneous catalysis field. By this simple method, the Au-NPs can be well dispersed on the surface of silica and separated from each other and on the other hand can be facilitate for the understanding of the gold-support interaction.

4.4 Conclusion

In the present work, we provided a strategy to synthesize Stöber silica coated by very small and homogeneous colloidal Au-NPs, in which the size of Au-NPs is controlled as the initial colloid (2-3 nm). This method is facile and inexpensive without either surfactant or catalytic-poisonous compound, thus providing an available path for this material utilized in the inorganic heterogeneous catalysis field. The Stöber silica with diameter much larger than the Au-NPs facilitated the high dispersion of Au-NPs and anti-clustering during calcination. The Au-NPs protected by PVA were bonded by silica, while the calcination process help the Au-NPs fixed on the silica surface by the residual hydroxyl species after combined removing of hydroxyl species in both PVA and silica structure. The satisfied part is that small nanoparticles still exist even after calcined at 300^{o}C for 4 h. The Au-NPs coated Stöber silica is very stable under temperature lower than 300^{o}C by this simple method, which can also be expended into SiO_2@Au structures (by increasing the content of Au), thus providing the perspective for the series of materials used in the inorganic heterogeneous catalysis field.

Bibliography

[1] O. Lopez-Acevedo, K.A. Kacprzak, J. Akola, H. Hakkinen, Quantum size effects in ambient CO oxidation catalysed by ligand-protected gold clusters, Nature Chemistry, 2 (2010) 329-334.

[2] A.S.K. Hashmi, G.J. Hutchings, Gold catalysis, Angewandte Chemie International Edition, 45 (2006) 7896-7936.

[3] S. Ivanova, W. Pitchon, Y. Zimmermann, C. Petit, Preparation of alumina supported gold catalysts: Influence of washing procedures, mechanism of particles size growth, Applied Catalysis a-General, 298 (2006) 57-64.

[4] X.H. Yan, J. Blacklock, J.B. Li, H. Mohwald, One-pot synthesis of polypeptide-gold nanoconjugates for in vitro gene transfection, Acs Nano, 6 (2012) 111-117.

[5] D.X. Li, Y. Cui, K.W. Wang, Q. He, X.H. Yan, J.B. Li, Thermosensitive nanostructures comprising gold nanoparticles grafted with block copolymers, Advanced Functional Materials, 17 (2007)

3134-3140.

[6] Y.G. Sun, Y.N. Xia, Shape-controlled synthesis of gold and silver nanoparticles, Science, 298 (2002) 2176-2179.

[7] J. Ye, B.V. de Broek, R. De Palma, W. Libaers, K. Clays, W. Van Roy, G. Borghs, G. Maes, Surface morphology changes on silica-coated gold colloids, Colloids and Surfaces a-Physicochemical and Engineering Aspects, 322 (2008) 225-233.

[8] D.X. Li, Q. He, J.B. Li, Smart core/shell nanocomposites: Intelligent polymers modified gold nanoparticles, Advances in Colloid and Interface Science, 149 (2009) 28-38.

[9] M.R. Mucalo, K.M. Babu, K.S.W. Wu, In situ characterisation of the aqueous gold colloid interface using CO as a surface probe: IR spectroscopic studies, Journal of Colloid and Interface Science, 310 (2007) 184-189.

[10] K. Shimizu, T. Yamamoto, Y. Tai, A. Satsuma, Selective hydrogenation of nitrocyclohexane to cyclohexanone oxime by alumina-supported gold cluster catalysts, Journal of Molecular Catalysis a-Chemical, 345 (2011) 54-59.

[11] J.D. Grunwaldt, M. Maciejewski, O.S. Becker, P. Fabrizioli, A. Baiker, Comparative study of Au/TiO_2 and Au/ZrO_2 catalysts for low-temperature CO oxidation, Journal of Catalysis, 186 (1999) 458-469.

[12] I. Fratoddi, I. Venditti, C. Battocchio, G. Polzonetti, C. Cametti, M.V. Russo, Core shell hybrids based on noble metal nanoparticles and conjugated polymers: synthesis and characterization, Nanoscale Research Letters, 6 (2011).

[13] J. Choma, D. Jamiola, P. Nyga, M. Jaroniec, Synthesis of rod-like silica gold core-shell structures, Colloids and Surfaces a-Physicochemical and Engineering Aspects, 393 (2012) 37-41.

[14] A. Penkova, J.M.M. Blanes, S.A. Cruz, M.A. Centeno, K. Hadjiivanov, J.A. Odriozola, Gold nanoparticles on silica monospheres modified by amino groups, Microporous and Mesoporous Materials, 117 (2009) 530-534.

[15] S.H. Joo, J.Y. Park, C.K. Tsung, Y. Yamada, P.D. Yang, G.A. Somorjai, Thermally stable Pt/mesoporous silica core-shell nanocatalysts for high-temperature reactions, Nature Materials, 8 (2009) 126-131.

[16] S. Mohapatra, Y.K. Mishra, D.K. Avasthi, D. Kabiraj, J. Ghatak, S. Varma, Synthesis of gold-silicon core-shell nanoparticles with tunable localized surface plasmon resonance, Applied Physics Letters, 92 (2008).

[17] W. Stöber, A. Fink, E. Bohn, Controlled growth of monodisperse silica spheres in the micron size range, Journal of Colloid and Interface Science, 26 (1968) 62-69.

[18] P.M. Arnal, M. Comotti, F. Schuth, High-temperature-stable catalysts by hollow sphere encapsulation, Angewandte Chemie International Edition, 45 (2006) 8224-8227.

[19] J. Choma, D. Jamiola, J. Ludwinowicz, M. Jaroniec, Deposition of silver nanoparticles on silica spheres and rods, Colloids and Surfaces a-Physicochemical and Engineering Aspects, 411 (2012) 74-79.

[20] D.X. Li, Q. He, Y. Yang, H. Mohwald, J.B. Li, Two-stage pH response of poly(4-vinylpyridine) grafted gold nanoparticles, Macromolecules, 41 (2008) 7254-7256.

[21] F. Osterloh, H. Hiramatsu, R. Porter, T. Guo, Alkanethiol-induced structural rearrangements in silica-gold core-shell-type nanoparticle clusters: An opportunity for chemical sensor engineering, Langmuir, 20 (2004) 5553-5558.

[22] J.H. Kim, W.W. Bryan, T.R. Lee, Preparation, characterization, and optical properties of gold, silver, and gold-silver alloy nanoshells having silica cores, Langmuir, 24 (2008) 11147-11152.

[23] C. Graf, S. Dembski, A. Hofmann, E. Ruhl, A general method for the controlled embedding of nanoparticles in silica colloids, Langmuir, 22 (2006) 5604-5610.

[24] E. Pensa, E. Cortes, G. Corthey, P. Carro, C. Vericat, M.H. Fonticelli, G. Benitez, A.A. Rubert, R.C. Salvarezza, The chemistry of the sulfur-gold Interface: In search of a unified model, Accounts of Chemical Research, 45 (2012) 1183-1192.

[25] C.H. Bartholomew, Mechanisms of catalyst deactivation, Applied Catalysis a-General, 212 (2001) 17-60.

[26] M. Yadav, T. Akita, N. Tsumori, Q. Xu, Strong metal-molecular support interaction (SMMSI): Amine-functionalized gold nanoparticles encapsulated in silica nanospheres highly active for catalytic decomposition of formic acid, Journal of Materials Chemistry, 22 (2012) 12582-12586.

[27] A. Noguchi, M. Kikuchi, H. Kamiya, K. Maeda, Synthesis and microencapsulation of organo-silica particles, Journal of Materials Chemistry, 16 (2006) 2170-2174.

[28] Q.J. Duan, J. Zhang, J. Tian, H.Y. Zhao, Silica nanorings on the surfaces of layered silicate, Langmuir, 27 (2011) 13212-13219.

[29] H. Hofmeister, P.T. Miclea, M. Steen, W. Morke, H. Drevs, Structural characteristics of oxide nanosphere supported metal nanoparticles, Topics in Catalysis, 46 (2007) 11-21.

[30] A. de Keizer, E.M. van der Ent, L.K. Koopal, Surface and volume charge densities of monodisperse porous silicas, Colloids and Surfaces a-Physicochemical and Engineering Aspects, 142 (1998) 303-313.

[31] J.Q. Cui, S.G. Han, Z.B. Zhou, C. Jia, Y. Zhang, Size-dependent aggregation behavior in monodisperse silica: a nitrogen adsorption study, Surface and Interface Analysis, 44 (2012) 166-169.

[32] O. Carmody, R. Frost, Y.F. Xi, S. Kokot, Surface characterisation of selected sorbent materials for common hydrocarbon fuels, Surface Science, 601 (2007) 2066-2076.

[33] A. Vazquez-Zavala, J. Garcia-Gomez, A. Gomez-Cortes, Study of the structure and selectivity of Pt-Au catalysts supported on Al_2O_3, TiO_2, and SiO_2, Applied Surface Science, 167 (2000) 177-183.

[34] H. Rojas, G. Diaz, J.J. Martinez, C. Castaneda, A. Gomez-Cortes, J. Arenas-Alatorre, Hydrogenation of alpha, beta-unsaturated carbonyl compounds over Au and Ir supported on SiO_2, Journal of Molecular Catalysis a-Chemical, 363 (2012) 122-128.

[35] H.F. Qian, M.Z. Zhu, Z.K. Wu, R.C. Jin, Quantum sized gold nanoclusters with atomic precision, Accounts of Chemical Research, 45 (2012) 1470-1479.

[36] R.D. Jean, K.C. Chiu, T.H. Chen, C.H. Chen, D.M. Liu, Functionalized silica nanoparticles by nanometallic Ag decoration for optical sensing of organic molecule, The Journal of Physical Chemistry C, 114 (2010) 15633-15639.

[37] C.L. Chen, Y. Li, S.Q. Liu, Fabrication of macroporous platinum using monodisperse silica nanoparticle template and its application in methanol catalytic oxidation, Journal of Electroanalytical Chemistry, 632 (2009) 14-19.

[38] F. Somodi, I. Borbath, M. Hegedus, A. Tompos, I.E. Sajo, A. Szegedi, S. Rojas, J.L.G. Fierro, J.L. Margitfalvi, Modified preparation method for highly active Au/SiO_2 catalysts used in CO oxidation, Applied Catalysis a-General, 347 (2008) 216-222.

[39] G.C. Bond, The effect of the metal to non-metal transition on the activity of gold catalysts, Faraday Discussions, 152 (2011) 277-291.

[40] H.Y. Xu, W. Chu, J.J. Luo, M. Liu, New $Au/FeOx/SiO_2$ catalysts using deposition-precipitation for low-temperature carbon monoxide oxidation, Catalysis Communications, 11 (2010) 812-815.

[41] H.Y. Xu, W. Chu, J.J. Luo, T. Zhang, Impacts of MgO promoter and preparation procedure on meso-silica supported nano gold catalysts for carbon monoxide total oxidation at low temperature, Chemical Engineering Journal, 170 (2011) 419-423.

[42] S. Ivanova, V. Pitchon, C. Petit, V. Caps, Support effects in the gold-catalyzed preferential oxidation of CO, Chemcatchem, 2 (2010) 556-563.

[43] A. Grill, Porous pSiCOH ultralow-k dielectrics for chip interconnects prepared by PECVD, Annual Review of Materials Research, 39 (2009) 49-69.

[44] L.S. Yuan, J. Efendi, N.S.H. Razali, H. Nur, Fine-tuning the local structure and catalytic activity of titanium-amine functionalized silica in oxidation of limonene by aqueous hydrogen peroxide, Catalysis Communications, 20 (2012) 85-88.

[45] R. Paul, S. Hussain, A.K. Pal, Characterization of nanocrystalline gold/DLC composite films synthesized by plasma CVD technique, Applied Surface Science, 255 (2009) 8076-8083.

[46] H. Aguiar, J. Serra, P. Gonzalez, B. Leon, Structural study of sol-gel silicate glasses by IR and Raman spectroscopies, Journal of Non-Crystalline Solids, 355 (2009) 475-480.

Chapter V Impacts of metal addition into Au/SS5-C applied as catalysts

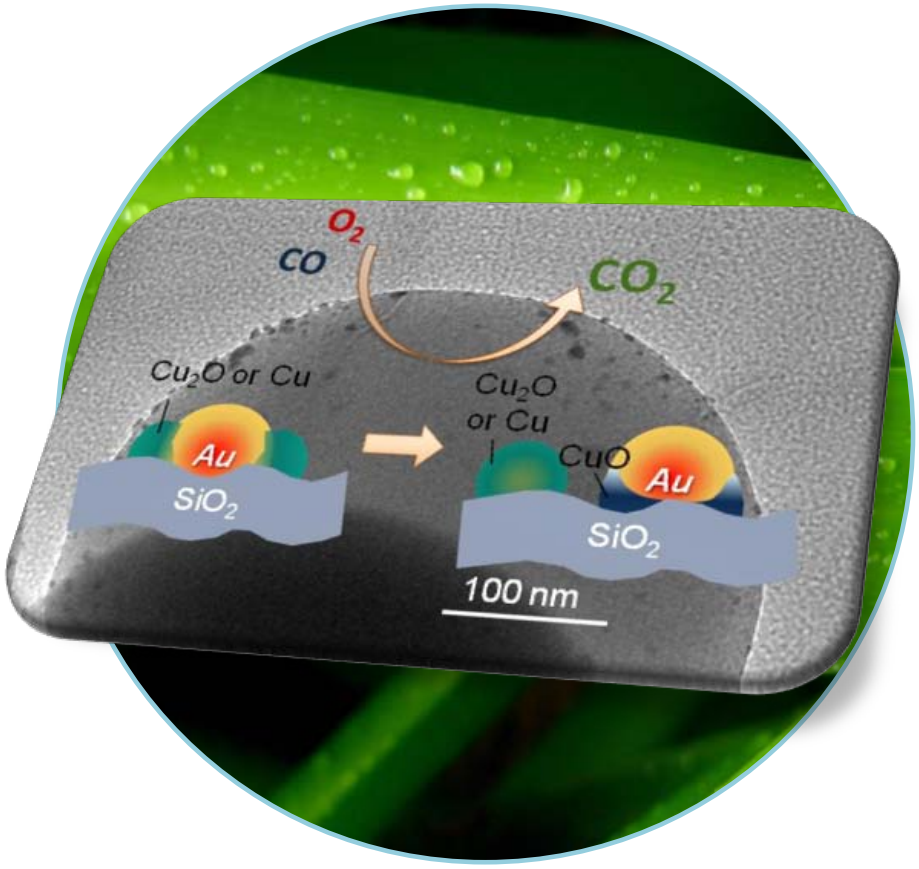

- The CO oxidation over the Au/SS5@M-C preferred the coexistence of neutral gold particles and small amount of oxidized Au-NPs.
- Metal addition facilitated the dispersion and fixing of Au-NPs on silica during reaction.
- The addition of metal (oxide) acted as important factor for changing the reaction mechanism of CO oxidation over gold catalysts.
- Non-porous Stöber silica possessed properties of being a novel and appropriate support for Au-NPs.

The gold nanoparticles (Au-NPs) supported on non-porous Stöber silica were synthesis and doped with metals (0.3 wt% of metal to silica) including copper, ion, and cobalt. The gold-based catalysts were measured by CO oxidation and characterized by X-Ray Diffraction (XRD), X-ray photoelectron spectroscopy (XPS), and Transmission Electron Microscope (TEM). The results showed that the 1 wt% Au/SS5-C without metal addition performed barren catalytic activity for CO oxidation below 300 ^{o}C. However, after doping with metals, the activity of supported Au-NPs was largely promoted. The study combining XPS and TEM revealed that by the metal additions, the mechanism of gold catalysts taking part into the CO oxidation was changed. The active oxygen species can be replenished by the lattice oxygen from the metal (oxides). For the copper doped gold material, the gold and copper (oxide) particles went through re-assembling during CO oxidation. The addition of metal helped the Au-NPs anchored onto the silica and largely enhanced the interaction between gold and support. The Au-support interaction was proved to be another essential factor for the catalytic activity beyond the size effect. The special structure of non-porous Stöber silica also contributed to the dispersion of metal nanoparticles, which matched the traditional mesoporous carriers and was considered a new and appropriate support for gold in catalysis field.

5.1 Introduction

Since the first discovery by Haruta et al.[1] of supported gold nanoparticles (Au-NPs) for low-temperature CO oxidation, the Au-NPs are now applied as excellent catalysts for various reactions including CO oxidation, alcohol oxidation, hydrogenation reactions, etc.[2-5] The CO oxidation can be applied extensively for the development of fuel cell feed gas purification, carbon dioxide laser, CO gas sensor and vehicle exhaust purification. Besides, the reaction is also low cost and structure sensitive,[6] which is commonly applied as a simple and typical reaction for probing the catalytic activity of supported Au-NPs. However, Au-NPs supported on inert support-silica synthesized by traditional methods, such as impregnation and deposition-precipitation, seemed unsatisfied.[7, 8] In order to obtain an active gold catalyst, the sizes of Au-NPs should be within 5 nm.[9, 10] The Au-NPs supported on inert carrier as silica could get active only under the condition that very small Au-NPs are highly dispersed on the surface of silica according to the reports. Nevertheless, the interaction between Au-NPs and silica is weak. The Au-NPs can be movable on the surface and the aggregations were easily formed. Under this circumstance, the new techniques and preparation methods for Au-NPs supported by silica that can perform approving catalytic activity were studied, which included the gas-phase grafting[11], chemical vapor deposition,[12] solvated metal atom dispersion (SMAD) technique,[13] etc. However, the above methods with high cost and complicated techniques do not fit for the normal application of catalysts.

The new types of catalysts exhibiting efficient catalytic activity have been reported, which were supported on cheap and easily available inert carrier promoted by active metal oxides. Venezia et al.[14] anchored Au-NPs onto TiO_2/SiO_2 by the sol-gol method and found that $Au/TiO_2/SiO_2$ catalysts with a TiO_2 loading of 5 wt% demonstrated better catalytic performance in CO oxidation than the Au/TiO_2 catalysts. Qian et al.[8] prepared supported Au catalyst with 6 wt% CoO_x promoting silica as carrier. Xu et al.[15, 16] also utilized 6 wt% addition of MgO or Fe_2O_3 to prepare the supported Au catalyst. The temperature of CO

complete conversion over the metal promoted catalysts was largely reduced. The impact of metal oxides into Au/SiO_2 seemed interesting and efficient. However, the sizes and distribution of supported Au-NPs were more likely to be dependent on the properties of supports and synthesize conditions. Besides, the Au-NPs coated non-porous Stöber silica with metal doping and applied in catalysis filed is still never heard. It is wondered what's the impact of metal addition for the morphology and catalytic activity of this kind of gold materials? Will it be effectual as in the traditional gold catalysts, or loss the superior function due to the special non-porous support that was considered improper as support for gold?

The reason we chose the Stöber silica (SS5) is that Au-NPs can be highly dispersed on the surface of the nonporous silica. The Au-NPs in the as-synthesized Au/SS5-C ("C" means after calcination under air at 300 ^{o}C for 4 h) will not be trapped in the pores and can be fully accessible to the reactants with more defects exposed on the small Au-NPs. In this way, the reaction mechanism and the role of Au-NPs can be studied accurately. Metal including copper, iron, and cobalt were doped onto the Stöber silica supported Au-NPs. The Au-NPs supported on Stöber silica without and with metal modification were tested by CO oxidation. The development of Au-NPs before and after CO oxidation, the impact of metal addition and the special morphology of samples, and the interaction between gold-metal particles and metal-support were discussed in detail.

5.2 Au/SS5@M-C samples applied for CO oxidation

The preparation method can be seen in Part 2.1.5 of Chapter II. CO oxidation is a famous and unfailing reaction model for estimating the catalytic activity of supported Au-NPs, which is also one of the earliest reactions found to be efficiently catalyzed by gold catalysts [17].

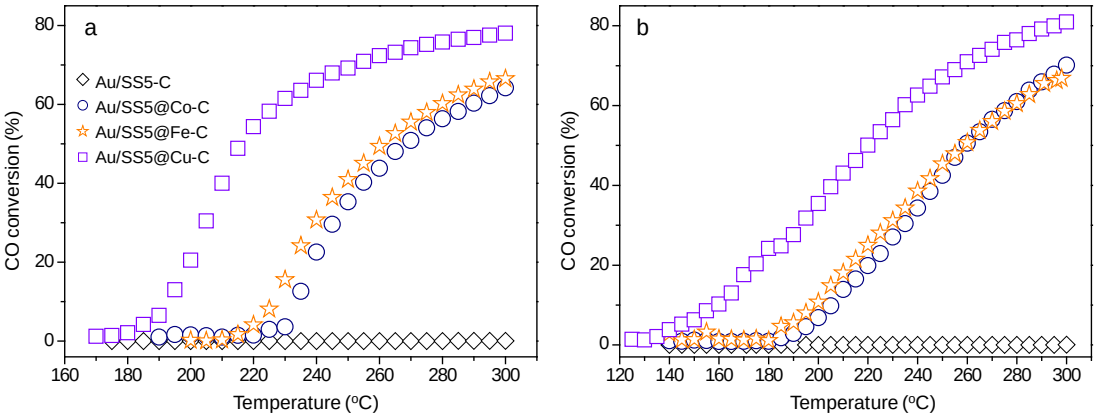

Figure 5.1 CO conversion during CO oxidation as a function of temperature over 50 mg Au/SS5@M-C catalysts: The first-time run (a) and the second-time run (b) of CO oxidation. "C" means calcination in air at 300 ^{o}C for 4 h.

The series of gold materials are tested by CO oxidation from room temperature to 300^{o}C with 1^{o}C/min rate as shown in Figure 5.1. 50 mg of samples are used as catalysts. The samples are tested by the CO oxidation for three times, the first run and second run of reaction results are shown. The Au/SS5-C catalyst without metal addition performs barren activity until 300^{o}C. The CO oxidation over 50 mg Cu/SS5-C (Cu loading is 0.3 wt% to silica) is also tested as comparison, unfortunately no activity is displayed (not shown). As it can be seen from the previous TEM images in Figure 4.6 of Chapter IV, the Au-NPs are dispersed on the surface of huge SS5 globules after calcination, the major parts of the small Au-NPs still exist, and only spots of gold aggregations are formed. In fact, the particle sizes of Au-NPs around 3 nm fall in the range of sizes active for the CO oxidation[18]. However, the Au/SS5-C is nearly futile during the CO oxidation below 300^{o}C, demonstrating that the size of Au-NPs is not the reason for the deactivation of Au/SS5-C. In other word, the sizes of Au-NPs are not the only critical parameter influencing the catalytic activity even over the inner silica carrier supported Au-NPs.

The Au/SS5@M-C catalysts display much better activity than either the Cu/SS5-C or Au/SS5-C for CO oxidation. In the first run of CO oxidation, the CO conversion raises rapidly

along with the temperature, the T_{10} (light-off temperature, temperature at 10% conversion) over Au/SS5@Co-C, Au/SS5@Fe-C and Au/SS5@Cu-C are 235, 227 and 192^{o}C, respectively. When the CO conversion reaches about 50%, the further increase of CO conversion with temperature becomes gentle. The final CO conversion under tested temperature (300^{o}C) do not arrive 100%. The Au/SS5@Cu-C possessing better activity gets about 78% CO conversion at 300^{o}C. The CO conversion at 300^{o}C over Au/SS5@Co-C and Au/SS5@Fe-C are similar of 67% and 64%. The activity behavior of Au/SS5@Co-C and Au/SS5@Fe-C differ not obviously. The Au/SS5@Fe-C is slightly preferable.

The three samples in Figure 5.1(a) are tested for the second run of CO oxidation. Comparing the first and second run of CO oxidation over the Au/SS5@M-C catalysts, they perform generally hysteretic catalytic activity during the first run, the T_{10} of which are about 40^{o}C higher than the second run. The second run of reaction as shown in Figure 5.1(b) over Au/SS5@M-C catalysts is accelerated at the beginning. But at the end of the reaction (300^{o}C), the corresponding CO oxidation are similar for each run over the same catalyst. During the second run and the third run of CO oxidation, the CO conversion over each sample maintains at the same level. It is a worth note that the amount of doping metal here is only 0.005Mr wt% to SS5 (about 0.3wt%, Mr is the mass of metal). However, the metal addition plays great importance for improving the catalytic activity of CO oxidation. The Au/SS5@Fe-C shows slightly lower light-off temperature and T_{50} (the temperature corresponding 50% CO oxidation) than Au/SS5@Co-C. The Au/SS5@Cu-C displays better catalytic activity than the other samples. The light-off temperature and T_{50} are 160 and 220^{o}C respectively, which is about 40^{o}C lower than the Au/SS5@Fe-C and Au/SS5@Co-C catalysts.

However, none of these gold catalysts arrive 100% conversion of CO until 300^{o}C. Thus the CO oxidation under the same operation conditions over 100 mg Au/SS5@Cu-C catalyst is carried out as comparison. By using different amount of Au/SS5@Cu-C catalyst (50 mg or 100 mg, 1 wt% of Au, atomic ratio of Au: Cu= 1: 1), the corresponding CO conversion varies not obviously below 150^{o}C, whilst the T_{50} decreases from 215 to 180^{o}C. The CO conversion

reaches its maximum (100%) at about 220°C. The previous work of Liu et al.[19] focused on the pretreatment of Au-Cu/SBA-15 catalysts with total metal loading of 6 wt% (Au: Cu molar ratio of 1: 1) for CO oxidation. It was reported that the 60 mg Au-Cu/SBA-15 catalysts after calcination without further pretreatment possesses T_{50} and T_{100} at 205 and 220°C, respectively. Ramírez-Garza et al.[20] also investigated the performance of Au/HMS-Fe (HMS: hexagonal mesoporous silica) catalyst for CO oxidation. For catalyst with 1.2 wt% Au loading and 10 wt% Fe after O_2 pretreatment, the T_{50} is about 210°C. However, the amount of catalyst for reaction is as high as 300 mg, which is 6 fold higher of the Au/SS5@Fe-C in our work. The current Au/SS5@M-C catalysts displayed no inferior activity comparing with the reported work although the reaction condition slightly differs, not to mention the much lower amounts of gold and metal contents in this work. No matter how, the Au/SS5@M-C catalysts with only 1 wt% gold loading after metal addition (about 0.3 wt% of metal to silica) is definitely effective for improving the catalytic activity of Au/SS5-C catalysts under the current operation system.

5.3 Formation of supported Au-NPs

5.3.1 X-Ray Diffraction of supported Au-NPs

Figure 5.2 shows the X-ray diffraction patterns of the Au/SS5-C catalyst and the metal added Au/SS5@M-C catalysts before and after CO oxidation. The broad and sharp peak around 22° is attributed to the diffraction peak of amorphous SiO_2 (JCPDS #27-0605).[15] No obvious peak corresponding to gold is observed in the fresh Au/SS5-C sample, which can be explained by either the very small and dispersive Au-NPs or the low content of gold that beyond the limitation of XRD detector. It is shown that both the Au(111) and Au(200) crystal phase exist in the metal doped gold materials. The average sizes of particles in the samples are calculated according to Scherrer equation by using the peak width at half height of the Au(111) face as shown in Table 5.2. Surprisingly, all the average size of metal doped Au/SS5@M-C samples decreases after CO oxidation.

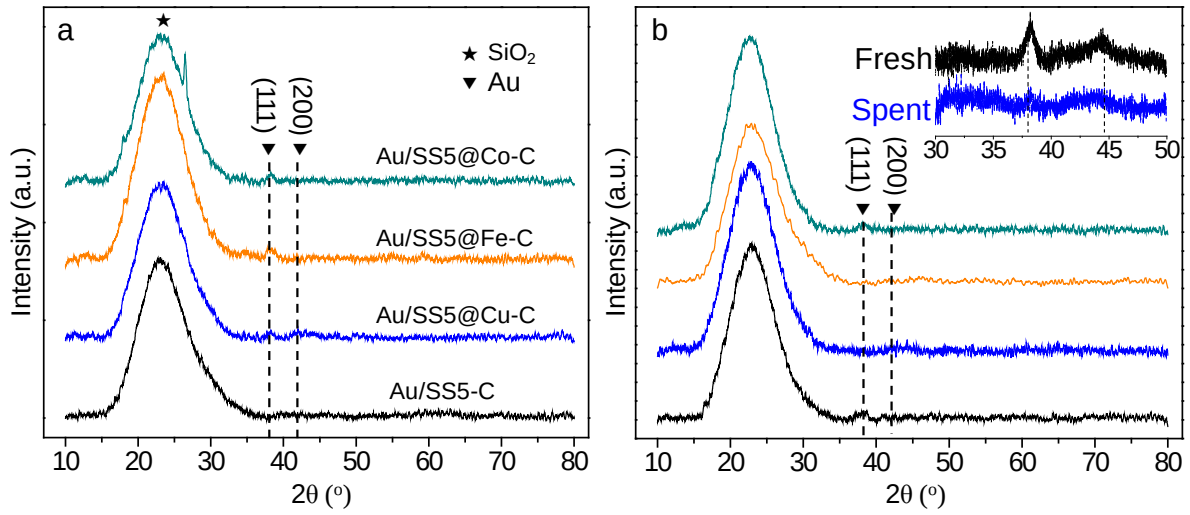

Figure 5.2 The XRD profiles of Au/SS5@M-C catalysts before (a) and after (b) CO oxidation. The inset picture of (b) is the comparison of fresh and spent Au/SS5@Cu-C in the range of 30-50^o.

Table 5.1 The possible XRD peaks of CoO_x, FeO_x, and CuO_x crystalline phases in the range of 30-50^o and their corresponding crystal faces.

Element	Crystalline phase	2θ (^{o})	Crystal face	2θ	Crystal face	2θ	Crystal face
Co[21-23]	Co	44.3	(111)				
	CoO	49.2	(200)				
	Co_3O_4	37.0	(311)	32.1	(220)	45.0	(400)
Fe[24]	Fe	44.7	(110)				
	FeO	36.0	(111)	41.9	(200)		
	Fe_2O_3	33.1	(104)	35.6	(110)		
	Fe_3O_4	35.5	(311)	37.1	(222)	43.1	(400)
Cu[25-27]	Cu	32.3	(220)	38.0	(311)	43.3	(111)
	Cu_2O	36.8	(111)	42.4	(200)		
	CuO	35.8	(-111)	38.9	(200)		

In order to identify the metal species more precisely, the zoomed XRD from 30-50^o of fresh and spent Au/SS5@Cu-C are performed as shown in the inset picture of Figure 5.2(b). The crystal faces corresponding to different crystallites of additional metals in the range of 30-50^o are listed in Table 5.1. However, there is still no observation of additional metal from the

zoomed XRD profiles, which ought to be resulted from the very low concentration (only about 0.3 wt% of the metal component to silica). The diffraction peaks in the spent Au/SS5@Cu-C samples are evidently weakened than in the fresh sample, indicating that the average size of spent Au/SS5@Cu-C is reduced- that is, the structure of the nanoparticles may change during the reaction. By the way, there is no evidence of the shifting of peaks around 38.2^{o} to confirm the formation of now composition from gold and copper combining species such as AuCu alloy.

Table 5.2 The average sizes of Au-NPs in each material before and after reaction.

Au/SS5-C		Au/SS5@Cu-C		Au/SS5@Fe-C		Au/SS5@Co-C	
Fresh	Spent	Fresh	Spent	Fresh	Spent	Fresh	Spent
-	14.3 nm	11.1 nm	7.6 nm	7.8 nm	5.6 nm	14.9 nm	8.4 nm

5.3.2 X-ray photoelectron spectroscopy of Au/SS5@M-C

XPS is a powerful technique for analyzing the surface components and the surface ratio between each species and elements. The Au/SS5-C after CO oxidation and Au/SS5@Cu-C catalyst before and after CO reaction stability test are analyzed by the XPS spectra as shown in Figure 5.3. For a comparison, the Au/SS5-C catalyst before and after 2 runs of CO oxidation is also shown. The results turn out that elements including Au, (Cu), O and Si exist on the surface of catalysts. The corresponding binding energy and surface components ratio calculated from XPS result are summarized in Table 5.3. The Au 4f spectra of all the samples possess two broad peaks and each peak can be fitted by two overlapped peaks. The peaks locating around 84 eV are ascribed to the metallic gold, and the peaks ranging from 84-86 eV correspond to the partially oxidized gold species $Au^{\delta+}$ ($0<\delta<3$). There is no observation of Au^{3+} species in both samples.

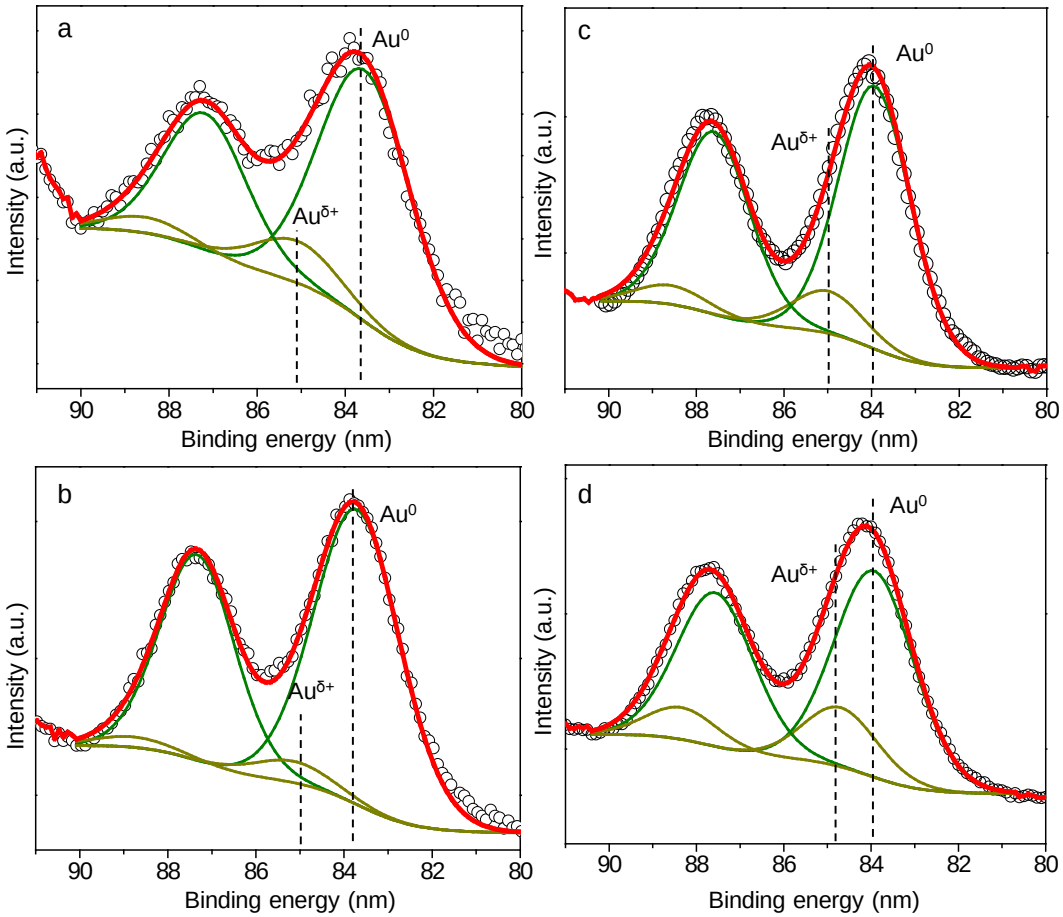

Figure 5.3 Au 4f XPS spectra of gold catalysts before and after CO oxidation: (a-b) fresh and spent Au/SS5-C after CO oxidation and (c-d) fresh and spent Au/SS5@Cu-C after stability test of CO oxidation. The balls illustrate the initial XPS spectrum, and the solid lines correspond to the fitted line.

The surface ratio of $Au^0/Au^{\delta+}$ and Au/SiO_2 are also shown in Table 5.3. The metallic gold species in both the fresh and spent Au/SS5-C catalysts are the major component with a small amount of partially oxidized gold species ($Au^{\delta+}$). The constitutions of Au^0 and $Au^{\delta+}$ in the fresh Au/SS5-C are 87.5% and 12.5%, respectively. However, after 2 runs of CO oxidation, the $Au^{\delta+}$ amount further decreases to 5.9%. In the Au/SS5@Cu-C after copper addition, the metallic gold species is still the domain component in the fresh sample.

Table 5.3 Au 4f and Cu 2p XPS results of Au/SS5-C and Au/SS5@Cu-C samples before and after reaction.

	Species	Au/SS5-C				Au/SS5@Cu-C			
		Fresh		Spent		Fresh		Spent	
		BE	Speci	BE	Specie	BE	Speci	BE	Speci
Au $4f_{7/2}$	Au^0	83.7	87.5	83.7	94.1%	84.0	90.9	83.9	80.9%
	$Au^{\delta+}$	85.1	12.5	85.2	5.9%	85.0	9.1%	84.7	19.1%
Cu $2p_{3/}$	Cu^0/C	-	-	-	-	932.8	100%	932.3	81.8%
	Cu^{2+}	-	-	-	-	-	0%	934.1	18.2%
Surface ratio		Au/Si 0.9%		Au/Si 1.1%		Au/Si 1.1%	Au/C 0.9	Au/Si 1.2%	Au/C 1.3

Different from the Au/SS5-C, the amount of metallic gold species of Au/SS5@Cu-C after the stability test decreases about 10%. The quantity of partially oxidized gold species ($Au^{\delta+}$) becomes two-fold as in the fresh Au/SS5@Cu-C. That is, during the stability test, few amounts of metallic gold species are bonded to oxygen species- either from the reactant oxygen gases or the oxygen species on the surface of support, to become positively charged gold species. It is mentionable that an early study of Bond and Thompson[28] suggested that the active sites of Au-NPs were consisted by large amount of Au^0 and small amount of cationic gold species fixed at the interface of gold-support. The cationic gold was essential for fixing the Au-NPs on the support as "glue".[28]

The Cu 2p XPS spectra of Au/SS5@Cu-C catalyst before and after CO oxidation stability test are as displayed in Figure 5.4. The XPS spectra in the range of 924-946 eV show the single Cu 2p peak of 932.8 eV and satellite peaks around 940-946 eV. In the spectrum of fresh Au/SS5@Cu-C catalyst, the large Cu $2p_{3/2}$ peak (927-938 eV) is intensive and symmetrical, which is consistent with the reported binding energy of Cu^0 or Cu^+ species.[29, 30]

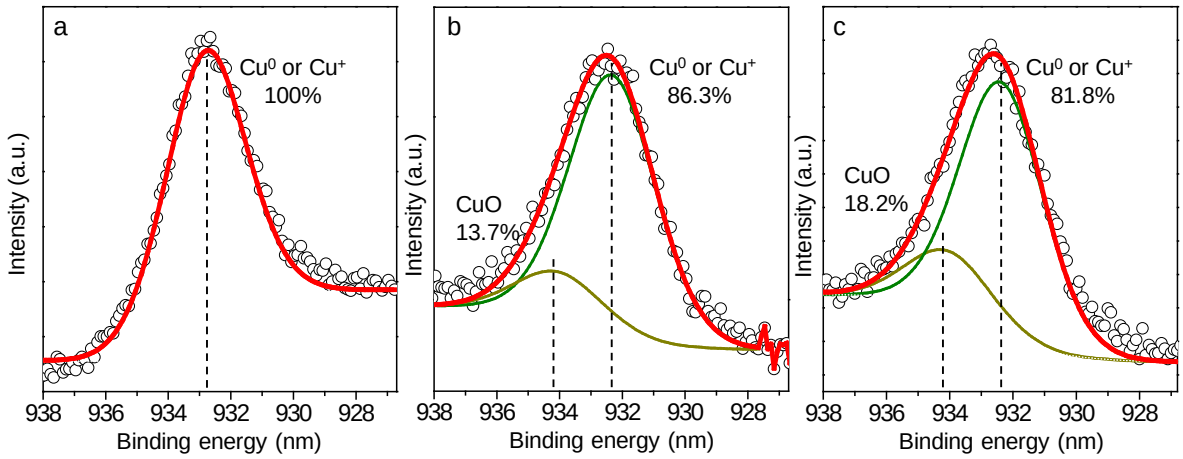

Figure 5.4 Typical deconvolution of Cu $2p_{3/2}$ XPS peak of fresh Au/SS5@Cu-C (a), Au/SS5@Cu-C after the first run of CO oxidation (b), and the spent Au/SS5@Cu-C after stability test (c). The balls illustrate the initial XPS spectrum, and the solid lines correspond to the fitted line.

Whilst after stability test (Figure 5.4(c)), such peak become broader and can be split into two overlapped peaks centered at 932.3 and 934.1 eV, respectively. The presence of later peak proves the generation of the Cu^{2+} species.[29] It is clearly that the Cu^0 or Cu^+ species are dominant in the freshly calcined Au/SS5@Cu-C catalyst. During the stability test, small amount of Cu^0 or Cu^+ species transform into Cu^{2+}, either in the CuO or some $Cu(OH)_2$ species connecting with silica. The atomic ratio between Au, Cu and Si elements are listed in Table 5.3. The Au/SS5@Cu-C after 2 times of CO oxidation from T_{room} to 300°C (just before stability test) is also detected as shown in Figure 5.4(b), in which the copper species should correspond to the light-off states of the materials. It can be observed that the two peaks related to Cu^0/Cu^+ and Cu^{2+} have already formed after 2 times of CO oxidation, demonstrating that the major amount of Cu^0/Cu^+ with small amount of Cu^{2+} species are more active and responsible for the reaction. The ratio between gold and silica is about 1.1%. The Au/Cu atom ratio in the fresh Au/SS5@Cu-C catalyst is quite equal to the theoretical atom ratio during synthesis (1:1), the atomic ratio of Au/Cu ratio raises from 0.9 to 1.3 after stability test.

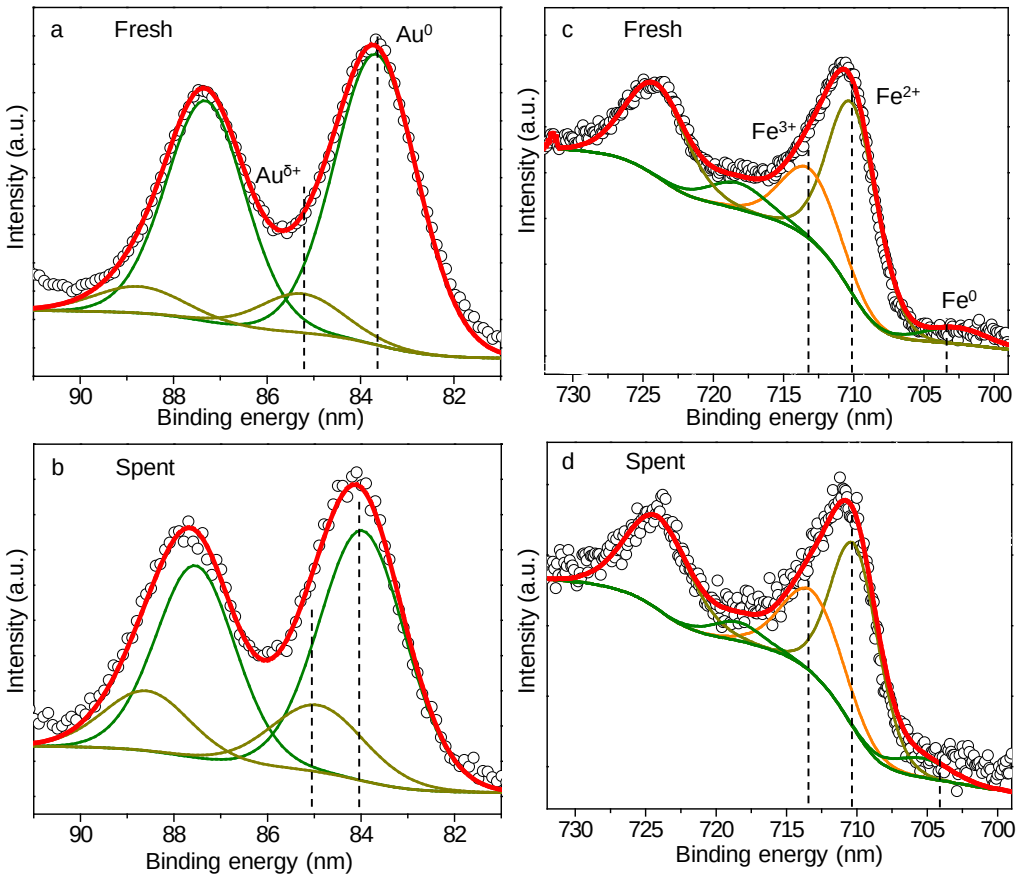

Figure 5.5 XPS profiles of Au4f (a-b) and Fe 2p (c-d) over fresh and spent Au/SS5@Fe-C catalysts after three times of CO oxidation from T_{room} to 300^{o}C. The balls illustrate the initial XPS spectrum, and the solid lines correspond to the fitted line.

For a better understanding of the acting roles of Au-NPs and assisted metal during reaction, the XPS spectra of Au/SS5@Fe-C and Au/SS5@Co-C catalysts before and after three runs of CO oxidation are also displayed in Figure 5.5. The corresponding results are listed in Table 5.4 and Table 5.5. It is worth to note that the catalyst is not deactivated after three runs of reaction. On the contrary, the activity of the Au/SS5@M-C after the first time CO oxidation until 300^{o}C becomes a little more active for the second run of reaction. The third run of reaction takes place at the similar reaction temperature of the second run. The states of tested elements in the samples are corresponding to the light off states. It can be seen from Figure 5.5 that the fresh Au/SS5@Fe-C after calcination also possesses large amount of metallic gold and minor amount of cationic gold species. After the CO oxidation, the amount of $Au^{\delta+}$ raises again to about

two-fold comparing with the fresh sample, the same case as the Au/SS5@Cu-C during reaction.

Table 5.4 Au 4f and Fe 2p XPS results of fresh and spent Au/SS5@Fe-C samples

Sample	Au $4f_{7/2}$ (eV)	Surface species	Fe $2p_{3/2}$ (eV)	Surface species	Atom ratio		
					Au/Si	Si/O	Au/Fe
Fresh	83.7	Au^0 (88.1%)	704.1	Fe^0 (7.2%)	2.1%	57.5%	0.3
	85.3	$Au^{\delta+}$ (11.8%)	710.0	Fe^{2+} (65.4%)			
			713.1	Fe^{3+} (27.4%)			
Spent	83.9	Au^0 (76.4%)	704.3	Fe^0 (7.3%)	2.0%	51.0%	0.4
	84.9	$Au^{\delta+}$ (23.6%)	710.1	Fe^{2+} (59.7%)			
			713.2	Fe^{3+} (33.0%)			

It was revealed by Fierro-Gonzalez et al.[31] that the CO molecules were only weakly and insufficiently adsorbed on the metallic gold above room temperature, and the cationic gold species strongly adsorbed the CO species, which may be significant on kinetics. The amount of cationic gold generated during the reaction can be considered as one of the reasons for the slight increase of the light-off temperature over Au/SS5@M-C samples during the second and third run CO oxidation.

The Fe 2p XPS spectra in Au/SS5@Fe-C before and after 3 times of CO oxidation are displayed in Figure 5.5(c-d), respectively. The large peaks ranging from 700-730 eV correspond to Fe 2p XPS spectra, which are fitted by three peaks. Both small amounts of Fe^0 and Fe^{3+}, possessing the binding energy around 705.3 and 713.1 eV, are present in the fresh Au/SS5@Fe-C sample. The major state with binding energy of 710.0 eV is ascribed to the ion components of Fe^{2+} species. Different from the fresh Au/SS5@Cu-C, the oxidized iron species exist in the spent catalyst. The Fe^0 species slightly transferred into oxidized iron species after oxidation, which is considered as a result of the oxidation effect from reactant gases.

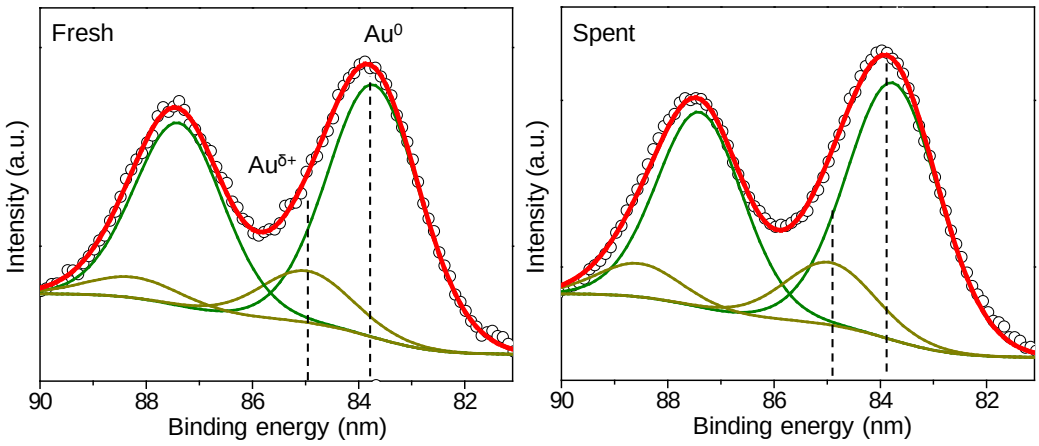

Figure 5.6 XPS profiles of Au 4f over fresh and spent Au/SS5@Co-C catalysts after three times of CO oxidation from T_{room} to 300°C. The balls illustrate the initial XPS spectrum, and the solid lines correspond to the fitted line.

Table 5.5 Au 4f XPS results of fresh and spent Au/SS5@Co-C samples

Sample	Au $4f_{7/2}$ (eV)	Surface species	Atom ratio	
			Au/Si	Si/O
Fresh	83.7	Au^0 (89.8%)	1.7%	65.9%
	85.0	$Au^{\delta+}$ (10.2%)		
Spent	83.9	Au^0 (83.0%)	1.4%	59.1%
	84.9	$Au^{\delta+}$ (17.0%)		

The Au 4f XPS of the fresh and spent Au/SS5@Co-C catalysts are also displayed in Figure 5.6. Unfortunately, the Co species in the fresh and spent samples are too difficult to be identified with large noise in the tested range. The change of the Co valent states are difficult to be recognized. No matter how, it can be realized that the majority of metallic gold species is still present in the freshly prepared Au/SS5@M-C after calcination. And once again, the apparent increase of $Au^{\delta+}$ species after reaction is evidenced. Comparing to the variation of $Au^{\delta+}$ in the fresh and spent Au/SS5@M-C and Au/SS5-C (M= Cu, Fe, and Co), it can be concluded that the increase of $Au^{\delta+}$ species is only the patent of Au/SS5@M-C with metal addition resulted from Au species bonded to oxygen species of the catalysts. It is also a confirmation of the Au-oxide interaction variation after metal addition.

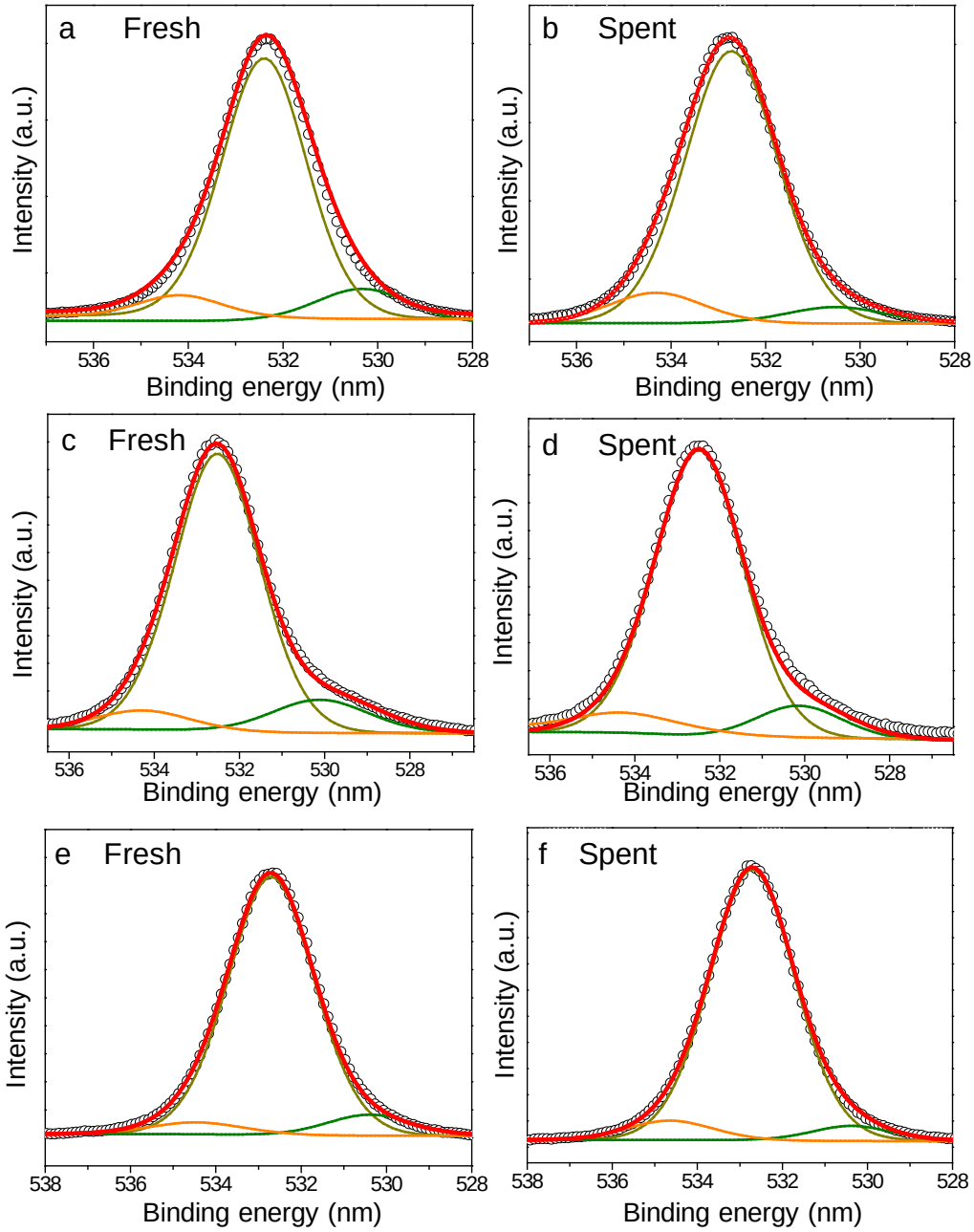

Figure 5.7 O1s XPS spectra of fresh and spent Au/SS5@Cu-C (a-b), Au/SS5@Fe-C (c-d), and Au/SS5@Co-C (e-f) catalysts for CO oxidation. The balls illustrate the initial XPS spectrum, and the solid lines correspond to the fitted line.

The O1s XPS spectra of Au/SS5@M-C catalysts before and after CO oxidation are also detected by the XPS technique. As shown in Figure 5.7, the large and broad oxygen peak is fitted by three peaks. The major peak centered around 532.7 eV can be attributed to the lattice

oxygen or Si-O-H species in the SiO_2 structures,[32] which is very huge and characteristic of SiO_2 supported catalysts. The two accompany peaks locating around 530.0 and 534.6 eV can be ascribed to the defected oxygen vacancy O^{2-} species in metal oxides and chemisorbed oxygen sites on the surface.[33]

Table 5.6 O 1s XPS results of Au/SS5-C and Au/SS5@M-C samples before and after CO oxidation.

	Au/SS -C		(O^c)%[d]	Au/SS5@Cu-C		(O^c)%
	O 1s (eV)	(%)		O 1s (eV)	(%)	
Fresh	530.2	0.8		530.2 [a]	12.0	
	532.7	97.8	-	532.6 [b]	79.3	0.42
	534.6	1.4		534.4 [c]	8.7	
Spent	-			530.3 [a]	5.5	
	532.6	100	-	532.7 [b]	81.8	0.70
	-			534.5 [c]	12.7	
	Au/SS5@Fe-C		(O^c)%	Au/SS5@Co-C		(O^c)%
	O 1s (eV)	(%)		O 1s (eV)	(%)	
Fresh	530.1	11.1		530.2	4.5	
	532.5	82.6	0.36	532.7	91.0	0.65
	534.4	6.3		534.5	8.5	
Spent	530.1	9.8		530.2	9.6	
	532.5	84.1	0.38	532.6	91.7	0.28
	534.5	6.1		534.6	3.7	

The superscripts a, b, and c are corresponding to three different oxygen species. [a] Binding energy corresponding to defected vacancy O^{2-} in the metal; [b] Binding energy corresponding to lattice oxygen or Si-O-H in the SiO_2 structure; [c] Binding energy corresponding to chemisorbed oxygen sites on the surface; d The O^c% is the ratio of O^c to the total amount of oxygen species from metal (not including the O^b), that is $O^c\% = O^c/(O^a + O^c)$.

It is well-known that the silica is inert and does not transform oxygen species to gold active sites. The O 1s spectra of Au/SS5-C should display negligible chemisorbed oxygen sites and defected oxygen vacancies as shown in Table 5.6. For the copper added Au/SS5@Cu-C, the fresh sample possesses apparently both the O^{2-} species in metal and the chemisorbed oxygen species. After CO oxidation, the amount of O^{2-} species obviously decreases while the amount of chemisorbed oxygen species rises on the contrary. The amount of lattice oxygen species in SiO_2 structure remains around 80% (Table 5.6) during the long term CO reaction with slight

increase after reaction, which is generally stable during the reaction. It seems that there is a continuous complementary effect of the oxygen vacancy O^{2-} species transferring into the chemisorbed oxygen sites during CO oxidation over Au/SS5@Cu-C. The O1s XPS spectra of the fresh and spent Au/SS5@Fe-C and Au/SS5@Co-C catalysts are also displayed in Figure 5.7(c-f), which are slight different from those of the Au/SS5@Cu-C system. Before reaction, the chemisorbed oxygen sites and O^{2-} species coexisted in the fresh Au/SS5@Fe-C catalyst. Both the amounts of chemisorbed oxygen sites and defected oxygen vacancy O^{2-} species slightly decline after the second run of CO oxidation. As it is mentioned above, the Au/SS5@Fe-C catalyst was partially activated during the second run of CO oxidation. Under this situation, it can be considered that the fluctuation of the chemisorbed oxygen species,[34] which is viewed as the active oxygen species during reaction, is going through a temporarily consumption. Herein, the complementary effect is again demonstrated that there exists the transformation of oxygen vacancy species into the active oxygen sites during CO oxidation. The Au/SS5@Co-C system possesses the general similar variation of O1s XPS spectra as the Au/SS5@Cu-C system. However, the amount of chemisorbed oxygen species and defected vacancy species in Au/SS5@Co-C are lower than the other two samples.

In addition, in order to understand what happened to the additional metal compounds, the variation percentage of chemisorbed oxygen species ((O^c)%) in the metal before and after CO oxidation is inspected as shown in Table 5.6. The (O^c)% of Au/SS5@Cu-C raises from 0.42 to 0.70 after CO oxidation, the obvious increase of chemisorbed oxygen species from defected vacancy O^{2-} in metal indicating that the variation of copper compound is a oxidized process during reaction. The variation of (O^c)% of Au/SS5@Fe-C are 0.36 and 0.38 before and after CO oxidation, suggesting a generally stable state of FeO_x species. The (O^c)% of Au/SS5@Co-C reduces from 0.65 to 0.28, corresponding to a reduction process of cobalt oxide species. The above analysis of additional metal oxide from (O^c)% variation happens to hold the same view from previous XPS spectra of metal species in the fresh and spent samples.

The XPS results confirm the changing of small amounts of Cu or Cu^{+} species to Cu^{2+} during the reaction in the Au/SS5@Cu-C. In fact, the Cu^{2+} is able to form Cu-O-Si species with silica. It is considered that the small amount of formed Cu^{2+} during reaction is more likely from the copper species linked with oxygen species on the silica surface.

5.4 Morphologies of fresh and spent gold catalysts

The morphology of the as-prepared Au/SS5-C after calcination can be seen as shown in Figure 4.6 of Chapter IV. Most of the small particles remain on the surface of large Stöber silica globules with diameter about 490 nm. Only small amount of Au-NPs are aggregated after the sample after calcination at 30 ^{o}C for 4 h. The major of the small particles still exists (4.4 nm ± 0.7 nm). However, this material does not possess obvious activity for the CO oxidation until 300^{o}C, although the sizes of Au-NPs are sufficient to active the reaction. The metal addition (molar ratio of M: Au is 1: 1, about 0.3 wt% of M to SiO_2) can greatly increase the catalytic activity for CO oxidation. Different from the previous work, in which the addition amount of Fe or Mg oxidized components are as high as 6wt%,[16, 35] the addition amounts here is amazingly low. The reason why is urgently required. It is also wondered that dose the specially morphology account somewhat for the catalytic properties of the catalysts?

5.4.1 Morphologies of the fresh Au/SS5@Cu-C

In the following work, we only take the Au/SS5@Cu-C sample with the higher CO oxidation activity as typical sample. The TEM technique is performed for understanding the growth of Au-NPs during CO oxidation, and the interaction between gold, copper and silica components. We also try to understand the mechanism of metal addition influencing the structure and activity of catalysts.

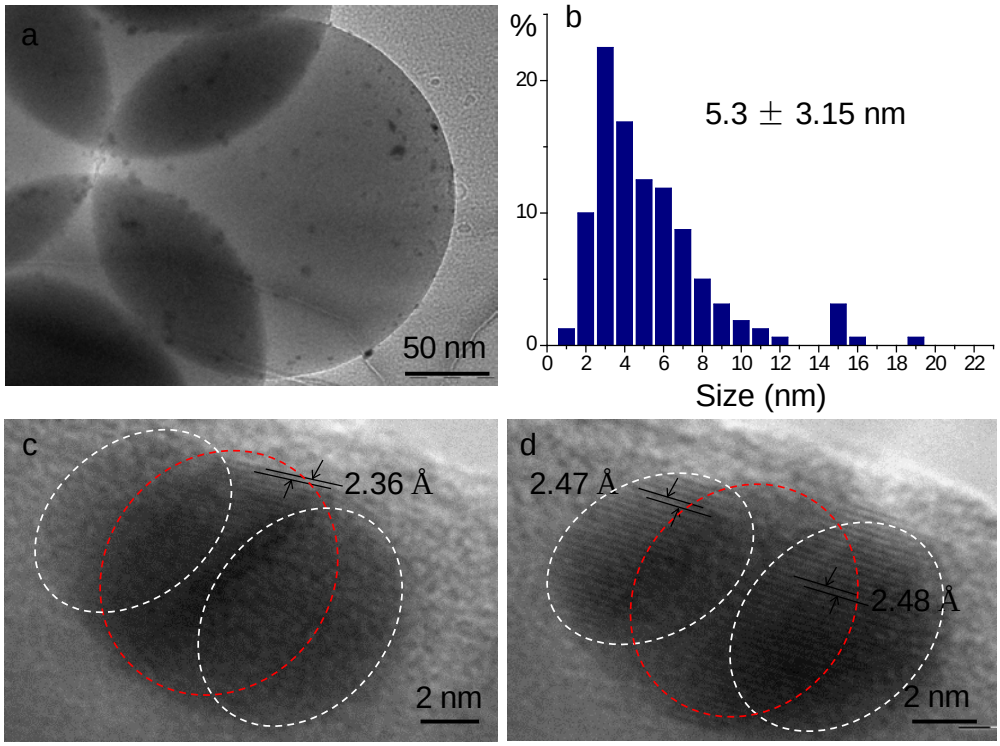

Figure 5.8 The TEM image (a) and size distribution based on 200 particles (b) of the fresh Au/SS5@Cu-C catalyst, and the high resolution of one single particle showing different crystal faces (c-d).

Comparing the TEM image and size distribution of Au/SS5-C sample without copper addition as shown in Figure 4.6 of Chapter IV, it can be clearly observed that the average particle size increases from 4.4 to 5.3 nm after copper addition, in which the particles larger than 8 nm is more frequently observed in the Au/SS5@Cu-C sample. There are also particles as large as 19 nm in the Au/SS5@Cu-C sample, which reveals a more intensive aggregation of the particles in this catalyst. In fact, some of reports always gave the assertions that the addition of metal (oxide) into supported Au-NPs could induce the high dispersion of Au-NPs due to some kind of synergetic interaction,[8, 36] which is seems not the case here. In order to understand the dispersion of gold and copper components and the formation process of larger aggregations, the high resolution TEM images are operated. The larger particles are mainly focused. Very interesting, two kinds of crystal faces in one large particle are observed sometimes. The particle in Figure 5.8(c-d) is the same one. The remarkable part is that two different interplanar spacing

are revealed. The crystal faces in Figure 5.8c with the interplanar spacing of 2.36 Å can be ascribed to the (111) crystal face of metallic Au.[37] While the crystal faces in Figure 5.8(d) with the interplanar spacing of about 2.47 Å is resulted from the (111) crystal faces of Cu_2O.[38] Some investigators reported that the gold and copper components in the catalyst can form AuCu alloy under special conditions (e.g. under heat treatment under at least 300^{o}C and then annealed in H_2-N_2 mixture at 800 ^{o}C),[39, 40] the interplanar spacings of which might ranges from 2.1 to 2.3 Å depending on the Au/Cu ratio. Under this point of view, it can be inferred that there is generally no AuCu alloy formed but only separated or conjugated Au and Cu (Cu_2O) particles or aggregations under current conditions. Combining the two TEM images of the same large particle, it is considered that the copper components partially encapsulates the Au-NPs and form one large aggregation, which might happened during either the preparation or the calcination process.

5.4.2 Morphologies of the spent Au/SS5@Cu-C

The Au/SS5@Cu-C displays an much improved catalytic activity for CO oxidation comparing to the Au/SS5-C, and the activity lasts for 7 h with only slight decrease of the activity, although the addition amount of copper is tiny. The spent Au/SS5@Cu-C sample is also observed by the TEM technique as shown in Figure 5.9. It is remarkable that the nanoparticles in the spent Au/SS5@Cu-C sample seem to be more dispersive with fewer large particles. The size distribution based on large amounts of particles is shown in Figure 5.9(d). Comparing the fresh Au/SS5@Cu-C sample, the percentage of nanoparticles smaller than 3 nm do not change obviously in the spent Au/SS5@Cu-C sample. Only partial of the nanoparticles ($\leq$ 2 nm) evolves into larger particles. However, the amount of nanoparticles smaller than 5 nm in the spent Au/SS5@Cu-C sample increases from 63.1% to 72.1% after reaction. The high-resolution TEM images over spent Au/SS5@Cu-C display some single spherical particles which are confirmed to be gold or Cu_2O particles by their corresponding interplanar spacing. During the observation, some interesting calabash-like particles are also observed as

shown in Figure 5.9(c). Combining with the XPS showing the appearance of Cu^{2+} species, it is considered that the calabash-like particle is consisted by the conjunction of Au-NPs and CuO patch, although only the Au(111) face is seen due to the observation angle.

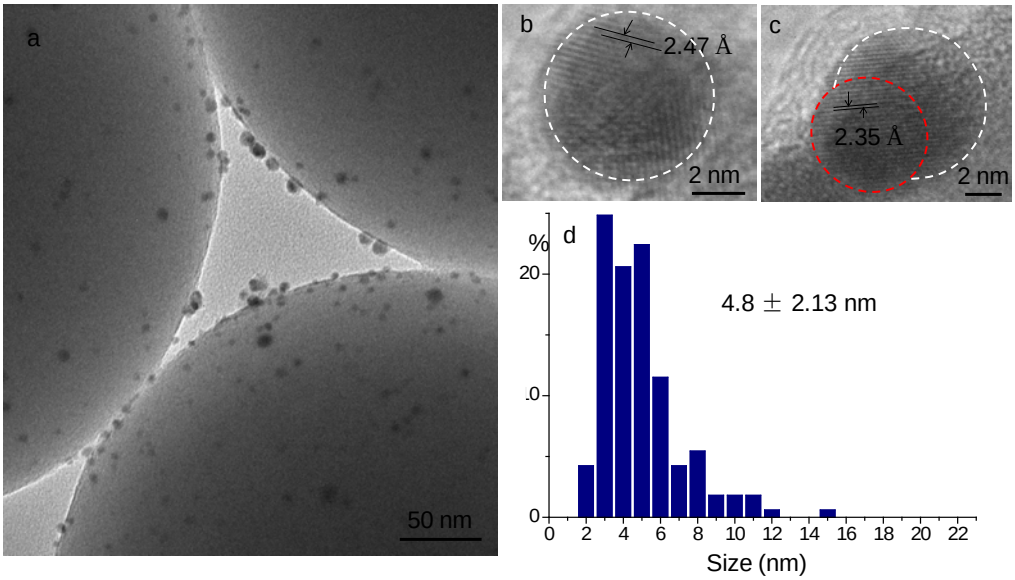

Figure 5.9 The TEM image (a-c) and size distribution based on 200 particles (d) of the spent Au/SS5@Cu-C catalyst.

5.5 Stability of Au/SS5@Cu-C and mechanism for CO oxidation

During the CO oxidation, the reaction temperature is carried out below 300 ^{o}C, which is nearly the limitation for smaller Au-NPs around 2 nm.[41] The question is that what about the stability of Au-NPs? Will they be aggregated intensely due to the long time staying under high temperature? If there are some aggregated gold with time, the CO conversion should largely fall along with the reaction time (since the CO conversion is a structure sensitive reaction), which is not desired by the industrial demands. Under this circumstance, the stability of CO oxidation at 270 ^{o}C over 50mg Au/SS5@Cu-C is measured as shown in Figure 5.10, the tested Au/SS5@Cu-C is after 3 times of CO oxidation from T_{room} to 300 ^{o}C (as shown in Figure 5.1).

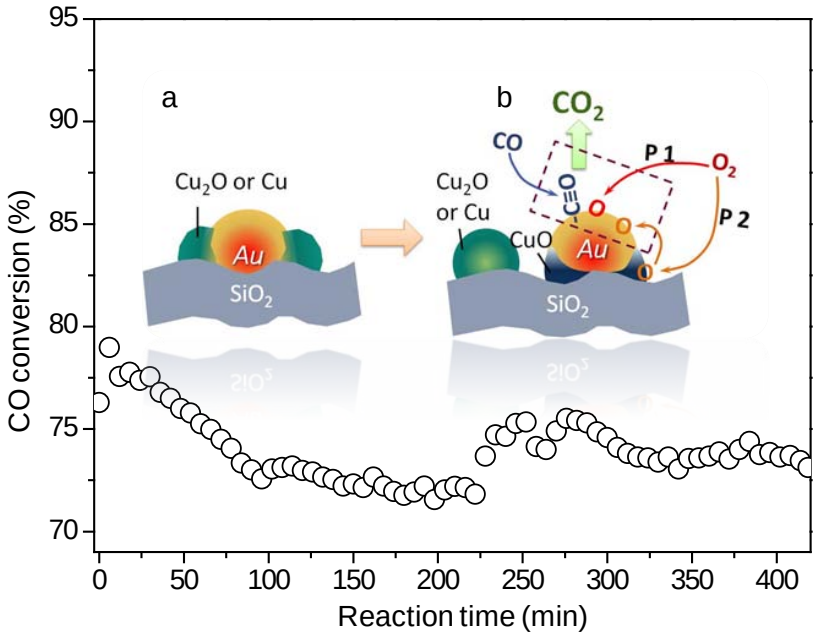

Figure 5.10 CO conversion as a function of time at 270 ^{o}C during 7 h over 50 mg Au/SS5@Cu-C catalyst.

At the very beginning during the stabilization, the CO conversion changes a little in the first 30 min due to the stabilization of temperature. It is thus stable at about 77% of CO conversion. During the next 2 h, a steady decrease of the CO conversion is observed with time and then become stable at 72%. The interesting part is that the CO conversion slightly rises back to 76% during 240-280 min, and then gently decreases to 73% until the end of the stability test. It is likely that there exists an equilibrium during the reaction, causing the slightly fluctuation of the CO conversion with time. During the tested 7 h, there is no obvious deactivation of the catalysts for CO conversion, demonstrating that the Au-NPs in the Au/SS5@Cu-C possess the capacity of anti-clustering at higher temperature.

It is considered that parts of Au-NPs can be interacted with copper oxide after the addition of copper compound and form the visible large particles as shown in Figure 5.10(a). And there is no formation of gold and copper alloy under the current situation (the formation of AuCu alloy needs a strict first oxidation-then reduction procedure). Confirmed by the TEM images after reaction, some of the Cu_2O particles get off the Au-NPs and become separate particles,

however some calabash-like particles are formed after reaction. The Au 4f XPS spectra of Au/SS5@Cu-C after reaction illustrates the increase amount of $Au^{\delta+}$, which demonstrates the enhancing interaction between Au-NPs and support. On the other hand, the Cu 2p XPS spectra suggest that Cu^{2+} species are also formed after reaction, either from the bulk CuO or copper species bonded to Si (Si-O-Cu). Combining the results of XPS and TEM, it can be inferred that the calabash-like particles should be formed by Au-NPs fixed by the residual CuO species bonding to the surface of silica as shown in Figure 5.10(b). One thing can be sure is that the addition of copper compound largely improve the interaction between Au-NPs and support. This is not about increasing the dispersion of Au-NPs as reported somewhere, since no evidence can confirm the obvious change of Au-NPs during CO oxidation.

For the pure silica supported Au-NPs, the CO and oxygen molecules can be competitively adsorbed on the exposed active sites of Au-NPs. Different from the active supports (e.g. TiO_2, CeO_2, etc.) supported Au-NPs, the oxygen molecules can be only dissociated on the surface of Au-NPs. The adsorbed CO species and dissociated oxygen species on the surface of Au-NPs thus form the CO_2 molecules. The rate-determining step should be the oxygen molecule adsorbed on the surface of Au-NPs, thus the sizes of the Au-NPs play the key role for the catalytic activity. However, the interaction between gold and silica is slightly weak as previously mentioned. The absorption and dissociation of oxygen molecules are easily blocked, causing the reduction of catalytic activity for CO oxidation.

For the Au/SS5@Cu-C with copper component doping, the case is different. The gaseous oxygen species can be adsorbed both on the surface of gold active sites fixed on the support (Path 1 in Figure 5.10(b)) and the surface of copper component (Path 2). In the Path 2, it was reported that for some semiconductors such as TiO_2, Fe_2O_3, etc.,[42, 43] the gaseous oxygen molecules can be directly adsorbed on the surface of these metal oxides and dissociated immediately to became the defected vacancy oxygen species in the metal supports. As previously revealed by the O1s XPS spectra of Au/SS5@Cu-C before and after CO oxidation, the replenishment from vacancy oxygen species in the copper oxide to chemisorbed oxygen

species is continuous during the reaction. The lattice oxygen species then spills over onto the interaction of Au-metal and produced the CO_2 molecules by reacting with adsorbed CO species. In a word, the addition of copper component helps to force the Au-support interaction, transport the active oxygen species, and also change the rate-determining step.

As we previously mentioned, even the addition of metal is efficient for the catalytic activity improvement, it is curious that such small amount of metal component addition significantly helps. The contribution of the special support must be taken into consideration. As it can be seen in Figure 5.8-5.9, the particles among the reaction are dispersed on the surface of large silica globules and easily exposed to the reactants. There does not exist the chance for the particles to be trapped into the pores of support since the silica is controlled to be non-porous. Different from the Au-NPs in the Au/SS5-C without metal addition, in which the Au-silica interaction is weak and the Au-NPs are easily move to form aggregations, the Au-NPs in Au/SS5@Cu-C are more likely to be fixed on the surface under the help of metal components. The redispersed Au-NPs maintain their forms and contribute to the reaction. It has to be mentioned that the non-porous SS5 indeed possess the ability for indirectly enhancing the activity. Distinctive from the frequently reported mesoporous supports including SBA-15 and MCM-41,[44] the non-porous Stöber silica also fulfill the capacity as a satisfied support and greatly benefit the catalytic activity of supported Au-NPs.

5.6 Conclusion

The Stöber silica supported Au-NPs by using gold colloid as gold precursor was modified by copper, iron, or cobalt addition. The bare Au/SS5-C without metal doping does not show activity for CO oxidation until 300^{o}C. Whilst after copper, iron, or cobalt addition, which was only about 0.3 wt% of metal to silica, the catalytic activity of Au/SS5@Cu-C was greatly improved comparing to the Au/SS5-C. By the combination of TEM images and XPS, the growth of Au-NPs and the impacts of metal addition were studied in detail. The conclusions are as below:

1. The CO oxidation over the Au/SS5@M-C preferred the coexistence of neutral gold particles and small amount of oxidized Au-NPs.

2. The present of metal (oxide) species facilitated the dispersion and fix of Au-NPs during the reaction onto silica.

3. The addition of metal (oxide) induced the participation of oxygen species in the metal oxides, in which the surface adsorption species could be replenished by the lattice oxygen from the metal oxides. In this case, the addition of metal (oxide) acted as an important factor for changing the reaction mechanism of CO oxidation over Au/SS5@M-C than the Au/SS5-C.

4. The Au-NPs dispersed on non-porous Stöber silica were fully accessible to the reactants; non-porous Stöber silica possessed the property of being a novel and appropriate support for Au-NPs.

Bibliography

[1] M. Haruta, N. Yamada, T. Kobayashi, S. Iijima, Gold catalysts prepared by coprecipitation for low-temperature oxidation of hydrogen and of carbon monoxide, Journal of Catalysis, 115 (1989) 301-309.

[2] M.C. Kung, R.J. Davis, H.H. Kung, Understanding Au-catalyzed low-temperature CO oxidation, Journal of Physical Chemistry C, 111 (2007) 11767-11775.

[3] S. Ivanova, C. Petit, V. Pitchon, Application of heterogeneous gold catalysis with increased durability: Oxidation of CO and hydrocarbons at low temperature, Gold Bulletin, 39 (2006) 3-8.

[4] B. Campo, C. Petit, M.A. Volpe, Hydrogenation of crotonaldehyde on different Au/CeO_2 catalysts, Journal of Catalysis, 254 (2008) 71-78.

[5] L. Wang, J. Zhang, X.J. Meng, D.F. Zheng, F.S. Xiao, Superior catalytic properties in aerobic oxidation of alcohols over Au nanoparticles supported on layered double hydroxide, Catalysis Today, 175 (2011) 404-410.

[6] V.P. Santos, S.A.C. Carabineiro, P.B. Tavares, M.F.R. Pereira, J.J.M. Orfao, J.L. Figueiredo,

Oxidation of CO, ethanol and toluene over TiO_2 supported noble metal catalysts, Applied Catalysis B-Environmental, 99 (2010) 198-205.

[7] A. Wolf, F. Schuth, A systematic study of the synthesis conditions for the preparation of highly active gold catalysts, Applied Catalysis a-General, 226 (2002) 1-13.

[8] K. Qian, W.X. Huang, Z.Q. Jiang, H.X. Sun, Anchoring highly active gold nanoparticles on SiO_2 by CoO_x additive, Journal of Catalysis, 248 (2007) 137-141.

[9] G.C. Bond, D.T. Thompson, Catalysis by gold, Catalysis Reviews-Science and Engineering, 41 (1999) 319-388.

[10] M. Haruta, Catalysis of gold nanoparticles deposited on metal oxides, Cattech, 6 (2002) 102-115.

[11] M. Okumura, S. Tsubota, M. Haruta, Preparation of supported gold catalysts by gas-phase grafting of gold acethylacetonate for low-temperature oxidation of CO and of H_2, Journal of Molecular Catalysis a-Chemical, 199 (2003) 73-84.

[12] C.M. Yang, M. Kalwei, F. Schuth, K.J. Chao, Gold nanoparticles in SBA-15 showing catalytic activity in CO oxidation, Applied Catalysis a-General, 254 (2003) 289-296.

[13] M.P. Casaletto, A. Longo, A.M. Venezia, A. Martorana, A. Prestianni, Metal-support and preparation influence on the structural and electronic properties of gold catalysts, Applied Catalysis a-General, 302 (2006) 309-316.

[14] A.M. Venezia, F.L. Liotta, G. Pantaleo, A. Beck, A. Horvath, O. Geszti, A. Kocsonya, L. Guczi, Effect of Ti(IV) loading on CO oxidation activity of gold on TiO_2 doped amorphous silica, Applied Catalysis a-General, 310 (2006) 114-121.

[15] H. Xu, W. Chu, J. Luo, T. Zhang, Impacts of MgO promoter and preparation procedure on meso-silica supported nano gold catalysts for carbon monoxide total oxidation at low temperature, Chemical Engineering Journal, 170 (2011) 419-423.

[16] H.Y. Xu, W. Chu, J.J. Luo, M. Liu, New $Au/FeO_x/SiO_2$ catalysts using deposition-precipitation for low-temperature carbon monoxide oxidation, Catalysis Communications, 11 (2010) 812-815.

[17] M. Haruta, S. Tsubota, T. Kobayashi, H. Kageyama, M.J. Genet, B. Delmon, Low-temperature oxidation of CO over gold supported on TiO_2, alpha-Fe_2O_3, and Co_3O_4, Journal of Catalysis, 144 (1993) 175-192.

[18] M.S. Chen, D.W. Goodman, Catalytically active gold: From nanoparticles to ultrathin films, Accounts of Chemical Research, 39 (2006) 739-746.

[19] X.Y. Liu, A.Q. Wang, L. Li, T. Zhang, C.Y. Mou, J.F. Lee, Structural changes of Au-Cu bimetallic catalysts in CO oxidation: In situ XRD, EPR, XANES, and FT-IR characterizations, Journal of Catalysis, 278 (2011) 288-296.

[20] R.E. Ramirez-Garza, B. Pawelec, T.A. Zepeda, A. Martinez-Hernandez, Total CO oxidation over Fe-containing Au/HMS catalysts: Effects of gold loading and catalyst pretreatment, Catalysis Today, 172 (2011) 95-102.

[21] J.U. Cho, J.H. Wu, J.H. Min, S.P. Ko, J.Y. Soh, Q.X. Liu, Y.K. Kim, Control of magnetic anisotropy of Co nanowires, Journal of Magnetism and Magnetic Materials, 303 (2006) E281-E285.

[22] H. Wang, J.L. Ye, Y. Liu, Y.D. Li, Y.N. Qin, Steam reforming of ethanol over Co_3O_4/CeO_2 catalysts prepared by different methods, Catalysis Today, 129 (2007) 305-312.

[23] Y.H. Li, K.L. Huang, Z.F. Yao, S.Q. Liu, X.X. Qing, Co_3O_4 thin film prepared by a chemical bath deposition for electrochemical capacitors, Electrochimica Acta, 56 (2011) 2140-2144.

[24] M. Rudolph, J. Erler, U.A. Peuker, A TGA-FTIR perspective of fatty acid adsorbed on magnetite nanoparticles-Decomposition steps and magnetite reduction, Colloids and Surfaces a-Physicochemical and Engineering Aspects, 397 (2012) 16-23.

[25] O.A. Lambri, J.I. Perez-Landazabal, A. Penaloza, O. Herrero, V. Recarte, M. Ortiz, C.H. Worner, Study of the phases in a copper cathode during an electrodeposition process for obtaining Cu-Li alloys, Materials Research Bulletin, 35 (2000) 1023-1033.

[26] S. Han, T.L. Lee, C.J. Yang, H.C. Shih, Trench gap-tilling copper by ion beam sputter deposition, Materials Chemistry and Physics, 97 (2006) 19-22.

[27] B.S. Li, K. Akimoto, A. Shen, Growth of Cu_2O thin films with high hole mobility by introducing a low-temperature buffer layer, Journal of Crystal Growth, 311 (2009) 1102-1105.

[28] G.C. Bond, D.T. Thompson, Gold-catalysed oxidation of carbon monoxide, Gold Bulletin, 33 (2000) 41-51.

[29] Y. Lv, L. Liu, H. Zhang, X. Yao, F. Gao, K. Yao, L. Dong, Y. Chen, Investigation of surface synergetic oxygen vacancy in CuO–CoO binary metal oxides supported on γ-Al_2O_3 for NO removal by CO, Journal of Colloid and Interface Science, 390 (2013) 158-169.

[30] D.A. Svintsitskiy, A.I. Stadnichenko, D.V. Demidov, S.V. Koscheev, A.I. Boronin, Investigation of oxygen states and reactivities on a nanostructured cupric oxide surface, Applied Surface Science, 257 (2011) 8542-8549.

[31] J.C. Fierro-Gonzalez, B.C. Gates, Evidence of active species in CO oxidation catalyzed by highly dispersed supported gold, Catalysis Today, 122 (2007) 201-210.

[32] I.K. Jung, J.L. Gurav, U.K.H. Bangi, S. Baek, H.H. Park, Silica xerogel films hybridized with carbon nanotubes by single step sol-gel processing, Journal of Non-Crystalline Solids, 358 (2012) 550-556.

[33] H.Y. Yang, S.F. Yu, S.P. Lau, T.S. Herng, M. Tanemura, Ultraviolet Laser Action in Ferromagnetic $Zn_{1-x}Fe_xO$ Nanoneedles, Nanoscale Research Letters, 5 (2010) 247-251.

[34] J.D. Stiehl, T.S. Kim, S.M. McClure, C.B. Mullins, Reaction of CO with molecularly chemisorbed oxygen on TiO_2-supported gold nanoclusters, Journal of the American Chemical Society, 126 (2004) 13574-13575.

[35] H.Y. Xu, W. Chu, J.J. Luo, T. Zhang, Impacts of MgO promoter and preparation procedure on meso-silica supported nano gold catalysts for carbon monoxide total oxidation at low temperature, Chemical Engineering Journal, 170 (2011) 419-423.

[36] K. Qian, S.S. Lv, X.Y. Xiao, H.X. Sun, J.Q. Lu, M.F. Luo, W.X. Huang, Influences of CeO_2 microstructures on the structure and activity of $Au/CeO_2/SiO_2$ catalysts in CO oxidation, Journal of Molecular Catalysis A: Chemical, 306 (2009) 40-47.

[37] G. Mattei, P. Mazzoldi, M.L. Post, D. Buso, M. Guglielmi, A. Martucci, Cookie-like Au/NiO nanoparticles with optical gas-sensing properties, Advanced Materials, 19 (2007) 561-564.

[38] X. Li, S.S.S. Fang, J. Teo, Y.L. Foo, A. Borgna, M. Lin, Z.Y. Zhong, Activation and deactivation of Au-Cu/SBA-15 catalyst for preferential oxidation of CO in H_2-rich gas, Acs Catalysis, 2 (2012) 360-369.

[39] G. De, G. Mattei, P. Mazzoldi, C. Sada, G. Battaglin, A. Quaranta, Au-Cu alloy nanocluster doped SiO_2 films by sol-gel processing, Chemistry of Materials, 12 (2000) 2157-2160.

[40] J.C. Bauer, D. Mullins, M.J. Li, Z.L. Wu, E.A. Payzant, S.H. Overbury, S. Dai, Synthesis of silica supported AuCu nanoparticle catalysts and the effects of pretreatment conditions for the CO oxidation reaction, Physical Chemistry Chemical Physics, 13 (2011) 2571-2581.

[41] F. Somodi, I. Borbath, M. Hegedus, A. Tompos, I.E. Sajo, A. Szegedi, S. Rojas, J.L.G. Fierro, J.L. Margitfalvi, Modified preparation method for highly active Au/SiO_2 catalysts used in CO oxidation, Applied Catalysis a-General, 347 (2008) 216-222.

[42] J.D. Grunwaldt, A. Baiker, Gold/titania interfaces and their role in carbon monoxide oxidation, Journal of Physical Chemistry B, 103 (1999) 1002-1012.

[43] A.K. Tripathi, V.S. Kamble, N.M. Gupta, Microcalorimetry, adsorption, and reaction studies of CO, O_2, and CO+O_2 over Au/Fe_2O_3, Fe_2O_3, and polycrystalline gold catalysts, Journal of Catalysis, 187 (1999) 332-342.

[44] E. Rombi, M.G. Cutrufello, C. Cannas, M. Occhiuzzi, B. Onida, I. Ferino, Gold-assisted E ' centres formation on the silica surface of Au/SBA-15 catalysts for low temperature CO oxidation, Physical Chemistry Chemical Physics, 14 (2012) 6889-6897.

Chapter VI New application for gold catalysts? – Oxidation of H_2S over Au/SS5-C and Au/SS5@Cu-C

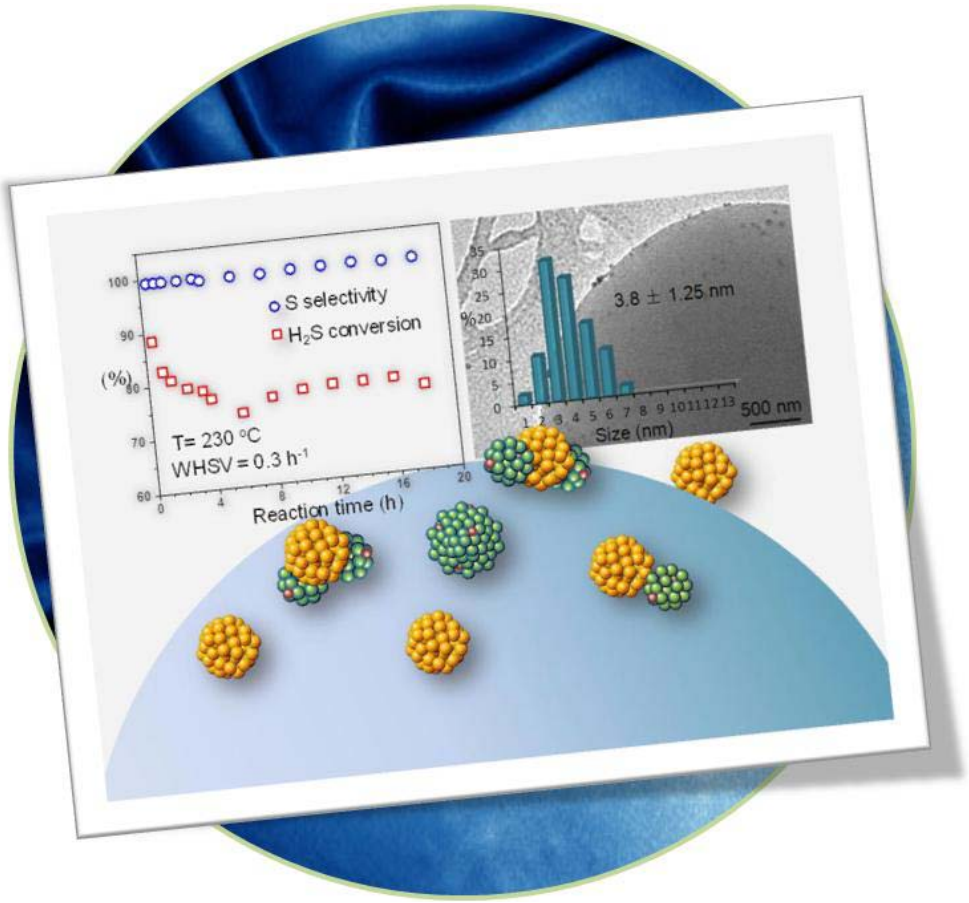

1. Stöber silica supported gold materials for the first time used for selective H_2S oxidation, possessing extremely high selectivity of sulfur.
2. Aggregation and sulfate were formed on Au/SS5-C after reaction.
3. The Au and CuO_x particles in Au/SS5@Cu-C re-assembled after the reaction.
4. Au-NPs were immune of sulfur poison and stable during long-term H_2S oxidation.
5. The non-porous silica globules helped to disperse Au-NPs, maximize the active sites exposure, limit the pressure drop and heat transfer, and facilitate to remove the sulfur vapor.

The selective oxidation of H_2S has always been an unauthorized reaction for gold catalysts. In this work, the selective oxidation of H_2S to Sulfur was tried as a probe for the Stöber silica (SS5) supported Au-NPs with and without copper addition (named as Au/SS5-C and Au/SS5@Cu-C). Interestingly, both the two samples possessed extremely high selectivity of Sulfur (95%- 98%). The H_2S conversion of Au/SS5-C was slightly feeble. However after copper addition (0.3 wt% of Cu to silica), the Au/SS5@Cu-C performed greatly enhanced H_2S conversion at Weight Hourly Space Velocity (WHSV) of 0.3 h^{-1} under 230 ^oC of about 80%- two-fold of that over the Au/SS5-C. The most exciting part was that, different from the large aggregations in the spent Au/SS5-C sample, the particles in the spent Au/SS5@Cu-C sample were even smaller than before reaction. The combining analysis of TEM and XPS revealed that the equilibrium existed during the reaction. Different from the Au/SS5-C that was affected by the sulfation and partial deactivation, the Au/SS5@Cu-C was more stable during the reaction and sulfur-resistant. Anyhow, the Au/SS5@Cu-C has provided a novel perspective for the supported gold nanoparticles to engage into the catalysis field.

6.1 Introduction

The H_2S is a main composition in the petroleum refining process, the industrial exhaust gas, the industrial syngas, and the natural gas, which must be carefully controlled before the gas release to avoid the pollution of environment.[1] The current main technique for disposing the H_2S is the Claus catalysis.[2] In the traditional Claus catalysis, the oxidation of H_2S was fulfilled by two or three reactors. The SO_2 was first produced and then reacted with H_2S to sulfur.[3] 3-5% of the H_2S cannot be transferred into sulfur due to the thermodynamic limitations. Under the catalytic conditions, the selective oxidation of H_2S can be processed under temperature range of 210- 240^{o}C by only one step, which is more simply equipped and environmental friendly.[4, 5]

Considering the mechanism of selective oxidation of H_2S, the efficient catalysts should toward sulfur at lower temperature:

$$H_2S + \frac{1}{2}O_2 \rightarrow \frac{1}{n}S_n + H_2O$$

However, under most reaction conditions, some by-products such as SO_2 and H_2SO_4 will be formed. In order to get the excellent selectivity from H_2S to sulfur, some secondary reactions must be controlled, which include:

$$\frac{1}{n}S_n + O_2 \rightarrow SO_2$$

$$H_2S + \frac{3}{2}O_2 \rightarrow SO_2 + H_2O$$

and $\frac{3}{n}S_n + 2H_2O \rightarrow 2H_2S + SO_2$ if in the presence of vapor.

The supported gold materials in nano-scale are very good at being catalysts for various reactions including (selective) oxidation reactions, hydrogenation reactions, hydrochlorination reactions, etc.[6-10] However, when the sulfur or sulfur-containing reactions are concerned, the gold catalysts become reticent. It is a common sense that the catalytic activity of gold catalysts would be largely reduced when even small quantity of H_2S or other S-containing compounds exist due to the poisoning effect of S.[11] The poisoning effect of Au-NPs (Au-NPs)

is that the special compounds strongly adsorbed on the active sites of Au-NPs and thus hinder the adsorption of real reactants. The early work by Bonzel and Ku[12] was focused on the poisoning effect of S in the CO oxidation. It was found that the CO can still be adsorbed on the metal surface in the present of sulfur; however the dissociation of oxygen molecules were hindered because of the occupation of adsorbed S on gold. Thus the CO production rate was greatly limited. Besides, most of these poison compounds can also change the structure of the sample, for example, which could cause the aggregation of Au-NPs.[13] The affinity between gold and S is great, which can be adsorbed onto gold surface both as atom and molecule, hence the S could easily poison the gold within several ppm.[14] In fact, the S poison can be removed by heat treatment. But it is undesirable for Au-NPs to maintain their sizes. That's why the publications in the field of inorganic heterogeneous catalysis always remind us the dangerous of using these compounds.[11] It's still considered a risk of gold catalysts possessing S-concerned impurity, not to mention to be used as catalyst for the sulfur containing reactions.

In a word, the application of Au-NPs is avoided to be touched by the S and S- containing compounds concerned reactions. But the fact is that if the S- component (e.g. H_2S and SO_2) acts as one of the reactants, it can be easily adsorbed on the surface of Au-NPs. Besides, Feria and co-workers[15] carried out a simulation and claimed that compounds including SO_2 can be dissociated on the surface of gold, which may be able to help carry out the Claus reaction, however, there is no further experiments operated.

It is believable that there exists a compatible activation level simultaneously appropriate for the reactants sorption and dissociation, selective transformation to sulfur, and regeneration of the active sites. In the Stöber silica supported Au-NPs system, the Au-NPs are highly dispersed on the surface of silica and separated from each other. The Au-NPs are fully accessible for the reactant gases and will never be deactivated by the accumulation of sulfur in pores as reported.[16] Besides, the Stöber silica globules with large interspaces between globules are helpful for limiting the pressure drop and heat transfer,[17] which is also one important role for the Claus catalysts.[1] The above properties of the as-synthesized Au-NPs may provide a modest environment for the selective oxidation of H_2S.

As far as we know, there is still no publication concerning the selective oxidation of H_2S to S over gold catalysts. In this work, we applied the Stöber silica (SS5) supported Au-NPs containing materials- named Au/SS5-C and Au/SS5@Cu-C ("C" means after calcination

under air at 300°C for 4 h), for the selective oxidation of H_2S. Different from the other supported gold catalysts, the current gold materials possessed very special morphologies- Au-NPs were dispersively separated on the surface of non-porous silica globules. Both the gold catalysts performed extremely high sulfur selectivity. The Au/SS5-C possessed inadequate conversion of H_2S, whilst the Au/SS5@Cu-C with copper addition (Au: Cu=1: 1 molar ratio) displayed an obvious promotion of 80% CO conversion (WHSV=0.3h^{-1}, 230°C). The reasons of the interesting behaviors of the materials were also analyzed by the transmission electron microscopy (TEM) and X-ray Photoelectron Spectroscopy (XPS) techniques.

6.2 Au/SS5-C for selective oxidation of H_2S

As we all know that sulfur is strong poison to gold catalyst, which makes the Au-NPs in the catalyst easily to form large aggregations or even deposition of AuS and sulfate, causing the deactivation of catalysts. This is also a reason why we utilize neither organic thiol nor surfactant containing sulfur during synthesis of the Stöber silica supported Au-NPs at the very beginning (Chapter IV). On the contrary there is another common sense that gold absorb the H_2S molecule easily, which is also an important step for the process of H_2S oxidation.[18, 19] The performance of 100 mg Au/SS5-C or Au/SS5@Cu-C mixed with 200 mg SiC (for diluting the sample and limiting the pressure drop, which do not influence the catalytic activity of gold catalysts) are tested by the selective oxidation of H_2S to S in the present of vapor. The detailed information for the selective oxidation of H_2S reaction process is shown in part 2.3.2 in Chapter II.

6.2.1 Selective oxidation of H_2S over *Au/SS5-C catalyst*

The results of selective H_2S oxidation over Au/SS5-C are shown in Figure 6.1. The reaction is first operated at WHSV (Weight Hourly Space Velocity) of 0.3 h^{-1} under 230°C. The H_2S conversion and S selectivity over Au/SS5-C reaches 94% and 90%, respectively.

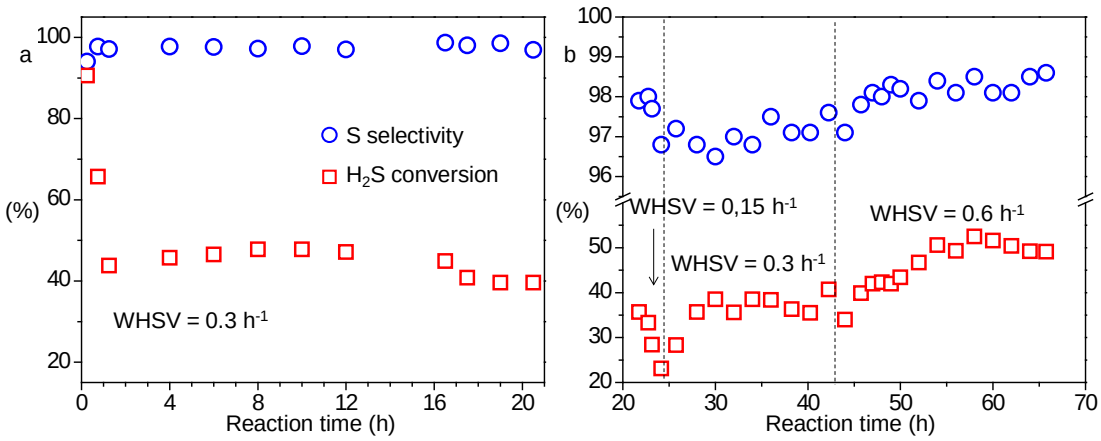

Figure 6.1 Performance of 100 mg Au/SS5-C catalyst (diluted by 200 mg SiC) with time for selective oxidation from H_2S to S at 230 ^oC (volume ratio of H_2S: O_2: water vapor = 1: 2.5: 30).

The first several measurements might be caused by the surplus gases in the chromatograph. The H_2S conversion reduces to 54% within 1 h, despite the slight increase of S selectivity to 98%. After 4 h measurement, the H_2S conversion stabilized at 40-50%. The H_2S conversion is lowered to about 38% after 20 h reaction due to the partially deactivation of the catalyst. By changing the WHSV from 0.3 h^{-1} to 0.15 h^{-1}, the conversion of H_2S rapidly decreases to about 20%. Adjusting the WHSV back to 0.3 h^{-1}, the conversion of H_2S recovers back to about 35%, gently lower than the results during the first 20 h under the same conditions. The further enhancement of the WHSV to 0.6 h^{-1} causes the improvement of H_2S conversion to more than 50%. During the tested 70 h, the selectivity of sulfur production maintains around 95%. However, comparing the performance during the first 20 h and 24-45 h, the H_2S conversion does irreversibly reduced for nearly 10%.

6.2.2 Morphology of spent Au/SS5-C

The TEM images of the spent Au/SS5-C catalyst after the selective oxidation of H_2S are shown in Figure 6.2. The globular structure of Stöber silica remains unchanged after long term reaction. However, large gold aggregations can be seen directly on the surface of silica. A part of one silica globule is displayed in Figure 6.2(b).

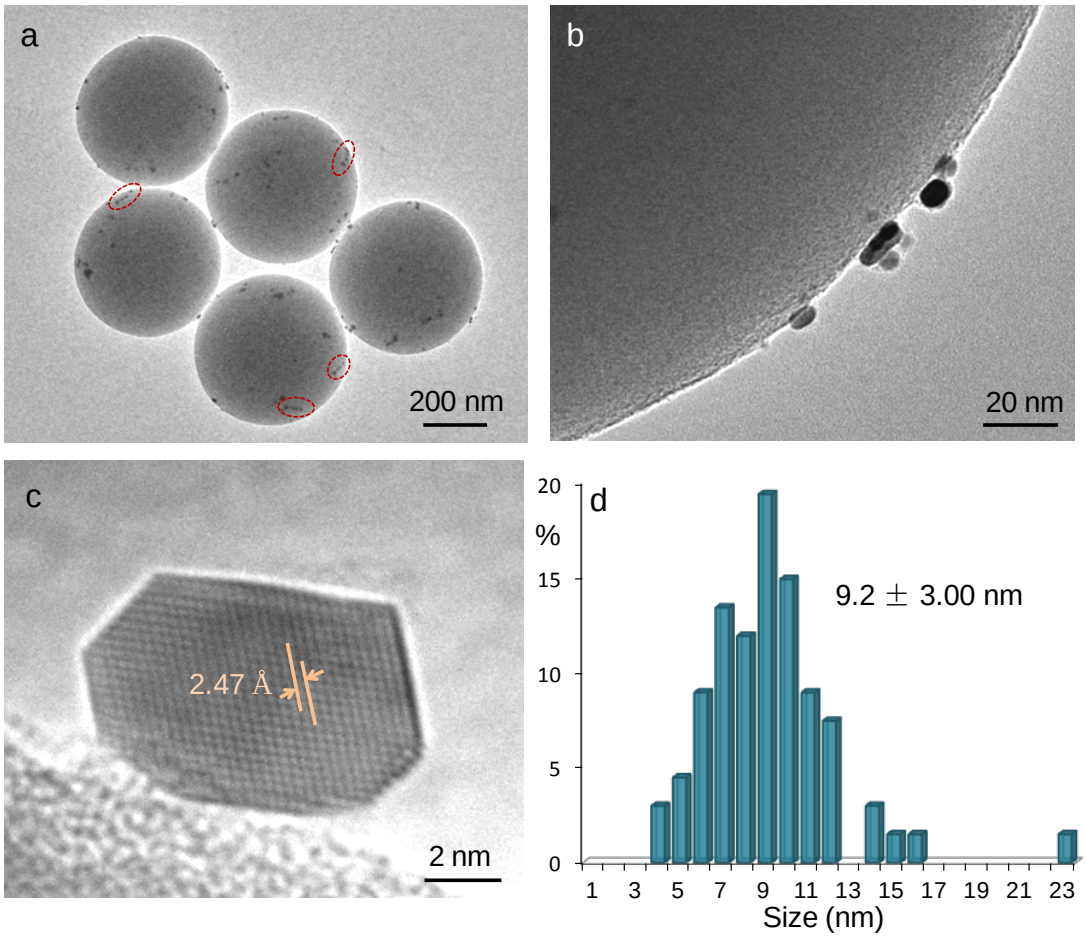

Figure 6.2 The TEM images and size distribution of spent Au/SS5-C sample.

There is nearly no small Au-NPs (< 4 nm) observed on the surface of silica. The intensive gold aggregation makes the large gold particles sporadically dispersed on the surface of the SS5. Besides, some of the gold aggregations seem to be linearly arranged as marked in the dotted circles of Figure 6.2(a), which might be a result of the S- containing compounds modifying the gold surface property as reported by Osterloh's work.[20] The average size of Au-NPs is 9.2 nm. The gold aggregations in the spent Au/SS5-C partially explain the irreversible H_2S conversion with time as shown in Figure 6.1.

6.2.3 Au 4f XPS of Au/SS5-C

The Au 4f XPS spectra and the related composition information of the fresh and spent gold catalysts are shown in Figure 6.3 and Table 6.1. The Au 4f XPS spectrum over Au/SS5-C before reaction can be fitted by four peaks. The peak locating at 83.7 eV and 85.1 eV are ascribed to the metallic Au^0 and $Au^{\delta+}$ ($0< \delta <3$) as reported everywhere.[21] The gold species in

the fresh AuSS5@Cu-C after calcination is consisted by majority of Au^0 species (87.5%) and minority of $Au^{\delta+}$ accounting for only 12.5%.

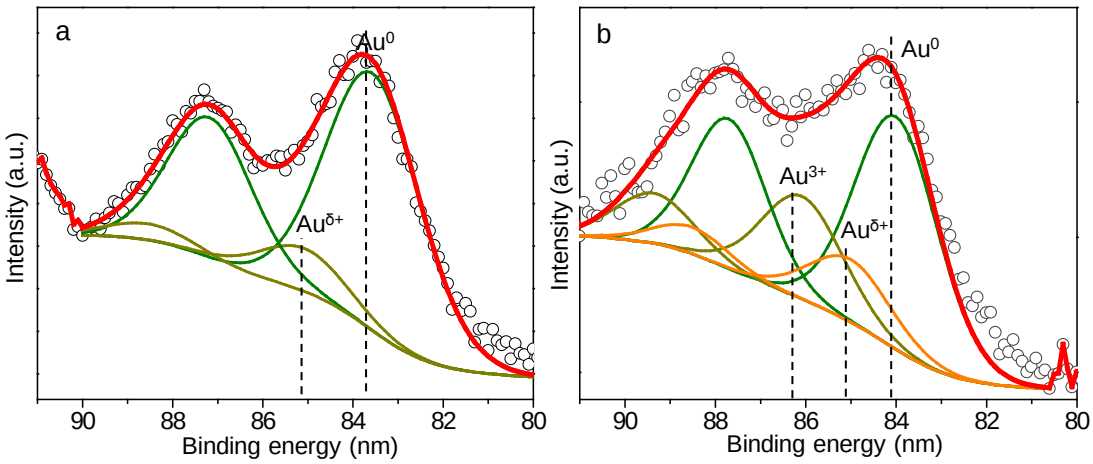

Figure 6.3 Au 4f XPS spectra of Au/SS5-C before (a) and after (b) selective oxidation of H_2S. The circle dots are the initial data, and the solid lines are the fitted lines.

Table 6.1 Information of Au4f, O1s, and surface atomic ratio from XPS spectra over the Au/SS5-C before and after selective H_2S oxidation.

	Fresh Au/SS5-C		Spent Au/SS5-C	
	BE (eV)	Species	BE (eV)	Species
Au $4f_{7/2}$	83.7	87.5%	84.0	61.1%
	85.1	12.5%	85.0	14.2%
	-	-	86.3	24.6%
O 1s	530.3	0.8%	530.4	17.2%
	532.7	97.8%	532.6	81.5%
	534.6	1.4%	534.4	1.3%
Atomic ratio	Au/Si 1.2%		Au/Si 1.4%	

Whilst after reaction, the composition of gold species largely varies as shown in Figure 6.3(b). Formation of new gold species with binding energy of Au $4f_{7/2}$ around 86.3 eV is observed, corresponding to Au^{3+} species.[22] The percentage of $Au^{\delta+}$ (14.2%) in the spent Au/SS5-C only slightly changes from the fresh sample (12.8%). However the Au^0 species decreases from 87.2% in the fresh sample to 61.1% after reaction, and the new Au^{3+} species accounts for about 24.6%.

6.2.4 O 1s XPS of Au/SS5-C

The existence of oxygen species in the catalysts is also an important indicator for the redox property of catalysts. The O 1s XPS spectrum of the fresh Au/SS5-C after calcination is shown in Figure 6.4(a), which can be fitted by three peaks. The huge peak centered at 532.7 eV is a characteristic peak of silica structure,[23] which is related to oxygen species bonded to silica structure, i.e. Si-O-H and Si-O-Si. Two tiny peaks around 530.3 eV and 534.6 eV are ascribed to the defected vacancy oxygen species (O^{2-}) in metal oxide and chemisorbed oxygen species on the surface,[24] respectively.

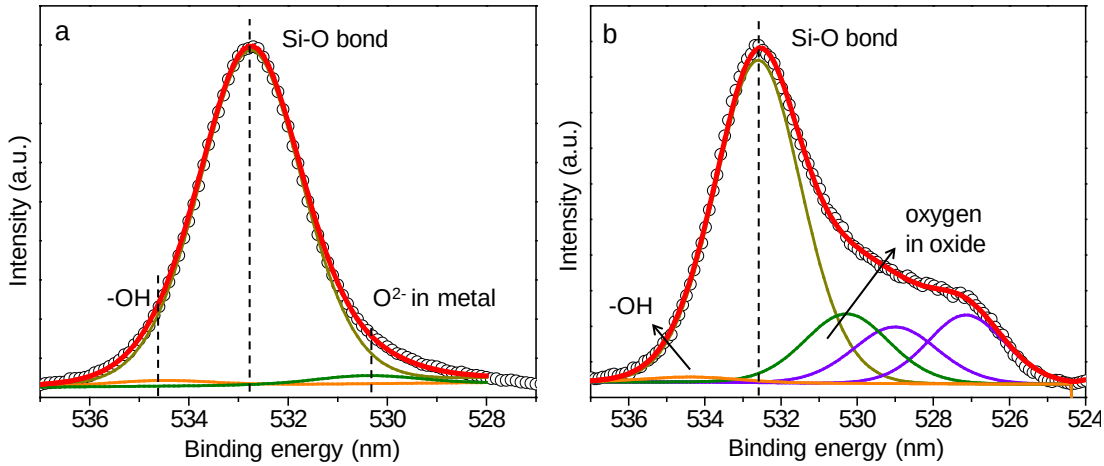

Figure 6.4 The O 1s XPS spectra over fresh (a) and spent (b) Au/SS5-C catalysts after selective H_2S oxidation.

As it was previously mentioned, the adsorption of oxygen species in the metal oxide and chemisorbed on the surface of Au/SS5 is negligible, due to the fact that silica is inert and do not responsible for adsorbing or transferring oxygen species. The detailed information of each peak is listed in Table 6.1. After the selective H_2S oxidation, the O 1s spectrum of spent Au/SS5-C is more complex. The chemisorbed oxygen species around 534.5 eV remains nearly the same. However, the intensity of peak corresponding to oxygen species in metal oxide greatly rises from 0.8% to 17.2% after reaction. It has to be mentioned that the peak related to oxygen species from O-S bond in the sulfate species also ranges in 530.0-530.73 eV.[25, 26] In this case, the increase intensity of peak locating around 530.5 eV witnesses the formation of sulfate on the spent Au/SS5-C.

6.2.5 C 1s XPS of Au/SS5-C

During the reaction, the SiC is mixed with the catalysts ($mass_{SiC}$: $mass_{Catal}$ = 2:1) for dilution. However, it is very hard to separate the SiC from gold catalyst after reaction. The powder is physically blended, and the SiC do not change during the reaction. In order to compare the spent gold catalysts with the fresh ones, the calculation is carried out to get rid of the interference from SiC in the C 1s spectra. The corresponding peak information of fresh and spent gold catalysts, the percentages of various carbon species based on different reference, and the calculation results are presented in Table 6.2. Since the C-Si peak around 282.8 is a characteristic peak of SiC compound, it is used as a reference to remove the background of SiC. In the SiC and spent samples, the Ri is defined as the relative ratio between other carbon species to C-Si bond, and can be calculated by:

$$R_i = \frac{A_{Ci}}{A} \tag{6.1}$$

A_{Ci} and A are the peak area of other carbon species and C-Si species.

The relative ratio $R_i`$ of i carbon species in spent samples without the interference can be obtained by:

$$R_i` = R_i^{catal} - R_i^{SiC} \tag{6.2}$$

R_i^{catal} and R_i^{SiC} are the value of R corresponding to the gold catalysts and pure SiC.

The real percentage A% of each carbon species in the gold catalyst without impurity is:

$$A\% = \frac{R_i`}{\sum_i R_i`} \times 100\% \tag{6.3}$$

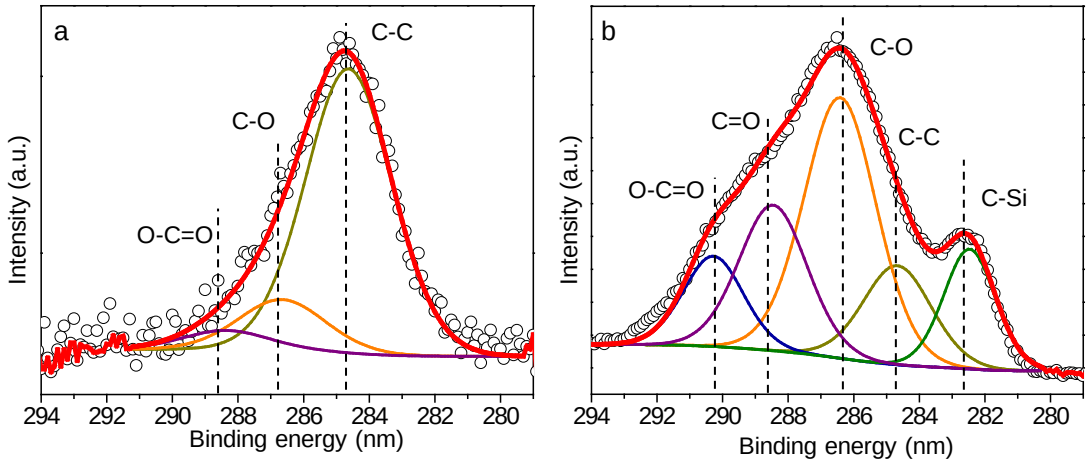

Figure 6.5 The C 1s XPS spectra of Au/SS5-C before (a) and after (b) selective oxidation of H_2S. The circle dots are the initial data, and the solid lines are the fitted lines.

The C 1s XPS spectra of gold catalysts before and after H_2S oxidation are also detected as displayed in Figure 6.5. The intensive peak around 284.6 eV is originated from C-C bond in graphite.[27] The smaller peaks centered at 286.7 eV and 288.5 eV are resulted from C 1s electrons adjacent to oxygen (C-O) and carboxyl (C=O), respectively.[28-30] The fresh Au/SS5-C before reaction possesses the graphite peak, which is partly resulted from oil contamination during XPS operation, and the two additional peaks from C-O and C=O species.

After reaction, the C=O species rapidly rise from 5% to 29.9% in the Au/SS5-C, and the amount of O-C=O species[31] also appears and increases to 15.3%, which should be an indication of coking on the surface of catalyst, probably from the residual carbon species in PVA compound.

Table 6.2 Information of C1s XPS spectra and the processed carbon species composition in the Au/SS5-C before and after selective H_2S oxidation.

C_i	SiC		Fresh Au/SS5-C		Spent Au/SS5-C			
	BE (eV)	R [a]	BE (eV)	A% [c]	BE (eV)	R	R` [b]	A%
C-Si	282.8	1.0	-	-	282.6	1.0	-	-
C-C	284.6	0.6	284.6	76.70%	284.7	1.1	0.5	10.40%
C-O	286.3	0.8	286.7	18.30%	286.4	3.0	2.2	44.40%
C=O	288.2	0.1	288.6	5.00%	288.5	1.6	1.5	29.90%
O-C=O	290.0	0.1	-	-	290.1	0.9	0.8	15.30%

[a] R is the relative amount of carbon species comparing to SiC (the R of C-Si bond at 282.8 eV is defined as 1). [b] R` is the relative amount of carbon species get rid of the influence of SiC existence. [c] A% is the real

percentage of carbon species in gold catalysts without interference of additional SiC.

6.3 Au/SS5@Cu-C for selective oxidation of H_2S

6.3.1 Performance of *Au/SS5@Cu-C catalyst*

The performance of Au/SS5@Cu-C sample for selective H_2S oxidation is illustrated in Figure 6.6.

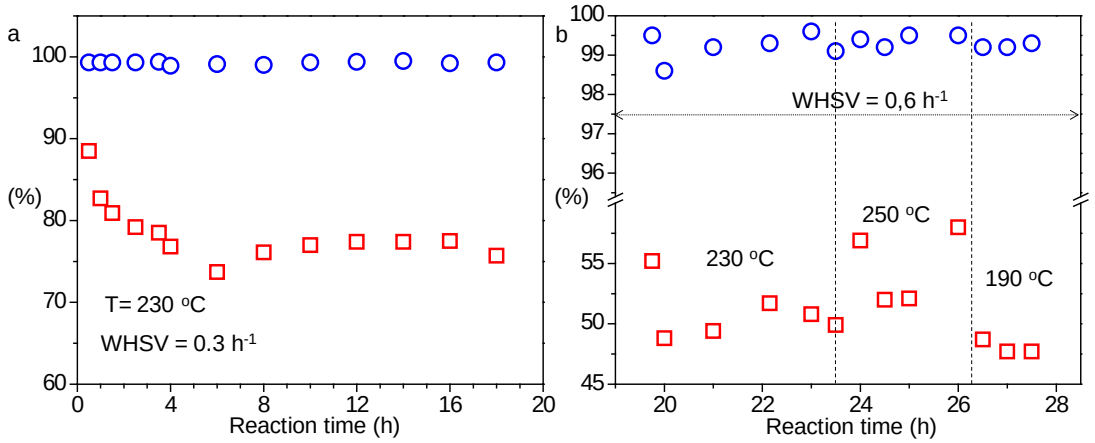

Figure 6.6 Performance of 100 mg Au/SS5@Cu-C catalyst (diluted with 200 mg SiC) with time for selective oxidation of H_2S to S (volume ratio of H_2S: O_2: water vapor = 1: 2.5: 30).

Comparing with the Au/SS5-C without copper addition, the H_2S conversion over Au/SS5@Cu-C is largely promoted. Besides, the selectivity of sulfur maintains above 98% throughout the reaction. By operating at WHSV of 0.3 h^{-1} under 230 °C, the H_2S conversion reaches 90% at the very beginning, then mildly decreases to 75% and become stable due to the surplus gases in the chromatograph. The H_2S conversion and the sulfur yield are about 2-fold over the gold catalysts without copper addition under the same operation conditions. By changing the WHSV to 0.6 h^{-1}, the variation of reaction temperature leads to the unobvious fluctuation of the H_2S conversion, that is, the increase of temperature generally corresponds to a slightly higher H_2S conversion. It has to be mentioned that the CuO based catalysts are also available for activating the H_2S oxidation. Marshneva et al.[32] tested lots of metal oxides and obtain the following order of oxides used for this reaction: V_2O_5 > Mn_2O_3 >

$CoO > TiO_2 > Fe_2O_3 > Bi_2O_3 > Sb_6O_{13} > CuO > Al_2O_3 = MgO = Cr_2O_3$. Besides, Laperdrix and co-workers[33] applied the CuO/Al_2O_3 as catalyst for the selective oxidation of H_2S at only 110°C. The CuO/Al_2O_3 with very high CuO loading (17.3 wt%) performed excellent H_2S conversion at the beginning. The CuO is the main active species, however the conversion decreased rapidly after about 20 h. They also found out that the CuO in the sample were easily sulfated during the reaction, causing the deactivation of catalyst. In fact, the main copper species in the fresh Au/SS5@Cu-C is not the CuO but the metallic Cu. In this case, even the increase of H_2S conversion may partially due to the addition of copper addition, the new catalyst seems more stable.

6.3.2 Morphology of spent Au/SS5@Cu-C

Different from the spent Au/SS5-C consisting by large Au aggregations, the Au-NPs in the spent Au/SS5@C-C sample are barely aggregated as viewed from Figure 6.7(a).

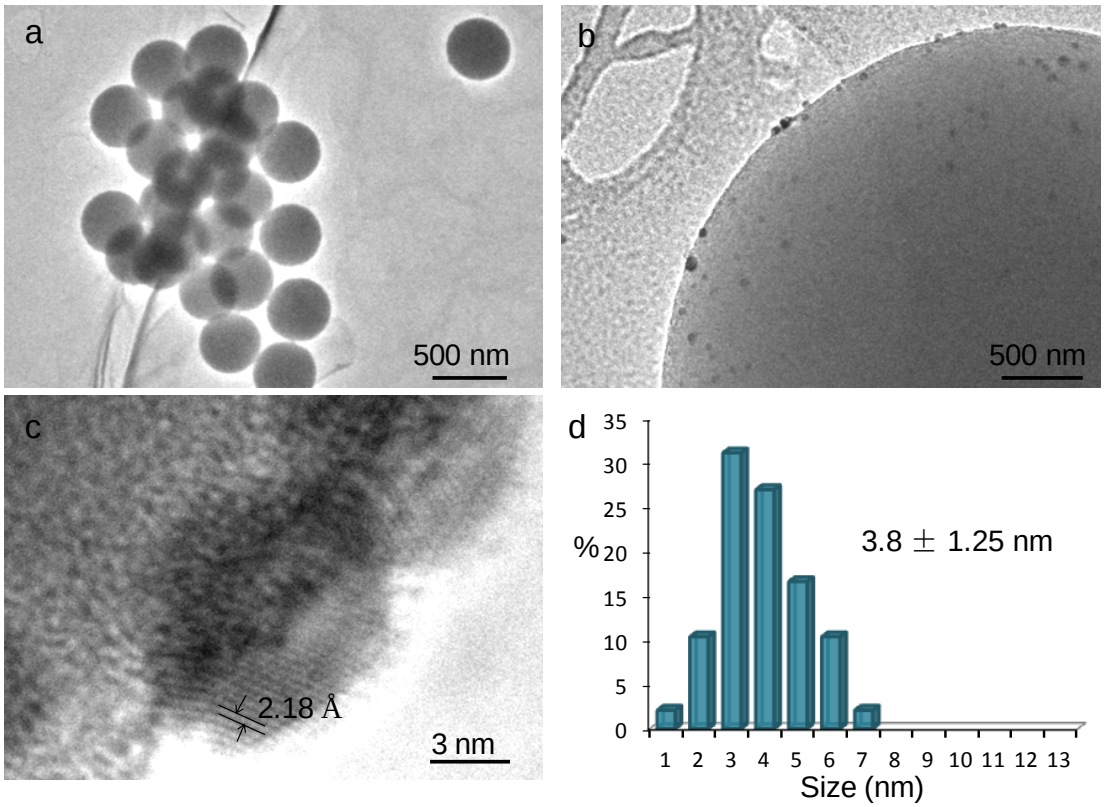

Figure 6.7 The TEM images and size distribution of spent Au/SS5@Cu-C sample.

Indeed, some of the metal particles are even smaller and seem to be more dispersive on the

globules surface after reaction. The size distribution of particles on the silica surface is displayed in Figure 6.7(d). Surprisingly, there are generally no particles larger than 8 nm. The average particle size is 3.8 nm, even smaller than that of the freshly calcined Au/SS5-C (4.4 nm) and Au/SS5@Cu-C (5.3 nm). However, the gold particles and copper (oxide) particles are very difficult to be separated directly from the TEM images. By observing the high resolution TEM images, there are also small parts of strange particles possessing special interplanar spacing (e.g. 2.18 Å as in Figure 6.4(c)), which do not belong to either pure Au or CuO_x lattice surface. In fact, the active components in the catalyst go through a slowly redox process under the coexistence of H_2S and O_2. It is inferred that small amounts of new species (i.e. AuCu alloy) are formed during the reaction.

6.3.3 Au 4f XPS of Au/SS5@Cu-C

Figure 6.5 displayed the formation of gold species in the fresh and spent Au/SS5@Cu-C from Au4f XPS. The detailed information is listed in Table 6.3. In both of the fresh and spent samples, only two gold species are observed. Comparing to the Au/SS5-C, there is no formation of Au^{3+} species after reaction.

Table 6.3 Information of Au4f, O1s, and Cu2p XPS spectra over Au/SS5@Cu-C before and after selective H_2S oxidation.

	Fresh Au/SS5@Cu-C		Spent Au/SS5@Cu-C	
	BE (eV)	Species	BE (eV)	Species
Au $4f_{7/2}$	84.0	92.9%	84.0	89.7%
	85.0	7.1%	85.1	10.3%
	-	-	-	-
O 1s	530.6	12.0%	530.4	9.6%
	532.6	79.3%	532.3	82.6%
	534.4	8.7%	534.3	7.8%
Cu $2p_{3/2}$	932.6	100%	932.4	92.7%
	-	-	934.1	7.3%
Atomic ratio	Au/Si 1.1%	Au/Cu 0.9	Au/Si 1.1%	Au/Cu 0.75

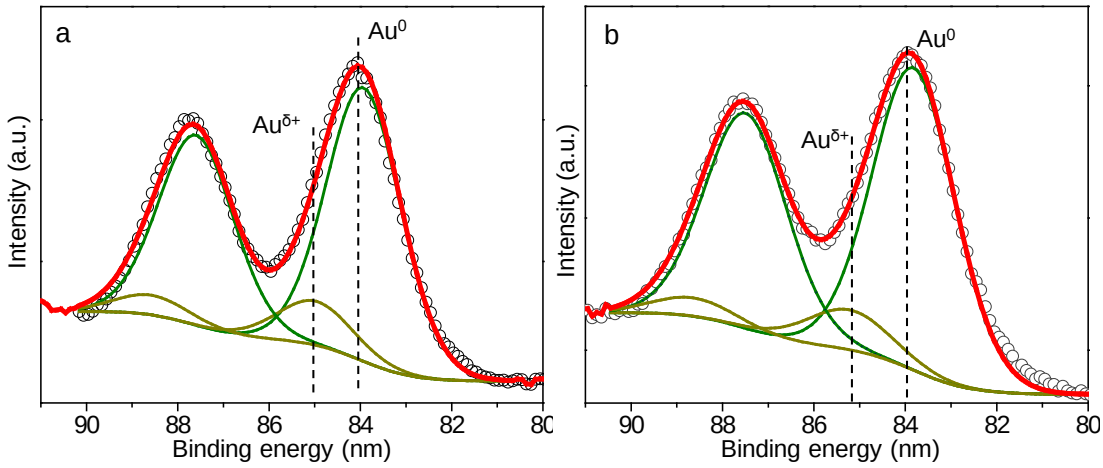

Figure 6.8 Au 4f XPS spectra of Au/SS5@Cu-C before (a) and after (b) selective oxidation of H_2S. The circle dots are the initial data, and the solid lines are the fitted lines.

The Au/SS5@Cu-C seems very stable going through the selective oxidation of H_2S. Both the binding energy and gold species composition of Au/SS5@Cu-C before and after reaction are generally unchanged (Figure 5.6(c-d)). Only the amount of Au^0 decreases very few (about 3% from Table 6.1) in return for minor increase of $Au^{\delta+}$ species. There is no direct evidence confirming that the gold species is affected by sulfur during the reaction.

6.3.4 Cu 2p XPS of AuSS5@Cu-C

Figure 6.9 displayed the Cu 2p XPS spectra of the fresh and spent Au/SS5@Cu-C catalysts for H_2S oxidation, and the corresponding information is listed in Table 6.3.

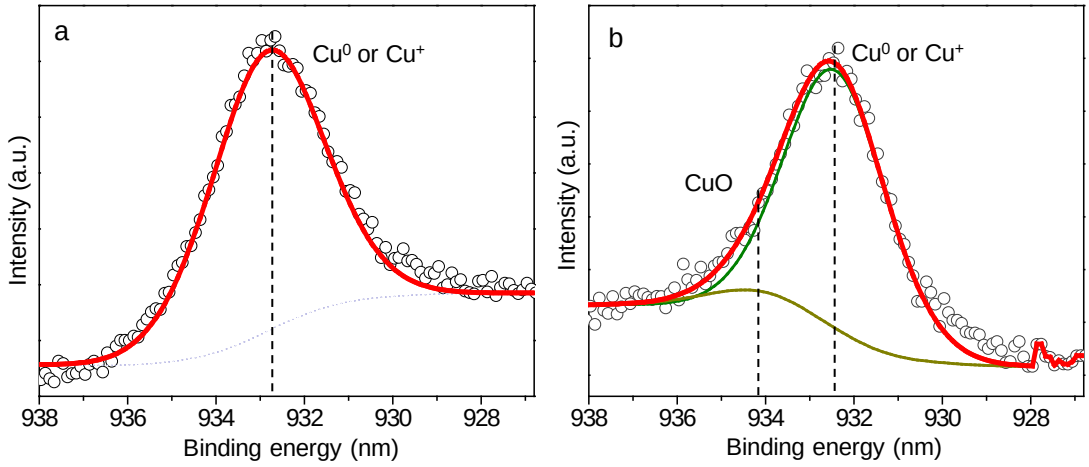

Figure 6.9 Cu 2p XPS spectra of Au/SS5@Cu-C before (a) and after (b) selective oxidation of

H_2S. The circle dots are the initial data, and the solid lines are the fitted lines.

In the fresh Au/SS5@Cu-C sample, only one symmetric peak (based on the background) is observed, which locates around 932.6 eV, ascribing to the Cu^0 or Cu^+ species in the sample. After the selective oxidation of H_2S, one huge and broad peak locating around 932.5 eV can be divided into two peaks with the binding energies (BE) of 932.4 and 934.1 eV, which are attributed to the Cu^0/Cu^+ species and Cu^{2+} species, respectively. The Cu^0 or Cu^+ species constitute the main parts in the copper component. Only very few amounts of CuO (about 7.3%) are present after reaction. The results indicate that the copper species does not go through drastic development during the long time reaction under O_2 and H_2S, and only very few parts of the copper species transfer into more oxidized copper species.

6.3.5 O 1s XPS of Au/SS5@Cu-C

The distribution of fresh Au/SS5@Cu-C after calcination is shown in Figure 6.10(a). Comparing with the fresh Au/SS5-C, the amounts of chemisorbed oxygen species and lattice oxygen species in metal become much higher. Even after 72 h reaction, the oxygen species generally remains as the same in the fresh sample, once again revealing the satisfied stability and the oxygen transition ability in the Au/SS5@Cu-C sample after copper addition.

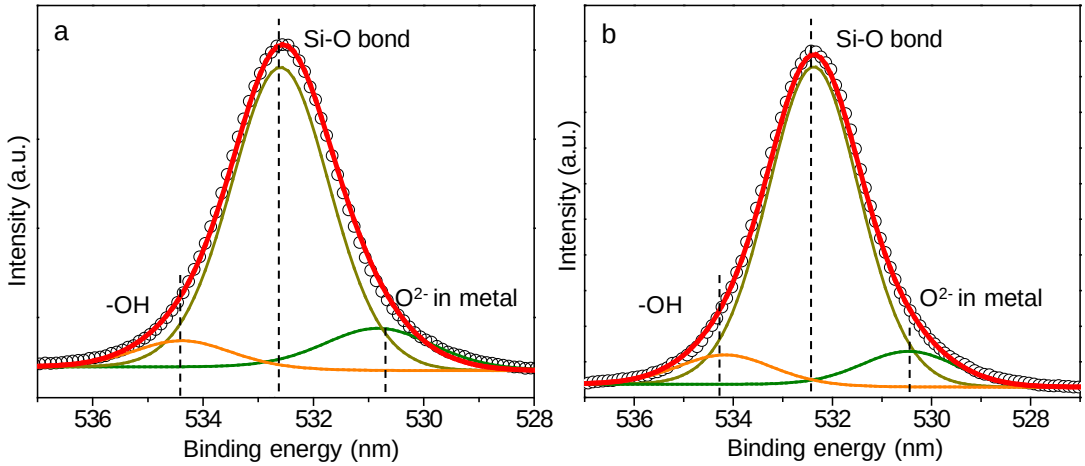

Figure 6.10 The O 1s XPS spectra over fresh (a) and spent (b) Au/SS5@Cu-C catalysts after selective H_2S oxidation.

6.3.6 C 1s XPS of Au/SS5@Cu-C

The C 1s XPS spectra of gold catalysts before and after H_2S oxidation are also detected as displayed in Figure 6.11. The intensive peak around 284.6 eV is originated from C-C bond in graphite.[27] The smaller peaks centered at 286.7 eV and 288.5 eV are resulted from C 1s electrons adjacent to oxygen (C-O) and carboxyl (C=O), respectively.[28-30] The fresh Au/SS5@Cu-C before reaction also possesses the graphite peak and the C-O and C=O species, similar to the fresh Au/SS5-C. After reaction, the C=O species is nearly the same amount of the fresh Au/SS5@Cu-C. There is no obvious coking formation observed from the C1s XPS of the spent Au/SS5@Cu-C.

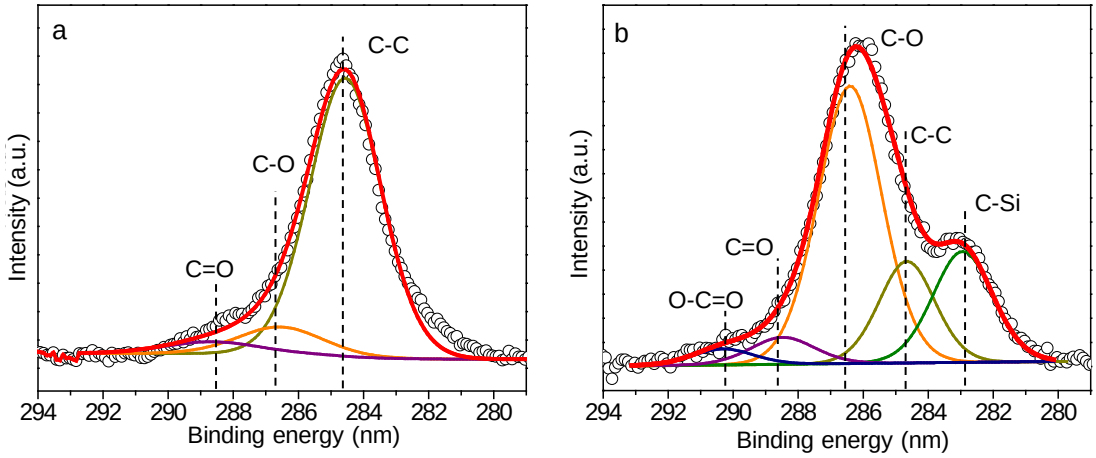

Figure 6.11 The C 1s XPS spectra of Au/SS5@Cu-C before (a) and after (b) selective oxidation of H_2S. The circle dots are the initial data, and the solid lines are the fitted lines.

Table 6.2 Information of C1s XPS spectra and the processed carbon species composition in the Au/SS5-C and Au/SS5@Cu-C samples before and after selective H_2S oxidation.

C_i	SiC		Fresh Au/SS5@Cu-C		Spent Au/SS5@Cu-C			
	BE (eV)	R [a]	BE (eV)	BE (eV)	BE (eV)	R	R` [b]	A%
C-Si	282.8	1.0	-	-	282.8	1.0	-	-
C-C	284.6	0.6	284.6	85.40%	284.7	1.2	0.6	22.70%
C-O	286.3	0.8	286.6	9.80%	286.4	2.7	1.8	70.20%
C=O	288.2	0.1	288.5	4.80%	288.5	0.3	0.1	5.70%
O-C=O	290.0	0.1	-	-	290.1	0.1	0	1.40%

[a] R is the relative amount of carbon species comparing to SiC (the R of C-Si bond at 282.8 eV is defined as 1). [b] R` is the relative amount of carbon species get rid of the influence of SiC existence. [c] A% is the real percentage of carbon species in gold catalysts without interference of additional SiC.

6.4 Discussion

By using the Au-NPs based catalysts, the selectivity of sulfur is excellent for more than 95%. It means that the rates of the side reactions are very slow or even negligible. The presence of Au-NPs should account for the high selectivity since the silica alone exhibits pore activity.[34, 35]

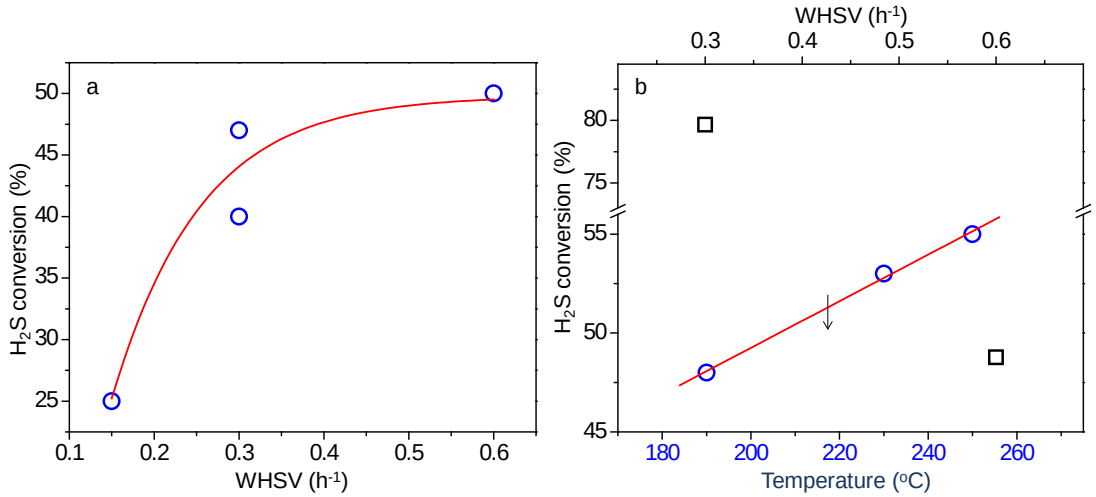

Figure 6.9 The variation trend between H_2S conversion and WHSV or reaction temperature over Au/SS5-C (a) and Au/SS5@Cu-C (b).

There is a very strange phenomenon if attention is paid to H_2S conversion changing as a function of WHSV (Figure 6.9). For the Au/SS5@Cu-C with copper addition, the H_2S conversion drops from 80% to 55% by accelerating the WHSV from 0.3 h^{-1} to 0.6 h^{-1}, which is a normal case as reported everywhere.[36] However, the variation of H_2S conversion over Au/SS5-C vs. the WHSV is definitely on the opposite. By adjusting the WHSV from 0.3 h^{-1} to 0.6 h^{-1} under 230^{o}C, the H_2S conversion varies from 35% to 55%. It is considered that reaction equilibrium exists during the H_2S oxidation over Au/SS5-C. The H_2S oxidation can be processed by the reaction between chemisorbed oxygen species and the absorption of H_2S- either physical absorption or dissociative chemisorption.[18, 19] Along with time, the amount of produced S increases and cannot be removed with vapor in time, covers parts of the active sites, hindered the sorption and dissociation of H_2S and O_2 temporarily, thus lowered the reaction speed. By increasing the WHSV from 0.3 h^{-1} to 0.6 h^{-1}, the flowing away of sulfur from Au-NPs is facile, making the active sites on Au-NPs re-exposed to the reactants.

Besides, the H_2S conversion only slightly increases along with the temperature. When the temperature is fixed at 230^oC, the sample is active for a 75% conversion. Further increase of temperature does not bring the beneficial enhancement of the H_2S conversion. On the other hand, the H_2S conversion decreases with the temperature (190^oC), due to the fact that amounts of sulfur may transformed into liquid phase as the temperature is lower than the dew point of sulfur, hindered the contact between reactants and active sites.

Combining with the TEM results and XPS spectra of Au/SS5-C before and after reaction, the gold species and nanoparticles in the Au/SS5-C sample encounter great aggregation during the reaction. After the reaction, the variation of gold species and formation of Au^{3+} species is considered to be resulted from the formation of Au^{3+} combining with S^{2-} from the dissociative absorption of H_2S[37] or even sulfate, which are easily bonded to the catalyst and nonreactive, causing the deactivation of materials.[38, 39]. The formation of Au^{3+} species consumes the metallic active gold species, partially accounts for deactivation of the catalysts. This is the case for the Au/SS5-C.

Whilst for the copper added Au/SS5@Cu-C, the situation is totally changed. After calcination, parts of the gold and copper (oxide) nanoparticles remain their sizes, and few parts of gold and copper (oxide) particles move together to form new aggregations (Figure 5.8 of Chapter IV). It has to be mentioned that the current calcination temperature is insufficient to make the formation of AuCu alloy, which can only be formed by first an oxidized condition and then reduced (e.g. annealed in H_2-N_2 mixture at high temperature).[40, 41] In this case, there exist Au-NPs, copper (oxide) nanoparticles, and Au-CuO_x but not AuCu alloy. After the selective oxidation of H_2S, the TEM images of spent Au/SS5@Cu-C catalyst displays particles even smaller and more dispersive. Besides, particles with interplanar spacing beyond pure gold or copper (oxide) are observed. It indicates that the gold and copper (oxide) components have been through a re-assembling process during the H_2S oxidation. From the XPS analysis, there is no Au^{3+} species formed in the Au/SS5@Cu-C after reaction. Besides, the variation of copper component, the oxygen species and carbon species are stable. The copper addition helps the gold species from sulfur-poisoning, making the gold species stable during the H_2S reaction.

It is also remarkable to concern the function of the special support- the non-porous Stöber silica globules. The TEM analysis of both spent Au/SS5-C and Au/SS5@Cu-C illustrate that

the metal particles dispersed on the surface of silica. It is previously reported that the high specific surface area of catalysts was one of the parameters for Claus catalyst.[1] However, even the temperature is higher than the dew point of sulfur, the special conditions may cause the produced S to be condensed in the pores and block the active sites, making the catalysts deactivated. In the non-porous Stöber silica case, there is no chance for the formed S to be trapped in the pores. The contact time of gold with sulfur is shortened. The metal nanoparticles are dispersed on the surface of silica and fully accessible for the reactants. The large distances between each globule facilitate the evacuation of sulfur vapor and avoid its condensation.

6.5 Conclusion

Sulfur is generally considered as the poison for gold nanoparticles in the field of inorganic heterogeneous catalysis, due to the fact that sulfur is so ready to adsorb onto the surface of gold nanoparticles and thus hindered the adsorption of the real reactants. Besides, the sulfur poison may change the structure of gold catalysts such as formation of gold aggregations during the reaction. However, it is believed that there is a modest activation level for the gold catalyst that it's good enough for the sorption and dissociation of reactants, and also available to avoid sulfating, thus avoid the poison of gold nanoparticles by sulfur.

In this work, the reaction of selective oxidation of H_2S to S was for the first time activated by the Stöber silica (SS5) supported Au-NPs (with and without copper addition, named as Au/SS5-C and Au/SS5@Cu-C). There were several conclusions obtained from the experimental part:

1. Both the Au/SS5-C and Au/SS5@Cu-C possessed extremely high selectivity of S. The Au/SS5@Cu-C (0.3 wt% of Cu to silica) performed greatly enhanced H_2S conversion at 0.3 h^{-1} under 230^{o}C of about 80%- two-fold of that over the Au/SS5-C.
2. The pure Au-NPs supported on SS5 intensely aggregated after reaction with partial deactivation. The XPS results confirmed that the sulfate was formed.
3. After copper addition, the Au and CuO_x particles went through re-assembling during the reaction. The copper addition illuminated the risk of gold to be poisoned by the sulfating and maked the catalyst stable during long-term H_2S oxidation.

4. The Stöber silica was applied as support for Au-NPs. The superiority of the non-porous globules- including the ability to disperse Au-NPs, maximize the active sites exposure, limit the pressure drop and heat transfer, and facilitate the sulfur vapor remove- were proved once again by using this special reaction.
5. This work may shed light on the supported Au-NPs for further engaged into the sulfur-containing catalysis field with the immunity of sulfur poison.

Bibliography

[1] A. Pieplu, O. Saur, J.C. Lavalley, O. Legendre, C. Nedez, Claus catalysis and H_2S selective oxidation, Catalysis Reviews-Science and Engineering, 40 (1998) 409-450.

[2] N.-K. Park, D.C. Han, T.J. Lee, S.O. Ryu, A study on the reactivity of Ce-based Claus catalysts and the mechanism of its catalysis for removal of H_2S contained in coal gas, Fuel, 90 (2011) 288-293.

[3] H.G. Karge, M. Łaniecki, M. Ziołek, UV-visible spectroscopic investigations of the modified claus reaction on NaX zeolite catalysts, Journal of Catalysis, 109 (1988) 252-262.

[4] P. Nguyen, J.-M. Nhut, D. Edouard, C. Pham, M.-J. Ledoux, C. Pham-Huu, Fe_2O_3/β-SiC: A new high efficient catalyst for the selective oxidation of H_2S into elemental sulfur, Catalysis Today, 141 (2009) 397-402.

[5] M.Y. Shin, C.M. Nam, D.W. Park, J.S. Chung, Selective oxidation of H_2S to elemental sulfur over VO_x/SiO_2 and V_2O_5 catalysts, Applied Catalysis a-General, 211 (2001) 213-225.

[6] J. Guzman, B.C. Gates, Structure and reactivity of a mononuclear gold-complex catalyst supported on magnesium oxide, Angewandte Chemie-International Edition, 42 (2003) 690-693.

[7] L.C. Wang, Y.M. Liu, M. Chen, Y. Cao, H.Y. He, K.N. Fan, MnO_2 nanorod supported gold nanoparticles with enhanced activity for solvent-free aerobic alcohol oxidation, Journal of Physical Chemistry C, 112 (2008) 6981-6987.

[8] M. Nishibori, W. Shin, N. Izu, T. Itoh, I. Matsubara, CO oxidation performance of Au/Co_3O_4 catalyst on the micro gas sensor device, Catalysis Today, 201 (2013) 85-91.

[9] M. Conte, A.F. Carley, G. Attard, A.A. Herzing, C.J. Kiely, G.J. Hutchings, Hydrochlorination of acetylene using supported bimetallic Au-based catalysts, Journal of Catalysis, 266 (2009) 164-164.

[10] S. Ivanova, V. Pitchon, C. Petit, V. Caps, Support effects in the gold-catalyzed preferential oxidation of CO, Chemcatchem, 2 (2010) 556-563.

[11] E. Pensa, E. Cortes, G. Corthey, P. Carro, C. Vericat, M.H. Fonticelli, G. Benitez, A.A. Rubert, R.C. Salvarezza, The chemistry of the sulfur-gold Interface: In search of a unified model, Accounts of Chemical Research, 45 (2012) 1183-1192.

[12] H.P. Bonzel, R. Ku, Adsorbate interactions on a Pt(110) surface. II. Effect of sulfur on the catalytic CO oxidation, The Journal of Chemical Physics, 59 (1973) 1641-1651.

[13] C.H. Bartholomew, Mechanisms of catalyst deactivation, Applied Catalysis a-General, 212 (2001) 17-60.

[14] T. Kiyonaga, T. Kawahara, H. Tada, Low-temperature photocleaning of sulfur-poisoned Au nanoparticles on titanium dioxide film, Electrochemical and Solid State Letters, 9 (2006) E9-E12.

[15] L. Feria, J.A. Rodriguez, T. Jirsak, F. Illas, Interaction of SO_2 with Cu/TiC(001) and Au/TiC(001): Toward a new family of $DeSO_x$ catalysts, Journal of Catalysis, 279 (2011) 352-360.

[16] M. Ziolek, J. Kujawa, A.B.M. Saad, O. Saur, J.C. Lavalley, Role of sulfates in the deactivation of alumina during the reaction between hydrogen-sulfide and oxygen, Bulletin De La Societe Chimique De France, (1987) 37-41.

[17] Y.F. Liu, L.D. Nguyen, T.H. Tri, Y. Liu, T. Romero, I. Janowska, D. Begin, P.H. Cuong, Macroscopic shaping of carbon nanotubes with high specific surface area and full accessibility, Materials Letters, 79 (2012) 128-131.

[18] M. Steijns, F. Derks, A. Verloop, P. Mars, The mechanism of the catalytic oxidation of hydrogen sulfide: II. Kinetics and mechanism of hydrogen sulfide oxidation catalyzed by sulfur, Journal of Catalysis, 42 (1976) 87-95.

[19] Z.L. Pan, H.S. Weng, H.Y. Feng, J.M. Smith, Kinetics of the self-fouling oxidation of hydrogen-sulfide on activated carbon, AIChE Journal, 30 (1984) 1021-1025.

[20] F. Osterloh, H. Hiramatsu, R. Porter, T. Guo, Alkanethiol-induced structural rearrangements in silica-gold core-shell-type nanoparticle clusters: An opportunity for chemical sensor engineering, Langmuir, 20 (2004) 5553-5558.

[21] A. Gazsi, A. Koos, T. Bansagi, F. Solymosi, Adsorption and decomposition of ethanol on supported Au catalysts, Catalysis Today, 160 (2011) 70-78.

[22] A. Karpenko, R. Leppelt, V. Plzak, R.J. Behm, The role of cationic Au^{3+} and nonionic Au^0 species in the low-temperature water-gas shift reaction on Au/CeO_2 catalysts, Journal of Catalysis, 252 (2007) 231-242.

[23] I.K. Jung, J.L. Gurav, U.K.H. Bangi, S. Baek, H.H. Park, Silica xerogel films hybridized with carbon nanotubes by single step sol-gel processing, Journal of Non-Crystalline Solids, 358 (2012) 550-556.

[24] H.Y. Yang, S.F. Yu, S.P. Lau, T.S. Herng, M. Tanemura, Ultraviolet Laser Action in Ferromagnetic $Zn_{1-x}Fe_xO$ Nanoneedles, Nanoscale Research Letters, 5 (2010) 247-251.

[25] S. Han, G. Zhang, H. Xi, D. Xu, X. Fu, X. Wang, Sulfated TiO_2 Decontaminate 2-CEES and DMMP in Vapor Phase, Catalysis Letters, 122 (2008) 106-110.

[26] P. Catalin-Florin, Alkaline oxidation of hydrosulfide and methyl mercaptide by iron/cerium oxide-hydroxide in presence of dissolved oxygen. Possible application for removal of Total Reduced Sulfur (TRS) emissions in the Pulp & Paper industry, PhD report, Université Laval, Québec, Canada, 2007.

[27] W.-S. Tseng, C.-Y. Tseng, C.-T. Kuo, Effects of gas composition on highly efficient surface modification of multi-walled carbon nanotubes by cation treatment, Nanoscale Research Letters, 4 (2008) 234 - 239.

[28] K. Emoto, Y. Nagasaki, M. Iijima, M. Kato, K. Kataoka, Preparation of non-fouling surface through the coating with core-polymerized block copolymer micelles having aldehyde-ended PEG shell, Colloids and Surfaces B-Biointerfaces, 18 (2000) 337-346.

[29] W. He, H.J. Jiang, Y. Zhou, S.D. Yang, X.Z. Xue, Z.Q. Zou, X.G. Zhang, D.L. Akins, H. Yang, An efficient reduction route for the production of Pd-Pt nanoparticles anchored on graphene nanosheets for use as durable oxygen reduction electrocatalysts, Carbon, 50 (2012) 265-274.

[30] T. Miller, J.M. Lin, L. Pirolli, L. Coquilleau, R. Luharuka, A.V. Teplyakov, Investigation of thin titanium carbonitride coatings deposited onto stainless steel, Thin Solid Films, 522 (2012) 193-198.

[31] S. Some, Y. Kim, E. Hwang, H. Yoo, H. Lee, Binol salt as a completely removable graphene surfactant, Chemical Communications, 48 (2012) 7732-7734.

[32] V.I. Marshneva, V.V. Mokrinskii, Catalytic activity of metal-oxides in hydrogen-sulfide oxidation by oxygen and sulfur-dioxide, Kinetics and Catalysis, 29 (1988) 854-858.

[33] E. Laperdrix, G. Costentin, O. Saur, J.C. Lavalley, C. Nedez, S. Savin-Poncet, J. Nougayrede, Selective oxidation of H_2S over CuO/Al_2O_3: Identification and role of the sulfurated species formed on the catalyst during the reaction, Journal of Catalysis, 189 (2000) 63-69.

[34] S.W. Chun, J.Y. Jang, D.W. Park, H.C. Woo, J.S. Chung, Selective oxidation of H_2S to elemental sulfur over TiO_2/SiO_2 catalysts, Applied Catalysis B-Environmental, 16 (1998) 235-243.

[35] M. Steijns, P. Mars, Catalytic-oxidation of hydrogen-sulfide - Influence of pore structure and chemical composition of various porous substances, Industrial & Engineering Chemistry Product Research and Development, 16 (1977) 35-41.

[36] K.V. Bineesh, M.I. Kim, G.H. Lee, M. Selvaraj, D.W. Park, Catalytic performance of vanadia-doped alumina-pillared clay for selective oxidation of H_2S, Applied Clay Science, 74 (2013) 127-134.

[37] H. Saussey, O. Saur, J.C. Lavalley, Infrared study of sulfur-compounds adsorption on anatase - Adsorption sites, Journal De Chimie Physique Et De Physico-Chimie Biologique, 81 (1984) 261-265.

[38] H.G. Karge, I.G.D. Lana, Infrared studies of SO_2 adsorption on a Claus catalyst by selective poisoning of sites, Journal of Physical Chemistry, 88 (1984) 1538-1543.

[39] H.G. Karge, Y. Zhang, S. Trevizan De Suarez, M. Ziołk, Studies on the modified Claus Reaction over alkaline faujasites by simultaneous infrared, kinetics, and esr measurements, in: N.I.J.P.J.V.B.K. P.A. Jacobs, G. Schulz-Ekloff (Eds.) Studies in Surface Science and Catalysis, Elsevier1984, pp. 49-59.

[40] G. De, G. Mattei, P. Mazzoldi, C. Sada, G. Battaglin, A. Quaranta, Au-Cu alloy nanocluster doped SiO_2 films by sol-gel processing, Chemistry of Materials, 12 (2000) 2157-2160.

[41] J.C. Bauer, D. Mullins, M.J. Li, Z.L. Wu, E.A. Payzant, S.H. Overbury, S. Dai, Synthesis of silica supported AuCu nanoparticle catalysts and the effects of pretreatment conditions for the CO oxidation reaction, Physical Chemistry Chemical Physics, 13 (2011) 2571-2581.

Chapter VII Conclusion and perspectives

7.1 General conclusion

The objective of the current work and the report is to look out for the new material based on gold applied in the catalysis field (e.g. CO oxidation) and understand the function and action roles of gold nanoparticles. We are mainly focused on the colloidal gold nanoparticles to be used as the gold precursor and the Stöber silica to be used as the support. As we mentioned at the beginning of this report, the colloidal gold nanoparticles possess special optical properties. People can realize the sizes and even the distributions of gold nanoparticles directly from the color, the plasmon resonance bond, and some simple measurements. Thus by using the gold colloid as precursor, the sizes of gold nanoparticles can be easily controlled before supporting process. On the other side, the Stöber silica synthesized in this work is proved to be non-porous. In this case the gold nanoparticles can be totally dispersed on the surface of support, available to be contacted by the reactant, and do not have the risk to be trapped into pores of support.

However, it was reported that the interaction between colloidal gold nanoparticles and supports were weak and lack of catalytic activity. And the colloidal gold nanoparticles supported on Stöber silica until now have never been used into the inorganic heterogeneous catalysis field. It is urgent and also interesting to introduce this kind of material into the catalysis field. We are trying to find a new way to prepare the Stöber silica supported gold nanoparticles without catalytic poisonous agents, understand what happened to the gold nanoparticles during the reactions, the catalytic activity and stability of gold nanoparticles. We also want to find an available path for accelerating this kind of supported gold nanoparticles with special structure into the catalysis field. And fortunately, the experimental results demonstrated the practical of this theory. The Au-NPs around 3 nm were successfully supported onto Stöber silica without organic compounds poisoning the Au-NPs in the catalytic activity. The above material after modification can be applied for CO oxidation with comparable activity as the parallel gold catalysts supported on silica after modification. What’s more, the Stöber silica was proof to be used as a novel support for Au-NPs and can catch up with the daily

used mesoporous carriers.

7.1.1 Synthesis of more controllable and divinable gold colloid

The colloidal gold nanoparticles could be synthesized by the $NaBH_4$ as reducer and PVA as protector (PVA: Au: $NaBH_4$ of 0.0197: 1: 5, molar ratio). The conditions were facile and with high repeatability. The plasmon resonance bonds revealed from UV-vis spectra and the color displayed by colloids were applied as the fundamental measurements for the Au-NPs. The home-made liquid diffusion test based on the same theory of column chromatography used in the organic chemistry was also utilized for providing further information of sizes and distribution of Au-NPs. The supposition of this simple test was evidenced by the SEM images. Here the possibility that the gold colloid with homogeneous and small Au-NPs could be directly indentified from the gold colloids (with various size distributions) during the colloid synthesis before the operation of TEM images, saving both money and time for the people working in the field concerning gold colloid.

7.1.2 Usage of Stöber silica as support

Five type of spherical silica with different diameters were prepared by Stöber method. Two kinds of silica with diameters of 50 nm and 490 nm were chosen as the supports. For the first time the controllably prepared Au-NPs (3 nm ± 0.7 nm) were coated on the surface of silica without the addition of organic coupling agent. And the mechanism of growth and anchoring of gold nanoparticles were studied by means of XPS, operand FTIR, and TEM. Small gold nanoparticles still exist after calcined at 300^{o}C for 4 h. Calcined gold particles are further fixed on silica by removing hydroxyl species.

7.1.3 Modification by metal addition

The gold nanoparticles supported on Stöber silica and tested by CO oxidation, however the activity of which was disappointed. The gold material performed much better activity for CO

oxidation after doping with trace amount of metal (Cu, Fe, Co, about 0.3 wt% to silica), especially for the copper doped catalysts. The detailed reason for the greatly enhanced activity of CO oxidation over the current catalysts was understood by using the CuO doped catalyst as example. The results displayed that during the reaction the active oxygen species can be replenished by the lattice oxygen from metal oxides. Before the CO oxidation, the Cu or Cu_2O partially covered the surface of Au-NPs and help the anchoring of Au-NPs on the surface of silica. After the reaction, most of the Au-NPs and copper compounds were split to be separate, whilst small part of the Cu or Cu_2O changed into CuO and become special contactor between Au-NPs and silica, making the interaction between gold and support more tightly, and largely enhanced the catalytic activity.

7.1.4 Novel application of Stöber silica supported colloidal Au-NPs

Finally, the application of the catalysts was considered for expended application in the sixth chapter. The Stöber silica supported gold nanoparticles before and after CuO addition were tested by a reaction that was never tried or even considered over supported gold nanoparticles- the selective oxidation of H_2S. The good stability, reactivity, and especially the excellent selectivity were observed over the synthesized gold nanoparticles. The mechanism of selective oxidation of H_2S over supported gold nanoparticles was for the first time analyzed.

7.2 Novelties and Perspectives

Based on the trinity of observing the color, the UV plasmon resonance peak, and results of the home-made liquid diffusion test, the morphology of gold nanoparticles in the colloid can be preliminarily estimated before microscopy. The simple method lowers the cost and show the guideline to the beginners of gold colloid.

The coating process of colloidal Au-NPs onto Stöber silica, without usage of coupling agent, gets rid of the risks of the poisoning Au-NPs. This aspect provided a perspective for the

Au/Stöber-silica from colloid to be applied in the heterogeneous catalysis field.

According to the 3.3 conclusion, the non-porous Stöber silica structure was also an assignable cause for dispersing the small Au-NPs and the enhancement of activity. The mesoporous silica is no longer a dictatorial material for the Au-NPs.

Based on the sulfur-tolerant ability of Stöber silica supported Au-NPs (with copper addition) extended the application of gold catalysts. It is hopeful that the gold nanoparticles do have the ability to provide more wonderful applications in catalysis field.

Jingjie LUO

Formation de nanoparticules d'or supportées sur silice Stöber: mécanismes et applications

Dans ce travail, les nanoparticles d'or supportées ont été étudiées en raison de leur fort potentiel dans les domaines de la catalyse. Des sphères de silice obtenues par la voie Stöber ont été synthétisées et utilisées comme supports des nanoparticules d'or. Les précurseurs d'or sont des solutions colloïdales possédant des nanoparticules d'or homogènes et de petite taille (environ 3 nm). Les matériaux préparés avec ou sans addition d'un nouvel élément ont été utilisés dans les réactions de l'oxydation du CO et une réaction inédite pour l'or: l'oxydation sélective de l'H_2S.

Les résultats indiquent que l'utilisation de colloïdes d'or comme précurseurs permet de contrôler la taille et la dispersion avant le dépôt et ceci est facilité par les propriétés optiques des nanoparticules de ce métal. Pour les propriétés catalytiques, outre la dispersion, on confirme très clairement par cette méthode de synthèse que l'interaction Au/Support joue un rôle majeur. L'addition d'un second métal augmente significativement l'activité des matériaux à base d'or. Les particules d'or et de Cu se rassemblent sous les conditions réactionnelles testées. Dans le cas de l'oxydation du CO, de petites quantités d'espèce d'or partiellement oxydée sont générées et forment une glue avec les espèces Cu^{2+} également formées au cours de la réaction et ceci permet de fixer les nanoparticules sur le support. Dans le cas de l'oxydation sélective de H_2S, il a été montré que le système est résistant au soufre, y compris sur une longue durée de test. Les silices Stöber se sont avérées comme des supports catalytiques très intéressants car non poreux et formés de particules de petites tailles, ils sont aptes à exposer les phases actives de l'or aux réactifs, diminuant la pression de surface et facilitant le transfert thermique. Il a également été prouvé que ce matériau peut être mis en compétition avec les matériaux mésoporeux, ces derniers étant jugés indispensables pour obtenir de hautes activités en catalyse hétérogènes jusque là.

Mots clés: Nanoparticules d'or, Colloïde, Silice Stöber, Croissance de particules, Oxydation du monoxyde de carbone

Formation of Stöber silica supported gold nanoparticles: mechanism and application

Supported gold nanoparticles have been focused on due to their high efficiency in the catalysis field. In this work, Stöber silica consisted by globules were synthesized and used as support for gold nanoparticles. The gold colloids with homogeneous and small nanoparticles (about 3 nm) were applied as gold precursor. The prepared materials with further metal addition were used to active the CO oxidation and another very special reaction-selective oxidation of H_2S.

The results suggested that by using the gold colloid as precursor the sizes of nanoparticles could be controlled before loading onto silica under the help of its optical properties. The results for catalytic reactions indicated that the interaction between Au-support is another essential factor impacting the activity beyond the size effect. The additions of metal largely enhance the activity of gold materials. The gold and copper (oxide) particles go through reassembling during the reactions. In the CO oxidation, small amounts of partially oxidized gold species were generated and "glued" strongly by the new formed Cu^{2+} species to the support. While in the selective H_2S oxidation, it was found that the material is sulfur-resistant during long time reaction. The Stöber silica is proved to be a very promising support, which is non-porous but beneficial to expose active sites of gold nanoparticles to the reactants, lower the pressure drop, and facilitate the heat transformation. It was proved even can be matched with the well-know mesoporous materials that is claimed to be indispensable for the high activity.

Keywords: gold nanoparticles, colloid, Stöber silica, development of nanoparticles, CO oxidation